

Final Report

Fly Myself Into the Future - With CESTREL

Circular Eco-friendly Short Take-off Range-
Extended Lifter

Group 22

AE3200 - DSE 2020



Final Report

AE3200 - DSE Project:
Fly Myself Into the Future - with CESTREL

With special thanks for support and guidance from

Tutor Dr. Irene Fernandez Villegas
Coach ir. Kushagra Vidyarthi
Coach Víctor Villalba Corbacho
TA Sam van Elsloo

by

Group 22

Name	Student Number
Jonas Appels	4682637
Yasser Elnily	4668669
Roosa Joensuu	4662407
Thomas Keesom	4668170
Timo van Maarschalkerweerd	4441958
Elise Scheers	4680847
Kasper Sijmons	4351088
Andrei Stefanidi	4680782
Aïcha van Veen	4660870

List of Abbreviations

Table 1: List of Abbreviations

Abbreviation	Meaning
ATC	Air Traffic Control
DSE	Design Synthesis Exercise
EOL	End of life
MTOW	Maximum Take-Off Weight
OEW	Operational Empty Weight
RAMS	Reliability, Availability, Maintainability, Safety
TRL	Technical Readiness Level
STOL	Short Take-off and Landing
SWOT	Strengths, Weaknesses, Opportunities, Threats
VTOL	Vertical Take-off and Landing
FFD	Functional flow diagram
FBS	Functional breakdown structure
ROC	Rate of climb
ROD	Rate of descent
AVL	Athena Vortex Lattice
HLD	High lift devices
MAC	Mean aerodynamic chord
cg	center of gravity
PLA	polylactide
PEI	Polyetherimide
PEEK	Polyether ether ketone
XPLE	Cross-linked polyethylene
RMP	rotations per minute
UAV	unmanned aerial vehicle
FEM	Finite element method
AoA	Angle of attack
SM	Stability Margin
TAS	True airspeed
BVI	blade-vortex interaction
ICAO	International Civil Aviation Organization

List of Symbols

Table 2: List of Symbols

Symbol	Meaning
C_D	Drag coefficient
C_L	Lift coefficient
C_{L_h}	Lift coefficient of the canard
$C_{L_{A-h}}$	Lift coefficient of the wing
$C_{L_{\alpha_h}}$	Gradient of the canard lift coefficient and AoA
$C_{L_{\alpha_{A-h}}}$	Gradient of the wing lift coefficient and AoA
$C_{L_{\alpha_v}}$	Gradient of the vertical tail lift coefficient and AoA
C_{D_0}	Zero lift drag coefficient
A	Aspect ratio
e	Oswald efficiency factor
S	Wing surface
V	Free-stream velocity
ρ	Density
M	Mach
W	Weight
g	gravitational acceleration
n	load factor
S	surface area
AR	Aspect ratio
T	Thrust
L	Lift
D	Drag
q	shear flow
I	moment of inertia
σ	normal stress
τ	shear stress
b	span
c	chord
Re	Reynolds number
m	mass

Contents

1	Introduction	1	9.3.3	Maximum Lift Coefficient and Drag Bucket	50
2	Executive Overview	2	9.3.4	The airfoils of the main wing, canard and vertical tail	51
3	Market Analysis	9	9.4	Lift and Drag estimation	52
3.1	Product Introduction	9	10	Stability and Control	53
3.2	Industry Overview	9	10.1	Functional analysis	53
3.3	Target Market	9	10.2	Requirement analysis	53
3.3.1	Target cost and selling units	10	10.3	Loading diagram and CG range	53
3.3.2	Target Customers	10	10.3.1	Loading diagram code verification	55
3.3.3	Selling points	11	10.3.2	Loading diagram code validation	55
3.4	Market Competition	12	10.3.3	Loading diagram sensitivity analysis	57
3.4.1	Indirect Competition	12	10.4	Stability and controllability during VTOL and wing configuration	57
3.4.2	Direct Competition	13	10.5	Stability and controllability during flight	59
3.4.3	SWOT-Analysis	13	10.5.1	X-plot code verification	61
3.5	Future Market Development	14	10.5.2	X-plot code validation	61
4	Resource Allocation	16	10.5.3	X-plot sensitivity analysis	63
4.1	Preliminary sizing	16	10.6	Vertical tail sizing	63
4.2	Resource allocation	17	10.6.1	Vertical tail code verification	65
4.3	Iteration logic	17	10.6.2	Vertical tail sizing sensitivity analysis	65
5	Functional Diagrams	18	10.7	Ground stability	65
5.1	Functional Flow Diagram FFD	18	10.8	Control Surfaces	66
5.2	Functional Breakdown Structure FBS	18	10.8.1	Aileron control surface sizing	66
6	Configuration and Layout	23	10.8.2	Rudder control surface sizing	67
6.1	Functional analysis	23	10.8.3	Elevator control surface sizing	68
6.2	Requirement analysis	23	10.8.4	Control surfaces code verification	70
6.3	Aircraft configuration and layout	23	10.8.5	Control surface sizing sensitivity analysis	71
6.4	Electric Block Diagram	25	10.8.6	Ailerons and elevators deflection during the VTOL mode	71
6.5	Hardware and Software block diagram	26	11	Material	72
6.5.1	Hardware	26	11.1	Functional analysis	72
6.5.2	Software	27	11.2	Requirement analysis	72
6.6	Data handling block diagram	27	11.3	Material choice for primary structures	72
7	Performance	31	11.3.1	Mechanical Properties	73
7.1	Functional Analysis	31	11.3.2	Sustainability and Recyclability	73
7.2	Requirement Analysis	31	11.3.3	Final Material Choice	75
7.3	Manoeuvring envelope (V-n) and Gust load diagram	31	11.4	Secondary structures and other components	75
7.3.1	Manoeuvring envelope (V-n)	32	11.4.1	Secondary structures	75
7.3.2	Gust load diagram	34	11.4.2	Other components	76
7.3.3	Verification and Validation	36	12	Structural Design	77
7.4	Revised mission profile	37	12.1	Functional analysis	77
7.5	Noise reduction	39	12.2	Requirement analysis	77
8	Power and Propulsion	41	12.3	Fuselage design	77
8.1	Functional analysis	41	12.3.1	Design Process	77
8.2	Requirement analysis	41	12.3.2	Verification and Validation	78
8.3	Cruise thrust and power	41	12.4	Landing gear design	80
8.4	VTOL thrust and power	42	12.4.1	Tire selection	81
8.5	Propulsion method	43	12.4.2	Main gear strut design and suspension	81
8.5.1	Range extender	44	12.4.3	Nose gear strut design and suspension	83
8.5.2	Fuel and battery calculations	44	12.4.4	Landing gear overview	83
8.5.3	Motor selection	44	12.4.5	Verification and Validation	84
8.6	Proprotor design	45	12.5	Wing Design	85
8.6.1	Verification and validation	46	12.5.1	Description and assumptions	85
8.7	Fuel system lay-out	47	12.5.2	Loads on wingbox	86
9	Aerodynamics	49	12.5.3	Moments of inertia of the cross-section	88
9.1	Functional Analysis	49	12.5.4	Stresses on the cross-section	90
9.2	Requirement Analysis	49	12.5.5	Buckling	93
9.3	Airfoil Selection	49			
9.3.1	Airfoil Thickness	49			
9.3.2	Airfoil Camber	50			

12.5.6	Wing structure	94	14.2.1	Environmental sustainability	118
12.5.7	Verification and Validation	97	14.2.2	Economical sustainability	121
12.6	Circular economy principle: joining method . .	99	14.2.3	Social sustainability update	123
12.6.1	Fairing	100	14.3	Sustainability development and conclusion . .	124
12.6.2	Landing gear joining	101	15	Technical Risk Analysis	125
12.6.3	Wing joining	101	15.1	Mitigated Risks	125
12.6.4	Canard joining	104	15.2	Current Risks	127
12.6.5	Tail joining	104	16	Development	132
13	Final Design	105	16.1	Project Design and Development Logic	132
13.1	Final Design Summary	105	16.1.1	PD&D Logic diagram	132
13.2	Budget Breakdown	105	16.1.2	Product lifetime cycle	132
13.3	RAMS characteristics	106	16.2	Project Gantt Chart	133
13.3.1	Reliability	106	16.3	Production Plan	136
13.3.2	Availability	106	16.3.1	Production plan diagram	136
13.3.3	Maintainability	107	16.3.2	Production phases	136
13.3.4	Safety	107	16.3.3	Circular economy	136
13.4	Cost breakdown	108	16.4	Operations and Logistics	138
13.4.1	Fixed costs	109	16.4.1	Operations	138
13.4.2	Variable costs	110	16.4.2	Ground Support	138
13.4.3	Total cost	110	16.4.3	Maintenance	139
13.5	Operational cost	111	16.4.4	Communication	139
13.6	Compliance matrices	111	16.4.5	Emergency procedures	140
13.7	Sensitivity analysis of the final design	116	16.4.6	Logistics	141
14	Sustainability development logic	118	17	Conclusion and Recommendations	143
14.1	Requirement analysis	118	References	144	
14.2	Sustainability analysis: checklist	118			

Introduction

This report looks into the final design of the aircraft of DSE group 22 with the theme "*Fly Myself into the Future*". The overall goal of the project is to design a personal aircraft, while making use of the circular economy concept. Over the years, flying frequency has been constantly increasing¹, resulting in concerns being raised about the sustainability of flight for the future. Various sources and statistics indicate that, as seen now, flying as a whole may perhaps never reach the status of a 'fully sustainable' means of transportation², the production of carbon dioxide being a particular issue raised by frequent flying. Based on current global developments, it is expected that flying will however continue to grow as a means of transportation. Firstly, global wealth has been increasing over the years³, which could have as a result more people affording to travel more often. Moreover, due to international collaboration and work travel seen from the number of people approximated to be currently working abroad (roughly 232million⁴), it is safe to assume that the general trend in air mobility will continue to increase. Airlines and aircraft manufacturers are nowadays attempting to balance out the environmental impact of flying through various methods such as planting trees in certain regions around the globe for a number of flown miles, or researching into new propulsion technologies to reduce emissions.

This report therefore looks into the final design approach taken for Cestrel (Circular Eco-friendly Short Take-off Range-Extended Lifter), a personal aircraft meant to improve the overall human air mobility, while simultaneously reducing the environmental impact and serving as a more sustainable means of air transportation of the future. First, [chapter 3](#) looks into the current market for such aircraft, together with the target of Cestrel in said market. Next, [chapter 4](#) investigates the resource allocation within the project for the aircraft, in order to have a clearer understanding of the expected outcome. In [chapter 5](#) the functional flow and breakdown structure of the aircraft are shown. The first rendering of the aircraft configuration and its layout is shown in [chapter 6](#), along with the electric block diagram, the hardware/software and the data handling diagrams of the aircraft. The overall performance of the vehicle is discussed in [chapter 7](#) including the manoeuvring envelope, the gust load diagram, the mission profile and certain techniques considered for noise reduction. Next, in [chapter 8](#) an analysis of the required thrust and power is performed, for both the cruise phase and VTOL phases, and lastly a propulsion method chosen along with the design of the propulsion system for the aircraft is discussed in detail. In [chapter 9](#), the selection of the airfoil and an analysis of the aerodynamics of the aircraft are conducted. Following this, [chapter 10](#) looks into the stability and control of the aircraft, by considering the loading diagrams and the x-plots obtained for the chosen configuration. The material choice for different components of the aircraft is done in [chapter 11](#) followed by the implementation of these materials in the analysis of the structural components of the aircraft in [chapter 12](#). Here, a detailed description of the analysis is done for the fuselage, landing gear and the wing structure. A final review of the complete design is given in [chapter 13](#), this including the RAMS analysis, cost breakdown, and operational cost of Cestrel. The sustainability of Cestrel is looked into in [chapter 14](#) taking into account the checklist set in earlier phases of the design and sustainability development. Next, the risks related to the aircraft, both from previous phases and from the final phase are described in [chapter 15](#). Lastly, the production plan, the operations and logistics, and the project design and development logic are addressed in [chapter 16](#), the report finalising with some concluding remarks and suggestions for the future in [chapter 17](#).

¹<https://www.statista.com/statistics/564769/airline-industry-number-of-flights/>, Accessed [22.06.2020]

²<https://flygrn.com/page/sustainable-air-travel>, Accessed [22.06.2020]

³<https://www.credit-suisse.com/about-us-news/en/articles/media-releases/global-wealth-report-2019-global-wealth-rises-by-2-6-driven-by-201910.html>, Accessed [22.06.2020]

⁴<https://www.trainingexperience.org/blog/2018/11/07/6-facts-working-abroad-will-make-understand-expats-better/>, Accessed [22.06.2020]

2

Executive Overview

This chapter provides a summary of the report as a whole. First a quick summary will be provided from the previous phases: Baseline phase and Midterm phase. Then it will include the topics of each chapter along with procedures and results where applicable.

Group 22 introduces Cestrel (Circular Eco-friendly Short Take-off Range-Extended Lifter), the personal aircraft of the future. It is a one-capacity, VTOL, low-noise aircraft with promising performance characteristics. On top of that, it is a new sustainable way of transportation due to the use of bio-fuel and batteries, due to the noise-reduction methods and, most importantly, it is designed according to the circular economy principle.

Baseline phase

To give a little bit of background, the previous two design phases were quickly summarised. The previous two phases are the baseline and midterm phase. During the baseline phase, the main focus was put on defining the requirements for the personal aircraft design. At the end of the baseline phase, the requirements contained quite a bit of unknown parameters, which were marked with '<tbd>'. The tbd's were removed from the requirements and substituted with known parameters as the project progressed. More and more became known in the later stages of the design.

Apart from the requirements, a few aircraft concepts were proposed. In addition, a design option tree was constructed to explore the possible options within the personal aircraft design.

Midterm phase

The main focus of the midterm phase of the project is the trade-off of the aircraft concepts that enter the trade-off. Of the proposed concepts of the baseline phase, four were selected to enter the trade-off: the flying car, flying wing, the bush plane and the tilt propotor design. The tilt propotor design was the most futuristic options. It is also able to vertically land and take off (VTOL). It was also expected that this design would perform well when trying to implement the circular economy to the structure of the design. These were the main reasons for the tilt propotor, which made it win the trade-off.

Market Analysis

In an industry overview relevant industries for the tilt propotor design are analysed. These are the existing long-distance transportation vehicles like cars, trains and airplane. The automotive industry is a large and dynamically involving industry that is readily available nowadays. Trains are also a common transportation method these days, it allows for cheap travel in populated areas. However, it is less flexible and private than travelling by car. Lastly the aviation industry is an important one to mention, which enables travelling faster from one city to another. Travelling by plane is currently still less flexible than by car.

The target market of Cestrel is mainly Europe. The main target customers are the business people who are in need of fast and flexible travel methods. Most preferably one that allows for sustainable travelling, such that business trips are not harmful for the environment. Next to that, the personal tilt propotor tries to reach revolutionary technology enthusiasts, which are key for the market of Cestrel as they are often willing to take the risk to buy a product from a not yet established manufacturer. After the early phase, the aircraft will also target customers which gained trust in the proven product.

The main reasons to sell the aircraft can be listed as selling points:

Sustainability, privacy and comfort, straight flight path, fast, flexible, being in control, fun, low operational cost, competitive purchase price, low repair cost, and lastly the high scrap value.

The aircraft will have to compete on the market with already existing competition and competition in development. The market competition can be split in two sorts: indirect competition and direct competition. The indirect competition is identified to be competitors which sell a different product with the same purpose. These include the personal car, public transport, conventional airplane and Hyperloop system. The direct competition are the competitors which do sell a similar product: a personal aircraft. The most relevant ones identified are: Boeing Passenger Air Vehicle, NASA Puffin, Airbus Vahana and the Lilium Jet.

Four phases of the product's life time on the market have been identified:

1. Introduction: this refers to introduction to the market without extra infrastructure.
- 2a. Growth: Hubs around the city will become available for landing.
- 2b. Growth: Regulations adapt and landing on streets and in cities becomes possible and legal.
3. Maturity: The market is (almost) saturated. Marketing should aim at fending off competition.
4. Decline: At some point the sales of the Cestrel will decline, which might have multiple reasons.

Resource Allocation

Before starting to design the complete aircraft, it is necessary make a preliminary sizing of the aircraft, including a mass estimation, a preliminary power estimation and a wing sizing. After the sizing, resources, such as mass, power, and cost, could be allocated to the subsystems. The main subsystems considered here are the structure, propulsion system, payload, fuel, and other. Payload and fuel have been taken into account here to have a complete mass allocation.

Functional Diagrams

The functional diagrams consist of the Functional Flow Diagram (FFD) and the Functional Breakdown Structure (FBS). The FFD will describe the three main functions during the phases of the aircraft's mission: production, operation and retirement. The diagram was already conducted in the Baseline report [6], however it was adjusted to fit the operation profile of the tilt proprotor design as more detail about all phases is present. The FBS will collect the functions together in form of an AND-tree and provide more detailed functions by going a level deeper in detail.

Configuration and Layout

The aircraft design is chosen such that it meets all of the requirements, which lead to the design of a vertical take-off aircraft for one person that is capable of a horizontal cruise of 220 km/h. To be able to do this, four tilting proprotors are used, one on each wingtip. This is possible as the aircraft has a main wing as well as a canard. The tilting ability of the proprotor is the reason why the aircraft can both take off vertically, as well as fly horizontally during cruise.

Also the electric components and its connections have been identified in an electric block diagram. Next to that, there is also a hardware and software block diagram. The hardware diagram shows the mechanical control in the aircraft, and the software diagram the required software for the hardware to be able to operate. Lastly, also a data handling block diagram is included, to show the data flows within the aircraft easily.

Performance

The performance of the aircraft is investigated by plotting the manoeuvring envelope (V-n diagram) and the gust load diagram. This is done for two mission phases: the VTOL/conversion phase where the proprotors are tilted and the airplane phase where the proprotors are positioned fully horizontally.

It is important to note that the true cruise speed is increased to $V_C = 61 \text{ m/s}$ (equivalent to 220 km/h) with respect to the minimum defined by requirement **DSE-22-SYS-P-07** of 160 km/h. This was to make sure that during cruise, all possible load factors could be reached as described by the CS-23 regulations and the value was found using iteration. By plotting the manoeuvring and gust diagrams, it is possible to determine the maximum load factor one should design for. The maximum load factors during VTOL/conversion mode for the manoeuvring diagram were determined by following the procedure in the CS-27 regulations and are equal to 2 and -1. In the aircraft mode the maximum load factors for manoeuvring were set by CS-23 regulations and are equal to 2.5 and -1. The gust loads gave values larger than those for manoeuvring: 2.92 and -1 and will therefore be considered for the design of structural elements.

The mission profile is revised for the new cruise speed. This time, the transition phases between vertical take-off, transition and horizontal flight is made clear, the same is done for the landing phase. This results in different rate of climb (ROC) and different rate of descent (ROD) in the climb and landing phases of the mission. The vertical rate of climb is determined by the maximum power that can be delivered, and is found to be 1.5 m/s. This same value is used to descent in fully vertical mode.

Research into noise reduction of aircraft resulted in a few methods that need to be taken into account in the further design process. The blade geometry for example should include a serrated trailing edge, and through testing, active flaps could also be implemented on the blades. Experiments on noise reduction effects of porous materials should be studied further. Additionally, the micro gas turbine should have acoustic liners and a turbine blade geometry optimised for noise reduction.

Power and Propulsion

The propulsion method chosen for this aircraft is a biodiesel, electric hybrid. This allows for high power but lightweight electric motors, these will rely on high power bursts from the batteries, but can also be powered by a micro turbine generator for the cruise flight. This allows for both high power bursts but also a lightweight energy storage for cruise. The proprotors will be connected to an electric motor each and the cruise electric power will be 25kW.

During cruise the combined power will be 25 kW. During a hover the combined power will be 160 kW. The fuel needed for the required 3 hour endurance is 38 kg. The lithium ion battery mass required for a 6 minute hover is 58 kg

Aerodynamics

In order to start with the analysis on the aerodynamic characteristics, it was necessary to determine the airfoils for the main wing, canard, and vertical tail first. This was determined based on a research on the camber and thickness. Once this was established, three 4-digit NACA airfoils were compared to each other, and for the main wing and canard the airfoil NACA 4412 was chosen, because of the wide drag bucket, high maximum lift coefficient, and high lift over drag ratio. The NACA 4412 performed best out of the research that was done on more airfoils, with these performances in mind.

Then, the aircraft without a fuselage was programmed in the Athena Vortex Lattice (AVL) program in order to compute aerodynamic characteristics. Through this program the lift coefficients for the total aircraft, as well as the individual contributors were determined. Also the drag coefficient during cruise was determined which lead to the total drag of the aircraft of 302 N. Furthermore, parameters that were needed for the stability and control characteristics were determined using AVL.

Once the maximum clean lift coefficient of 1.404 was known, it was also possible to start sizing the main wing. This was done while taking the sizing of the canard into account as well, as they are both lift generating contributors to the aircraft. After a few iterations, the surface area of the main wing was determined to be 9 m^2 , the wing span to be 6 m, and a chord length of 1.5 m.

Stability and Control

In this chapter, the wing configuration as well as the sizes and positions of the horizontal stabiliser and basic control surfaces will be determined. The aircraft will not have any high lift devices (HLDs) as the aircraft will not need them. The aircraft has a VTOL mode to be able to take-off and land vertically.

For the positioning of the horizontal stabiliser, it is important to know the cg range of the aircraft. For this a loading diagram tool was created in python which calculated the cg range of the aircraft. For this is assumed that the payload includes the pilot and his/het baggage. It also assumed that their cg location are at the same position. The cg range of the aircraft is calculated to be between -82.73 and -78.43 %MAC. This is logical as they are in front of the main wing, like it should be for a canard aircraft.

The aircraft will have a VTOL mode. For stability during VTOL it is beneficial to have a canard configuration as the propulsion system of the aircraft will be mounted on the tips of the wings. For canard configurations, generally the wings are positioned further apart compared to a conventional aircraft configuration. Another good reason to have the canard configuration is that the wings will both create positive lift during nominal flight, which allows both the main wing and the canard to be smaller as they work together to generate the necessary lift to keep the aircraft in the air.

Apart from the canard configuration, the main wing will be a positioned high on the fuselage to prevent prop wash of the proprotors on the canard from hitting the main wing during transition from VTOL mode to nominal flight.

To position and size the canard, an X-plot tool was programmed to size the canard to meet the stability and control requirements. It also helps to position the canard. The aerodynamic data needed from this was taken from the aerodynamics department. The main wing will be positioned at 3.741 m from the nose and the canard will be positions at the very tip of the nose of the aircraft. The canard will have a surface area of 2.286 m^2 , with a span of 3.81 m and a cord of 0.6 m.

The sizing for the vertical tail was critical for an engine failure that causes asymmetric thrust. The idea is to have a control system that limits the asymmetric thrust in the event of an engine failure. The control system should be able to let some rotors generate less or more thrust. If the maximum asymmetric thrust is assumed to be 92 N, the vertical tail was sized to have a surface area of 0.947 m^2 , with a cord of 0.910 m and a span of 1.04 m.

The control surfaces were sized using preliminary methods [37]. The ailerons were designed to meet a roll rate requirement of 60 degrees in 1.3 seconds. This means that the ailerons had to have a total area of 1.89 m^2 and a span and cord of 2.10 and 0.9 meters respectively. The ailerons would start at 2.45 m and ends at 3.5 m on the wings.

The rudder was designed for a particular maximum rudder deflection. This resulted in a rudder with a surface area of 0.128 m^2 and a span and cord of 1.2 and 0.11 meter.

Lastly, the elevators, which were the hardest to size. This is because the method to size the elevators used data from all departments. The critical case for the sizing of the elevators is rotation during take-off. However, the personal aircraft is not planned to perform nominal take-offs where the aircraft gains speed on the ground. The idea was to try and size the elevators for a nominal take-off anyway such that the aircraft could also take-off nominally in future operations. Unfortunately, the sizing method pointed out that the selected elevator size would stall during rotation. It was decided to check if the elevators would be appropriately sized for the next most critical phase, which is landing. This was the case, so the idea of the aircraft being able to perform a nominal take-off was discarded and the elevator size is given to be: 0.456 m^2 for the surface area and 3.81 and 0.12 m for the span and cord.

Materials

The materials for the aircraft were selected based on an analysis for each type of structure - primary load carrying structures, secondary load carrying structures and for structures that do not carry loads. For the primary structures first, the main aspects that were looked into are the mechanical properties such as yield, critical and fatigue strengths, and then the sustainability. For sustainability it was important whether the material was recyclable and if parts made out of said material are reusable. For the secondary structures and non-load carrying components a similar analysis was performed, however the sustainability was considered more important than high-performance for these elements. The result of the analysis showed that the material which fulfils all the requirements set was aluminium 6061 T6 for primary structures, as it is one of the most available alloy type as a recycled aluminium alloys, while simultaneously having good mechanical properties. For secondary structures the thermoplastic PEI will be used. Manufacturing by 3D printing will reduce waste and moreover, the thermoplastic parts can be reused by patching cracked parts. This can be done by heating up the material which will then fill up the cracks present. The plan for the future remains to switch to PLA however the feasibility of long-term outdoor use of PLA has to be researched in more depth before this application will be possible.

Structural Design

Fuselage design

The fuselage structure will not be of a tubular form and in order to enable the shaping of the irregular form, a load-carrying truss structure with a non-load-carrying fairing will be designed. The truss structure itself is designed using iterative CATIA and ANSYS analysis, in order to investigate the stresses posed by the loads on the trusses. The trusses itself are made of Aluminium 6061 and have a 20 mm radius circular cross-section with a 3mm wall thickness which are then welded to each other. This thickness has not yet been optimised per section, which will be done in the future. The fairing will be made of a thermoplastic material, with a thickness that can be optimised for each fairing section.

Landing gear design

The aircraft will have fixed landing gear due to the low cruise speed, low complexity, low weight and low maintenance cost. They will be configured in a tricycle landing configuration with 2 main landing gears and one smaller nose gear. The positioning of the landing gear will make sure that ground stability is met, which includes longitudinal and lateral tip-over criteria (as given in Roskam [35]) and to make sure the nose gear takes up enough loads for good steerability, without overloading it. The nose gear will be positioned at 1.12 m from the aircraft nose, the main gear is positioned at 3.38 m.

The tires were selected based on the static and dynamic load they should be able to carry, and by looking into reference aircraft (Cessna 180). By looking into a reference aircraft that lands horizontally, the landing gear of Cestrel will exceed the requirements for the wheel during VTOL operations which are less demanding on the tire. However for a future mission profile, allowing for horizontal STOL landings, a bigger tire was selected. The selected main wheel is of type 6.00-6 (dimensions in inches), together with a fitting main wheel tube, main wheel assembly and main wheel brake assembly. The nose gear has the 5.00-5 dimensions, with nose wheel tube and a wheel assembly.

The main gear suspension is achieved by using a spring steel strut design. The strut has a rectangular cross-section made out of steel 300M, due to its high strength, toughness and fatigue strength. This means it allows for proper suspension (the strut will bend) without plastically deforming it. The strut will have a length of 1.05 m, and will be positioned at a 43 degree angle with the horizontal. The nose wheel strut mechanism will consist of a oleo pneumatic shock absorber, with a steel 300 M strut. The height of the strut is such that the aircraft on ground is fully levelled, allowing for better vertical take-off.

Wing design

For the main wing, the canard and the vertical tail, the primary load-carrying structure is a wingbox, made out of aluminium 6061 T6.

First, the maximum load case was identified as the VTOL phase of the mission, including the load factors from the V-n diagram and a safety factor. The wingbox was thus designed to withstand the loads in this ultimate situation. Additionally, the wing box was tested for both positive and negative load factors that can occur during its operation. The wingbox is designed such that it will not buckle under the loads.

The next step was to look into the fatigue stress to which the wingbox can be exposed. The results were that the stresses in the wingbox of the canard and the main wing do not exceed the fatigue limit stress of the chosen material for normal use of the aircraft, i.e. with load factors set to 1.

The results of the structural analysis performed are presented in [Table 2.1](#). Naturally, the number of stringers changes per spanwise section, based on load requirements.

Table 2.1: Wingbox sizes for wing, canard and vertical tail

Parameter	Wing	Canard	Vertical tail	Unit
Load case	VTOL	VTOL	-	-
Max shear stress	14	17	31	MPa
Max compressive stress	221	232	124	MPa
Max tensile stress	273	285	148	MPa
Top skin stringers at root	21	7	6	-
Bottom skin stringers at root	11	5	3	-
Ribs	11	7	3	-
Mass of wingbox	14	13	5	kg

The structure can still be optimised further by adjusting the thicknesses at each web or spar. Additionally, the top and bottom skin could be made to adhere to the curvature of the airfoil.

For the LE and TE of the wing, canard and vertical tail it was decided that they will be made out of PEI, with a 3D printed honeycomb structure. A thick lining of honeycomb is used, about 5cm, with an infill percentage that should be optimised for impact resistance where necessary, and otherwise weight.

Circular economy principle: joining method

At the end-of life (EOL), the aircraft will be disassembled into different parts and components to sort them into recyclable, reusable or refurbishable units.

- ✈ **Reuse:** The part goes back into the assembly street for new aircraft right away. With very little cost the full value is sustained.
- ✈ **Refurbish:** The part is thoroughly checked for functionality and repairs are made if necessary. Then it also goes back into the assembly street. With slightly higher cost the most of the value can be sustained.
- ✈ **Recycle:** If the part cannot be reused or refurbished only the material value can be sustained. Different recycling procedures apply to different materials. The mostly used Al 6061 can be melted and reshaped. This is the least favourable solution since it destroys most of the part's value.

For reusing and refurbishing non-permanent joining mechanisms are crucial to allow for a non-destructive disassembly of the parts. Therefore the joining methods will consist whenever possible of non-permanent fastener types such as bolts and screws. For recycling it is important that the different materials can be easily separated. For an easy disassembly it is important to have a good accessibility over the whole aircraft. This will also simplify the replacement or repair of parts in case of local damage. It is achieved by making the fuselage structure from trusses. These trusses will carry all the loads, and therefore fairing, wing, canard and tail will directly be joined to this structure. The fairing will be made out of several pieces, such that it can be easily removed one by one in order to access the truss structure. On top of that, a 'door' with hinge will be incorporated where the engines are located such that inspections can be performed without having to disassemble any covering parts. The two wing halves will be joined to each other by a pin and lug design that will take up the bending moment and by another pin/lug mechanism that introduces the lift into the truss structure. These mechanisms also allows for easy disassembly and replacing.

Final Design

The final design is a tilting proprotor design for one person that can take-off vertically, as well as fly horizontally during cruise. Each of the wingtips has a tilting proprotor which enables the aforementioned functions of the aircraft. The final design has a mass of 775 kg.

Sustainable Development Logic

To access the sustainability of the final design, the sustainability checklists were again used.

The environmental sustainability was awarded a 3.1/4. Mainly because the recommendations with regards to the propulsion system were taken into account. The aircraft now has a propulsion system this able to run on all sorts of fuels. Not just fossil fuels, but also more sustainable fuels such a biofuel. Circular economy was also greatly taken into account for the structure of the aircraft.

The economical sustainability of the aircraft was awarded with 3.8/4. This is because the aircraft is expected to do well in the future market and has a very low operational cost. With regards to social sustainability the group is still holding on. Although the current workload can not be sustained for a very long time, no one will be burned out at the end of this project.

There is also a choice made in the fuel which could affect the overall sustainability of the aircraft. The use of Bio fuel could decrease the equality because it could compete with food production. With respect to the midterm quite some improvement was made with regards to sustainability. Overall, the scores increased quite a bit. The part of sustainability that the team is most proud of is trying to implement the circular economy and the propulsion system.

Technical Risk

For this section, the risks were divided into two categories: risks which were already mitigated through the design choices made, and risks which are new or that were not mitigated yet. For the risks that were already mitigated at this stage of the project, a table was generated presenting the risks, their initial scores for likelihood and severity along with the corresponding risk level, followed by the design choice which mitigated the risk and how this happened. The next step was to present the new scores for each risk as perceived after the mitigation took place. For the risks which were not mitigated yet, this was either due to the risks being directly related to the production phase of the aircraft or due to the risks being newly identified from the design choices. A similar approach was taken for these risks, however this time the table presenting the actions which are planned for the future mitigation. This was once again followed by a table indicating the anticipated risk levels after the mitigation will take place. To conclude this part, the remaining risks which are considered the most important out of the remaining ones for future phases of development are as follows: engine failures during operation which have to be mitigated through the addition of stabilisation software on the aircraft once this software is fully developed, risks of structural failures during operation which are to be mitigated through proper maintenance and care of the aircraft, the risks of aircraft overstress during operation which can be mitigated by proper training and by setting in place strict procedures for the safe operation of the aircraft which the pilot has to follow at all times, and lastly any failure of the turning subsystem for the proprotors, which once again has to be mitigated through a combination of maintenance and proper training for the pilot with regards to emergency procedures, should this ever occur during flight.

Development

The development chapter discusses the post-DSE phase of the project, this includes the Project design and development logic (PDD logic), the project Gantt chart, the production plan, and the operations and logistics.

The PDD logic discusses all the post-DSE activities, these activities also count for the business aspects of the project, for example, fund raising, sales, legislative work, etc. The next phase starts with evaluating the DSE period, making a business plan, and contacting investors. After raising funds, further design phases will be started, the conceptual design will be revised first then the preliminary design phase will start, followed by the detailed design. The testing and production phase are started afterwards. A more detailed diagram is created in this chapter with all the intermediate activities included. This section is followed by a project Gantt chart with all the tasks included in the PDD logic up to the production phases, since it is not really possible to estimate the durations of the other activities. The chart shows a very rough estimate for the duration required for the listed activities, these estimated will be refined in the next phase. For now, it is estimated that a first flight of the aircraft will be possible after 4.5 years.

The production plan of the aircraft consists of three main phases, manufacturing, assembly, and integration; the assembly phase is divided into two sub-phases, firstly the the components assembly, then the subsystems assembly. Once all the subsystems are assembled, the integration phase start, where the aircraft starts to get into its final shape. Some of the parts will be manufactured in-house from scratch, some will be provided by suppliers, and others will

be refurbished and used from retired aircraft. Same strategy goes for the components, some might be outsourced, assembled in-house, or refurbished and used from retired aircraft. Quality checks will be done throughout the entire production process, after each phase, parts, components, or subsystems will be quality-checked before they are approved to be used in the next phase. After the integration phase, full testing of the aircraft start. Finally, prior to manufacturing, disassembly of the retired aircraft will be done, and parts will be sorted. The exact details about how each part or component will be treated at the end of life are to be determined after the detailed design is finalized.

Finally, the operations and logistics section first discusses the operations. The operations is divided into three main phases, pre-flight, in-flight, and post-flight activities; the first one is divided into three main blocks, take-off, landing, and landing/loitering. It should be noted that operating the aircraft will required the pilot to have both PPL(H) and PPL(A) licenses as well as a multi engine rating. Secondly, the ground support is discussed, in the case of the aircraft being owned, the owner will either have his own garage, or rent a garage in the airport he is operating from. In the future, a leasing option will be considered. For the refueling of the aircraft, current infrastructure already exist in the airports, however, in the future, more fueling will be needed in urban areas. On the ground, batteries will be charged by a normal plug in method, while during the flight, they will be charged using a range extender. The aircraft will require pre-flight inspections which checks for visible damages. According to the EASA regulations, a detailed maintenance should be done every 100 flying hours or yearly. A communication diagram is also created showing the interaction of the system with the environment, i.e., communication between the pilot and ATC and other aircraft. It should be noted, however, that all the aircraft should be registered and and connected to the UTM (Unmanned Aircraft Systems Traffic Management) provider. In addition, Emergency procedures are looked into, this looks into emergency scenarios for example, motor failure during cruise, range extender failure, etc, and what procedures will be followed in these cases. Lastly, the logistics plan of the project is to be studied during later phases of the project, once the detailed design and manufactured plan are finalized.

Conclusion and Recommendations

During the earlier phases of the project, a trade-off process was done in order to choose a design concept which is able to comply with the customer requirements. The trade-off winner was a tilt-proprotor canard aircraft with VTOL capability. During the final phase of the project, the conceptual sizing of all the subsystems was done, resulted in and aircraft that has a range of 660 km, cruise speed of 220 km/h, endurance of 3 hours and payload mass of 150 kg. The circular economy concept was embraced throughout the entire design process, recyclable materials were chosen, sustainable energy options etc. In the next phases of the project, the preliminary and detailed design will be done, the production plan will be refined as well.

In order of the mass of the aircraft to converge in the next design phases, other components should be considered in more details, for example, avionics and instrumentation. This mass change, however, will affect the structural design of the aircraft, a lighter aircraft means lighter loads, and therefore lighter structure. In addition to this, some structural changes are recommended in the future in order to have a more optimised structure; for example, deflections should be looked into, buckling effects on the structure, and changing the rectangular structure of the wing into a curved one. Finally, during this phase of the project, only 4-digit NACA airfoils were considered, however, in the future using 5-digit NACA airfoils, which are more detailed, can improve the aerodynamics characteristics. The stability and control of the aircraft should be reassessed as well, currently, the cg range is very narrow, having a wider range means a more stable and controllable aircraft.

3

Market Analysis

The market analysis describes the market as it is right now and how this will be influenced by the aircraft as well as how it influences the aircraft. To be able to do this, first the product will be introduced in [section 3.1](#), then an industry overview is given in [section 3.2](#). This is followed by the target market in [section 3.3](#), which looks into the target price, target customers and also describes the selling points of the aircraft. This is then followed by a market competition in [section 3.4](#) and a Strength, Weakness, Opportunities and Threat (SWOT) analysis. Then the future development is described in [section 3.5](#).

3.1. Product Introduction

Based on the ever-existing dream to have flying cars, a gap in the market was found: to have a direct, fast, and flexible way to travel while being sustainable as much as possible. This led to the idea to design a personal aircraft in the form of a tilt propotor: Cestrel (Circular Eco-friendly Short Take-off Range-Extended Lifter), as this concept was found to be most successful in the mid-term report [7]. The aircraft will be sustainable by reducing the emissions and noise levels as much as possible. Another very important factor of why this aircraft will be able to fit the market is the circular economy concept that is implemented. The technical aspects of the aircraft that will have a big influence of the market analysis as well are the short take-off of maximum 50 meters, the minimum range of 300 km, and the minimum endurance of 3 hours. However, in order to see how feasible this idea is, it is needed to assess the current market and its development. This way additional factors that are important for the design will be identified and can thus be implemented.

3.2. Industry Overview

The tilt propotor that is being designed is a better solution for long distance travelling than cars, trains, or other aircraft. However, before it is possible to state the specifications that make the tilt propotor better, it is necessary to research and analyse the relevant industries. These industries are the existing long distance transportation vehicles, being cars, trains, and other aircraft.

The automotive industry is an immensely large and dynamic industry, as there are cars readily available for any purpose and price range. Within the automotive industry innovations are also always an ongoing process, making sure the automotive industry follows the current trends. These days, this means making cars as environmentally friendly as possible, and as such hybrid or electric cars came to exist for example ¹. Another innovation has been to make the cars (partially) autonomous to get self-driving vehicles. Therefore, the autonomous industry has proven so far that it has almost endless options to innovate. Product wise, cars usually have a range of approximately 400 to 600 km ². This in combination with all of the gas stations means it is possible to go anywhere with the car which is a big reason as to why the automotive industry is so large. The automotive industry is currently also an important part of the economy and is integrated in the whole society.

Another long distance transportation industry is the rail industry. Trains are a common method of transportation, which is used both in short and long distances. Often, there are subscriptions available which make this type of transportation a cheaper option to travel. Especially in densely populated areas, and from one of those said areas to another, this is a popular travelling method. It differs from a car as a transportation by not being as flexible, and for longer distances having to transfer trains. However, in trains it is possible to relax or work as you do not have to steer the vehicle.

Then finally the last industry to take into account is the aviation industry. On a larger scale, this industry is used to travel fast from one big city to another. It provides the fastest way of travelling, but it is a lot less flexible than for example a car. However, the total travel time is still less fast as it is necessary to go through airport security.

3.3. Target Market

The target market describes the first estimation of the target cost and selling units as previously described in the Baseline report [6] in [subsection 3.3.1](#). It will describe the specific market suitable for the aircraft, including the cus-

¹https://www.valueline.com/tocks/Industries/Industry_Analysis_Automotive.aspx#.Xu9dxkUzaUk [accessed on 21-06-20]

²<https://evadoption.com/statistics-of-the-week-comparing-vehicle-ranges-for-gas-bevs-and-phevs/> [accessed on 21-06-20]

tomers, their need, and how the aircraft aids in providing this need (see [subsection 3.3.2](#)) This section also includes the selling points of the aircraft in [subsection 3.3.3](#).

Since the aircraft was designed to comply with the European regulations CS-23 and CS-27 the target market will be Europe. If the first roll-out in European countries is successful, other markets can be developed. This is further explained in the life-cycle phases in [section 3.5](#).

3.3.1. Target cost and selling units

A first estimate on the cost of the aircraft was performed in the Baseline report [6]. In this analysis, the target cost of the personal aircraft was estimated by conducting a literature study and researching into the cost of already existing reference aircraft or aircraft currently in development. These reference aircraft were chosen as they have similar aircraft performance characteristics, that meet the top level requirements from [6] set for the design. A cost estimation was performed for the futuristic aircraft designs which include: Lilium Jet ³, Airbus Vahana ⁴, Boeing Passenger Air Vehicle ⁵, Opener Blackfly ⁶, Volocopter ⁷ and Ehang AAV ⁸. The average cost of these aircraft was calculated to be €275,000. According to requirement **DSE-22-SYS-C-01** the maximum allowable cost for Cestrel shall be less than 150% of that of the reference aircraft. These extra costs include costs needed for incorporating innovative technology into the aircraft and sustainability aspects which can add extra costs. The maximum target cost (including this 50% margin) was therefore set to be €412,500. When all aircraft parameters of Cestrel are fixed, a more accurate and detailed cost analysis will be performed in [section 13.4](#). Both a development cost estimate and operational cost estimate will be provided.

The amount of units to be sold is determined by taking into consideration that the amount of manned aircraft to be used in urban areas by 2035 is 30,000 units⁹. It is assumed that the fleet will rise a market share of 25% and 7,500 Cestrels will be sold in 15 years time span. The 25% estimation comes from the fact that currently no personal air vehicles are fully developed yet and it is estimated that 3 competitors will have a finished design at the same time of Cestrel. The average units sold per year is therefore equal to 500.

3.3.2. Target Customers

A suitable application of the Cestrel would be for business purposes. People that use a personal aircraft for business purposes want to travel quick and flexible. The amount of total travellers that travel for work is almost 20 % and airline profit as of now also comes mainly from the business traveller ¹⁰. As can be seen in [Table 3.1](#) and [Figure 3.1](#) the most used means of transport for the business traveller is the car with a share of almost 50%. The airplane is second with about 27% of the business journeys. With a range of 660km (see [chapter 7](#)) the Cestrel is very similar to the car or even exceeds the range of many cars. If the Cestrel successfully competes with the car it can gain a high market share. Additionally it has the potential to take up a part of the airplane share since the range could substitute most domestic flights and even some intra-European flights.

Since the awareness for the environment is steadily increasing many business travelers also demand a sustainable product. Also that is delivered by the Cestrel. The payload of 150kg is ideal for business trips since rarely more payload is needed. When travelling for business the value of the product or service is important which does not mean that the customers want the lowest price but they want the best value for the money ¹¹. Later in [section 13.4](#) the cost for the Cestrel is determined to be approximately 314,000€. This is surely more expensive than a car and also quite a few train tickets can be bought from that purchase price but as it is described in the selling points it can deliver added values like no other means of transport.

³<https://lilium.com/the-jet>, [Accessed 29.06.2020]

⁴<https://www.airbus.com/innovation/zero-emission/urban-air-mobility/vahana.html> [Accessed 29.06.2020]

⁵https://en.wikipedia.org/wiki/Boeing_Passenger_Air_Vehicle [Accessed 29.06.2020]

⁶https://en.wikipedia.org/wiki/Opener_BlackFly, [Accessed 29.06.2020]

⁷<https://www.volocopter.com/en/> [Accessed 29.06.2020]

⁸<https://www.ehang.com/ehangaav> [Accessed 29.06.2020]

⁹https://www.sesarju.eu/sites/default/files/documents/reports/European_Drone_Outlook_Study_2016.pdf [Accessed 29.06.2020]

¹⁰<https://www.condorferries.co.uk/business-travel-statistics> [accessed on 26-06-20]

¹¹<https://www.citicar.com.au/latest-news/top-7-things-business-travellers-really-want/> [Accessed: 22.06.2020]

Means of transport	Volume	Share in %
Flight tickets	2,268,000	26.8
Car rides	4,180,000	49.4
Train tickets	1,370,000	16.2
Other	644,000	7.6
Total	8,462,000	100

Table 3.1: Share of means of transport 2015 for multiple day business journeys in Austria¹²

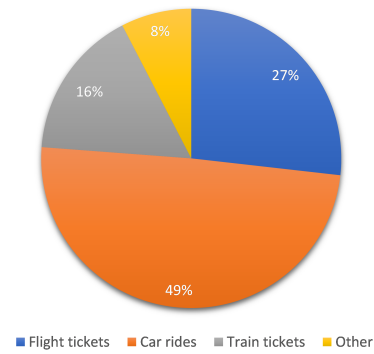


Figure 3.1: Table 3.1 in a pie chart

Next to people travelling for business there are quite many potential customers that consider themselves as pioneers for revolutionary technology. These are quite important in the early phase of the market entry since they are willing to buy the product even if the infrastructure is not fully deployed yet. This is comparable to the success story of Tesla¹³ which mainly depended on customers that believed in this novel technology and were willing to take the risk to buy a product from a not yet established manufacturer. These customers usually are more wealthy and are willing to spend the money to be one of the first owning such a revolutionary product. Therefore they are key for the Cestrel as well and must be reached and triggered by the product through the proper marketing.

Once the early phase was mastered more experience about the usability of the Cestrel is gained and the product attracts the attention of other customers as well. By then a new target customer group can be approached which is still rather wealthy but not willing to be the first to test a product.

3.3.3. Selling points

From the research done on the existing industries, it is clear that there is not yet a sustainable personal flying VTOL-vehicle for one person as readily available as cars are. However, there are many benefits that come with a personal flying vehicle, combining many positive aspects of other transportation means. All the advantages of the Cestrel are summarised in its selling points below.

1. **Sustainability** Due to the reusability, recyclability and low operational cost the Cestrel excels in sustainability metrics as it is further described in [chapter 14](#).
2. **Privacy and Comfort** While flying to the hubs close to the city centre with the Cestrel allows the customer to enjoy a maximum of privacy and comfort in their personal aircraft.
3. **Straight flight path** Living in remote areas where a good road connection is difficult due to topographical conditions (e.g. if the streets must follow a long valley) and where the next highway is far away, is not a problem anymore. With the Cestrel the customer is not dependent on the road network anymore.
4. **Fast** With a cruise speed of 220 km/h the Cestrel is much faster than the allowed maximum speed for cars on highways in most countries.
5. **Flexible** Public transport, Hyperloop and conventional airplanes operate or will operate according to fixed schedules and routes. With the Cestrel the customer can flexibly decide on his own departure time and destination.
6. **Being in control** Flying the Cestrel gives the customer the control over a powerful yet sustainable aircraft.
7. **Fun** Flying an airplane is already fun. The Cestrel is not only an airplane it also has a VTOL-mode making it even more fun to fly.
8. **Low operational cost** The operational cost has been found in [section 13.5](#) to be only 36.7 €-cents per kilometer. Since the aircraft will be easy to disassemble at the end of life, it is also easy to disassemble it partially to do maintenance or repairs, which will reduce the costs.
9. **Competitive purchase price** With a purchase price of €314,344 the aircraft is very competitive on the market and delivers high value for the money.
10. **Low repair costs** Due to its modular design the cost to repair a damage are minimal compared to other aircraft. During design it was ensured that all components can be easily accessed and are replaceable.

¹³<https://www.investopedia.com/articles/personal-finance/061915/story-behind-teslas-success.asp> [Accessed 22.06.2020]

11. **High scrap value** The Cestrel was designed for a circular economy. This also has direct benefit for the customer who profits from the high scrap-value at the end of the aircraft's life (EOL). To be correct, the aircraft at EOL is no scrap but it includes valuable parts that will be reused in a new aircraft or can be recycled.

3.4. Market Competition

In order to make sure the aircraft will sell, one should look at the already existing projects and projects in development that will serve a similar purpose. This is to find out whether this project is different and even better than compatible ones. In order to do so, the market competition will be investigated. This includes two types of competitors: first, one could identify indirect competitors. These consist of other means of transport, which however offer solutions to the same problem. The goal of these indirect competitors is a decrease of travel time. Another type is the direct competition, which are companies that sell a similar product: a personal aircraft.

3.4.1. Indirect Competition

The indirect competition mainly consists of already existing means of transport such as a car, public transport and conventional aircraft. These means of transport are widely used over the whole world and proven transportation methods. Therefore they are big competitors for the personal aircraft. Also the Hyperloop system, which is a new concept, shows some promising developments. All of these competitors will be discussed one by one and some advantages and disadvantages over the personal aircraft design will be listed.

Personal Car

The personal car is probably the largest competitor currently available on the market. Due to its wide usage, all infrastructure to support transportation by a personal car is readily available. The personal aircraft will need no infrastructure during the in-flight phase (such as roads for cars), reducing the already existing infrastructure cost. However, need for extra landing spots and parking areas (garages/storage boxes) will arise, as well as air-traffic-control (ATC) systems costs. This investment can be rather costly, however it is expected that once the system is set up the cost for operation will be lowered over the years. In terms of mobility, the personal car has a similar advantage as a personal aircraft, as they both offer the user freedom in transportation. Also similar ranges can be reached. The personal tilt proprotor design currently has a maximum estimated range of 660 km (for a cruise speed of 220 km/h and endurance of 3h, requirement **DSE-22-SYS-P-01**), which is similar to cars with internal combustion engines. Electric cars have a slightly lower range of about 300 km. When comparing to internal combustion cars, the personal aircraft will provide a more sustainable way of transportation by using bio diesel, while still reaching the same range. Electric cars or hybrid models however have even lower emissions, but this comes with the cost of handing in the maximum achievable range. Another advantage of the personal tilt rotor, is the ability to travel in straight flight paths when no airspace restrictions are set. This combined with a larger travel speed (220 km/h) results in travel times that are significantly shorter than those of car travelling. Also due to the three dimensional travelling directions, a larger volume of traffic can be handled at the same time, therefore solving the problems of the current traffic jams. This results in one of the biggest advantages of the personal aircraft, namely the certainty of arriving at your destination at a desired time.

Public Transport

Public transport is another example of already proven transport methods. This includes trains, buses, metro stations,... The public transport scores very well in terms of sustainability. Due to larger groups travelling at the same time, costs and emissions can be divided over the passengers, lowering both. However the limited comfort and scheduled travelling times are a large drawback for public transport compared to the personal aircraft. The personal aircraft will provide a comfortable way of travelling in very flexible travelling times, determined by the user itself.

Conventional Airplane

In the conventional aircraft category, only the short-haul flights can be considered to have some competition on the personal aircraft design, again due to the fact that it is already existing and similar ranges can be reached. However, the personal aircraft would make travelling by aircraft more easy as no long duration check-in procedures need to be followed, and departure times can be decided on.

Hyperloop

Lastly a transportation method that is not yet fully developed is considered to be a potential competitor for the personal aircraft: the Hyperloop system. The system promises to enable travelling faster than the personal aircraft with speeds that can reach subsonic or even sonic speed regimes. Another advantage is the range not being limited by the energy available on board but only by the expansion of infrastructure. Which directly also indicates a disadvantage for the Hyperloop system: the need of building underground tunnels in already crowded places, which are both very costly and difficult to implement. Due to the latter, it is questionable whether the Hyperloop system will be a major competitor to the personal aircraft and further developments will need to prove otherwise.

3.4.2. Direct Competition

For the direct competition category, other personal aircraft, currently tested or in development, were considered. Therefore some advantages and disadvantages will be investigated for some reference personal aircraft with a few similar performance characteristics.

Boeing Passenger Air Vehicle

The Boeing Passenger Air Vehicle is an autonomous VTOL personal aircraft developed by Boeing and Aurora Flight Sciences¹⁴. The aircraft is currently in development and has a planned introduction data on 2024. A big advantage of this vehicle is that it is fully electrically powered and therefore does not have any emissions. However, it does have the disadvantage of having a maximum range of only 80 km, and cruise speed of 180 km/h and therefore can not compete in terms of performance with the personal tilt proprotor design.

NASA Puffin

The NASA puffin concept has very similar characteristics as the personal proprotor design. The concept is also a low-noise personal VTOL aircraft with proprotors, capable of hovering. The advantage of puffin is again the fully electric propulsion, and therefore good sustainability characteristics. It can reach similar, and even higher cruise speeds of 241 km/h¹⁵. Due to all these promising characteristics, it can therefore be considered a close competitor on the market. The only aspect in favour of the personal tilt proprotor design, is the fact that it can reach 7.5 times the range of the puffin (only 80 km) and therefore meets the range requirement (DSE-22-SYS-P-01) set by the user of the project, where this is not the case for the NASA puffin concept.

Airbus Vahana

Vahana is a personal, tilt-wing aircraft able to take-off and land vertically financed by Acubed, Airbus and Airbus Urban Mobility. It has a slightly lower cruise speed of 190 km/h¹⁶, but again due to its fully-electric propulsion system it has a very limited range of only 50 km. It does again have a high sustainable value due to its zero emissions and low noise.

Lilium Jet

The last competitor considered in the analysis is the Lilium Jet designed by Lilium GmbH¹⁷. It is currently still under development but already has successfully flown prototypes. The introduction is planned in 2025. Although it serves quite a different purpose as it is not a personal aircraft but has a capacity of 5 people, it is still considered in the analysis due to its very promising performance and sustainability characteristics. The Lilium jet is able to reach cruise speeds of 280 km/h and has a maximum range of 300 km, all of this while also being fully electric.

Overall it can be said that there is quite some direct competition to the personal tilt proprotor aircraft. All of these concepts have zero-emissions and are therefore very appealing for futuristic personal air transportation. On the other hand, this often comes with a price of performing worse for range and cruise speed requirements. In order to meet the 300 range requirement and to enable fast travelling to a desired location, it was unfeasible for the personal tilt proprotor design to have zero-emissions. The sustainability aspect is however widely covered in the whole design by decreasing the amount of emissions using biofuel, incorporating noise reduction, and having the circular economy concept as a big part of the design.

3.4.3. SWOT-Analysis

From the above analysis, one can come up with strengths and weaknesses related to our business itself, which can be considered to be internal aspects. Also opportunities and threats can be identified for the external factor: market and environment. These are summarised in a SWOT-table as seen in [Table 3.2](#).

¹⁴https://en.wikipedia.org/wiki/Boeing_Passenger_Air_Vehicle, [Accessed 21.06.2020]

¹⁵<https://evtol.news/aircraft/nasa-puffin/>, [Accessed 21.06.2020]

¹⁶<https://www.airbus.com/innovation/urban-air-mobility/vehicle-demonstrators/vahana.html>, [Accessed 21.06.2020]

¹⁷https://en.wikipedia.org/wiki/Lilium_Jet, [Accessed 21.06.2020]

Table 3.2: SWOT-analysis

Our business (intern)	Market/Environment (extern)
<p>Strengths:</p> <ul style="list-style-type: none"> • Good reputation as TU Delft graduates • Product offers comfort and privacy • Good investor present • Team is young and highly motivated • Soon many design methods will be protected by patents 	<p>Opportunities:</p> <ul style="list-style-type: none"> • No very similar product existing yet • Climate change boosts need for sustainable mobility • Traffic congestion issues in cities increase need for aerial mobility • Positive change in regulations that allow for more applications of the aircraft (flying into cities, flying in bad visibility conditions (with automation systems)) • Aircraft has the potential to be a substitute for cars
<p>Weaknesses:</p> <ul style="list-style-type: none"> • Start from 'zero', no existing business yet, no machines, no shop floor • very high start-up costs: high market entry barrier • No profit in first years/decades • Team has no or little experience in the industry • The team is still too small and has too little time to fully complete the design of the aircraft • All members have same background (e.g. no marketing knowledge, however it is needed) 	<p>Threats:</p> <ul style="list-style-type: none"> • Increasing digital working/home office: no need to commute to work • Regulations don't (sufficiently) change • No/little acceptance in society (noise, disturbance, privacy concerns (flying over gardens/houses), safety concerns (crashing into urban areas)) • Shortage in bio fuels • Competitor develops similar product • Downturn in economy reduces sales

3.5. Future Market Development

Once a product enters the market its life-cycle on the market starts. This can be divided into 4 phases, which are introduction, growth, maturity and decline. These phases will be described in more detail in the following.

1. **Introduction: Introduction to market without extra infrastructure** After finishing the development, the certification and the set-up of the series production the first aircraft can be produced and delivered to the customers. This marks the time of entering the market. At this time the product is not yet well known in the public and in the legislative. Therefore it is unlikely that until then it was possible to have an impact on the regulations to drastically change them. Thus the product must fully comply with the current regulations. In the first phase, the Cestrel can be used comparable to a helicopter. This means it is allowed to land everywhere where local restrictions do not prohibit that and where the necessary space is available. Many cities (e.g. London, New York) however do have restrictions which limits the use of the aircraft. In less densely populated areas, - for instance - the back yard of the customers country house could be an appropriate landing spot. The customer of this phase is more of a pioneer since the infrastructure is not yet present to make good use of the product. Those pioneers believe in the product and its capability to provide a sustainable but flexible mobility. The market share will be rather small in the beginning, since only a few sold units are sold so far. The main goal of the introduction phase is to gain attention in media and society. Hence promotion and marketing for the product are important to build up a demand for the product. This should already start before the Cestrel is produced in series by showing prototypes on exhibitions, by inviting journalists on test flights etc.. Additionally, once there are multiple units of the Cestrel flying around, this will be a form of marketing as well.
- 2a. **Growth: Hubs around city become available for landing** If the product is perceived well in public it will enter the phase of growth in which the number of sales starts to increase. This implies that also more people will make their pilots licence in order to be allowed to fly the Cestrel. Parallel to that, an infrastructure must established to handle the increasing traffic. As it was explained in the Baseline Report [6] hubs at the edge of the city need to be build and need to be connected to public transport and road network. These hubs are a compromise between the individual traffic, which is demanded by many customers, and the more efficient mass transport. The connection to the public transport will keep the individual traffic outside of the city which reduces the pollution by noise and emissions in the cities and it avoids that too many personal aircraft are parked inside the city where space is already a rare commodity. At the same time the major part of the journey is done in the personal aircraft which increases flexibility and reduces travel time. While this infrastructure develops, more and more customers are appealed by the advantages of the product and the sales increase. Also the modular

¹⁷https://www.abta.at/wp-content/uploads/2012/12/Gesch%C3%A4ftsreise-Analyse-final_V5.pdf [Accessed: 29.06.2020]

design will slowly start to pay off if damaged parts need to be repaired. The Circular Economy effects itself are not that relevant yet since the fleet of aircraft is still very young and none of them has reached its regular end of life-time. If the European market starts to grow successfully the introduction to the US market can slowly start. This would require a reassessment of the development to check if design adjustments are needed to comply with FAA regulations.

- 2b. **Growth: Regulations adapt and landing on streets and in cities becomes possible and legal** Still in the growth phase, the product starts to be widely accepted as a new means of transport. This will put pressure on the legislative to start to adapt the regulations to allow the product to deploy more of its capabilities. This includes flying over cities and landing in them (probably on top of buildings). That however will come at an increased cost for the operator since the space in the city is limited. The hubs at the edge of the city will remain for the mass traffic. This is comparable to the road traffic: one either drives the car into the city (expensive) or one uses park&ride-offers (cheaper). To only allow part of the traffic into the city, new regulations are needed that prescribe smart routes to reduce emission and noise pollution in the cities. Also more resources should be put into developing noise reduction methods for the Cestrel. Another favourable change in the regulations would be to allow the implementation of autonomous flight controls and the abolition of the duty to have a pilots license if these autonomous flight controls are present. This would give more people access to flying this aircraft. With the adapted regulations the product has the capability to develop to a mass means of transport which boosts the sales. Also the break-even point should be reached during this phase. If the market launch in the US is also successful other markets in Asia, Australia etc. can be captured as well. Especially Dubai and Singapore appear to be suitable cities for a market launch in Asia due to their open-minded policy towards novel technologies.
3. **Maturity** In the phase of the maturity the market is (almost) saturated. The marketing should aim at fending off competition. To sustain the business, altered products need to be developed to reach different market segments. For instance a two or more person aircraft was already addressed in the Baseline Report [6]. New models should be developed that use new technologies which will be available by then. New energy storage methods that allow for fully electric flight while being easily recyclable or models which are tailored to carriage of freight can be considered. Also models with increased or decreased range and endurance can be researched depending on the performance of the Cestrel on the market. If the Cestrel is very successful in the long-term future the expected sales volume could be that most of the middle and upper class cars are replaced by a Cestrel. This is quite ambitious though since such a development will take a couple of decades and involves many risks. Also the Cestrel will certainly not have the full market share since other companies are going to join the market already during the growth phase. Also the competition guardians will not allow the Cestrel being a monopoly on the market and will take actions against it.
4. **Decline** At some point the sales of the Cestrel will decline. This might be due to multiple reasons. Either the technology is outdated and other models from competitors - or the same company - are simply better. The need for this product could disappear (for instance due to increased home-office which vanishes the need to travel or another means of transportation which offers a better performance than the Cestrel). When the sales of the first model drop it must be analysed for how long it is economically feasible to continue the production. In the end it is time to phase the model out and to finally stop its production. This means that slowly all existing aircraft of this model will reach their end of life and cannot be fed back into production of the same aircraft anymore. To remain sustainable it must be investigated how the components of this phased-out model can be recycled or reused in the new models. A trade-off is needed to assess the advantages and disadvantages of reusing old components and implementing more efficient new components which were produced using new technologies and materials.

The plans described in the four phases are quite ideal. In reality many things will change unexpectedly and not everything will work out as it was planned. The ability to quickly react and to adapt to changes and new circumstances is what defines a good and economically sustainable company. When building up the company that is supposed to produce the Cestrel huge emphasis should be put on the agility and flexibility. This is particularly important for disruptive business-models, which the Cestrel surely has the potential to be.

Resource Allocation

This chapter focuses on the resources which are to be used for different areas of the design. These include the general sizing of the aircraft in [section 4.1](#), the general resource allocation in [section 4.2](#), and lastly the iteration logic for the process in [section 4.3](#).

4.1. Preliminary sizing

Mass

Before the design of subsystems can start, some preliminary sizing is made and resources are allocated to the subsystems. The MTOW of the aircraft was estimated in the Midterm Report to be 1,480 kg [7]. This is taken as the maximum MTOW that the aircraft should have, and it is considered necessary to leave tolerance for the weight of the aircraft to increase due to unexpected mass increments throughout the design process [13]. Therefore using a contingency or tolerance of 25%, the MTOW that will be designed for becomes 1,180 kg [7].

Power

Here it must be noted that the power estimation made in the Baseline Report [6] is not exactly applicable to the design, because the reference vehicles used for the futuristic category are purely electric and do not fit under tilt rotor category. The first estimation for power consumption is made according to the calculations explained later in [chapter 8](#), which is based on the book on Helicopter Theory by Johnson [25]. In the calculations the power coming from hovering and vertical climb is taken into account, which is assumed to lead to the maximum power use. For the first estimate it is assumed that all 4 proprotors have the same dimensions, all having a 1m radius. The VTOL thrust is assumed to be equal to the take-off weight, and the thrust to be equally divided over the 4 proprotors. Based on requirement **DSE-22-SYS-P-06** a climb speed of 5 m/s is used as the first value. The found maximum power needed is 420kW. This value also has uncertainty, which will be discussed in [chapter 8](#).

Wing sizing

Next, the actual size of the wing can also be determined. The wing sizing is critical for the stall speed that the aircraft needs to adhere to according to the CS-23 requirements [32], which is 31 m/s. The weight over surface area ratio (or wing loading W/S) can be calculated using [Equation 4.1](#). The maximum clean lift coefficient ($C_{L_{max_{clean}}}$) refers to the one of the main wing without any deployed high lift devices. The wing loading of the aircraft is then converted to a main wing surface area using the estimated mass of the aircraft. The air density at 3,048 m (maximum cruise altitude) was taken as it would result in a lower wing loading ratio, which results in a bigger main wing surface area.

For the first calculations, it was assumed that the main wing generated all the lift to keep the aircraft in the air. This resulted in a surface area of 10.22 m². The span of the main wing is limited to 9 meters according to the requirement **DSE-22-SYS-AC-03**. However, it was decided to position the proprotors of 1 meter at the wingtips. This means that the span of the aircraft's main wing is limited to 7 m. This results in a chord of 1.7 m for the main wing.

However, after many iterations, the mass of the aircraft got significantly reduced. In addition, the canard configuration means that the canard surface will also produce positive lift. This means that the main wing is no longer fully responsible for creating all the lift to keep the aircraft in the air. These changes mean that the main wing surface size could be drastically reduced. This was also beneficial for the propulsion system as the rotor radius could be increased, to increase the propulsive efficiency and to limit the noise. The span of the aircraft was now set at 6 m. The maximum clean lift coefficient was also iterated many times, which is more clearly explained in [section 9.4](#), ultimately the value of 1.4 was used.

Because of the low mach number that the aircraft cruises at, $M = 0.186$, the geometry of the main wing can stay simple. This is why a simple rectangular wing was selected for the main wing. It was decided that no sweep is necessary, as this only starts to become useful in the event of cruising at trans-sonic mach numbers. The final wing size and dimensions are described in [Table 4.1](#).

$$\frac{W}{S} = 0.5\rho V_{cruise}^2 C_{L_{max_{clean}}} \quad (4.1)$$

Table 4.1: The dimensions of the main wing

Surface area (S) [m ²]	Span (b) [m]	Chord (c) [m]
9	6	1.5

Table 4.2: Preliminary resource allocation

Subsystem	Component	Mass [kg]	Power [kW]	Cost [Euro]
Structure		261	-	?
	Wing	90	-	?
	Fuselage	108	-	?
	Tail	27	-	?
	Landing gear	36	-	?
Propulsion		554	420	?
	Electric motors	136 ¹	powers rotors	51,040 ²
	Gas turbine	91 ³	generates power	?
	Batteries	147	power storage	?
	Rotor	135	420 ⁴	?
	Fuel system (excl. fuel)	45	-	?
Other		85	1	?
	Avionics	45	1 ⁵	20,000 ⁶
	Instruments	9	-	?
	Other	31	?	?
Payload		150	-	-
Fuel		130⁷	-	-
Total		1180	421	412.500

4.2. Resource allocation

The total mass is divided to different subsystems, taking into account structures, the propulsion system, and components, such as avionics and flight instruments. All mass assumptions for the components are based on fractions found in [26], unless otherwise specified within Table 4.2. The power is calculated from the need to rotate the propellers in vertical flight mode while climbing. The micro gas turbine is used to generate power, batteries for energy storage, and the electric motors to power the propellers. The losses in the power system are not considered yet, but these will add uncertainty. Another component that needs power is the avionics. The total cost was estimated to 412,500 euros in the Baseline Report [6]. This estimation is still used, although the design does not correspond exactly to the reference aircraft. The cost has the most uncertainty out of the three parameters that are considered. A price for the electric motors and avionics is found from off-the-shelf products. In Table 4.2 the resource allocation of mass, power and cost is shown. A '-' is used, when the parameter is not applicable to the component. A '?' is used when no estimation could be made for the component.

4.3. Iteration logic

The design will be subjected to many iterations in the order depicted in Figure 4.1. The first step, mass estimation, is obtained from the Class I weight estimation [7], as discussed in section 4.1. The second step, wing sizing, is also discussed in section 4.1.

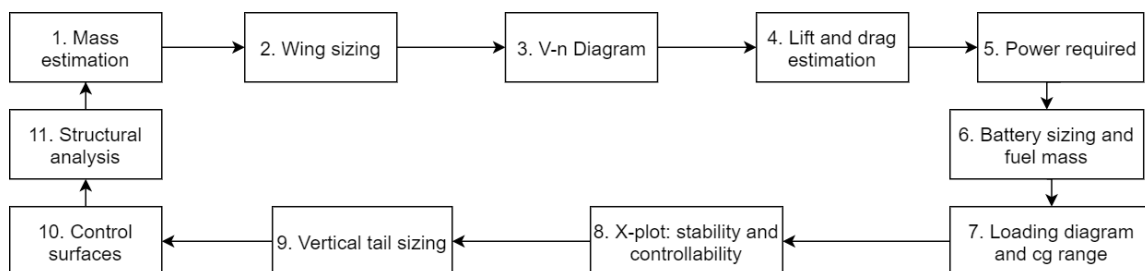


Figure 4.1: Iteration logic

¹Based on off-the-shelf product. <https://www.mgm-compro.com/products/50-80kw-electric-motors/> [Accessed 21.06.2020]

²Based on off-the-shelf product. <https://www.mgm-compro.com/products/50-80kw-electric-motors/> [Accessed 21.06.2020]

³Based on off-the-shelf product. <http://www.hkmmotors.com/en/Industrial/car.aspx> [Accessed 21.06.2020]

⁴First estimate of max power consumption.

⁵Based on off-the-shelf product. <https://www.intelligent-aerospace.com/commercial/article/16539709/fanless-800watt-power-supply-for-avionics-aerospace-military-and-missile-applications-introduced-by-gaia> [Accessed 21.06.2020]

⁶Based on off-the-shelf product. <https://www.flyingmag.com/story/avionics/avionics-retrofits/> [Accessed 21.06.2020]

⁷From Midterm Report.

Functional Diagrams

This chapter shows the revision of the Functional Flow Diagram (FFD) in [section 5.1](#) and the Functional Breakdown Structure (FBS) in [section 5.2](#). Both diagrams will show the functions the system has to perform with their unique identifier F#.

5.1. Functional Flow Diagram FFD

The FFD was revised from the previous version that was presented in the Baseline report [6]. The diagram is split into three main phases: production of the air transportation capability, the operation of the air transportation capability and the retirement of the air transportation capability. The first level phases are colour coded and the colour scheme is used in the different levels. The revision of the FFD was needed as a lot more is now known about the personal aircraft design: the tilt proprotor. The FFD was adjusted to fit the operational profile of the tilt proprotor.

The FFD was split in two pages. This is because a fourth level was added. The levels 1 to 3 of the FFD can be found in [Figure 5.1](#). Level 4 of the FFD can be seen in [Figure 5.2](#). The asterisk symbol at the top of a block means the block itself is expanded in a deeper level.

A separate FFD was made for the emergency procedures that will identified in [subsection 16.4.5](#). This was done to keep the nominal operational procedure separate from the emergency procedures. The emergency procedures FFD is presented in [Figure 5.3](#).

5.2. Functional Breakdown Structure FBS

In [Figure 5.4](#), the revised FBS is shown. As can be seen, the FBS is now expanded to a fifth level. It goes one level deeper than the FFD. The expansions that have not been mentioned in the FFD can be seen as listed items which are not presented in blocks. These items could be either level 4 or 5 items. The items that are not presented in blocks are not in the FFD as they were considered too detailed for the FFD or they did not add to the flow of the FFD. The level 4 items are still indicated using a four-decimal number, the level 5 items are indicated using letters in alphabetical order. In this diagram the same colour code is used as in the FFD, depicting the first level phases of the mission.

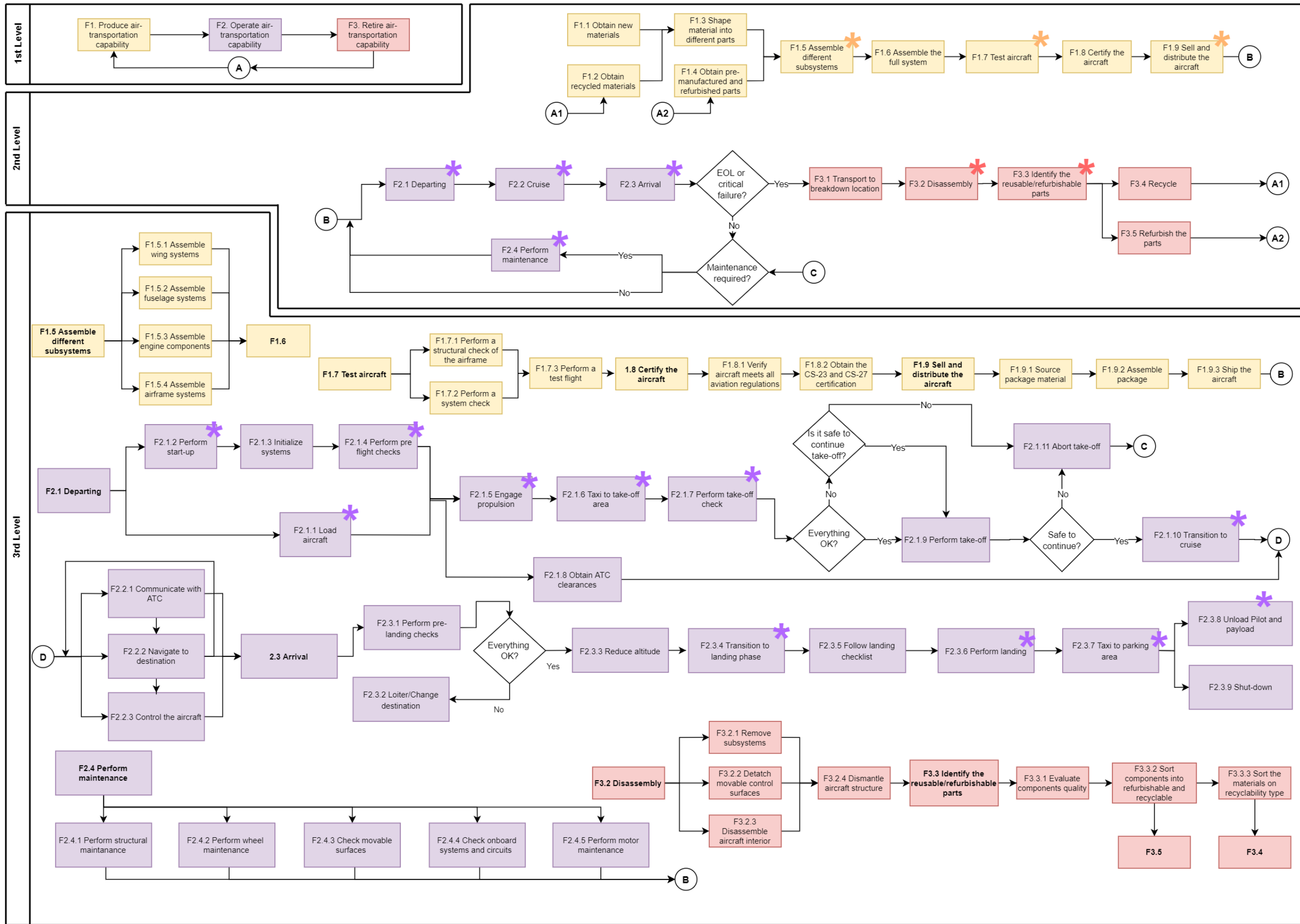


Figure 5.1: Functional flow diagram with the levels 1 to 3.

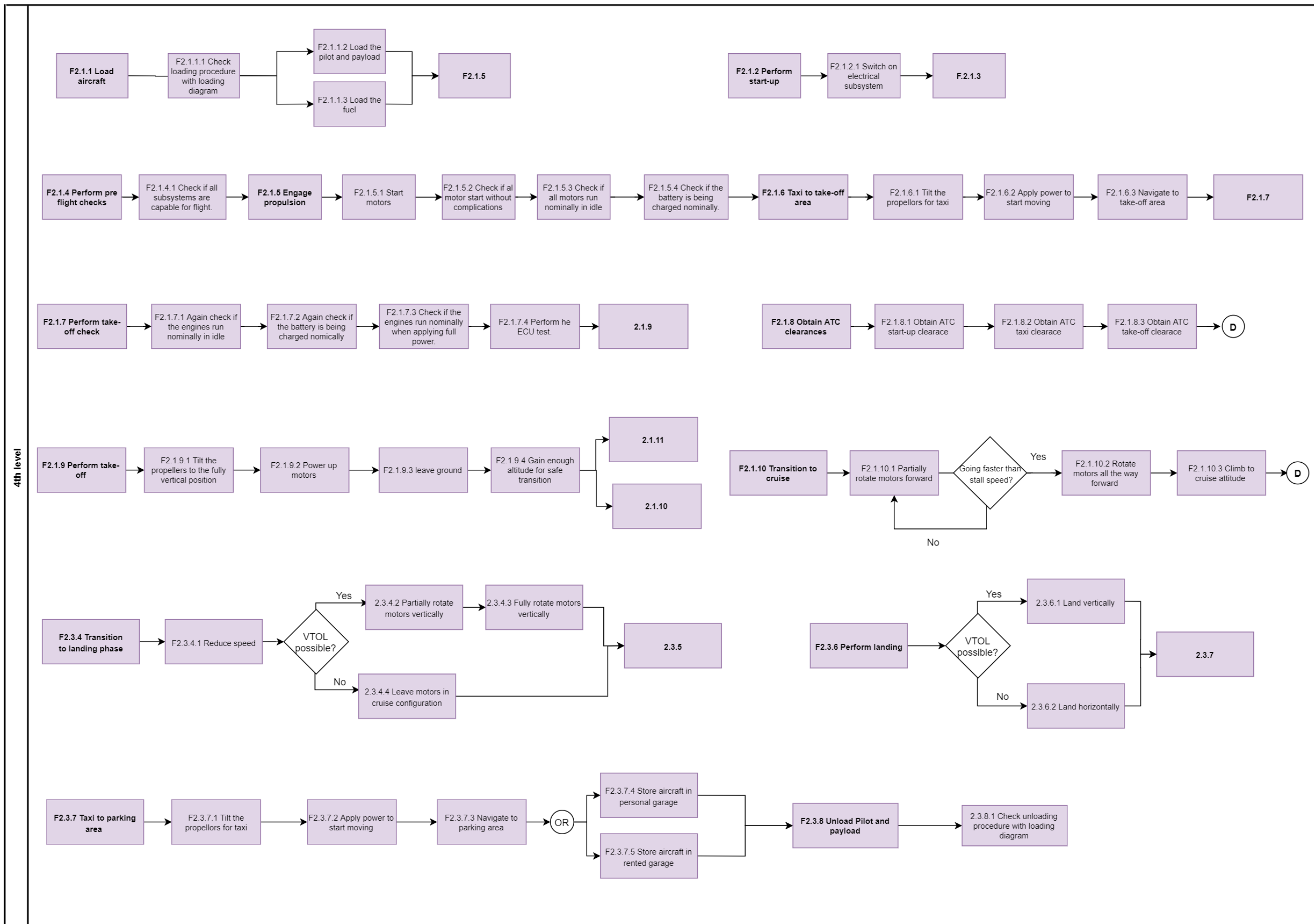


Figure 5.2: Level 4 of the FFD

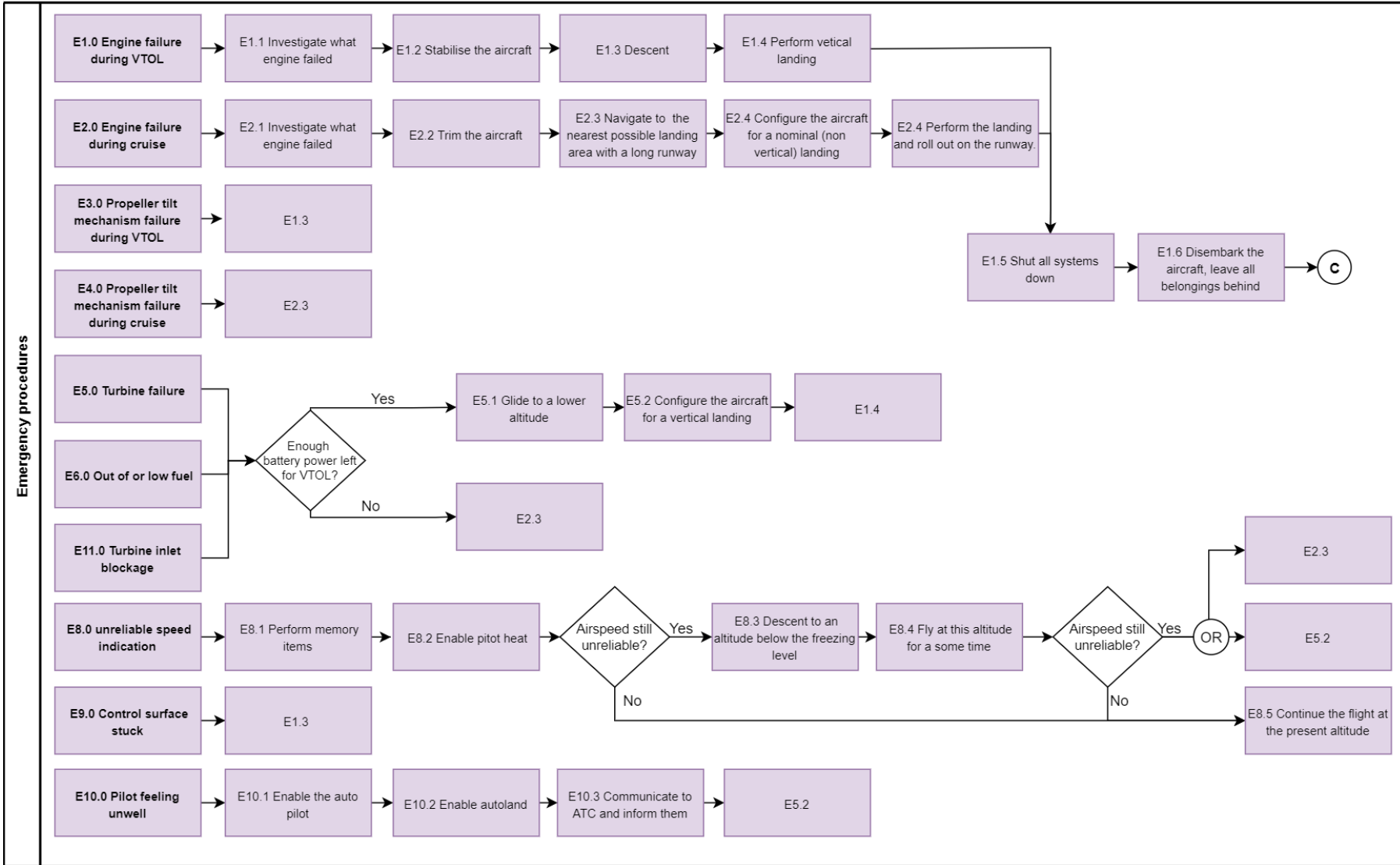


Figure 5.3: The emergency procedures FFD.

DSE Project 22: Fly myself into the future

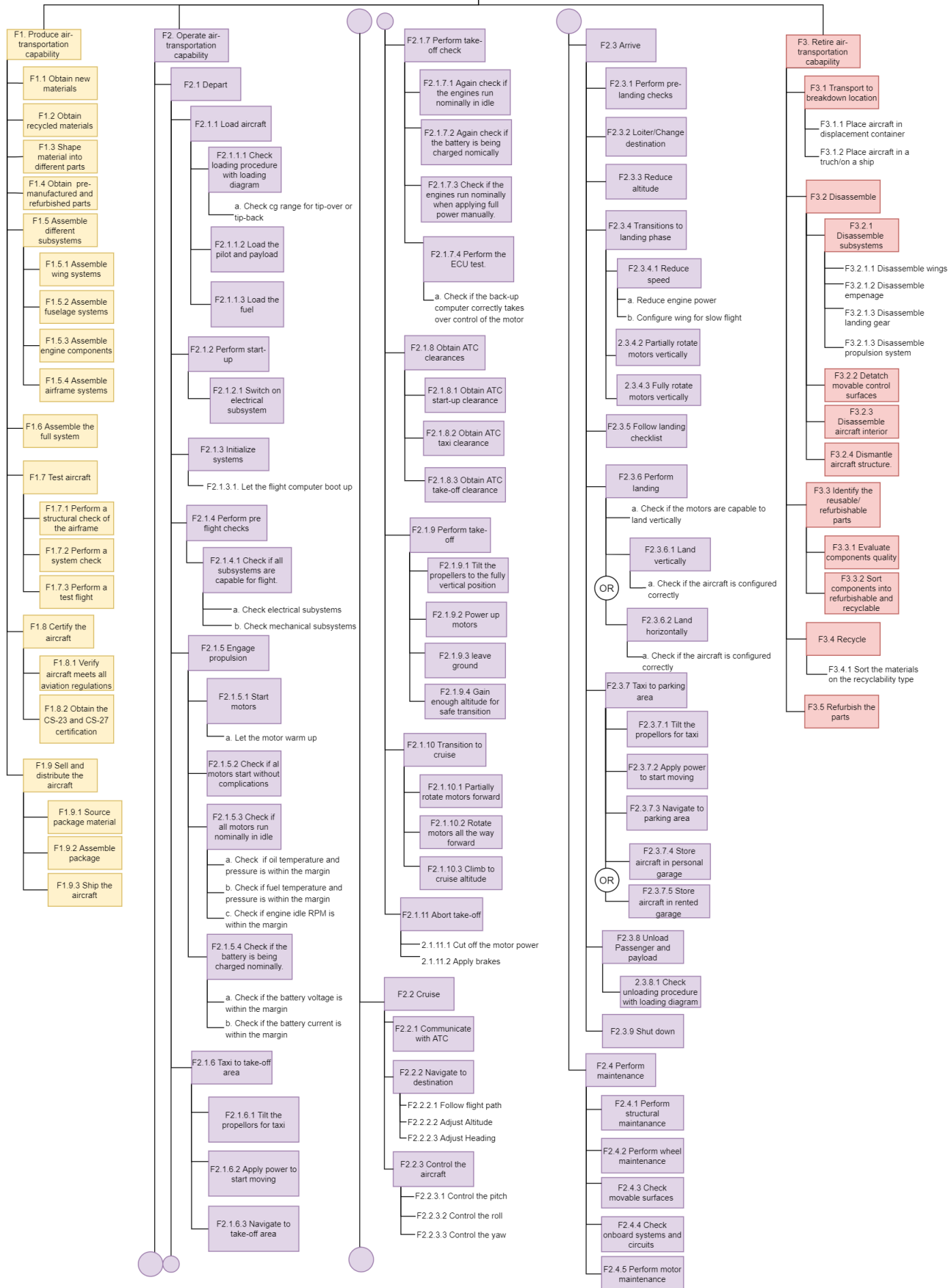


Figure 5.4: Functional Breakdown Structure

6

Configuration and Layout

This chapter will discuss the configuration and layout chosen for this aircraft in order to perform the mission required. It first starts with the functional analysis in [section 6.1](#), then the requirements analysis in [section 6.2](#). It then discusses the aircraft configuration and layout in [section 6.3](#). That is then followed by the electrical block diagram in [section 6.4](#), and after this, the hardware and software block diagrams of the aircraft are explained in [section 6.5](#). Finally, the data handling block diagram is shown in [section 6.6](#).

6.1. Functional analysis

By looking at the functional breakdown structure, the configuration and the layout of the aircraft should be chosen such that the following functions can be performed properly:

- ✈ F2.4: "Perform maintenance":
Configuration and layout should allow for easy maintainability of the aircraft.
- ✈ F2.1.1: "Load aircraft":
It should allow for loading and unloading the aircraft by customers during its lifetime.
- ✈ F2.1.10: "Transition to cruise":
Since it is a tilt-proprotor aircraft, the configuration should allow for transition from VTOL to horizontal flight mode.

6.2. Requirement analysis

During the design process, some requirements has to be taken into consideration while choosing the configuration of the aircraft:

- ✈ **DSE-22-STAK-02:** The aircraft shall comply with the current safety and reliability requirements [3].
- ✈ **DSE-22-STAK-03:** The aircraft shall have a capacity of one person [6].
- ✈ **DSE-22-SYS-P-03:** The aircraft shall have take-off and landing distance within 50m [6].
- ✈ **DSE-22-SYS-AC-04:** The aircraft shall be able to accommodate pilots between 153.5cm and 185.5cm height [6].
- ✈ **DSE-22-SYS-P-07:** The aircraft shall have a minimum cruise speed of 160 km/h [6].

The mentioned requirements have a great influence on the configuration of the aircraft. That is why requirements will be taken into account for the configuration of the aircraft.

6.3. Aircraft configuration and layout

The design solution that was chosen for meeting all the requirements is a one person vertical take-off aircraft that is capable of a horizontal cruise of 220 km/h. To accommodate this, a tilting proprotor is attached to each wingtip. This decision is based on a trade-off in the midterm report [7]. The aircraft has a canard configuration, making both horizontal surfaces load carrying. The proprotors will be oriented upwards at take-off, making the aircraft function like a quadrotor, which is capable of vertical flight. After taking off, the proprotors will start to tilt forward and the aircraft will start to accelerate horizontally. This will gradually continue until the airframe produces enough lift for horizontal flight and the proprotors are completely tilted horizontal. A visual representation of the aircraft in vertical flight mode can be seen in [Figure 6.1](#). In transition the aircraft looks like [Figure 6.2](#). In [Figure 6.3](#) the aircraft is shown in horizontal flight mode. The aircraft will be powered by 4 electric motors in the 4 rotating wingtip pods. These motors will be powered by a hybrid system consisting of a lithium ion battery and a turbine range extender. The battery will be used during vertical flight mode as this flight mode has a very high power demand. The turbine range extender will provide the power during cruise. The residual power during cruise can be used to re-charge the battery. When the aircraft has landed it can also refuel its batteries using a power grid at the airport making it a plug-in hybrid power system.

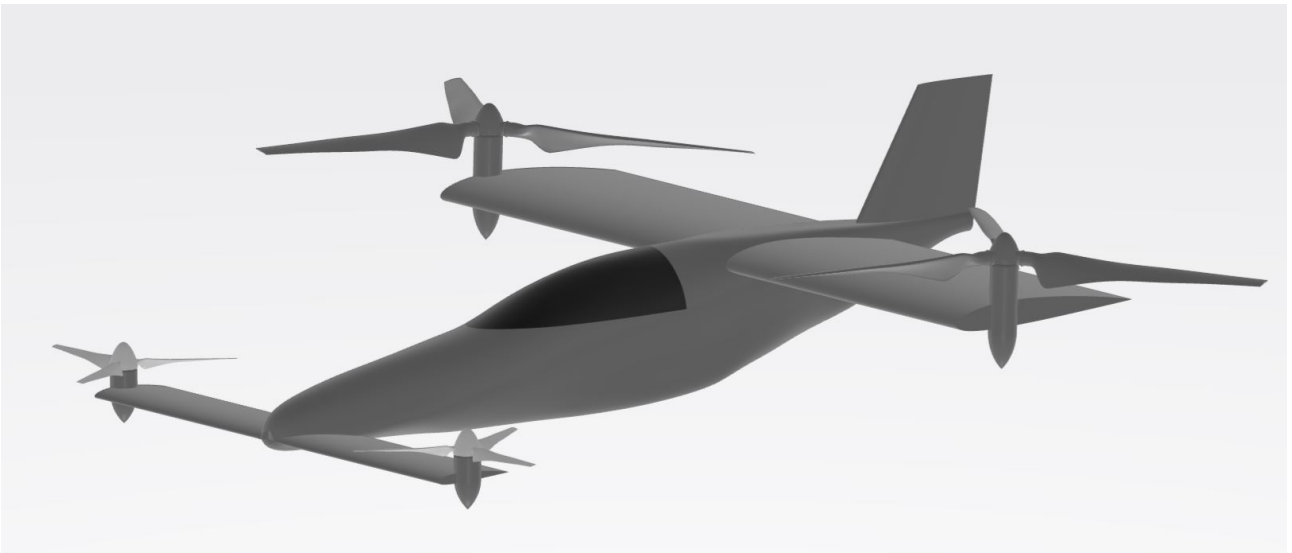


Figure 6.1: Aircraft in Vertical Flight Mode

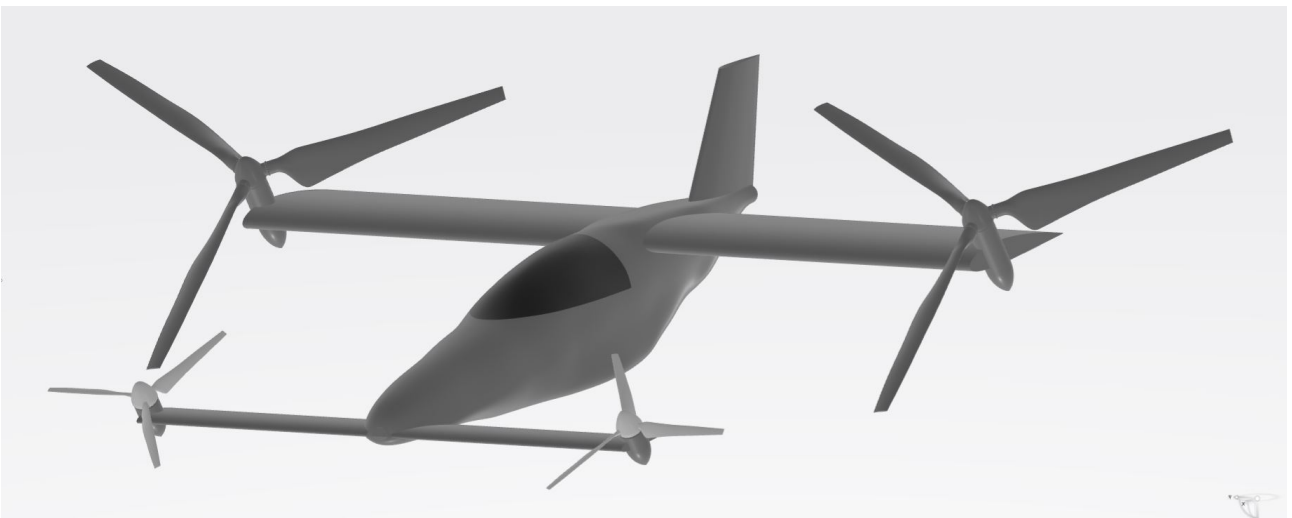


Figure 6.2: Aircraft in Transitional Flight Mode

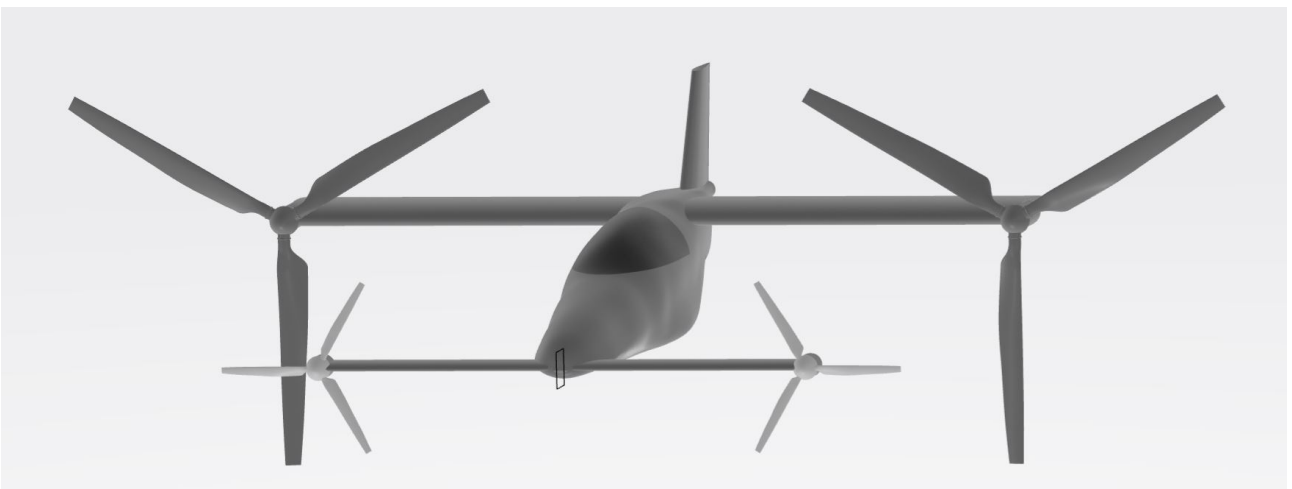


Figure 6.3: Aircraft in Horizontal Flight Mode

The layout of all the subsystems in the aircraft is determined to get the centre of gravity of the empty aircraft at the location that was determined in the aerodynamic sizing ([chapter 9](#)). The range extender is positioned behind the

cabin underneath the wing. The batteries are in the nose to shift the centre of gravity forward. The cabin will be close to a cockpit you find in a glider aircraft. The fuel tank is not positioned in the wings but behind the pilot. This makes the shift in centre of gravity minimal while draining the tank in flight. All these components and the attachment points of the main wing and the canard, are shown in [Figure 6.4](#).

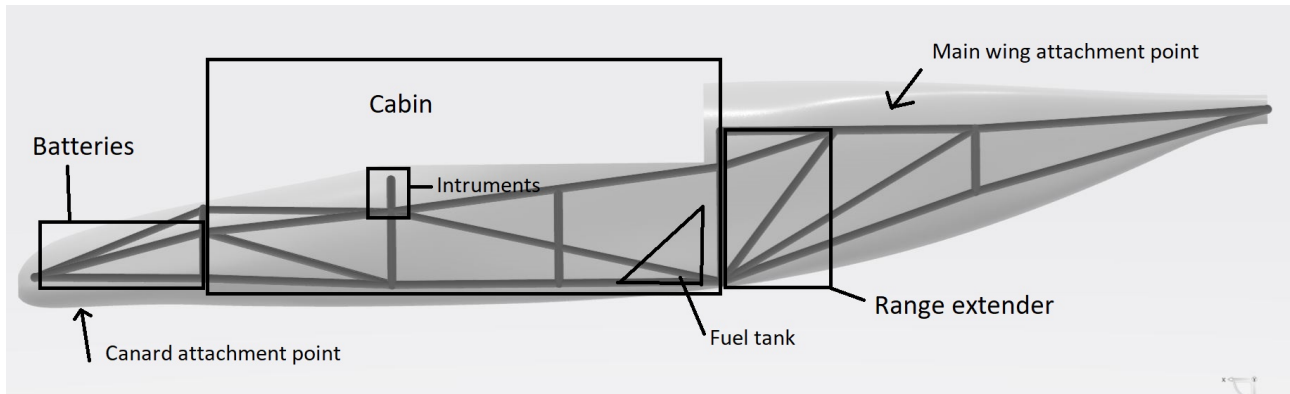


Figure 6.4: Aircraft layout

6.4. Electric Block Diagram

In [Figure 6.5](#) the electric block diagram is shown. This diagram shows all electric components and its connections as found in the tilt proprotor aircraft. The thick lines indicate high voltage connections. These are used to directly power the motor controllers from the battery. These lines carry the bulk of the power. That is why the battery bus voltage will be chosen to match the motor controller input voltage. No conversion will be necessary in these power connections thus reducing any conversion losses. This also means that the battery voltage needs to be stepped down before it can be connected to the other aircraft systems. The DC/DC converter will take care of this. After this conversion, the thin lines indicate the low voltage power going to the other electric hardware in the aircraft.

The dashed lines indicate an alternating current. This for example comes out of the range extender due to its rotational generator. This AC signal is then converted to a DC signal by the rectifier containing a diode bridge and some filtering. This DC power can be used to either charge the battery or power the motors directly. The selection of input power for the motors happens in the input selector. This will be draining the battery during hover and will be using the range extender during cruise. The yellow lines indicate signal connection and the black lines indicate a power connection.

Each electric motor has a separate motor controller to control the speed and power going into the motor. This controller needs the position of the motor to match the produced waveform. The motors will be three-phase motors, this being the reason why the motor controller output will look like [Figure 6.6](#)¹. The waveform shown in this illustration has to match the orientation of the permanent magnets in the middle, otherwise the input signal could be braking the motor if the propeller hits a small gust.

The position of the tilting mechanism will be controlled by a mechanical lever with a number of steps. Therefore no tilting mechanism is shown in the electric block diagram. This part of the mechanical control system will be discussed in more detail in [section 6.5](#).

To mitigate the risk of the low voltage circuit going dead, a second backup DC/DC converter is used that is directly connected to the battery. In case anything fails between the battery and the low voltage output of the DC/DC converter, this backup can be switched on which is directly connected to the battery. Another single point of failure in this diagram is the input selector. This component will be operated by the software on board. In case this system fails a manual override switch will be placed inside the cockpit. In case of failure the pilot will be able to manually switch between battery and range extender power. This switch is however left out of the diagram because it is exactly the same as the input selector that is now in the diagram, and adding it would overcrowd the illustration. The only difference is that the manual switch does not have a signal input.

¹How Brushless motor and ESC work, <https://howtomechatronics.com/how-it-works/how-brushless-motor-and-esc-work/> [accessed on 26-06-2020]

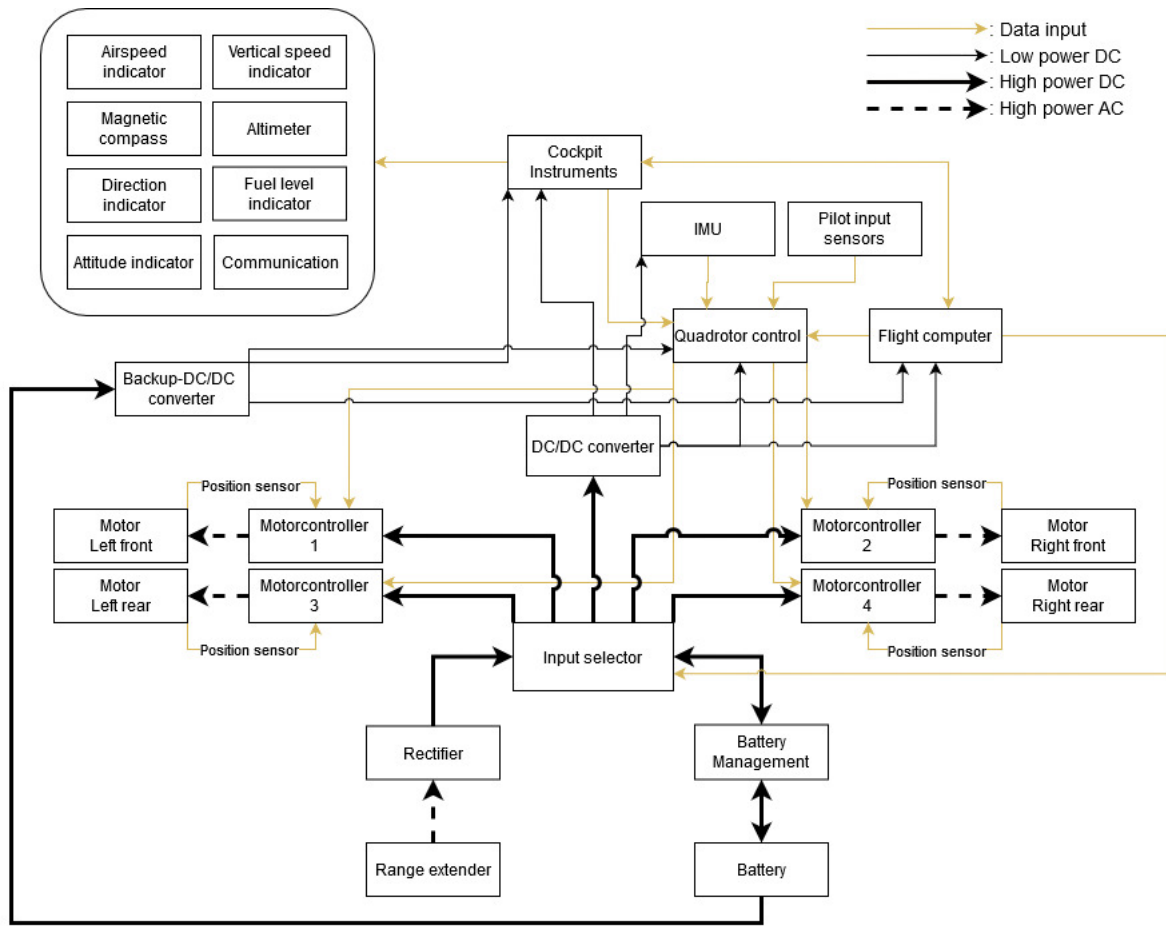


Figure 6.5: Electric block diagram

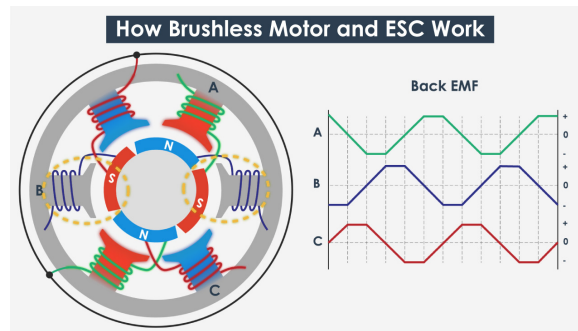


Figure 6.6: Motor controller wave explanation

6.5. Hardware and Software block diagram

The section provides the hardware and software block diagrams to describe the aircraft hardware systems and software systems

6.5.1. Hardware

Two different hardware diagrams are shown in Figure 6.8. The first one indicates the electrical wiring in the aircraft. The arrows indicate the flow of electricity in the aircraft, apart from the blocks software and sensors. The software of the flight computer will be explained in Figure 6.9, and the sensors in Figure 6.10. The electrical system was already shown in more detail in Figure 6.5. In the hardware diagram the converters are not shown, and the power management systems are only indicated by one block, although there are multiple ones, for example one for each motor. The possible future addition of automated fly-by-wire system is indicated in grey. Additionally, for now only mechanical tilting of proprotors is considered, but in the future this could be done by fly-by-wire controls, with the mechanical system left as emergency system. Same goes for the canopy.

In the right diagram of Figure 6.8 the mechanical control is indicated. The main control surfaces are the ailerons, the

elevators and the rudder. Additionally a mechanical lever will be added to open and close the canopy, and to levers to tilt the proprotors. The tilting mechanism is shown separately in the loop below the mechanical control diagram. The lever for tilting the rotors will have angle position locks which will be used by the pilot as an indicator of the angle of the proprotors, and changed manually by the pilot based on the indicated airspeed, similar to flaps setting selection. A visual representation of the lever can be seen in [Figure 6.7](#). Within the figure, the following numbering can be found:

- ✈ 1 - Lever for proprotor tilting
- ✈ 2 - Holes for setting of motor at certain prescribed angles
- ✈ 3 - Retractable pin connected to lever for angle setting selection
- ✈ 4 - Button on lever for pin retraction/lock
- ✈ 5 - Cruise setting (motors in cruise configuration)
- ✈ 6 - VTOL setting (motors in VTOL configuration)

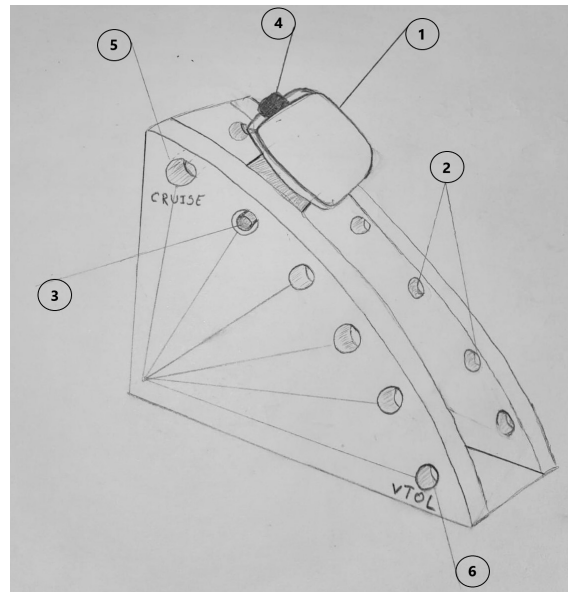


Figure 6.7: Proprotor Tilting Lever

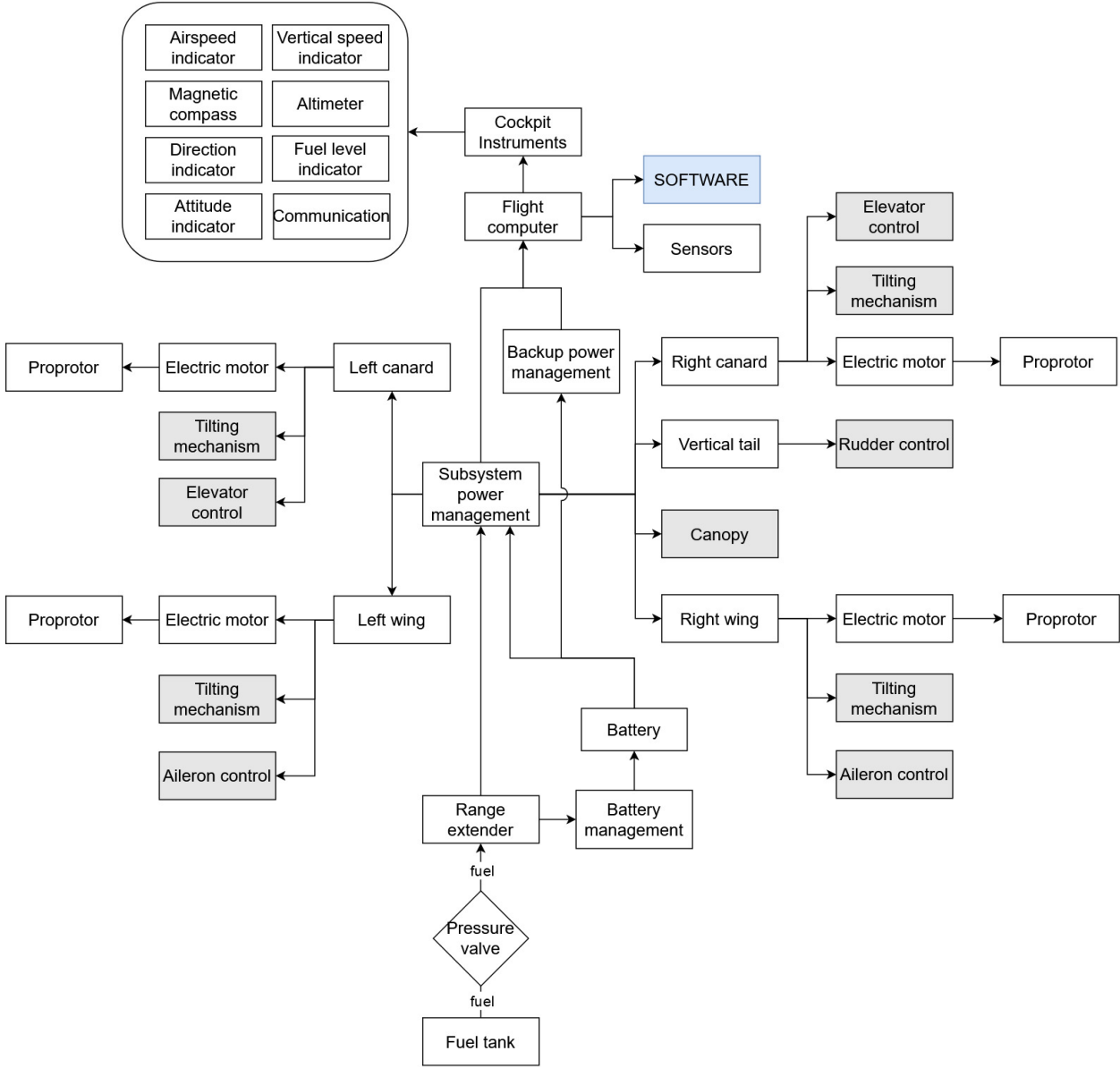
6.5.2. Software

The software diagram as seen in [Figure 6.9](#) presents the required software for the hardware installed on the aircraft. On the right side of the diagram, some blocks have been marked in grey, indicating software that could be used in future models of the aircraft, once more automation is included. This would include an autopilot capable of operating the vehicle almost entirely, making it easier to fly, most probably at the price of a more elevated cost for the advanced models with these additional options. In the diagram, the connection between the blocks indicate as well (where needed) the elements/information which is input/output for the operation.

6.6. Data handling block diagram

The Data handling block diagram in [Figure 6.10](#) shows the data flows within the aircraft. The blocks represent the subsystems in the aircraft. The data flow is defined by the arrow coming out of or going into the block. If it is not clear what output or input a specific subsystem will produce, a grey box is added identifying the different data flows. Most flows of data are sensor data. These are coming from the the different sensors. There are three blocks that will give different outputs. These are the autopilot, electronic control system and the motor controller. These all send commands to the next block. The autopilot will be an optional feature of the aircraft which is not yet worked out. It will give commands on the angle of the rudder, elevator and ailerons. It will receive all system information which it will use to control the aircraft. The electronic control system will control all the servos used by the autopilot system as well as the engine settings during VTOL mode. During VTOL all inputs of the pilot in yaw, pitch and roll need to be converted to engine settings of the 4 electric motors. This translation is done by the electronic control system. The motor controller controls the speed of the motors such that it provides the right input to the motors. At last, the red blocks in the diagram identify the outside information going into the aircraft.

Hardware diagram 1: Electric wiring



Hardware diagram 2: Mechanical control

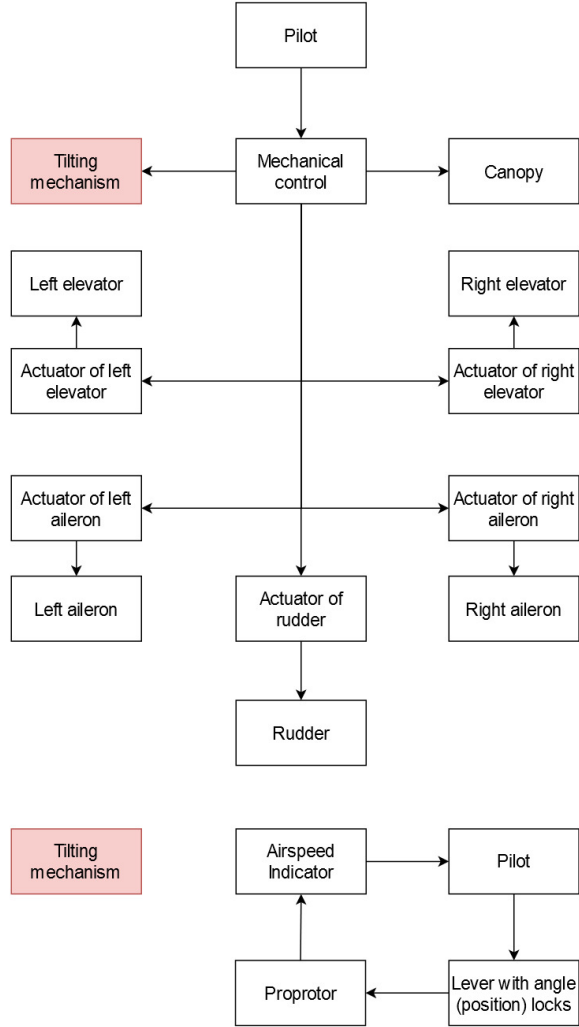


Figure 6.8: Hardware Diagram

Software diagram: VTOL software and future automation

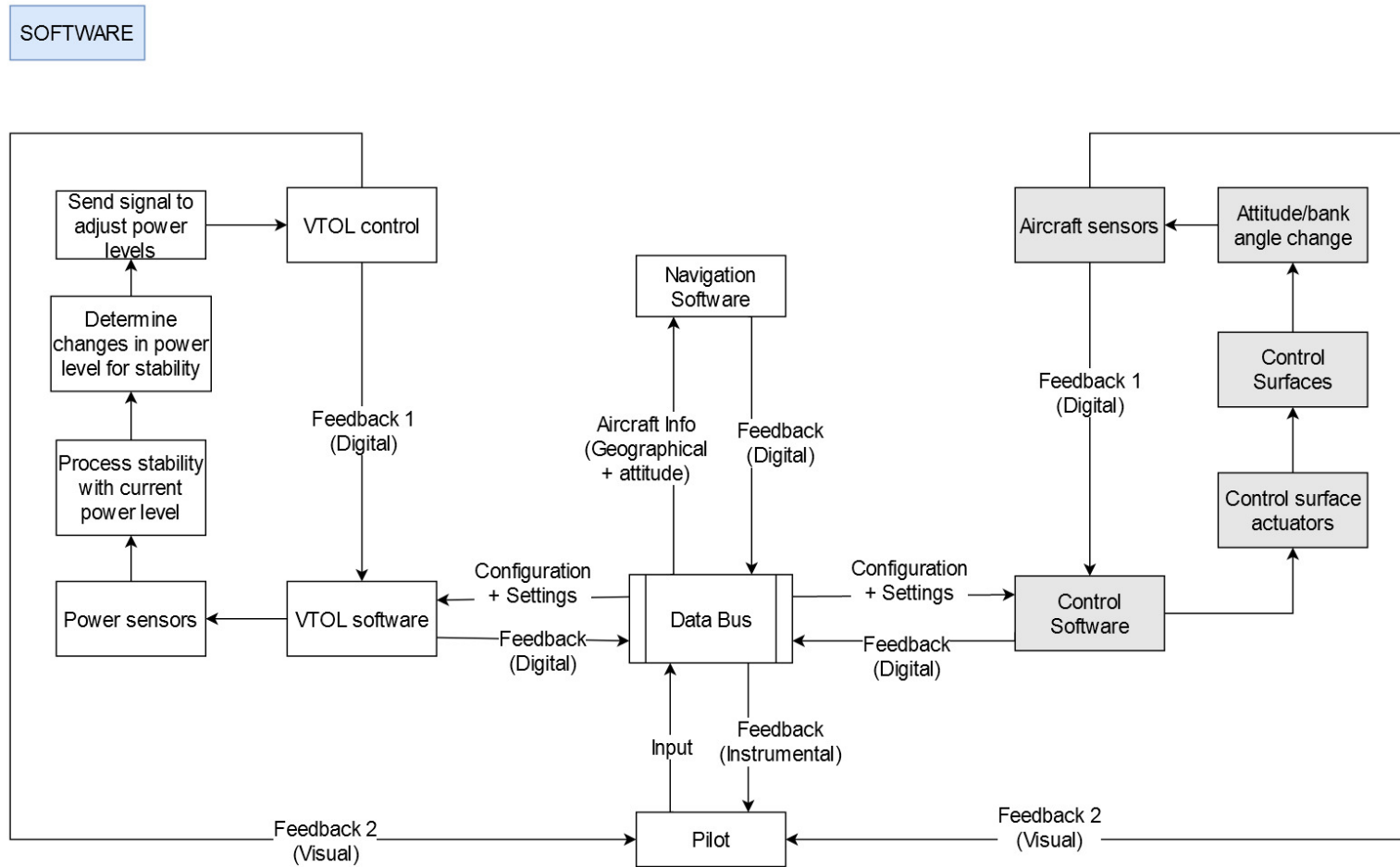


Figure 6.9: Software Diagram

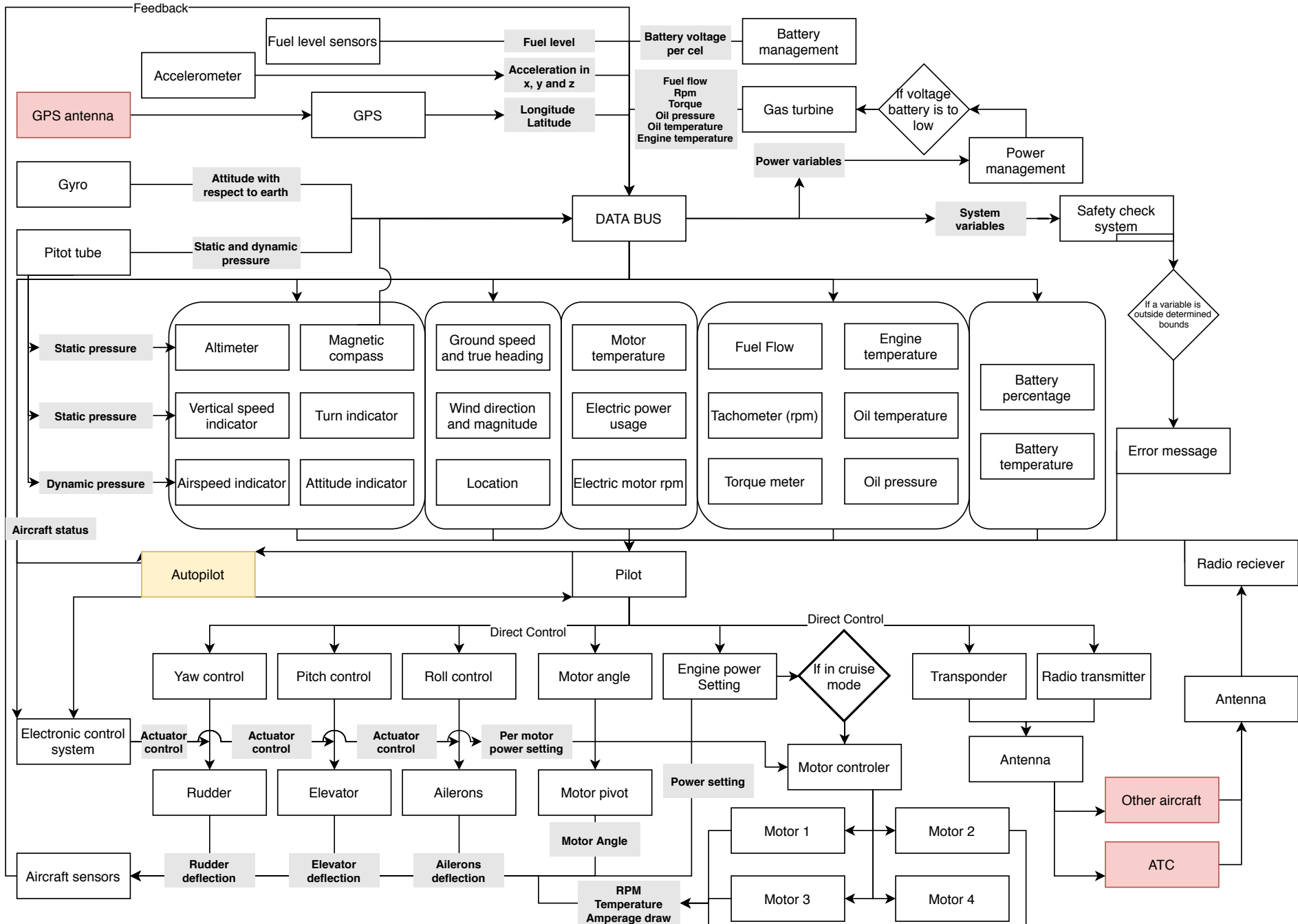


Figure 6.10: Datahandling diagram

Performance

This chapter will describe the performance characteristics of the tilt proprotor design. First the functional analysis is performed in [section 7.1](#), then the requirement analysis in [section 7.2](#). The manoeuvring envelope and gust diagram will be plotted in [section 7.3](#) together with the verification and validation. A revised mission profile is given in [section 7.4](#). Lastly the noise reduction methods will be described in [section 7.5](#).

7.1. Functional Analysis

The aircraft performance should always allow it to perform certain functions. According to [Figure 5.2](#), these functions are:

- ✈ F2.1.9: "Perform take-off":
The aircraft should always be able to perform vertical take-off.
- ✈ F2.3.2: "Loiter/change destination":
In special cases, the aircraft might have to loiter or change the destination, the performance should allow for this.
- ✈ F2.3.3: "Reduce altitude":
Prior to landing or just during cruise, the aircraft should be able to descend.
- ✈ F2.3.4: "Transition to landing phase":
Aircraft should be able to switch from horizontal flight to vertical landing mode by tilting the proprotors.
- ✈ F2.3.6: "Perform landing":
In normal cases, the aircraft has to land vertically, in emergency cases when the tilting mechanism is not working it should be able to land horizontally.

7.2. Requirement Analysis

In order for the aircraft to perform the functions mentioned in the previous section, the following requirements should be met.

- ✈ **DSE-22-STAK-01:** The aircraft shall have performance characteristics such that it is competitive on the market [6].
- ✈ **DSE-22-STAK-02:** The aircraft shall comply with the current safety and reliability requirements [3] [1].
- ✈ **DSE-22-STAK-03:** The aircraft shall have a capacity of one person [6].
- ✈ **DSE-22-SYS-P-01:** The aircraft shall have a range of at least 300 km [6].
- ✈ **DSE-22-SYS-P-02:** The aircraft shall have a minimum endurance of 3 hours [6].
- ✈ **DSE-22-SYS-P-03:** The aircraft shall have take-off and landing distance within 50m [6].
- ✈ **DSE-22-SYS-P-04:** The aircraft shall have a loiter time of minimum 45 minutes [6].
- ✈ **DSE-22-SYS-P-05:** The aircraft shall have a maximum service ceiling of 3048 m [6].
- ✈ **DSE-22-SYS-P-06:** The aircraft shall have a minimum rate of climb of 304.8 meters per minute [6].
- ✈ **DSE-22-SYS-P-07:** The aircraft shall have a minimum cruise speed of 160 km/h [6].
- ✈ **DSE-22-SYS-SR-06:** The aircraft shall only be landed on streets within the operational cross wind limit. (CS-23.333 [3]).
- ✈ **DSE-22-SYS-S-05:** The noise level limitation shall be identical to motor vehicles (82 dB(A)) [6].

All the requirements will be used to determine the flight envelope of the personal aircraft. This will be done in the shape of a V-n and gust load diagram. Lastly, the noise of the aircraft will be looked into using the last mentioned requirement.

7.3. Manoeuvring envelope (V-n) and Gust load diagram

In this section the methodology to come up with the V-n diagram and gust load diagram will be provided for two configurations: the aircraft configuration and VTOL configuration. Both diagrams are shown for an altitude of 10,000 ft (= 3,048m), which is the maximum service ceiling of the aircraft.

7.3.1. Manoeuvring envelope (V-n)

The manoeuvring envelope, shown in Figure 7.1, is a combination of the envelope during the VTOL-phase and the envelope during regular airplane flight. Since the VTOL-phase also includes velocities greater than 0 it can also be considered as conversion-phase (CONV). The diagram shows the outlines of the safe region of operation. When flying the aircraft, one should make sure to stay in the manoeuvring diagram, which poses a restriction on the maximum (positive and negative) load factors the aircraft may encounter for a specific speed. Specialised control systems or cockpit warnings should prevent the pilot from reaching higher load factors.

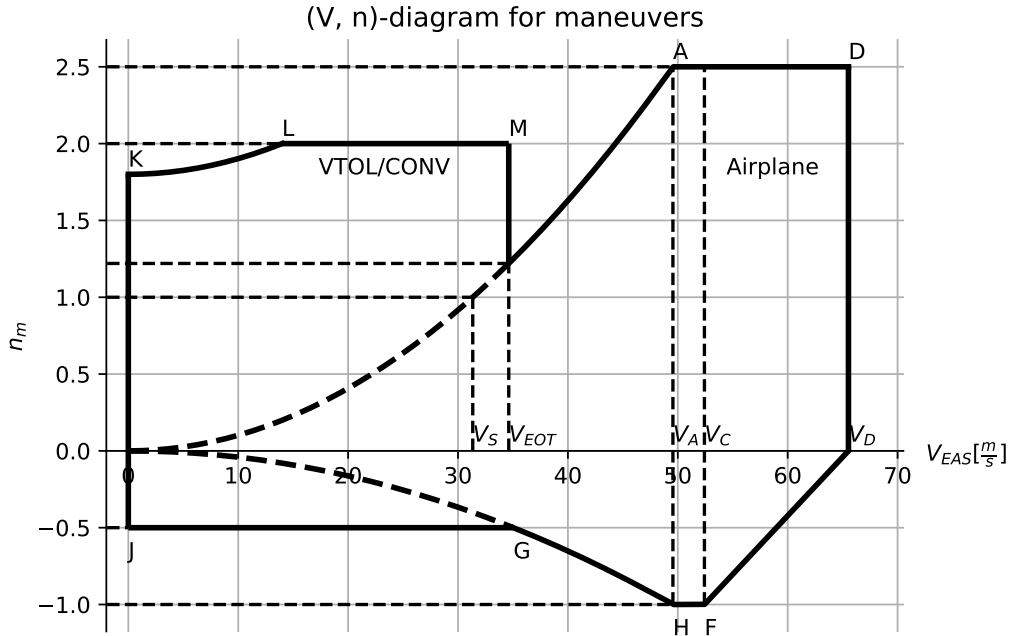


Figure 7.1: Manoeuvring diagram

The manoeuvring envelope for the **normal aircraft configuration** was set up for an upper positive load factor of 2.5 (n_{max}) and a maximum negative load factor of -1 (n_{min}), as was found in CS-23 [3] for the commuter aircraft category. The first step in setting up this diagram is to come up with the definitions and values for the important speeds: Stall speed V_S , Design manoeuvre speed V_A , cruise speed V_C and dive speed V_D . For the formulas in Equation 7.1, 7.2, 7.3 and 7.4, the values seen in Table 7.1 are used.

Table 7.1: Values for formulas ¹

$C_{L_{max}}$ [-]	S [m^2]	m [kg]	h [ft]	ρ_0 [kg/m^3]	$\rho_{@h}$ [kg/m^3]
1.41	9.00	775	10,000	1.225	0.905

Stall speed, V_S was found by setting the weight equal to the lift and re-organising the formula for the speed as seen in Equation 7.1. It should be noted that the density at sea-level (ρ_0) was used in order to achieve the equivalent airspeed.

$$V_S = \sqrt{\frac{2mg}{\rho_0 C_{L_{max}} S}} \quad (7.1)$$

According to the CS-23 regulations [3], V_A , the design manoeuvre speed, should not be less than the multiplication of the computed stall speed with the limit manoeuvring load factor. This is shown as the formula in Equation 7.2.

$$V_A = V_S \sqrt{n_{max}} \quad (7.2)$$

¹ $C_{L_{max}}$, S and m were found when looking at the aerodynamics of the aircraft in chapter 9 and were iterated in the calculations for the performance characteristics as provided in this chapter.

The cruise speed itself was found using iteration. The requirement **DSE-22-SYS-P-07** posed a minimum cruise speed of 160 km/h, however this velocity is close to the stall speed and results in a maximum load factor of only 1.49 during cruise at maximum cruise altitude. This value is unacceptably low, as this would mean almost no manoeuvring could be performed during cruise. Therefore, it was decided to increase the cruise speed to a value such that during cruise all possible allowable load factors defined by CS-23 can be reached. This resulted in a minimum cruise speed of 208 km/h. It was chosen to slightly higher this value to 220 km/h to have a small margin for convenience. This results in updated cruise speed of 61 m/s (true airspeed TAS), which will be used throughout the rest of the calculations and design. One should note that this is however the true cruise speed at maximum cruise altitude of 10,000 ft, which converts to 52.4 m/s of equivalent airspeed using the correction factors as seen in [Equation 7.3](#).

$$V_{CEAS} = V_{CTAS} \sqrt{\frac{\rho}{\rho_0}} \quad (7.3)$$

Lastly, the design dive speed (V_D) equation was also found in the CS-23 regulation [3] and can be found using the formula [Equation 7.4](#).

$$V_D = \frac{V_C}{0.8} \quad (7.4)$$

Filling in the equations with the values found in [Table 7.1](#), the important speed values are found and summarised in [Table 7.2](#).

Table 7.2: Speed values in EAS

V_S [m/s]	V_A [m/s]	V_C [m/s]	V_D [m/s]
31.34	49.56	52.42	65.53

Now that the speed values are determined, the manoeuvre envelope can be plotted. The parabolic line from point 0 to point A is found using the following relation:

$$n = \frac{L}{W} = \frac{C_{L_{max}} 0.5 \rho_0 V^2 S}{mg} = \frac{V^2}{V_S^2} \quad (7.5)$$

A similar relation is used to plot the line from the origin to point H, reaching a load factor of -1 at V_A

$$n = -\frac{V^2}{V_A^2} \quad (7.6)$$

The line from point A to point D is simply horizontal due to the maximum positive load limitations set in the CS-23 regulations [3], the same goes for the horizontal line connecting point H to point E, which is limited to the maximum negative load factor. Lastly, point F and the horizontal axis are connected by a straight line.

Now that the V-n diagram was set up for pure horizontal flight, the manoeuvre envelope in **VTOL-configuration** can be considered. For this CS-27 regulations [1] were followed. Here it is stated that the limit load factor range from a positive 2.0 (n_{max}) to a negative -0.5 (n_{min}) in case the probability of exceeding the values is proven by analysis and flight tests to be very remote. If no proof/explanation can be given higher load factors must be used. The lower limits were considered due to the fact that high loading factors in the VTOL-mode would result in high point loads, pointing in upward direction, at the mountings of the proprotors. This will require a sufficiently strong structure. By decreasing the load factors to the smallest possible values (+2.0 and -0.5) the structure can be lighter which increases the sustainability. The price of this however is that manoeuvres exceeding these load factors are not possible anymore and must be blocked by the flight control system. This price is acceptable since the aircraft is not intended to fly heavy manoeuvres. It is a personal air transportation vehicle that should be operable by a broad range of customers. Since this can include humans that are not in a sporty physical condition, high load factors should be avoided anyway.

Point K is the maximum load factor at $V_{EAS} = 0$ (hovering). This value is the maximum available lift that can be produced by the propellers during VTOL mode. It is assumed to be 1.8, which is the same value as for the V-22 Osprey (see [Figure 7.3](#)). For VTOL the structure is designed for the higher load factor of 2. The lower load factor at lower speeds does not have an impact on the structures design during the conceptual design phase. Therefore it was decided to not go more in depth about the calculation of point K.

By gaining flight velocity the wing starts to provide lift. Thus the possible load factor increases with V_{EAS} . The lift factor is given in [Equation 7.7](#), where L_p is the lift force of the propellers during VTOL. The maximum possible lift

from the wings is produced by flying at $C_{L_{max}}$. This line goes until the load factor reaches the limit load of $n=2$ at point L.

$$n(V) = \frac{L_p + C_{L_{max}} 0.5 \rho_0 V^2 S}{W} \quad (7.7)$$

Then again, the V-n diagram shows a horizontal line between points L and M, from the limiting maximum positive load factor and from J to G from the maximum negative load factor according to the CS-27 regulations [1].

When converting from purely vertical flight mode to horizontal flight, one should slightly rotate the propellers from a 90° angle (vertical) to a 0° angle (horizontal). This results in the thrust vector to be tilted as well, and therefore having both a vertical (upward) and a horizontal (forward) velocity component. The aircraft will lose some of its vertical velocity component, and therefore climb at a lower rate of climb or it will even not climb at all, but it will gain forward velocity. This process should be performed gradually, where both the tilt angle is gradually changed, as well as the delivered thrust to hold the aircraft in the air. The maximum forward speed considered in this transition phase V_{EOT} (EOT= end of transition) is found by determining the end of the transition phase. Full conversion to 0° angle is only safe to perform once the stall speed of the airplane-mode is exceeded, then the lift is such that it can hold the aircraft's weight in the air, and it would be possible to fully rely on horizontal flight mode. However, for safety reasons it was decided to increase this value after the stall limit speed. Otherwise the maximum possible load factor at the end of the conversion-phase would be 1 which is very dangerous since the slightest manoeuvre would cause the aircraft to stall. The speed at which the transition phase can be safely finalised was found by considering the possibility of turning the aircraft into a 35° bank angle in aircraft mode. The corresponding load factor of this bank angle can be found with [Equation 7.8](#) and results in $n=1.22$.

$$n = \frac{1}{\cos\theta} \quad \text{where } \theta \text{ is the bank angle} \quad (7.8)$$

The speed at the load factor $n=1.22$ is determined by [Equation 7.5](#) and found to be 34.62 m/s. Following from that the smallest possible radius at that speed can be calculated using [Equation 7.9](#) as seen in lecture 3 from the flight mechanics course [34].

$$R = \frac{V^2}{g\sqrt{n^2 - 1}} \quad (7.9)$$

This results in a minimum turn radius of 174.82 m which is quite a short turn, ideal for short turns in urban areas. It must be noted that in reality it is not safe to fly that close to stall but this calculation shows that the load factor of 1.22 indeed determines a safe speed to transition fully to airplane mode.

7.3.2. Gust load diagram

The gust load diagram for the **normal aircraft configuration**, shown in [Figure 7.2](#), was again defined using the CS-23 regulation [3]. The gust envelope will show the loads achieved when the aircraft experiences sudden wind gusts during flight. From the regulations the aircraft should be designed to withstand to the following:

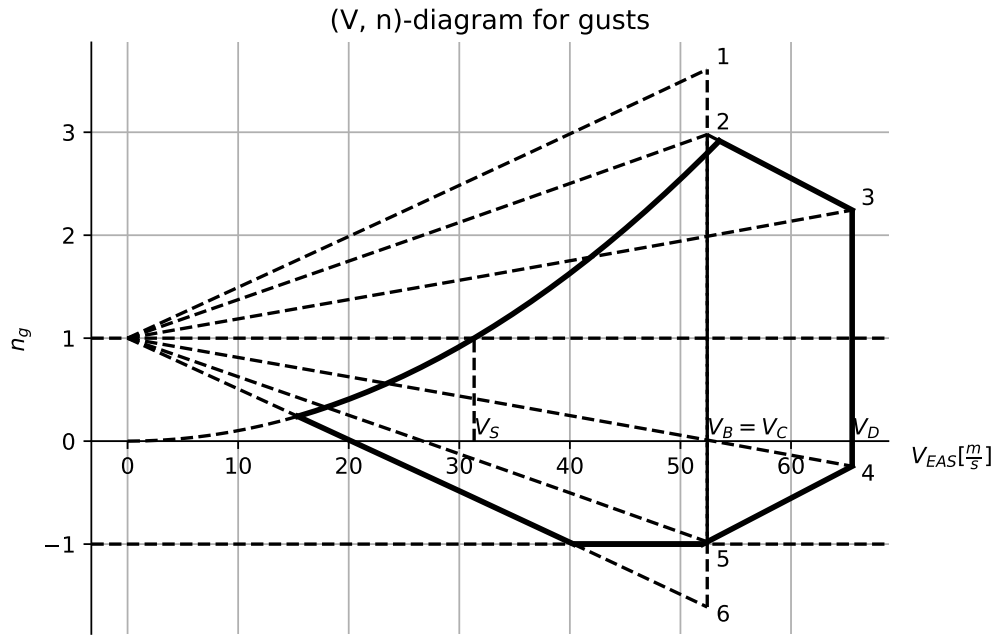


Figure 7.2: Gust diagram

- ✈ Positive (up) and negative (down) gusts of 50 ft/s (=15.24 m/s) at V_C for altitudes between sea level and 6069 m (CS-23.333 [3]).
- ✈ Positive and negative gusts of 25 ft/s (=7.62 m/s) at V_D for altitudes between sea level and 6096 m (CS-23.333 [3]).
- ✈ Positive and negative rough air gusts of 66 ft/s (=20.12 m/s) at V_B for altitudes between sea level and 6096 m (CS-23.333 [3]).

To calculate the gust load factors the method from the CS-23 regulations [3] was followed. The gust load factor is defined as

$$n = 1 \pm \frac{k_g \rho_0 U_{de} V a}{2(W/S)} \quad (7.10)$$

where

$$k_g = \frac{0.88 \mu g}{5.3 + \mu g} = \text{gust alleviation factor} \quad (7.11)$$

and

$$\mu g = \frac{2(W/S)}{\rho \bar{C} a g} = \text{aeroplane mass ratio} \quad (7.12)$$

and U_{de} = derived gust velocities as mentioned above (m/s);

ρ_0 = density of air at sea level (kg/m^3);

ρ = density of the air at altitude considered (kg/m^3);

W/S = wing loading (N/m^2)

\bar{C} = mean geometric chord (m);

g = gravitational acceleration (m/s^2);

V = aircraft equivalent speed (m/s);

a = Aircraft normal force coefficient curve slope. (estimated to be $C_{L\alpha}$ in 1/radians)

The gust diagram for the aircraft shown in Figure 7.2, poses a new, and higher, maximum design load factors on the aircraft. The highest positive load factor is found to be 2.92 at the maximum service ceiling (10,000 ft altitude). This load factor seems to be quite high, however it is only the maximum design load factor the aircraft shall be able to withstand. In real life, the pilot would check the weather forecast and would adapt the mission (change in flight level or circumvent the region) to avoid the high possibilities of strong gusts. The largest negative load for the gust diagram was cut of at -1, due to the fact that the aircraft is built to use as a personal air transportation vehicle and a broad range of customers will operate it, there is no need to design it for more drastic loads. This action was also found in the example flight envelope in CS-23 regulations [3, CS 23.333 (d)] and is therefore considered as a correct measure.

Also in the **VTOL configuration**, gust loads appear, and according to the CS-27 [1] the aircraft should be able to withstand all loads coming from a gust speed of 9.1 m/s. However these will not be considered in the design phase of the aircraft for two main reasons. First, a rotorcraft reaction to gusts is less severe than compared to fixed wing aircraft [12, p.8]. The gust loads however are not insignificant and will become more important when increasing airspeed. [12, p.8] This gives a second reason to disregard them in the design phase: the aircraft will only perform VTOL at lower velocities and will only reach higher velocities in the airplane mode.

7.3.3. Verification and Validation

The verification and validation procedure of the V-n and gust diagram will mainly check whether the correct methods are used and if the plots give the corresponding output.

A first, and very easy test, is to check whether the manoeuvring envelope shows a similar form as a reference tilt-rotor design. For this reference the V-22 Osprey was considered, its flight envelope can be found in Figure 7.3². When comparing the flight envelope in Figure 7.3 with the one for the proprotor design in Figure 7.1, it can be seen that the shapes are very much alike, except for the load factors of the V-22 exceeding the ones for the designed aircraft. This makes sense as the V-22 Osprey is a military aircraft operating at higher loads than a personal air vehicle. On top of that, Figure 7.3 shows the different maximum speed in VTOL configurations as a function of the tilt rotor angle, where in a particular configuration, the same 'cut-out triangle' can be found as seen in Figure 7.1. Even though this triangle poses some constraints on the maximum operable load factors in this particular region and requires a well-programmed control system, it can be considered valid due to the fact that it is similar in the V-22 Osprey case.

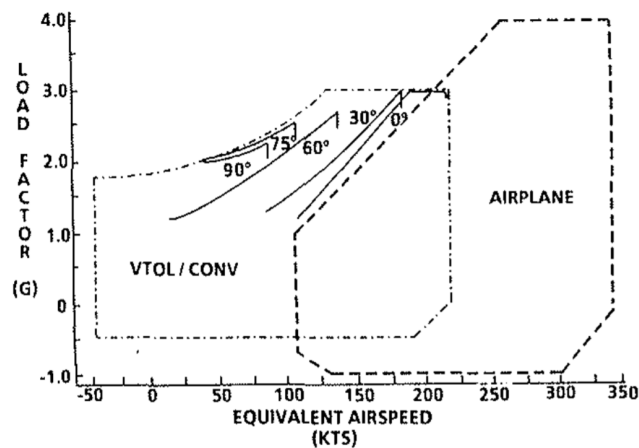


Figure 7.3: Flight envelope V-22 Osprey

Secondly, a sensitivity analysis on the diagrams is performed. In this analysis, some values will be changed to see what the effect is on the outcome and whether the effect makes sense. The measures taken will be:

1. Change of cruise speed
2. Change of $C_{L_{max}}$
3. Change of $C_{L_{\alpha}}$

The first action taken is to change the true cruise speed to a higher number of 100 m/s (which is an equivalent cruise speed of 85.94 m/s). The estimated outcome for the manoeuvring diagram is that the V_C line will shift to the right, as well as the V_D line, because the V_D value is dependent on the cruise speed as seen in Equation 7.4. The V_S and V_A should remain unchanged by this action. The new plot is depicted in Figure 7.4 and show the exact same changes as estimated.

²<https://dSPACE-erf.nlr.nl/xmlui/bitstream/handle/20.500.11881/2582/ERF1990-Vol2-II-7-3.pdf?sequence=1> [accessed 18.06.2020]

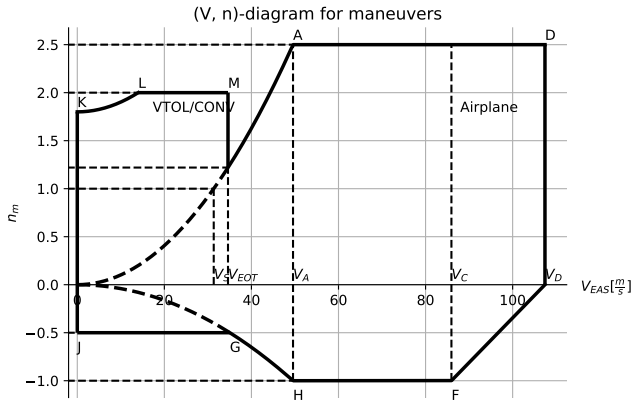


Figure 7.4: Manoeuvring diagram for larger cruise speed

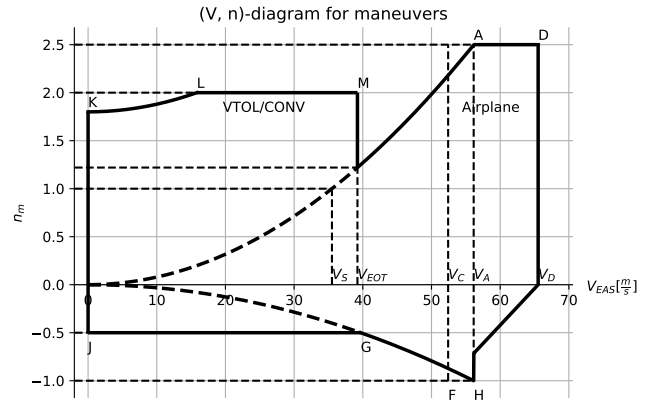


Figure 7.5: Manoeuvring diagram for lower $C_{L_{max}}$

During the programming, it was clear that a change in $C_{L_{max}}$ had a large impact on the manoeuvring diagram, therefore it will now be checked whether the change results in correct outcomes. The original value of $C_{L_{max}}$ is seen in Table 7.1 and is equal to 1.41. The maximum lift coefficient is mainly determined by the airfoil selection, due to proper selection this value is quite high. If another airfoil was chosen with significant lower $C_{L_{max}}$, this will have an impact on the curves, which is a good reason to investigate it. This second sensitivity action lowers the $C_{L_{max}}$ to 1.10. This time we expect the opposite to happen with respect to action 1: V_S will change according to Equation 7.1, and will therefore also affect V_A . V_C and V_D remain unchanged by this action. In Figure 7.5 the outcome is plotted which shows the changes as estimated. It is important to note that, when lowering the $C_{L_{max}}$ to 1.10, the design manoeuvring speed V_A becomes higher than the cruise speed V_C . This can be explained due to the low cruise speed and low $C_{L_{max}}$, and means that during cruise the maximum load factor is limited by stall and not by the general value of 2.5 anymore.

Another thing noticed when programming, is the effect of $C_{L_{\alpha}}$ on the gust envelope. Therefore, as a third action, this value will be changed from the original 4.569 (per radians) to a lower value of 3.50. This means that the change due the angle of attack has a lower change on the total lift of the aircraft. Since gusts basically create a change in angle of attack and by that a change in C_L it is expected that the lower $C_{L_{\alpha}}$ would also reflect in a lower load factor due to gust. The outcome of this change is seen in Figure 7.6. Compared to the original gust diagram Figure 7.2 all diagonal dashed lines moved closer to the horizontal center line at $n=1$ and with that also the envelope shrank. This action shows that the code works at least qualitatively correct.

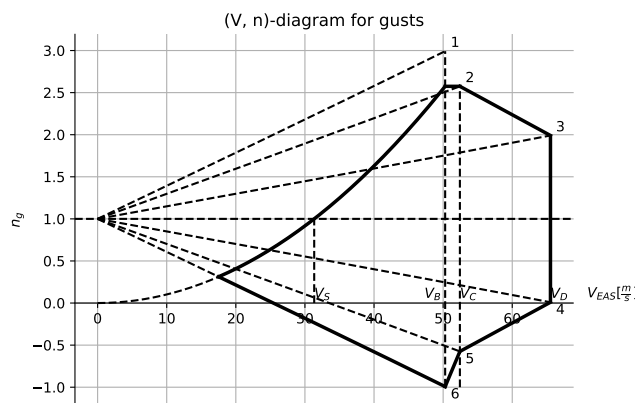


Figure 7.6: Gust diagram for lower $C_{L_{\alpha}}$

7.4. Revised mission profile

This section provides the revised mission profile from the previous one provided in the Midterm report [7]. This example mission profile is revised with respect to the aircraft’s newly defined cruise speed as mentioned in section 7.3, and it includes a clear transition phase in the flight profile. From this the following mission phases can be established:

- ✈ *Departure.* This phase includes engine warm-up, taxi, take-off and ends with flying out of the aerodome airspace. The departure procedure is however not shown in the mission profile as it is too short compared to the climb, cruise and descent phase [6] [7].
- ✈ *Purely vertical take-off.* In this phase, the tilted proprotors are positioned at a 90 degree angle. In [25, Chapter 7, p.424] it was found that for helicopters pure vertical take-off is only performed until about 5 m altitude, after which the pilot will accelerate forward. Therefore, it was determined to let the tilt proprotor perform its purely vertical take-off at a rate of 1.5 m/s until this specified 5 m altitude.
- ✈ *Transition to horizontal flight.* After the vertical take-off, the aircraft will slowly rotate its proprotors from the 90 degree angle to fully horizontal position (0 degree angle). During this transition, it will gain forward speed and will climb at a different (lower) climb rate compared to the VTOL mode. The total time the aircraft can provide its full thrust in VTOL mode is set by the battery capacity to be 6 minutes (from subsection 8.5.2).
- ✈ *Horizontal climb.* The aircraft is now in fully horizontal aircraft mode and can climb to its desired cruise altitude. For this, the power available and power required are calculated (see chapter 8) in order to find the rate of climb in horizontal mode.
- ✈ *Cruise.* In cruise the aircraft will fly at a speed of 220 km/h. The minimum cruise altitude was set to 1,000 ft (304.8m), the maximum cruise altitude is equal to 10,000 ft (3,048m).
- ✈ *Horizontal descent.* Similar to the horizontal climb, the aircraft will start its descent in fully horizontal mode.
- ✈ *Transition to VTOL.* The horizontal descent is then followed by transition phase, this time from horizontal mode to the vertical mode. The rotors will gradually rotate from 0 degree angle to a 90 degree angle and prepare for vertical landing.
- ✈ *Purely vertical landing.* The aircraft will land in pure vertical mode at a rate of 1.5 m/s.
- ✈ *Loiter.* When needed, the aircraft will descent to its loiter altitude and loiter to its desired location. The loiter time of 45 minutes was added to the 3 hours of endurance, as seen in requirement **DSE-22-SYS-P-04**.

An example mission profile is provided in Figure 7.7. The figure gives the flight profile for cruise at minimum altitude of 304.8m , maximum altitude of 3,048 m and an example flight at altitude 1,500m.

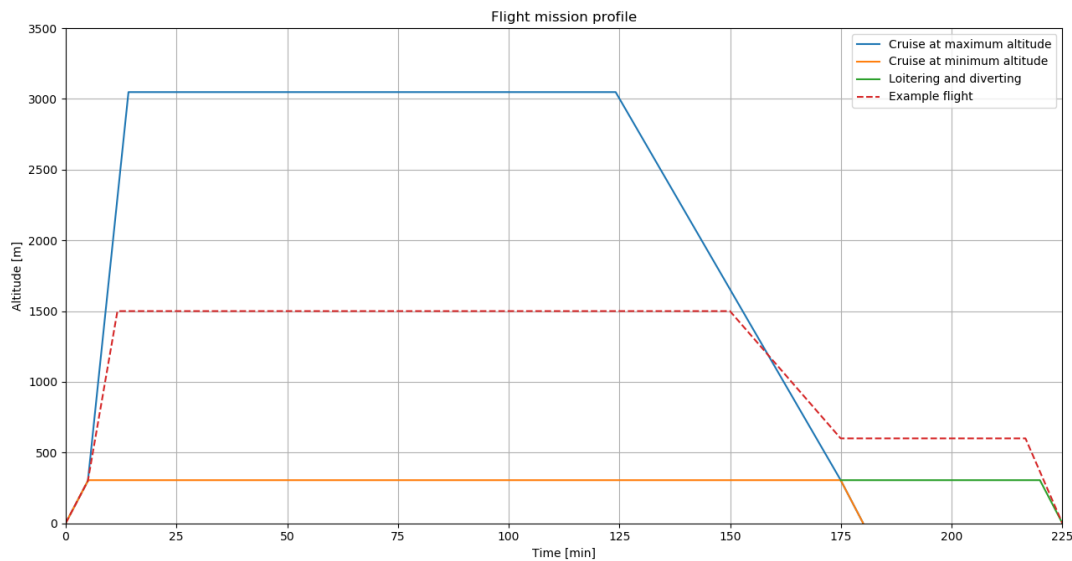


Figure 7.7: Mission profile

Due to the different phases: Vertical climb, transition climb and horizontal climb, the aircraft will fly at different rate of climb for each of the phases. This can clearly be seen in Figure 7.8. The same is valid for the descent phase where aircraft will fly at different rate of descent.

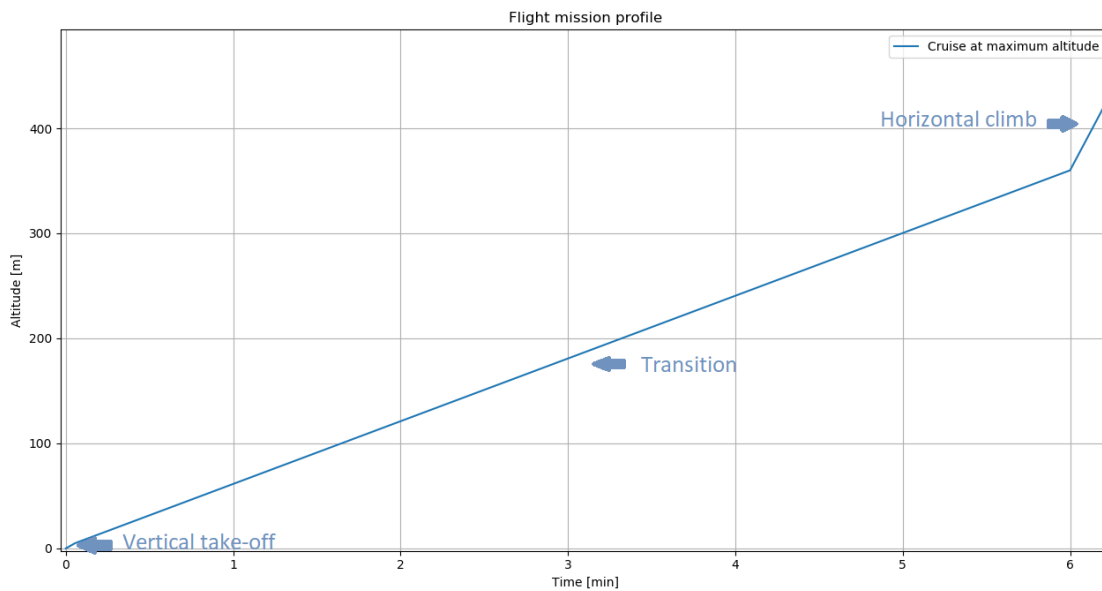


Figure 7.8: Differences in rate of climb in mission profile

7.5. Noise reduction

A requirement considering the noise level of the aircraft was set by the user and was translated in requirement **DSE-22-SYS-S-05**. However, as was explained in the Midterm report [7], the actual noise level is impossible to accurately estimate without experimental testing. After a discussion with a staff member of Delft University of Technology, B. von den Hoff, who is specialised in noise, it was decided to focus on finding noise reduction methods that can be implemented in the design, instead of estimating the noise level of the vehicle.

The main sources of noise in the aircraft are its proprotors and the turbine range extender. First looking into the proprotors; they are likely to generate more noise in VTOL than in cruise, because of the high rotational speeds. According to Johnson, helicopters noise is mainly influenced by rotor tip speed, and the frequency range of the noise is lowered by decreasing the rotational speed [25]. ICAO study on noise reduction technologies in helicopters identifies different types of noise [22], and the ones that are relevant in VTOL operations are listed here.

In hover, two main forms of noise are the thickness noise and the blade loading noise. The first one is generated by the periodical displacement of air through the rotor, and the second one is caused by the rotating forces acting on the air. In approach, a third noise is recognised, known as blade-vortex interaction (BVI). It is produced when a blade is disturbed by the tip vortex of a preceding blade [22].

Following measures are recognised by ICAO to reduce the noise [22]:

- ✈ Reduction of rotor rotational speed
- ✈ Increasing number of rotor blades
- ✈ Advanced rotor blade design
- ✈ Active technologies

The reduction of rotational speed will be taken into account in choosing the motor and the RPM-torque combination that will provide the required power, however, from performance perspective high RPMs might be required in VTOL.

The number of rotor blades can still be adjusted with the blade design. Additionally, advanced methods can be used in the blade design. Serration of the trailing edges of blades has proven to reduce the noise in multiple studies. According to Candeloro, et al., serration is the most effective way of adjusting blade geometry to noise reduction [10]. In the same report the use of porous materials is also suggested, as this has already been studied for wind turbine blades [10]. In a study about UAV propellers with trailing edge serrations it was concluded, that the performance in hover was not affected by the serration, but the noise was reduced by up to 7.5dB [41]. Serrated trailing edges are also actively used in wind turbines for noise reduction, as shown in [Figure 7.9a](#)³. From these results it can be said that serration should be used in the blade design, and the effects tested experimentally. The use of porous material requires more experimental research.

Active technologies include for example the Blue Pulse technology, which uses active trailing edge flaps on rotor blades to reduce vibrations and noise. Flaps are displaced with piezoelectric actuators in optimal frequency regarding the ro-

³<https://blog.greensolver.net/en/operation-wind-farm-serration/> [Accessed 21.06.2020]

tor revolutions [30]. The active flap is presented in yellow in Figure 7.9b⁴. The feasibility of integrating this technology in the design would need more research. The active flaps should not decrease the aerodynamic performance of the blades, the blade structure should be able to withstand the new loads, and the actuators need to be placed within the proprotor.

In the Midterm Report [7] the use of duct around the proprotors was also recommended, but due to the large size of the proprotors in diameter this structure would be substantially large, adding a lot of weight and stress on the wings. Because of this reason, ducts are the most unreasonable option out of all of the above-mentioned ones and are therefore left out of the design.

Now as the turbine range extender will be bought off-the-shelf, the possibilities of adding noise reduction mechanisms are limited, unless the manufacturer is willing to adjust the product after discussions. Two methods for noise reduction are identified from an ICAO report: firstly, acoustic liners can be added around the turbine or incorporated in optimal locations in the component, and secondly, the turbine blade geometries can possibly be designed for noise reduction [27].



(a) Serrated wind turbine blade



(b) Active flap on a rotor blade

Figure 7.9: Noise reduction mechanisms

⁴https://www.nasa.gov/topics/aeronautics/features/smart_rotor.html [Accessed 21.06.2020]

Power and Propulsion

The amount of thrust that is needed for the aircraft and the propulsion method that is selected for the aircraft are discussed in this chapter. The chapter again starts with a functional analysis in [section 8.1](#) and a requirement analysis in [section 8.2](#). Then the cruise thrust and power calculations are provided in [section 8.3](#). The VTOL thrust and power calculations are given in [section 8.4](#). The propulsion method will be explained in [section 8.5](#). The proprotor design is addressed in [section 8.6](#). This chapter is concluded by providing the fuel layout system in [section 8.7](#).

8.1. Functional analysis

[Figure 5.2](#) shows the list of functions that should be performed during production, operation, and end-of-life of the aircraft. Some of these functions has to performed by the power and propulsion subsystems:

- ✈ F2.1.5: "Engage propulsion":
After the pre-flight checks, the propulsion system should be ready to be engage.
- ✈ F2.1.6: "Taxi to takeoff area":
Provide enough power to the aircraft to taxi from the parking area to the takeoff area.
- ✈ F2.1.9: "Perform takeoff":
providing enough power to the aircraft to takeoff vertically.
- ✈ F2.3.7: "Taxi to parking area":
After landing, enough power should be provided by the propulsion system for taxiing.

8.2. Requirement analysis

A detailed list of requirements was identified in the baseline report[6], out of which, some are related to the power and propulsion subsystem. These requirements are as follows:

- ✈ **DSE-22-STAK-01:** The aircraft shall have performance characteristics such that it is competitive on the market [6].
Market competitive performance affects choice of propulsion.
- ✈ **DSE-22-STAK-02:** The aircraft shall comply with the current safety and reliability requirements [3] [1].
The propulsion system needs to be safe in operation.
- ✈ **DSE-22-STAK-05:** The aircraft shall be environmentally friendly [6].
Sustainability is also a big part of the propulsion system, largely because of the emissions.
- ✈ **DSE-22-SYS-P-05:** The aircraft shall have a maximum service ceiling of 3048 m [6].
The propulsion system should be able to propel the aircraft to an altitude of 3048 m.
- ✈ **DSE-22-SYS-P-06:** The aircraft shall have a minimum rate of climb of 304.8 meters per minute [6].
The ROC during nominal horizontal flight is largely dependant on the available power of the propulsion system.
- ✈ **DSE-22-SYS-AC-03:** The aircraft shall have a maximum wing span of 9m [6].
Because the propellers will be mounted at the wing tips, the span requirement needs to be taken into account when placing the engines. The propellers will effectively change the total span of the aircraft.
- ✈ **DSE-22-SYS-S-05:** The noise level limitation shall be identical to motor vehicles (82 dB(A)) [6].
The noise created by the propulsion system needs to be minimised.

8.3. Cruise thrust and power

The cruise thrust is assumed to be equal to the drag experienced in cruise flight.

As the thrust is known, the required cruise power can be computed. The power is computed for each proprotor individually. The computation for ideal power is done according to the actuator disk theory ¹, with [Equation 8.1](#).

$$P_{ideal} = \frac{1}{2} T u_0 \left[\left(\frac{T}{A_{disk} u_0^2 \frac{\rho}{2}} + 1 \right)^{\frac{1}{2}} + 1 \right] \quad (8.1)$$

¹<https://web.mit.edu/16.unified/www/FALL/thermodynamics/notes/node86.html> [Accessed 19.06.2020]

Here u_0 notes the flight velocity, the A_{disk} the propeller disk area, and ρ the cruise density, taken for the altitude 1,500m.

As there are losses caused by the propeller, the ideal power is converted to a required power by multiplying with propeller efficiency, as done in [Equation 8.2](#). The efficiency is assumed to be 0.8, as this is typically the peak that can be achieved ² [32].

$$P_{req} = \eta P_{ideal} \quad (8.2)$$

In order to verify the calculation, the cruise thrust value, and the proprotor dimensions are also tested with the Software JavaProp [28], more about this will be explained in [subsection 8.6.1](#). A standard blade geometry is used, because no blade airfoil is specified. For now the number of blades is set to three. For a given propeller configuration and desired thrust the software determines the most efficient RPM value and a torque. The power values only differ by 0.1 kW from those calculated, when the efficiency reaches 0.79, which is the highest one found.

The values in [Table 8.1](#) are computed for the latest iteration and include uncertainty, because the mass value for which the thrust and power are computed could still change.

Table 8.1: Cruise thrust and power

Mode: cruise	Canard	Wing
Number of proprotors	2	2
All values below are per proprotor		
Thrust [N]	68	83
Radius [m]	1.0	1.5
Area [m ²]	3.14	7.07
Cruise velocity [m/s]	61	61
Efficiency [-]	0.8	0.8
Power (estimated) [kW]	5.2	6.3
Power (JavaProp) [kW]	5.3	6.4

8.4. VTOL thrust and power

The total VTOL thrust needed is assumed to be equal to the MTOW of the aircraft. Naturally, more thrust would be needed in order to accelerate. It is assumed that the vertical climb velocity is achieved by adjusting power output of the individual motors, for each proprotor separately.

The Canard and wing lift fractions are found from the center of gravity (cg) range in [chapter 10](#), same fractions are used for the thrust that needs to be generated by the main and canard proprotors in VTOL. Fraction of main wing proprotors is 59% of the thrust, and 41% for the canard ones.

The total required power to perform vertical climb consists of four components: induced power, climb power, rotor profile power, and parasite power. The reference used for the following power calculations is Johnson's Helicopter Theory [25].

The power induced is the power needed to produce lift, thus the power overcoming rotor drag induced by the mass flow of air going through the rotor disk. To calculate the induced power per proprotor [Equation 8.3](#) is used.

$$P_i = T v_i \quad (8.3)$$

where v_i is the induced velocity, from [Equation 8.4](#)

$$v_i = \sqrt{\frac{T}{2A\rho}} \quad (8.4)$$

Variable A being the disk area, that varies with chosen proprotor radius.

The climb power is computed as thrust times climb velocity, using [Equation 8.5](#).

$$P_c = T v_c \quad (8.5)$$

²<https://web.mit.edu/16.unified/www/FALL/thermodynamics/notes/node86.html> [Accessed 26.06.2020]

In [section 7.4](#) the climb rates used for different climb phases are introduced. In CS-27 regulations [4] it is mentioned that the maximum descent rate is 1.5 m/s. This value will also be used for climb in pure vertical flight mode, as a lower climb rate requires less power. If higher climb rate is wanted in pure vertical flight mode, for example to avoid obstacles, more power needs to be added to the system, and a check needs to be made that enough thrust can still be delivered.

In transition phase the climb rate will stay below 5 m/s. In horizontal flight mode the minimum climb rate of 5 m/s is determined, from requirement (DSE-22-SYS-P-06).

To make sure that this climb rate can be reached without implementing the maximum thrust, which should be used in vertical flight mode only, [Equation 8.6](#) from the Aerospace Design and Systems Engineering Elements course [32] is used. Here the thrust required for the climb rate of 5 m/s is computed, using the most recent iteration of weight, a cruise velocity of 61 m/s and a most recent estimation of total drag.

$$T = \frac{ROC * W}{V} + D \quad (8.6)$$

The thrust is found to be 924.2N for the most recent iteration with a mass of 775kg and drag of 301 N, this value being only a small portion of the VTOL thrust, approximately 12%. It can be said that the aircraft can easily reach higher climb rates than 5 m/s in horizontal mode, without having to use maximum settings.

The rotor profile power is the power to rotate the proprotor, it can also be computed as the torque times the rate of rotation. For now this is assumed to be half of induced power, as according to Johnson induced power usually accounts for 60% of the total required power, and rotor profile losses 30% [25]. This assumptions is made because the RPM of the motor can be adjusted to the required power value by changing current and torque, this will be further discussed in [section 8.6](#).

Considering the last power component, the parasite power: it can normally be computed as drag times velocity, and it is dependent on the vertical drag of the vehicle. For now the parasite power is neglected, as it is very low in comparison to the three previously mentioned ones. However in the motor choice it has to be taken into account, that the motor should be able to provide more power than what is calculated here.

Similarly to that of cruise flight, the values in [Table 8.2](#) are computed for the latest mass iteration and include uncertainty.

Table 8.2: VTOL thrust and power

Mode: VTOL	Canard	Wing
Number of proprotors	2	2
All values below are per proprotor		
Thrust [N]	1495	2212
Radius [m]	1.0	1.5
Area [m ²]	3.14	7.07
Induced velocity [m/s]	15	12
Climb velocity [m/s]	1.5	1.5
Power induced [kW]	22.4	26.9
Climb power [kW]	2.2	3.3
Rotor profile power [kW]	11.2	13.5
Total power per proprotor [kW]	35.9	43.7

8.5. Propulsion method

For the propulsion method selection two options were considered: either running the propellers directly on a chemical fuel engine, or using a completely electric set-up. Chemical combustion has the disadvantage that the engines are quite heavy per kW that they need to produce. The advantage is that they use chemical fuels in the combustion process, and these fuels have a very high specific energy. This type of energy production does not need to consume much fuel in order to provide enough propulsion for the aircraft for the entire flight. The second option is fully electric, with the propellers powered by an electric motor. These motors are very light for the amount of power they produce. The energy storage of electric power still has a very low specific energy, and the batteries would need to be substantially large in size to last for the duration of the flight.

The first option would be the best for the cruise phase of the aircraft, as the cruise takes a long time with a relatively low power output. The required engine and fuel tank would be quite small. The second option would be best for the

VTOL phase of the aircraft. This phase only takes a very short time but requires a lot of output power. The battery will not be too heavy in this case, as it only needs to store enough energy for the short VTOL duration.

A third option was created using this knowledge: a hybrid of the two. This means taking the advantage of the electric motors in their low weight and combining this with the specific energy of the chemical fuels. During VTOL the electric motors will be powered by a battery that has a high discharge rate. However, when the battery is empty and the aircraft is in cruise, a generator will be used to power the electric motors. This range extender can also charge the battery when necessary.

8.5.1. Range extender

The first thing to consider is the range extender. It could be just a reciprocating combustion engine with a generator attached. This option is very simple, and it has been proven to work, but it is not very efficient. There exists a better option, that is currently in development: a micro turbine generator. This consists of a small turbine engine which powers a high speed electric generator. UAV Turbines has produced a system that uses this principle³. It has made a hybrid electric setup from which the turbine generator produces 25 kW and weighs 27 kg. This generator was chosen to be used in the design of the aircraft. These turbine generators are already used as an emergency power generator for their efficiency and low maintenance. The efficiency of this specific generator is not mentioned anywhere, but these turbines can reach an electrical efficiency of 25% to 33% [9]. Because the turbine from UAV Turbines is a lightweight version, the 25% efficiency was used for the fuel calculations.

8.5.2. Fuel and battery calculations

The turbine can run on a wide variety of fuels. For the calculations biodiesel was used as this is one of the more environmentally friendly chemical fuels available. To calculate the amount of fuel for the aircraft the following parameters are needed: the cruise power, the specific energy of biodiesel, the turbine efficiency and the electrical efficiencies of the electric power-train. The turbine efficiency taken at 0.3 is the highest contributing factor to the efficiencies. This equation is shown in Equation 8.7. This came down to a fuel mass of 38 kg for a 3 hour endurance with loitering, which was rounded up to 40 kg for coming calculations. This lead to an operational cost of €18.02 for the fuel.

$$\text{Fuelmass} = \frac{P_{\text{cruise}} \cdot \text{Endurance}}{\text{Specific Energy} \cdot \text{efficiencies}} \quad (8.7)$$

For the battery choice it was decided that lithium-ion batteries have the best performance for the design. They are the lightest batteries per kWh available. The battery mass depends on the power needed during vertical flight, the specific density of lithium-ion batteries, and the electric efficiencies of the power-train. This is almost the same as Equation 8.7 with the cruise power and VTOL power exchanged. The range extender efficiency is replaced by the battery efficiency. For 6 min of vertical flight, which was estimated to be plenty of time to transition to horizontal flight, a battery mass of 53 kg was calculated. 10 % was added to this to account for any wiring, or a battery management system. The final battery mass is 58 kg.

8.5.3. Motor selection

For selecting a motor, the output power is the most important factor. This value is somewhat determined by the size of the motor housing. The torque and operating RPM can still be adjusted by winding the motor differently. For this aircraft the REB 50 was chosen from MGM Compro⁴, as the website states this motor can be customised to fit the RPM needs. The VTOL RPM will be within the standard operating RPM of this motor. During cruise the RPM will probably be lower than the operating RPM on the manufacturers website. However the manufacturer states that the motor can be customised for the customers needs. Usually this lower limit is a cooling restriction. However during cruise the motor will use a lot less power than the maximum power. This means the motor can also be used at this power setting and RPM. This does however need to be validated by contacting the manufacturer. This motor will be controlled by a motor controller. The controller creates a waveform that matches the RPM of the motor. The motor controller will adjust the voltage of this waveform to adjust the torque provided by the motor. The RPM will be depending on the torque provided and the load on the motor. For cruise flight the most efficient combination of RPM and torque for the proprotor size is found with the software JavaProp [28]. The required thrust, number of blades, and the proprotor radius are set as input parameters. A range of different RPM values is also tried as inputs, and from these software outputs the efficiency of the proprotor, the required power and the torque. For now the RPM that gives the highest efficiency and therefore also the lowest required power is chosen as the most suitable one. However, it is possible to choose a higher RPM for the propeller in horizontal flight mode to fit the operational range of the motor. The efficiency of the propeller would not be as high in this case, and more power would be required. This again could lead to needing more fuel, and should therefore only be considered if necessary.

³Hybrid Electric micro turbine, <https://www.flightglobal.com/news/uav-turbines-unveils-hybrid-electric-microturbine-for-drones/135703.article> [Accessed 22-06-2020]

⁴REB 50, <https://www.mgm-compro.com/products/30-50kw-electric-motors/> [Accessed 22-06-2020]

In order to find a range of RPM and torque values that the motor should provide for the VTOL a different approach is used, as the JavaProp software is not designed for rotor design. For VTOL it is important, that the aircraft is capable of providing the necessary thrust. Thrust-delivering capability of the proprotor is dependent on the density of the air, the tip speed of the blades, and the thrust coefficient, which can be found with [Equation 8.8](#).

$$C_T = \frac{T}{\rho \pi R^2 V_t^2} \quad (8.8)$$

To compute a range of suitable RPM values and the torque that follows from it, the thrust coefficient for the proprotors is assumed to be between 0.005 and 0.01, as this is within the range of thrust coefficients that are used on a tilt rotor modelling study [43]. Now the tip speed is still an open variable, and it is computed for the lowest and highest thrust coefficients, assuming cruise altitude of 1500m. In order to avoid transonic flow on the blades, the tip speed is however limited to Mach 0.7. If the tip speed with the lowest thrust coefficient, 0.005, exceeds Mach 0.7, the thrust coefficient is increased to stay at this Mach.

The RPM and the torque are then computed from the blade tip speed with [Equation 8.9](#)[25].

$$RPM = \frac{V_t}{R} \frac{60}{2\pi}, \quad \text{Torque} = \frac{30P_{req}}{\pi RPM} \quad (8.9)$$

The range of RPM values for the canard proprotors is found to be very limited. With a thrust coefficient of 0.01, the tip speed would become 200 m/s. This translates to RPM and torque of 1900 1/min and 180 Nm respectively. With a thrust coefficient of 0.005 the tip speed would exceed Mach 0.7, and therefore the thrust coefficient is increased. For the maximum tip speed, 235 m/s, a thrust coefficient of 0.008 is required. This leads to RPM of more than 2200, and torque of 150 Nm.

For the main wing proprotors the range is less limited due to the longer radius. For a thrust coefficient of 0.01, the tip speed becomes 170 m/s, leading to RPM of 1100 and a torque of 390 Nm. Mach 0.7 is exceeded when the thrust coefficient 0.005 is used. For the maximum tip speed of 235 m/s, the required thrust coefficient becomes 0.0054. For this tip speed the RPM is 1500 and torque 280 Nm. A RPM value of 1500 would fit in the operational range of the currently found motor⁵.

The thrust coefficient of the rotor will eventually depend on the design choices. As mentioned above, the RPM of electric motors can still be adjusted. A higher RPM leads to more noise, as is discussed in [section 7.5](#), and it also causes higher centrifugal forces on the blades, which means that the blade structure has to handle higher stresses. A lower RPM on the contrary has more torque, and electric motors are usually found to be more efficient with higher RPM values.

Table 8.3: Proprotor design parameters

Mode: cruise	Canard	Wing	Mode: VTOL	Canard	Wing
All values below are per proprotor					
Radius [m]	1.0	1.5	Radius [m]	1.0	1.5
Nr. of blades	3	3	Nr. of blades	3	3
Thrust [N]	68	83	Thrust [N]	1495	2212
Power req. [kW]	5.3	6.4	Power req. [kW]	35.9	43.7
RPM	1000	800	RPM range	1900-2200	1100-1500
Torque [Nm]	50	76	Torque range [Nm]	180-150	390-280
Blade tip Mach	0.31	0.37	Blade tip Mach range	0.60-0.70	0.50-0.70

The results are summarised in [Table 8.3](#). It should be noted that the values presented in this section do still include some uncertainties. The propulsion system is highly dependent on the mass of the aircraft, which could still change at later stages. Additionally, not all losses within the system are taken into account yet, and these should be considered in the future.

8.6. Proprotor design

In the design process a three-bladed proprotor was considered. There are already existing propellers that would fit close to the wanted RPM range and have the right dimensions, a 1m radius for the front proprotors and a 1.5m radius for the back proprotors. An example off-the-shelf propeller is found by Aeroprop⁶, which has a diameter of 1.9m, and

⁵REB 50, <https://www.mgm-compro.com/products/30-50kw-electric-motors/> [accessed on 22-06-2020]

⁶<https://aeroprop.aero/en/products/propellers/u-1900/> [Accessed 22.06.2020]

optimal RPM of 2100.

However, it is desirable to design the blades instead of buying them off-the-shelf, because in this way the blade design could account for noise performance. In [section 7.5](#), methods of noise reduction are explained, and some of them should be implemented in the blade design. Design considerations are for example serration of trailing edges, possible use of porous materials, and including active flaps.

The performance of the proprotor is naturally the key aspect of blade design. The proprotors should be able to generate the required thrust in VTOL and in cruise. From noise reduction perspective it is beneficial to run the proprotors with lower RPM, which means that the blades should have high performance, to be able to provide the required VTOL thrust in lower RPM values.

The use of variable pitch propellers can be considered later to increase performance in VTOL. In this case the drag-caused power losses in cruise could also be minimised, reducing the energy needed to fly the aircraft. The material choice for the blades is also an important sustainability consideration.

8.6.1. Verification and validation

As is mentioned in [section 8.3](#), the power required by the proprotors was first computed by hand, following the actuator disk theory. In the calculation the assumption was made, that the propeller efficiency would be 0.8. The required power was then computed with the software JavaProp, setting the radius, number of blades, required thrust and cruise forward velocity as inputs. Another required input for the software is the RPM value, which was adjusted to find the highest efficiency.

The found maximum efficiency was 0.79. For this efficiency, the required power only differed from the computed one by 0.1 kW, verifying the both the assumptions for the efficiency and the first computed value for required cruise power.

The RPM and torque values that give the maximum efficiency on JavaProp are for now assumed to be good estimations for the proprotor performance in cruise conditions, but these should be tested experimentally.

The calculation tool for VTOL power required is verified first by testing with values for a known helicopter, the Robinson R22. From the pilot's operating manual [11], the maximum take-off weight and the rotor diameter are found. Additionally, the document gives a TOP (take-off power) rating for the powerplant. The maximum rate of climb is determined to be 1200 feet/min⁷. The outputs of the tool are shown in the following table. The results show that the calculated maximum total power is close to the maximum TOP rating. The difference can be explained by the assumed high rate of climb at take-off, which in reality is not possible immediately without having any forward velocity. The results given by the VTOL power tool are considered reasonable.

Table 8.4: Robinson R22 Power

Input parameters for tool	
Mass [kg]	620
Rotor radius [m]	3.8
Climb velocity [m/s]	6
Output parameters from tool	
Induced velocity [m/s]	7.4
Disk loading [N/m ²]	13.7
Power induced [kW]	45.0
Profile power [kW]	22.5
Climb power [kW]	37.1
Total power [kW]	105
From pilot's operating handbook [11]	
TOP rating [kW]	92

Additionally, to confirm that the calculations are valid for a tilt proprotor configuration with multiple rotors, the computed disk loading and hover lift efficiency are compared to those found in the graphs in [Figure 8.1](#). The [Figure 8.1a](#) is from the Krossblade Aerospace VTOL project⁸ and [Figure 8.1b](#) is from the Airbus Vahana project⁹. The disk loading and hover lift efficiency are computed for the design with [Equation 8.10](#).

⁷<https://www.skybrary.aero/index.php/R22> [Accessed 20.06.2020]

⁸<https://www.krossblade.com/disc-loading-and-hover-efficiency> [Accessed 20.06.2020]

⁹<https://acubed.airbus.com/blog/vahana/vahana-design-process-part-ii-preparing-for-lift-off/> [Accessed 20.06.2020]

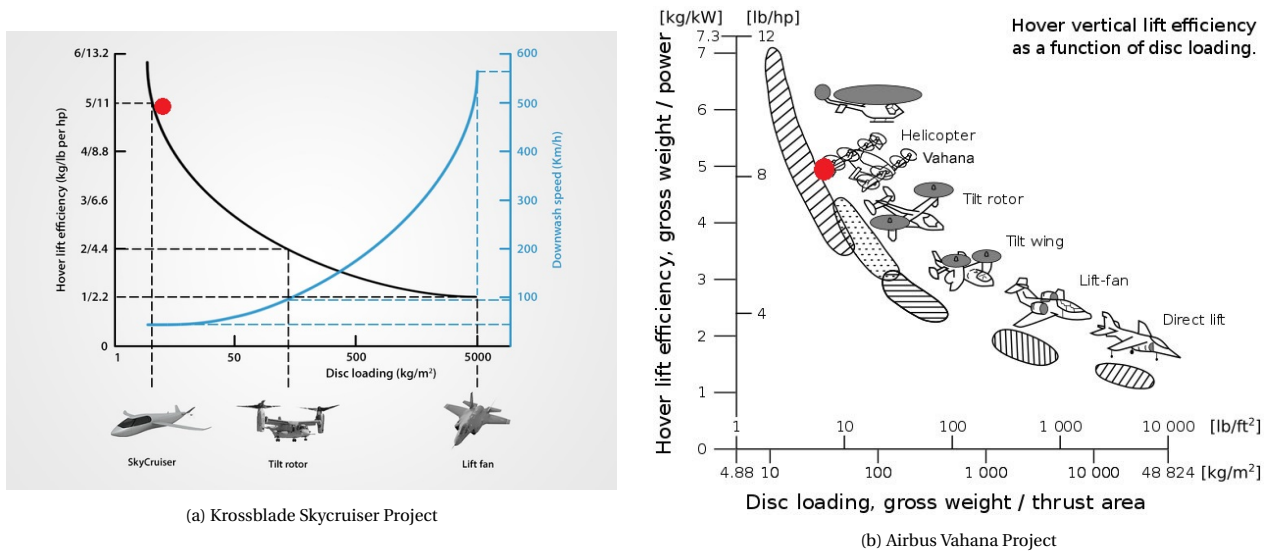


Figure 8.1: Hover lift efficiency versus disk loading

$$DL = \frac{MTOW}{A_{disk}}, \quad \eta_{hl} = \frac{MTOW}{P_i + P_p} \quad (8.10)$$

In this equation A_{disk} is the total disk area, taking into account all four proprotors, and for the hover lift efficiency η_{hl} only the hover power is taken into account, which consists of power induced P_i and rotor profile power P_p .

The design is indicated in the graphs as a red dot, with disk loading of 37 kg/m² and hover lift efficiency of 5 kg/kW. It can be seen that the disk loading is lower than that of common tilt rotor aircraft, but higher than that of helicopters. The hover lift efficiency is higher than that of tilt rotors. It is good to note, that the design fits close to the Skycruiser from Krossblade Aerospace¹⁰ and Vahana from Airbus project¹¹. The skycruiser is can fold away its eight rotors in cruise, and Vahana has eight fans on tilting wings. Even though the tilting proprotor design does not fit in the tilt rotor category on the two graphs, it is close to the two mentioned vehicles, that are both in the small personal aircraft category. This validates the VTOL power tool.

8.7. Fuel system lay-out

This section aims to give an overview of what the fuel system will look like. In [Figure 8.2a](#) and [8.2b](#), sketches of the fuel system can be found.

The component that are numbers in the sketches are now explained.

1. The batteries:
They are placed in front of the aircraft. The total mass of the batteries is 59 kg, with a volume of 21.6 l.
2. The power lines:
These power lines transport the electrical energy generated by the turbine (9.) to the batteries in front of the aircraft. The power lines run through the middle on the bottom of the aircraft and will be fixed to the aircraft thrus structure.
3. Fuel pumps:
Fuel pumps are needed as the turbine is located higher then the lowest point of the fuel tank. Note that two fuel pumps are installed on either side of the fuel tank. This is done due for redundancy. Would a fuel pump fail during flight, an other fuel pump is still able to take over and provide fuel to the turbine such that it can keep producing electrical energy.
4. The fuel tank:
The fuel pump is located directly behind and underneath the seat of the pilot, this is to keep the cg range small. On the other side, it will be fixed to the aircraft structure. Because the fuel tanks is so restricted in between the pilot seat and aircraft structure, it will be better protected during a possible crash. Due to restricted space, it also has a triangular shape. The fuel tank will have to be able to hold 40 kg of fuel with a volume of 45.5 l. The total mass of the fuel system (including the fuel tank, but excluding the turbine) was estimated to be 45 kg in the resource allocation in [chapter 4](#).

¹⁰<https://www.krossblade.com/disc-loading-and-hover-efficiency> [Accessed 20.06.2020]

¹¹<https://acubed.airbus.com/blog/vahana/vahana-design-process-part-ii-preparing-for-lift-off/> [Accessed 20.06.2020]

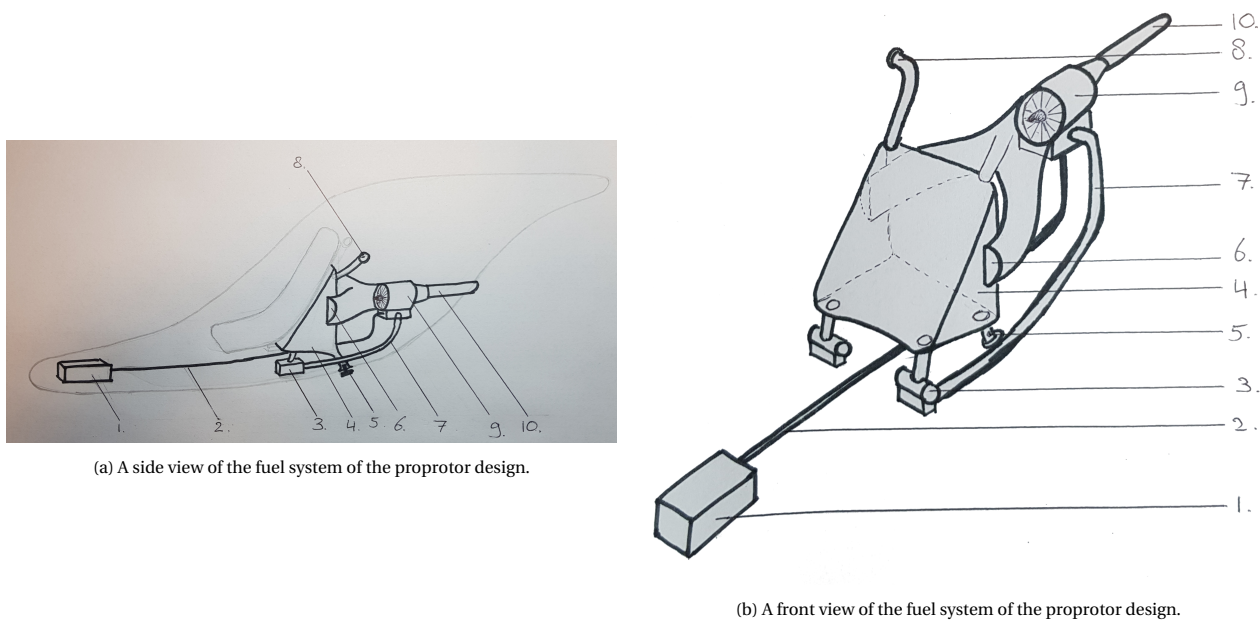


Figure 8.2: Hover lift efficiency versus disk loading

5. The fuel inspection valve:

Just like general aviation aircraft, the aircraft has a fuel inspection valve to check if no water or anything else entered the fuel tank. It is positioned on the left side of the aircraft. The fuel inspection valve takes fuel from the lowest part in the fuel tank. This is done to prevent any of the water or debris in the fuel tank from being led towards the turbine. The fuel that is taken from the fuel tank that goes to the turbine is always positioned a bit higher in the fuel tank. Because the fuel is not taken from the lowest point in the tank, it results in always having a bit of left over fuel in the tank. This fuel is unusable for combustion. For some general aviation aircraft, this unusable fuel is a bit more than 5% of the total fuel capacity¹²

6. Turbine air inlet:

To provide the turbine with air for combustion, an inlet will be positioned on either side of the fuel tank, which takes free stream air into the turbine.

7. The fuel pipe:

This fuel pipe leads the fuel from the fuel tank to the turbine.

8. The refuelling opening:

From here, the tank can be refuelled. One of these openings is positioned on either side of the aircraft at around the middle of the height of the fuselage. This way, this opening can easily be reached from the ground. The refuelling opening is conveniently positioned underneath the main wings. This also prevents water and other debris from entering the fuel tank via this opening.

9. Turbine:

The turbine converts fuel to electrical energy that is stored in the batteries.

10. Exhaust duct:

After combustion, the exhaust gases are led through this duct to be released in the airflow behind the aircraft. The duct is kept as short as possible to prevent leakage and limit its weight.

Fuel tank crash worthiness

In the event of a possible crash, it is important that the best efforts are put in protecting the fuel tank and its contents.

As was already explained, the fuel tank is going to be positioned in the fuselage. The fuel tank will be positioned behind the pilot seat in the lower part of the fuselage. This way the fuel tank is more protected compared to if they were in the wings. The fuselage structure will provide protection comparable to a roll cage in a car.

In addition to the positioning of the fuel tank, it will be made even more crash damage resistant, a kevlar lining will be put into the fuel tank. This will prevent leakage when the fuel deforms due to impact of the crash. The kevlar lining is also recyclable¹³.

¹²<https://airplaneacademy.com/why-do-aircraft-have-an-unusable-amount-of-fuel/>, [Accessed 29.06.2020]

¹³http://ballisticrecycling.com/Kevlar_Recycling.html, [Accessed 26.06.2020]

Aerodynamics

In this chapter the aerodynamic characteristics of the aircraft are calculated and analysed. The chapter starts off with a functional analysis in [section 9.1](#), and a requirement analysis in [section 9.2](#). After selecting an airfoil for the wing and the canard in [section 9.3](#), wing sizing is done in ?? and the lift and drag estimation is provided in [section 9.4](#).

9.1. Functional Analysis

It should be insured that the aerodynamic design of the aircraft will be able to perform the following functions:

- ✈ F2.1.10: "Transition to cruise":
Airfoil should allow for easy transition
- ✈ F2.3.4: "Transition to landing phase":
Airfoil should allow for easy transition
- ✈ F2.2.3: "Control the aircraft":
The wing size and dimensions should make the aircraft controllable during cruise and other phases of flight

9.2. Requirement Analysis

The following requirements are important when it comes to aerodynamic characteristics and are thus taken into account when designing the characteristics. All of these requirements have been met.

- ✈ **DSE-22-SYS-P-07:** The aircraft shall have a minimum cruise speed of 160 km/h [6].
This requirement is used to design the wing for a particular Reynolds number of airflow.
- ✈ **DSE-22-STAK-02:** The aircraft shall comply with the current safety and reliability requirements [6]: CS-23 and CS-27 [3].
 - The aircraft shall have a stall speed no higher than 61 kts (31 m/s) (CS-23) [3].

The stall speed is used to size the area of the main wing.

- ✈ **DSE-22-SYS-P-05:** The aircraft shall have a maximum service ceiling of 3048 m (10,000 feet) [6].
The density at the this maximum altitude will be used to determine the Reynolds number to size the wing.

9.3. Airfoil Selection

The airfoil of the main wing and the horizontal stabiliser of the aircraft was selected based on a few parameters that are of big influence on the performance: the camber, thickness and maximum lift coefficient of the airfoil. In order to get a feeling for these parameters, the camber and thickness effects were tested in Javafoil [21]. This is a program that allows for an analysis of particular airfoils at a desired Reynolds number. Additionally, aerodynamic data found on an online tool called 'airfoil tools' was used to compare and research the airfoils ¹. In order to make the geometry investigation a bit easier due to time constraint, focus was put on the 4-digit NACA airfoils for now. These digits each represent a valuable parameter of the airfoil. The first two digits represent the camber of the airfoil, and the last two digits the thickness of the airfoil with respect to the chord length. As an example, NACA 4412 means that the airfoil has a 2% camber at 40 % of the chord length. The 12 stands for the 12 % thickness over chord ratio that the airfoil has.

9.3.1. Airfoil Thickness

A test was done to see what thickness would be the most beneficial for the airfoil at the Reynolds number that corresponds to the minimum cruise speed of the aircraft. The Reynolds number of the aircraft was estimated with [Equation 9.1](#). The program Javafoil was then used to investigate three airfoils of different thicknesses, but with the same amount of camber to see what thickness would be the most efficient. The efficiency of a particular airfoil is expressed in the so called lift over drag ratio (C_l/C_d). This ratio shows how much lift an airfoil is able to generate for the amount of drag that is generated. In short, the higher the lift over drag ratio the more efficient a particular airfoil is at generating lift.

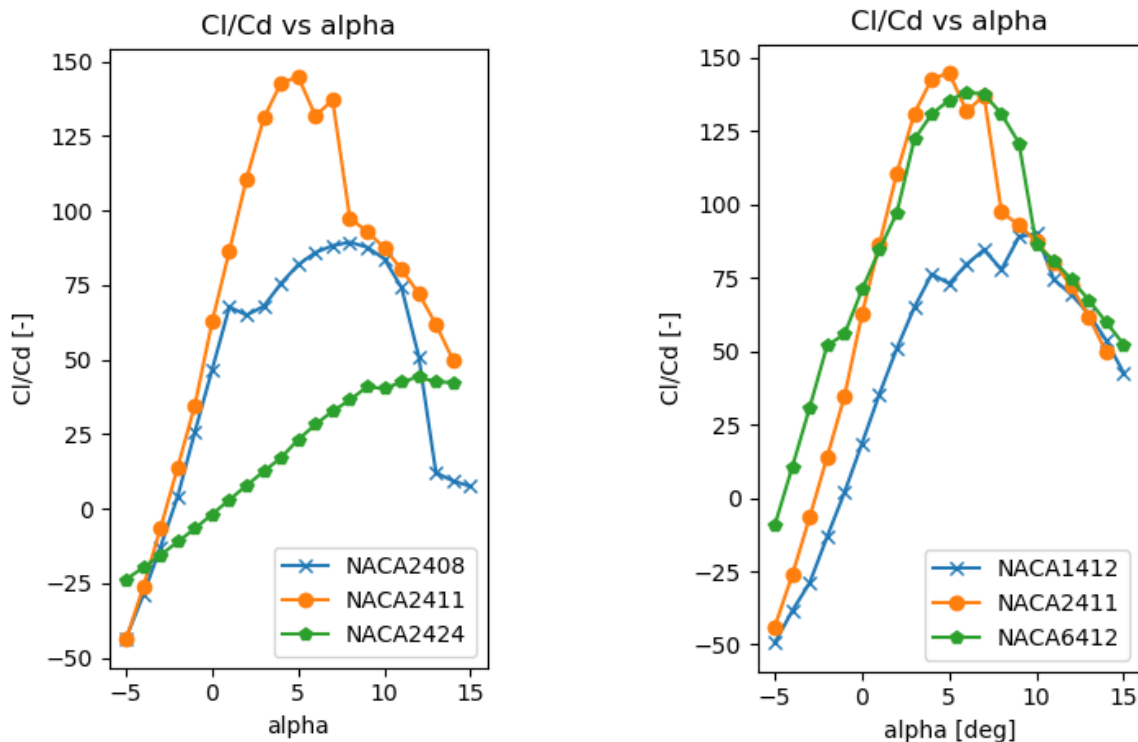
¹<http://www.airfoiltools.com/> [Accessed 29.06.20]

$$Re = \frac{Vc\rho}{\mu} \quad (9.1)$$

In Javafoil three airfoils were tested to see which would have the best lift over drag ratio at any particular angle of attack. The three airfoils that were investigated for the thickness are: NACA2408, NACA2411 and NACA2424. In a [Figure 9.1a](#), a python plot is shown which shows the effect of the thickness at a Reynolds number of 2,300,000. This is not the same as the current Reynolds number, however iterations through reasoning and the use of airfoil tools were done to make sure the arguments were still valid. From the figure it becomes clear that the middle ground with regards to thickness is the most suitable for the aircraft due to the high lift over drag ratio. Thus, an airfoil thickness of around 11% or 12% would be best.

9.3.2. Airfoil Camber

A similar test was performed to investigate what camber would work best for the aircraft. For this test, the NACA1412, NACA2412 and NACA6412 were chosen to perform the test on. The results can be seen in [Figure 9.1b](#).



(a) The airfoil thickness comparison, at $Re=2,300,000$.

(b) The airfoil camber comparison, at $Re=2,300,000$.

Figure 9.1: Hover lift efficiency versus disk loading

From the figure it actually turns out that the lift over drag ratio is very similar for a wide range of airfoils with a different camber. So, it was decided that another method had to be chosen to find the perfect airfoil. This was then done by researching airfoils with a high maximum lift coefficient and a wide drag bucket, to reach the best lift to drag ratio.

9.3.3. Maximum Lift Coefficient and Drag Bucket

The maximum lift coefficient ($C_{l_{max}}$) of an airfoil occurs at a particular angle of attack, after which the aircraft will start to stall. When this occurs, the airflow will start to get separated from the airfoil surface, which means that the airfoil will produce less lift. It is therefore also important to consider the drop of the lift coefficient after the maximum. For a few airfoil of a different camber with a constant thickness, the maximum lift coefficient is given in [Table 9.1](#). As can be seen, there seems to be a linear increase of the maximum lift coefficient with camber, which is why it is also important to take into account the width of the drag bucket.

Table 9.1: The maximum lift coefficients of a three airfoils with a constant thickness, but with varying camber [24].

Airfoil	$C_{l_{max}}$
NACA2412	1.6
NACA4412	1.64
NACA6412	1.7

Another aspect that is very important to select the most optimal airfoil is the width of the drag bucket. It is desired for this to be as wide as possible, such that a higher lift to drag ratio is available for more lift coefficient values throughout the flight. These discussed parameters, the width of the drag bucket, lift over drag ratio, and maximum lift coefficient are thus the most important factors that determine the airfoil to be chosen.

9.3.4. The airfoils of the main wing, canard and vertical tail

For the main wing, the airfoil NACA 4412 is selected due to its wide drag bucket, high lift over drag ratio and high maximum lift coefficient. Its representative polar curves are given in Figure 9.2². From a structural perspective the NACA 4418 airfoil was also considered to have more freedom for design in the Structural Department. However, after some iterations, it became clear this was not needed, and thus the airfoil that performs best aerodynamically was chosen. As a canard configuration is the case for this personal aircraft, a cambered airfoil is chosen as well. This was decided upon because of stability and control, which showed that a cambered airfoil for the canard is more beneficial than a symmetrical one to reduce upwash on the main wing [19]. The same reasoning as for the main wing regarding airfoil performance also counts toward the reasoning for the canard, therefore the canard also uses the NACA 4412 airfoil.

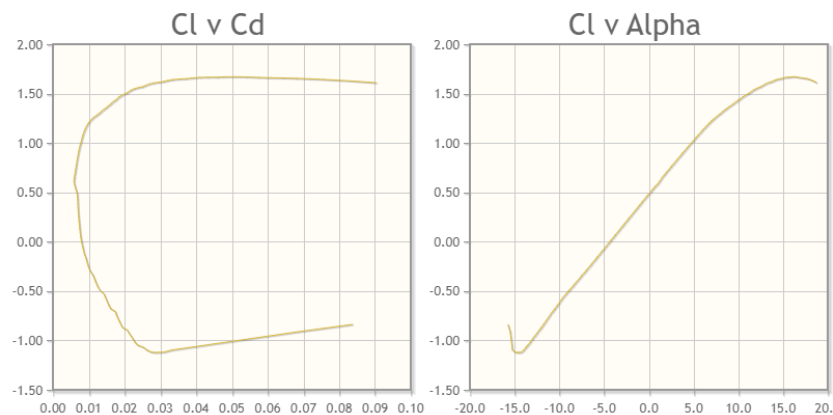


Figure 9.2: Polar curves of the NACA 4412 airfoil

For the vertical stabiliser, symmetric airfoils were considered as in symmetric flight, the vertical tail is not supposed to create lift. The vertical tail is only supposed to create lift if a side slip angle occurs on the aircraft due to a disturbance as an example. As the vertical tail has to perform well in the same Reynolds number as the other wings, the found optimal thickness of the airfoil of around 12% still applies. This is why the NACA0012 was selected for the vertical tail. During iterations, it also became clear the the cruise speed of the aircraft had to increase to 220 km/h (around 61 m/s). This is described in section 7.3. This means that the Reynolds number changed to about 4,000,000. However, the results that were presented so far remain valid as the testing again revealed the same results.

A summary table of all the airfoils of the aircraft can be seen in Table 9.2.

Table 9.2: A summary table with the wing surfaces and their corresponding airfoils.

Wing	Airfoil
Main wing	NACA4412
Canard	NACA4412
Vertical tail	NACA0012

²<http://www.airfoiltools.com/> [accessed on 29-06-20]

9.4. Lift and Drag estimation

In order to estimate the lift and drag characteristics, the Athena Vortex Lattice (AVL) program was used. Within this program it was possible to recreate the aircraft without the fuselage, so this means it included the canard, main wing, and vertical tail, as can be seen in [Figure 13.1](#). It is possible in AVL to create the fuselage as well, however this is a complicated process and not possible within the time frame. Therefore, the found lift and drag parameters are slightly different than they would be if a fuselage had been included, but this is justified as the wings and canard have the biggest impact on these parameters. Including the fuselage would increase the drag.

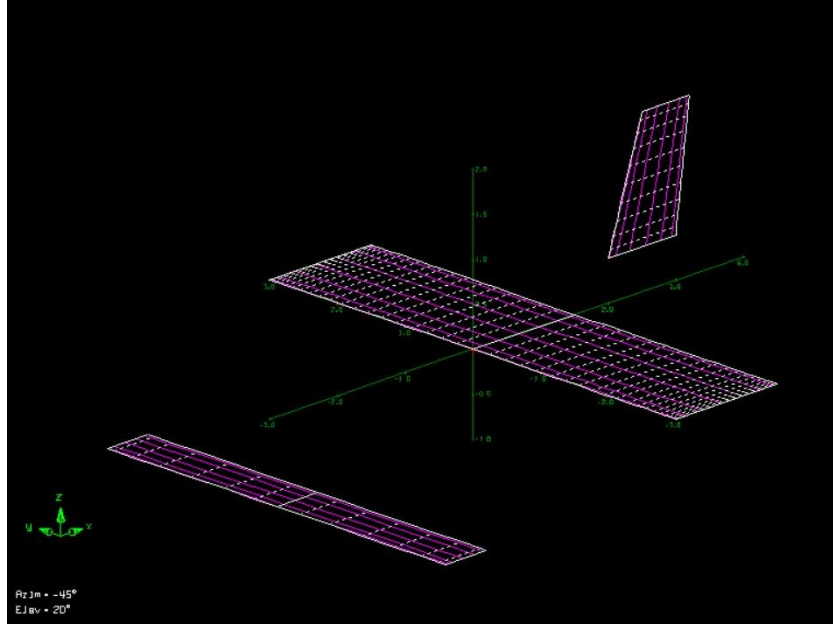


Figure 9.3: The personal aircraft programmed in AVL

After inputting the cruise values for the aircraft, including the cruise speed and density, and the NACA airfoils that were used, the program was able to output aerodynamic characteristics for different angles of attack. These aerodynamic characteristics were given both for the full aircraft and the individual parts. This way it was possible to determine the different parameters needed for the calculations done in [chapter 10](#). These parameters were the lift coefficients of the vertical tail C_{L_v} , of the canard C_{L_h} , and of the aircraft without the tail $C_{L_{A-h}}$, and their slopes. All of the lift coefficients were taken at the cruise angle of attack of 5 degrees. This was determined in AVL by plotting the lift to drag ratio for different angles of attack, and it was found that the highest lift over drag ratio occurred at 5 degrees. The program also outputs the drag coefficient at any point, using an input value for the zero-lift-drag coefficient (C_{D_0}). This value was determined using [Equation 9.2](#) and [Equation 9.3](#) with a Mach number of 0.19 and a wetted surface area of $7,95 \text{ m}^2$. The C_{D_0} is thus 0.003 [32].

$$C_{D_0} = C_f \cdot \frac{S_{wet}}{S} \quad (9.2)$$

$$C_f = \frac{0.455}{(\log_{10} Re)^{2.58} (1 + 0.144M^2)^{0.65}} \quad (9.3)$$

These input values have lead to the outputs given in [Table 9.3](#). With the outputs of AVL it was also possible to estimate the drag, which has been determined to be 302 N and is be used by the Propulsion Department to calculate the thrust needed. This drag value has been calculated from the cruise drag coefficient which was found to be 0.0199 in AVL. The overall $C_{L_{maxclean}}$ was determined to be 1.4.

Table 9.3: Output values from AVL

Parameter	Value
C_{L_h} [-]	0.664
$C_{L_{\alpha_h}}$ [1/rad]	4.75
$C_{L_{A-h}}$ [-]	0.287
$C_{L_{\alpha_{A-h}}}$ [1/rad]	2.99
$C_{L_{\alpha_v}}$ [1/rad]	3.7

10

Stability and Control

This chapter focuses on the stability and control of the design. Firstly, a functional and requirement analysis is performed to see what parts of the design need to be taken care of by stability and control. This will be described in [section 10.1](#) and [section 10.2](#). The loading diagram of the aircraft will be discussed in [section 10.3](#). How the aircraft will be made stable and controllable during the VTOL mode will be explained in [section 10.4](#). The wing configuration will become clear in this section. After this, the stability during flight in [section 10.5](#) will be discussed. In which, the horizontal stabiliser will be sized. The sizing of the vertical tail is discussed in [section 10.6](#). Next, some notes will follow on the ground stability in [section 10.7](#). Lastly, the sizing of the control surfaces is discussed in [section 10.8](#). For the sizing methods that have their own python sizing tool, a code verification (and validation if applicable) and sensitivity analysis is performed.

10.1. Functional analysis

A look is taken in [section 5.1](#) to see what functional tasks the stability and control (S&C) needs to take care of. Stability and control is important on the ground and in the air. In the air, the aircraft will need to be stable and controllable during VTOL mode and nominal flight. This means that the S&C plays a big roll in the blocks:

- ✈ F2.1.6: "Taxi to take-off area":
Ground stability particularly comes into play here.
- ✈ F2.1.9: "Perform take-off":
During the take-off, the aircraft will be in a pure VTOL mode, so stability and controllability during VTOL is important here.
- ✈ F2.2: "Cruise":
During the longest part of flight it is important that the aircraft is stable and controllable like any other aircraft.
- ✈ F2.1.10: "Transition to cruise":
During this phase, the aircraft will tilt its propellers forward to start gaining forward speed to make the wing generate lift. This is a critical phase where the aircraft is partly flying using its wings and partly in VTOL mode.
- ✈ F2.3.4: "Transition to landing phase":
Just like for the transition to cruise, the transition from cruise to the landing configuration needs to be performed just before the aircraft reaches its destination.

10.2. Requirement analysis

Following from the requirement that were set for this project, the aircraft design has to fulfil the following requirements when it comes to stability and control according to CS-23 [3]:

- ✈ **DSE-22-STAK-02:** The aircraft shall comply with the current safety and reliability requirements [6]: CS-23 and CS-27.
 1. The aircraft shall be stable during all phases of flight (CS-23.171) [3].
 2. The aircraft shall be controllable during all phases of flight (CS-23.171) [3].
 3. The aircraft shall have a minimum roll rate of 60 degrees in 1.3 seconds [31].
 4. The aircraft shall have a particular amount of rotational angular acceleration during rotation of 4 to 5 °/s² (CS-23.51d) [3].
 5. The aircraft shall be stable and controllable after an engine failure (CS-23.147) [3].

All phases of flight include taxi, take-off, transition, cruise and landing. Also note that CS-23.171 and CS-23.147 summarise the requirements necessary for stability and control during flight and an engine failure situation. These regulations are to extensive to all mention in this report.

10.3. Loading diagram and CG range

To make the aircraft stable and controllable in flight, the main wing and horizontal stabiliser need to be at a specific position. To determine these positions, it is important to know what the range of the center of gravity (cg) range of the aircraft is. The cg range and positions is also important to know when positioning the landing gear. To determine this cg range, investigating what components can be loaded on the aircraft that will alter the cg position of the operational

empty aircraft is needed. The cg of the aircraft is only able to shift due to two components: fuel and payload. In [chapter 4](#) the masses of these individual components are mentioned.

The cg position shift will depend on where each individual components will have its cg position. When a particular component is loaded on the aircraft, the new aircraft cg position can be determined using the [Equation 10.1](#). This equation can be derived from moment equilibrium of all particular components loaded to the aircraft. The moment equilibrium equation is then rearranged to obtain [Equation 10.1](#).

$$x_{cg_{i+1}} = \frac{(x_{cg_0} m_0 + x_{cg_i} m_i)}{m_0 + m_i} \quad (10.1)$$

The subscript i indicated the current mass or cg position of a particular component. The subscript 0 indicated the last cg position of mass. Lastly, $i + 1$ indicated the new mass or cg position.

The new mass can be calculated by summing the masses of the particular components that are loaded into the aircraft, as can be seen in [Equation 10.2](#).

$$m_{i+1} = m_0 + m_i \quad (10.2)$$

The range of the cg positions can be determined by looking into all possible orders that particular components are loaded onto the aircraft. In the case of the personal aircraft design, there are only two possible ways to load the two components onto the aircraft: first the payload is loaded onto the aircraft and the fuel is loaded afterwards, or the other way around.

The cg positions are expressed in a percentage of the mean aerodynamic chord (%MAC). This because the stability of the aircraft is really dependant on positions like the neutral point (np), center of pressure (cp) and aerodynamic center (ac) with respect to the cg positions. As the np, cp and ac are usually expressed in %MAC, the same is done for the cg positions.

The Cartesian coordinate system is generally used during the design. The x coordinate is defined as zero at the nose of the aircraft and positively increases towards the rear of the aircraft. To convert from the x coordinate system to the MAC coordinate system, [Equation 10.3](#) can be referred to.

$$x[\%MAC] = \frac{x[m] - x_{LEMAC}}{MAC} \quad (10.3)$$

A python tool was created to create a plot of the loading diagram. The tool also outputs the cg range of the aircraft. First, the tool considers one of the possible loading situations and calculated the new cg position and weight of the aircraft. Then, its does the same for the other loading situation. The most forward and aft cg positions are given as an output, as the cg range of the aircraft during loading.

In [Table 10.1](#), the input values can be seen that produced the loading diagram and the cg range of the personal aircraft.

Table 10.1: The input values used to produce the loading diagram of the personal aircraft.

CG position	Value [m]	Masses	Value [kg]
$x_{cg_{OEW}}$	2.5	OEW (m_0)	585
$x_{cg_{payload}}$	2.7	Payload mass ($m_{payload}$)	150
$x_{cg_{fuel}}$	3	Fuel mass (m_{fuel})	40

The [Figure 10.7](#) contains the loading diagram of the personal aircraft. It shows that the maximum cg range of the aircraft is given to be: 0.043 %MAC, with a maximum forward positioned cg of -0.8273 and a maximum aft cg position of -0.7843 %MAC.

10.3.1. Loading diagram code verification

With regards to the code of the loading diagram, a function was created called: "Potato". This function takes the position of the leading edge of the MAC (x_{LEMAC}) as its only numerical input. The output is the cg range as well as a plot of the loading diagram.

The verification will be structured in terms of unit tests to see if the small building blocks have been implemented correctly. After this a few small units will be combined in blocks and tested separately. Lastly, a system test will be performed to see if the entire code works as intended.

Unit tests

Firstly, it was checked if the equations that calculate the new masses and cg positions were implemented correctly. This was done by checking the equation syntax in the code. In other words, were the equations implemented correctly in the code? No discrepancies were found here.

The same thing was done for the code used to plot the loading diagram. This plot will be used for the next step of the verification. The plot will also present the actual loading diagram of the aircraft. This is why the code was checked to make sure that the loading diagram will get the desired lay-out. Here again, no discrepancies were found.

Block tests

As a block test, the plot of the loading diagram was used. When a particular component was loaded. It was checked if the mass and cg position changed as expected. For example, the cg of the empty aircraft would be in the middle of the aircraft and some payload is loaded in front of the aircraft. It is expected that the total mass increases and the cg position of the aircraft will shift forward, towards more negative %MAC coordinates. According to the plots, the tests that were performed always matched the expectations.

System test

As this is a relatively small code, the two building blocks can immediately be combined to check if the whole code works properly. This is why no separate block tests were performed.

For this system test, a plot was created for the cg range for all possible locations of the leading edge of the MAC (x_{LEMAC}). What is expected to be seen is that the cg range varies linearly over the length of the fuselage. This is because the loading only consists of two components: payload and fuel. In normal loading diagrams, the cg range itself also changes over the length of the fuselage due to the multiple rows of passenger seats that need to be loaded. As in this situation, only one passenger is loaded, it is expected that the cg range has the same length over the entire fuselage length [16]. In [Figure 10.1](#), the verification result is shown.

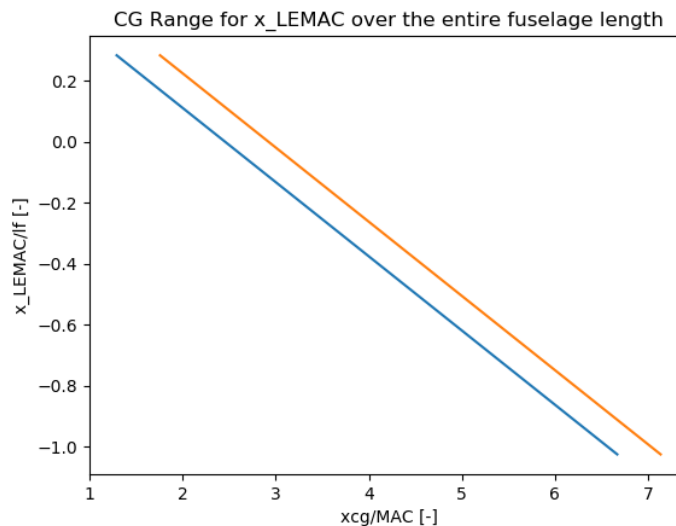


Figure 10.1: The CG range for a x_{LEMAC} over the entire fuselage length.

The result is expected, the cg range varies linearly over the fuselage length. The cg range also has the same width, which is also expected.

10.3.2. Loading diagram code validation

For the validation of the loading diagram code, data of an existing general aviation aircraft was used as this data is readily available. The general aviation aircraft which was used is the Diamond DA40. With the help of the DA40 operational manual, the cg range was calculated. In addition, the code was also used to calculate the cg range. Both

results can be directly compared to see if the code achieves the same result as the method of the operational manual. [Table 10.2](#) contains the data that was used for both methods to determine the cg range.

Table 10.2: The input values used for the code validation of the loading diagram tool.

Input	Value	Unit
OEW	900	kg
Payload mass	150	kg
Fuel mass	84	kg
$x_{cg_{OEW}}$	2.496	m
$x_{cg_{payload}}$	2.3	m
$x_{cg_{fuel}}$	2.63	m
MAC	1.121	m
x_{LEMAC}	2.194	m
length fuselage	8.007	m

To make this calculation applicable to the situation of the personal aircraft, it is assumed that the DA40 also only carries payload in the front seat. It is also assumed that the aircraft carries the fuel in its wings and does not make use of any other tanks. The MAC was assumed to be positioned at the position of the wing root, as the aircraft has a very small sweep angle of 1 degree.

The method for calculating the cg position as described in the operational manual was used to calculate the most forward and backward cg position while the aircraft is being loaded. The operational manual uses the nose of the aircraft as its datum. The method in the operational manual is based on determining the moments created by all the separate components. Then, in the end, the total moment is divided by the total mass to obtain the new cg of the aircraft.

The most forward cg would be created by loading the payload first. In [Table 10.3](#) the calculation is shown as done in the operational manual.

Table 10.3: The forward cg position as determined by the DA40 operational manual.

Component	x [m]	m [kg]	M [kgm]
OEW	2.496	900	2246.4
Payload mass	2.3	150	345
Total	2.468 (= 0.245 %MAC)	1050	2591.4

Note that the forward cg value is also expressed in terms of %MAC.

The same thing was done for the aft cg position, [Table 10.4](#) contains the results.

Table 10.4: The most aft cg position as determined by the method in the operational manual for the DA40.

Component	x [m]	m [kg]	M [kgm]
OEW	2.496	900	2246.4
Fuel mass	2.63	84	220.9
Total	2.507 (= 0.2796 %MAC)	984	2467.3

The MTOW and final cg position are presented in [Table 10.5](#).

Table 10.5: The cg position at MTOW for the DA40 after loading is completed.

Component	x [m]	m [kg]	M [kgm]
OEW	2.496	900	2246.4
Payload mass	2.3	150	345
Fuel mass	2.63	84	220.9
Total	2.480 (= 0.255 %MAC)	1134	2812.3

Now the same thing was done using the loading diagram tool. The output can be found in Figure 10.2. The cg range calculated by the tool was given to be 0.244 %MAC for the forward cg and 0.2796 %MAC for the most aft cg. The final cg position as determined by the tool is 0.255 %MAC.

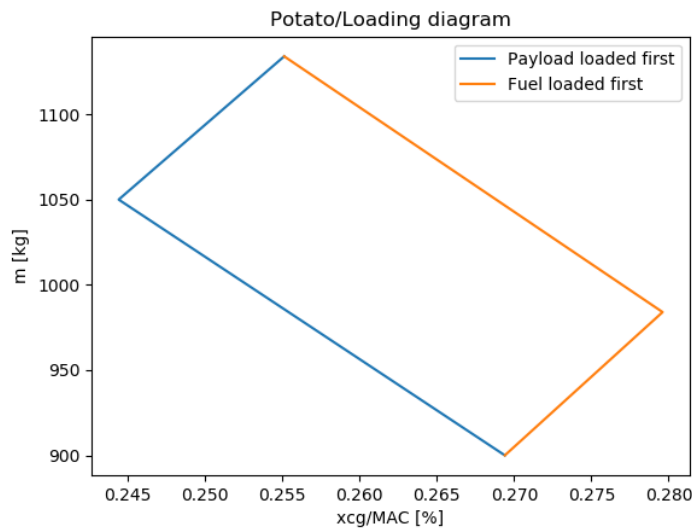


Figure 10.2: The plot created by the loading diagram tool using the DA40 data.

The code has the exact same output as the method used in the operational manual.

10.3.3. Loading diagram sensitivity analysis

The parameter that has the most effect on the width of the cg range is the overall difference in cg positions and masses of the individual components. The further apart the cg positions, the larger the moment arms for the weight to act on. The same goes for the masses, the larger the differences masses, the larger the moment created by these weights.

The position of the cg range is mostly linked to the position to the position of the cg of the operational empty aircraft. This is logical as this is the cg position with the biggest weight assigned to it. Small masses will this not be able to relocate the cg of the aircraft as much.

10.4. Stability and controllability during VTOL and wing configuration

For stability and controllability in the air, two separate conditions can be identified: Stability and controllability during VTOL and nominal flight (mainly cruise).

One can imagine that during VTOL, the aircraft does not have any forward speed. This means that the wings do not generate any lift and therefore the stability and controllability of the aircraft during VTOL is fully dependant on the thrust created by the engines which will be placed at the tips of the wings. The propellers are placed at the wing tips such that they encounter the least disturbed free stream flow.

The wings of the personal aircraft will be positioned in a canard configuration. This means that the horizontal stabilising surface will be positioned in front of the main wing as oppose to at the rear like conventional aircraft. Generally, canard aircraft have their main wings positioned more towards the rear and the horizontal stabiliser positions more towards the nose of the aircraft. This means that the horizontal wing surfaces will be positioned further apart compared to conventional aircraft. In addition, the cg range of canard aircraft lie just in front of the main wing, instead of on the MAC for conventional aircraft. This is beneficial for stability during VTOL, as the propellers need to generate less thrust.

In [Figure 10.3](#), a conventional tail configuration aircraft with propellers at the end of its main wing and conventional horizontal tail tips is sketched during a VTOL situation. The cg position of the aircraft is in front of the main wing and the horizontal stabiliser. This situation is referred to as situation 1.

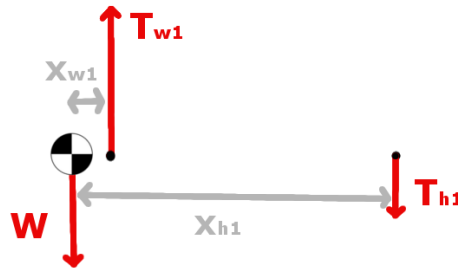


Figure 10.3: Situation 1: The force equilibrium situation during VTOL for a conventional tail configuration aircraft. Note, the forces are not to scale.

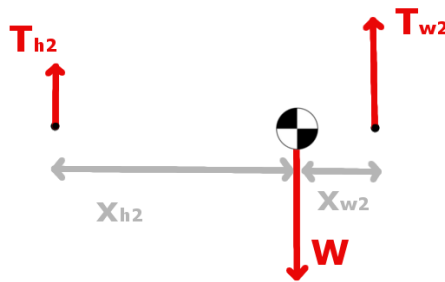


Figure 10.4: Situation 2: The force equilibrium situation during VTOL for a canard configuration. Note, the forces are not to scale.

In [Figure 10.4](#), situation 2 is sketched. Situation 2 is a canard configuration aircraft with propellers at the tips of the main wing and canard. The cg of the aircraft is located in front of the main wing, but behind the horizontal stabiliser.

When looking at force and moment equilibrium, it can be seen that the moment equilibrium equation, taken around the cg, is the same for both situation 1 and 2. However, the force equilibrium functions are different, as can be seen in [Equation 10.4](#) and [10.5](#). If the force equilibrium equations are rearranged, it can be concluded that less thrust force is needed in situation 2 to keep the aircraft stable during VTOL. In situation 1, the thrust on the main wing needs to fight the downward force of the weight as well as the tail thrust. In situation 2, the main wing and canard thrust both fight the weight of the aircraft. Going for the lower thrust option allows for a lower usage of resources such a fuel and means that the electric motors powering the propellers can be smaller.

$$1: T_{w1} = W + T_{h1} \quad (10.4)$$

$$2: T_{w2} + T_{h2} = W \quad (10.5)$$

Another good thing about the canard configuration is that because both wing surfaces create upward lift, the wings both contribute to creating positive lift for the aircraft. This means that the main wing no longer has to create all the lift required to keep the aircraft in the air and the wing surfaces for the canard configuration aircraft will be smaller compared to the conventional horizontal tail configuration.

For these reasons, the canard configuration is chosen as the wing configuration for this personal aircraft. In addition, the customer is interested in a futuristic looking aircraft. A canard configuration achieves this goal as not many aircraft have this wing configuration.

The reasons why many aircraft do not have this configuration is because it is harder to make the canard configuration stable and controllable during flight. The design space for a stable and controllable canard configuration is smaller

compared to a conventional tail configuration [16]. How the aircraft will be made stable and controllable during flight is discussed in [section 10.5](#).

During VTOL mode, it is extremely hard for the pilot to focus on where he/she is going to land and keeping the aircraft stable during the landing. This is why a control system will be designed that keeps the aircraft stable during the VTOL mode. It will do this by manipulating the thrust on all the four motors at the wing tips. This way, the pilot can focus on landing the aircraft in the correct position.

Between the VTOL mode and forward flight, there is a phase where the aircraft transitions from VTOL mode to forward flight mode. During this transition, the rotors will slowly tilt forward as the aircraft gains forward speed. When the propellers on the canard tilt forward, the prop wash of the propellers risk to hit the main wing of the aircraft. To avoid this problem all together, the main wing will be positioned high on the fuselage.

This means that the personal aircraft will have high wing, canard configuration.

10.5. Stability and controllability during flight

For stability during flight, use is made of a tool called the X or scissor plot [16]. The X-plot helps to determine the positions of the main wing and canard as well as the canard size to achieve stability and controllable during flight.

In the X-plot, consists of a plot where the canard size ratio with respect to the main wing (S_h/S [-]) is plotted against the x coordinate of the cg position of the aircraft in terms of %MAC (x_{cg}/MAC [%MAC]). The X-plot will show the feasible design space for a horizontal tail size and cg position range.

The controllability limit line is defined by [Equation 10.6](#) and the stability line if defined by [Equation 10.7](#) [16].

$$\frac{S_h}{S} = \frac{1}{\frac{C_{L\alpha_h}}{C_{L\alpha_{A-h}}} (1 - \frac{d\epsilon}{d\alpha}) \frac{l_h}{c} (\frac{V_h}{V})^2} x_{cg} - \frac{x_{ac} - SM}{\frac{C_{L\alpha_h}}{C_{L\alpha_{A-h}}} (1 - \frac{d\epsilon}{d\alpha}) \frac{l_h}{c} (\frac{V_h}{V})^2} \quad (10.6)$$

$$\frac{S_h}{S} = \frac{1}{\frac{C_{L_h}}{C_{L_{A-h}}} \frac{l_h}{c} (\frac{V_h}{V})^2} x_{cg} - \frac{\frac{C_{m_{ac}}}{C_{L_{A-h}}} - x_{ac}}{\frac{C_{L_h}}{C_{L_{A-h}}} \frac{l_h}{c} (\frac{V_h}{V})^2} \quad (10.7)$$

The X-plot of a conventional configuration aircraft looks something like what can be seen in [Figure 10.5](#). The design space for the horizontal stabiliser is located on top of the controllability and the stability line. It forms an up side down triangle. The green line in the figure is the cg range in this example. For a particular cg range and position, a particular tail size can be selected in the X-plot to make the aircraft stable and controllable in flight.

As can be seen, the equations contain lift coefficients and lift coefficient gradient. Their subscripts indicate that they are lift coefficients and gradient of main instead of the aircraft. This data was obtained from the aerodynamics department, where AVL was used to estimate these lift coefficients and gradients.

Other important things to note is that for the canard configuration the tail length (l_h) is negative by definition, as the tail is located in front of the main wing. The downwash and angle of attack gradient ($\frac{d\epsilon}{d\alpha}$) is zero for a canard configuration as the canard is not affected by the downwash created by the main wing. This also means that the main wing and canard encounter the same air flow. This means that the airflow ratio of the canard with respect to the main wing (V_h/V) is equal to 1. The stability margin (SM) is implemented for extra safety.

These differences are the reason that the X-plot of a canard configuration aircraft looks different from the X-plot of a conventional configuration aircraft. An example of an X-plot of a canard configuration aircraft can be seen in [Figure 10.6](#). The feasible design space is not located between the controllability and stability line above the point where the two lines cross. As can be seen, the design space for a stable and controllable canard configuration is much smaller compared to the design space of an aircraft with an conventional horizontal stabiliser. As said in [section 10.4](#), it will be harder to make the aircraft stable in flight due to this smaller design space. This is price that was payed for stability and a lower thrust level during VTOL mode.

To be able to easily design the canard size and position, a tool for the X-plot was created in python. This tool consists of four functions. The first two functions define the control and stability lines in the X-plot. These functions calculate the tail size ratio for a particular location of the cg. These points are saved in lists such that the following function can easily plot the points to visualise the X-plot. The function TailSize uses the location of the main wing and the cg range determined by the loading diagram python tool to determine the tail size for that situation. Lastly, the function called ShSmin calculated the minimum tail size for the given inputs. This means that this function can optimise the

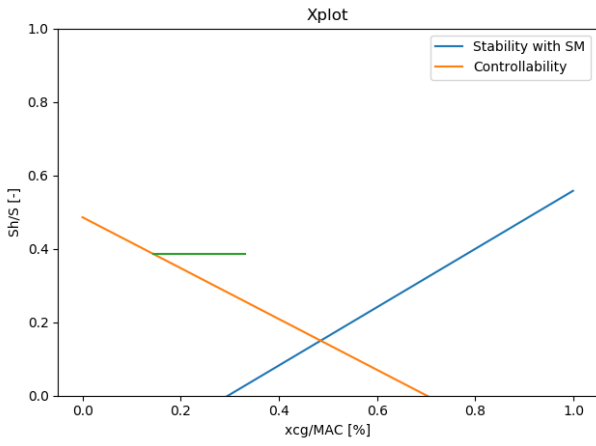


Figure 10.5: An example of an X-plot of a conventional configuration aircraft

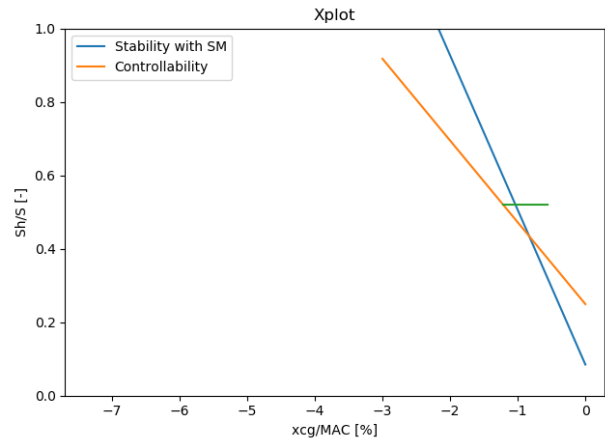


Figure 10.6: An example of a X-plot of a canard configuration aircraft.

cg position and the location of the wing in order to obtain the smallest possible canard size.

The X-plot of the personal aircraft is given in Figure 10.7 and 10.8. The main wing will be positioned at 3.741 m from the nose and the canard will be positions at the very tip of the nose of the aircraft.

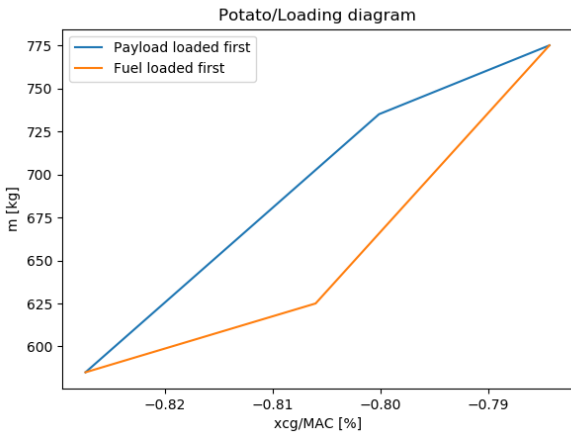


Figure 10.7: The loading diagram of personal aircraft.

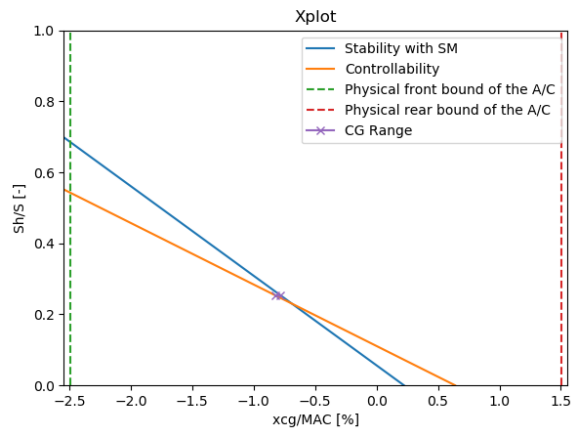


Figure 10.8: The X-plot of personal aircraft.

According to the given X-plot, the final dimensions of the geometry of the canard can be found in Table 10.6.

Table 10.6: The final dimensions of the canard.

Parameter	Value	Unit
S_h/S	0.254	-
b_h/b	0.635	-
c_h/c	0.4	-
S_h	2.286	m^2
b_h	3.81	m
c_h	0.6	m
AR_h	6.35	-

10.5.1. X-plot code verification

The verification will be done in terms of unit, block and system tests.

Unit tests

The standard unit tests of checking if equations such as the stability and controllability equations were implemented correctly were performed. As well as making sure that the conversion from the x coordinate in meters to %MAC worked as intended. No discrepancies were found.

Block tests

The controllability and stability functions that define the controllability and stability limits were tested to see if they produced the correct output. This was tested with some data from a course called SEAD [16] of the Delft university of Technology. One of the ways to check this is to see if the lines cross x-axis of the X-plot in the correct locations. The stability line should cross the x-axis at: $x_{ac} - SM$.

The controllability line should cross the x-axis at: $x_{ac} - \frac{C_{mac}}{C_{L_{A-h}}}$.

In addition, the slope is checked to see if the line calculates the correct positions in the X-plot. These things were all confirmed by looking at a plot of the X-plot. The functions worked as intended.

The next thing that was checked is how the code determines the corresponding tail size. For the calculated cg range by the loading diagram tool, the tail size was determined where the cg range would be above the controllability line. This means it would be in the feasible design space. For the tail size to be a feasible solution, the whole cg range needs to fit in the design space. So it was checked if the most aft cg position in the cg range did not lie outside the design space on the right side of the stability line. This check was performed for many cg ranges. The code would always return that there is no feasible solution in the form of a string, if the cg range did not fit inside the design space or it would need to have a canard bigger than the main wing (in other words $S_h/S > 1$).

The last function that needed to be tested was the function that locates the minimum tail size for a particular cg range. Here, the same check was performed as for the previous function. I needed to be checked in the selected cg range would fit in the design space. However, here it also needed to be checked if the selected tail size really was the theoretical minimum as proposed by the X-plot. This was checked by doing the analysis again for the last previous points that the function discarded as minimum tail sizes. It was checked if the margin between the cg fitting in the design space indicated that the cg was outside the design space. It was also checked if this margin becomes bigger for points further away from the indicated minimum. This was confirmed after manual analysis.

System test

To see if the entire code works as intended, only the last function was considered. This is the function that was able to determine the minimum tail size for a particular cg range as input. The reason this works as a system test is because this ShSmin function uses all the previously defined functions in the code. If this function works, it proves that all the other functions also work together correctly.

This system test was performed by creating a plot, where the tail size points considered by the program are visualised. This way it can easily be tracked what points the program considered, but it can also clearly be seen where the program stopped.

The plotted points help to identify the actions the program takes to identify the minimum tail size. It can also clearly be seen that the program gives a tail size that is in the feasible design space and not in the space between the lines below the point where they cross. The cg range is not that wide in this case, so the program could have also chosen a point in the non feasible design space where the cg range fits between the lines. This plot proves that the program does what it is supposed to do and properly selects a minimum tail size in the feasible design space.

10.5.2. X-plot code validation

The validation of the code for the X-plot will be done using data of a canard aircraft that has a similar size as the personal aircraft: the Rutan VariEze. A picture of the aircraft is shown in [Figure 10.11](#)¹.

For the validation, input data was compiled using online sources. This online data is then fed into the X-plot code to see if the real tail size of the Rutan VariEze is comparable to the tail size that the code calculates.

The following assumptions were made with regards to the input data for the Rutan VariEze:

- ✈ The aerodynamic centre was assumed to be at 25% of the MAC.
- ✈ The MAC length was calculated by taking the average of the tip and root chord of the aircraft:

$$MAC = \frac{c_t + c_r}{2}$$

¹<https://www.eaa.org/aaa/aircraft-building/kits-and-plans/h—l/long-ez>, [Accessed 21.06.2020]

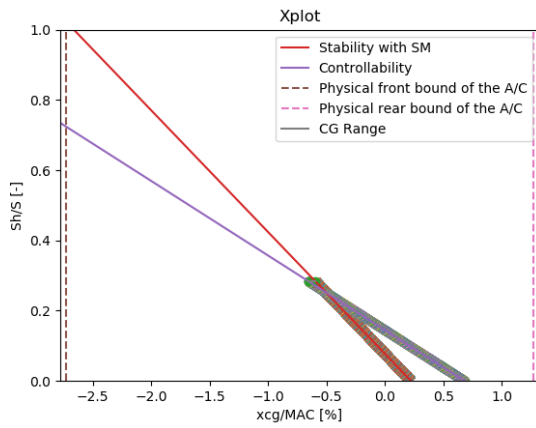


Figure 10.9: The X-plot with the considered tail size points visualised on the stability and control lines.

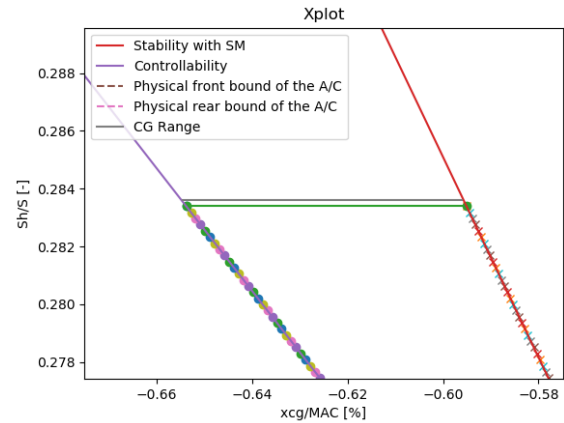


Figure 10.10: A zoomed in X-plot with the visualised tail size points.



Figure 10.11: The Rutan VariEze aircraft in flight

- ✈ The pilot and the luggage cg location were assumed to be positioned in the same spot.
- ✈ The location of the MAC ($x_{LEM\text{AC}}$) is assumed to be positioned at the same x position as the back of the cockpit window [36].

In Table 10.7, all the Rutan VariEze input data that was used for the validation can be found. Note that all the cg positions have the nose of the aircraft as a reference.

Table 10.7: The validation input data of the Rutan VariEze.

CG location data		Source	Mass data		Source
x_0 [m]	2.794	[36]	OEW [kg]	242.76	[36]
$x_{payload}$ [m]	2.032		$m_{payload}$ [kg]	145.15	
x_{fuel} [m]	2.616		m_{fuel} [kg]	106.59	
Dimension data			Aerodynamic data		
$x_{LEM\text{AC}}$ [m]	3.175	[36]	$C_{m\alpha}$ [-]	0	[42]
x_{ac} [%MAC]	0.25		C_{L_h} [-]	0.15	
MAC [m]	2.032		$C_{L\alpha_h}$ [rad^{-1}]	0.9004	
l_h [m]	-2.7		$C_{L_{A-h}}$ [-]	0.35	
l_f [m]	4.928		$C_{L\alpha_{A-h}}$ [rad^{-1}]	5.239	

In Figure 10.12 and 10.13, the loading diagram and the X-plot of the Rutan VariEze can be found. These plots were created by the X-plot tool.

Most of the data was found in the owner's manual of the VariEze [36]. The wing and canard surface area are mentioned,

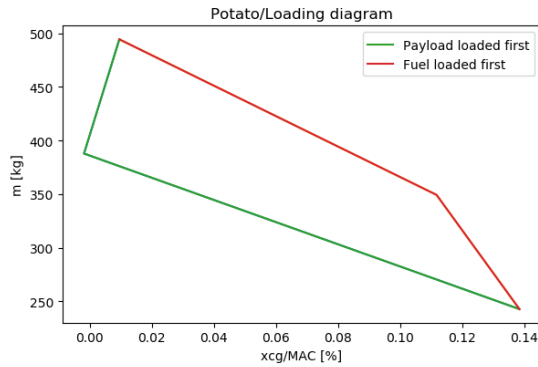


Figure 10.12: The loading diagram of the Rutan VariEze that the X-plot tool created.

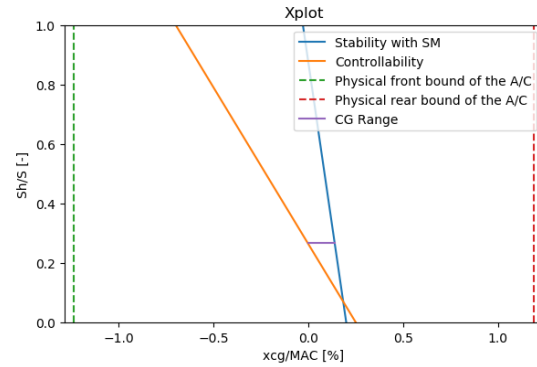


Figure 10.13: The X-plot of the Rutan VariEze that the X-plot tool created.

which gave the aircraft a tail size ratio of: $S_h/S = 1.14/4.98 = 0.229$.

According to the X-plot tool the tail size ratio is equal to: $S_h/S = 0.266$. The tail size ratio only differs with an error of around 16% from the one obtained from the owner's manual. However, this error is expected to mostly be caused by the aerodynamic data. This data was read from graphs in the document which contained data on the wind tunnel testing of the Rutan VariEze [42], which was really hard to do accurately as all the aerodynamic graphs were drawn by hand.

The error can also have occurred due to the assumptions that were made to be able to do this calculation. For example, the leading edge location of the MAC might be quite wrong. However, the X-plot tool also outputs the leading edge location of the MAC together with the minimum tail size ratio. Compared to the value of 3.175 m that was used for the leading edge of the MAC. However, after iterating the tail size a few times, the code showed the leading edge location of the MAC is at 2.513 m from the nose for the already mentioned minimum tail size ratio. This shows that the assumption of the leading edge of the MAC location was wrong. However, the code corrected for it itself.

Due to this reasons, there is still a high confidence level that the X-plot code is able to determine the tail size accurately.

10.5.3. X-plot sensitivity analysis

After a lot of experimenting with the code. It became clear that the X-plot method most sensitive to changes in the cg range. A small change in cg range can drastically change the minimum tail size. This is logical as a small cg range means that it will be easier to fit the cg range between the controllability and stability lines. Because of this, it was decided to keep the cg range as small as possible. This is why it was decided to place the fuel in a tank close to the pilot instead of in the wings. The fuel in the wings drastically increased the tail size of the aircraft due to a wider cg range. By keeping the cg positions of the payload and fuel close to each other, the cg range can be made less wide.

The next thing the X-plot method is sensitive to is the ratio between the lift coefficients and lift coefficient gradients. This is because this ratio greatly affects the slope of both lines. Situations were encountered that for certain lift coefficient gradient ratios, the controllability line's slope would be too high. So high that it did not even cross the stability line, which means that no feasible design space exists. However, the ratio could also have a very positive effect in the sense that it would create a very shallow slope, which creates a very large design space.

Another parameter that greatly influenced the slopes of the controllability and stability lines is the tail arm (l_h). Smaller values for the tail arm created small design spaces as well as tail sizes. The larger the tail arm length, the smaller the tail sizes. This is logical as a large tail arm creates large moment arms. The larger the moment arm the smaller the amount of force required to generate a particular moment. This is why it is the most beneficial to position the canard at the most forward position on the aircraft. However, structurally, it needs to be possible to position the canard as far forward as possible.

10.6. Vertical tail sizing

A vertical tail is important to counter disturbances that create a side slip angle for the aircraft during flight. Side slip angles can be created by wind gusts. However, the situation that is critical for designing the vertical tail is asymmetric thrust during nominal flight. In the case of the personal aircraft, asymmetric thrust could occur during an engine failure or when one side of the aircraft produces a different amount of thrust compared to the other side.

Because the engines of the aircraft will be very powerful, very large asymmetric thrust situations could occur during the event of an engine failure. This is especially true for during the VTOL mode. This is why the idea of a control system was introduced that is able to sense abrupt changes in thrust and will determine the best possible solution in terms of making other propellers generate less thrust. If the control system does this in a timely manner the time that the aircraft will be exposed to differential thrust will be minimised. This idea is feasible as the aircraft has four electric motors that all drive a propeller. The risk that more than two electric motors fail at the same time is extremely unlikely. This is why it is deemed possible to lower the thrust created by one motor to limit the differential thrust. It will also limit the maximum differential thrust that the aircraft will be exposed to. This maximum differential thrust is very important when it comes to the sizing of the vertical tail.

The sizing of the vertical tail as done using a method from the SEAD course of the Delft University of Technology [16]. In Figure 10.14, the method for sizing the vertical tail for a propeller aircraft is shown.

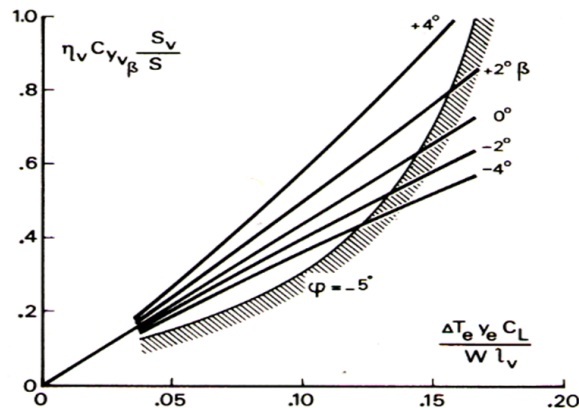


Fig. 9-22. Effect of sideslip on vertical tailplane area required to cope with engine failure

Figure 10.14: Vertical tail sizing figure [16].

First, the value on the x-axis of the of Figure 10.14 is determined. The following parameters were used to determine the x-axis value. Some assumptions are also mentioned.

- ✈ The differential thrust (ΔT_e) was assumed to have a maximum value of 92 N. It is thus assumed that the control system is able to equalise the thrust on both sides of the aircraft before the maximum differential thrust is reached. The 92 N was experimentally obtained by playing with the code and seeing what the corresponding tail size would be. The differential thrust was fixed at the point where the engineers found it to be acceptable. Note that the differential thrust is not only caused by the engine that is still running, but also by the drag created by the inoperative engine.
- ✈ The arm of the differential thrust (y_e): is equal to half the span: $b/2 = 3.5m$.
- ✈ The lift coefficient in the figure is the lift coefficient of the aircraft during cruise (C_L) [16]. This includes the effects of the canard and main wing.
- ✈ The Weight (W) is assumed to be the minimum weight during cruise, as this will create the largest possible tail size. The weight is assumed to be equal to the OEW and the payload mass: $W = OEW + m_{payload}$. This will slightly over estimate the size of the vertical tail. Using the most critical weight is set by CS-23.147(b) point VI [2].
- ✈ Lastly, the vertical tail arm (l_v) indicated the position where the side force created by the vertical tail acts. It is assumed to be all the way at the back of the fuselage. Just like the horizontal tail, the vertical tail arm is defined from the leading edge of the MAC of the main wing: $l_v = l_f - x_{LEMAC}$, where l_f is the length of the fuselage.

In the figure a few lines with particular a side slip angle are presented. This is the side slip angle at which the aircraft continues its flight after the engine failure. This is selected by the engineers. Note that the bigger you choose this equilibrium side slip angle, the larger the vertical tail becomes. A negative side slip angle means that the aircraft side slips towards the side of the broken engine, which the aircraft will do naturally. Thus this requires a small tail size. A positive equilibrium side slip angle means that the aircraft slips towards the still operational engine. Note that a bigger vertical tail is necessary for this.

Differential thrust will at first create a yawing moment. As the yawing and rolling motion are coupled, the yawing moment will also induce a bank moment. The tail size is limited by an initiated bank angle due to the engine failure of 5 degrees according to the figure.

When the x-axis value is determined and the equilibrium side slip angle is selected, the appropriate vertical tail size parameter can be read of from the y-axis of the figure. So obtain the vertical wing size, the y-axis parameter needs to be divided by a few other parameters:

- ✈ The ratio of airflow across the vertical tail compared to the free stream velocity (η_v): this value was assumed to be equal to 0.96 [16].
- ✈ The slope of the lift curve of the vertical tail. This lift coefficient gradient can be assumed to only depend on the aspect ratio of the vertical tail as vertical tails of aircraft generally have low aspect ratios: $C_{L_{\alpha_v}} = \frac{\pi}{2} AR$. This means that the side force created by the vertical tail will depend on the span of the vertical tail instead of the surface area [16]: $Y = L_v = \rho q C_{L_{\alpha_v}} \beta = \rho q \frac{\pi}{2} AR \beta = \frac{\pi}{2} b^2 \beta q$.

This method was put into python code to make it easy to iterate the vertical tail size. From the figure, it can be seen that all lines corresponding to a particular equilibrium side slip angle all go through the origin of the figure. This is convenient for putting the lines in code. The slopes of all lines were determined using their highest value on the graph and the coordinate of the origin. The function in python calculates the x-axis parameter for a specified vertical tail span and equilibrium side slip angle. Then using the correct line, it determines the y-axis parameter from which it calculates the corresponding vertical tail size.

The final geometry parameters of the vertical tail are given in [Figure 10.14](#).

Table 10.8: The final dimensions of the vertical tail.

Parameter	Value	Unit
S_v/S	0.105	-
b_v/b	0.173	-
c_v/c	0.607	-
S_v	0.947	m^2
b_v	1.04	m
c_v	0.910	m
AR_v	1.14	-

10.6.1. Vertical tail code verification

As the vertical tail sizing is quite a preliminary method, the verification and validation of this method will be limited. The main thing that could be verified is the correct implementation of this method into the code.

The first thing that was checked was the correct calculation of the x-axis and y-axis parameters. They were just checked by inspection. No discrepancies were found.

The next and last thing that can be checked is the correct implementation of the equilibrium side slip lines. These were implemented by carefully reading the values out of the graph and then calculating the slope in the code. The calculated equilibrium side slip lines by the code was checked to see if it matched the one in the figure. There is a limit to the accuracy to which this can be checked as it can only be checked by reading out the figure. However, the side slip equilibrium lines seemed to be implemented well and matched the ones shown in the graph.

As this method is based on statistical data, it does not really make sense to validate this method. Also because this is quite a preliminary method, uncertainties are still included in this sizing method.

10.6.2. Vertical tail sizing sensitivity analysis

While working with code, it became apparent quickly that the code was most sensitive to the differential thrust (ΔT_e) input. As soon as this value became large, it gave results that fell outside the scope of the method.

As can be seen in [Figure 10.14](#), as soon as the x-axis parameter gets value of above 0.16, the method has no feasible solution for a vertical tail size for any of the equilibrium angles. The other inputs in the x-axis parameter are more or less fixed, so the only thing that can influence the x-axis parameter and thus the vertical tail size is the differential thrust during an engine failure.

10.7. Ground stability

Stability on the ground while taxiing also needs to be considered. This means that the main landing gear have to be far enough apart in order to prevent tip over of the aircraft during taxiing. Also, the landing gear need to be positioned such that the nose gear carries at least 8% of all the weight to make the aircraft steerable on the ground [35, part IV]. This is for a tricycle gear set-up.

The landing gear design is closely linked to the structural design of the aircraft this is why the landing gear design and positioning was described in [section 12.4](#). The results for the landing gear positioning can be found in [Table 12.1](#) and [12.4](#).

10.8. Control Surfaces

Proper designing of control surfaces is crucial for flight safety, a bad controllability of an aircraft may result in fatal accidents. Thus, it has to be looked into carefully during all the design phases of the aircraft. However, since our concept is a VTOL aircraft, high-lift devices (HLDs) are not considered. That is because of the fact that they are used during horizontal takeoff and landing only, nonetheless, other control surfaces are considered. In [subsection 10.8.1](#), aileron design is considered, followed by the rudder design in [subsection 10.8.2](#). Finally, elevator design is discussed in [subsection 10.8.3](#).

10.8.1. Aileron control surface sizing

The aileron of this aircraft is designed to meet the Class I, small & light airplanes, roll requirements. The requirements state that the aircraft shall be able to roll 60 degrees in 1.3 [31]. A tool is created, where the aileron dimensions are given as inputs, and the maximum deflection angle required to meet this requirement as output. The chord dimension of the aileron is constrained by the spar location of the wing, which is currently at 60% of the MAC, i.e. the aileron chord to wing chord ratio is 0.4. The span of the aileron is the dimension that can be changed in the tool in order to get a different maximum deflection; namely, b2 and b1, the end and the start points of the aileron relative to the wing span.

The roll rate of the aircraft is calculated using [Equation 10.8](#)[31]:

$$P = -\frac{C_{l_{\delta\alpha}}}{C_{l_p}} \delta\alpha_{\max} \left(\frac{2V}{b} \right) \quad (10.8)$$

where:

- ✈ $C_{l_{\delta\alpha}}$ is the aileron control derivative.
- ✈ C_{l_p} is the roll damping coefficient.
- ✈ $\delta\alpha_{\max}$ is maximum deflection required to achieve this roll rate.

The control derivative depends also on the aileron effectiveness, which can be obtained from [Figure 10.15](#). It should be noted, however, that this graph is used to obtain the effectiveness of any of the control surfaces, thus, it is also used for rudder and elevator sizing. Both control derivative and damping coefficient are also computed in the tool, the calculation method can be found in [31].

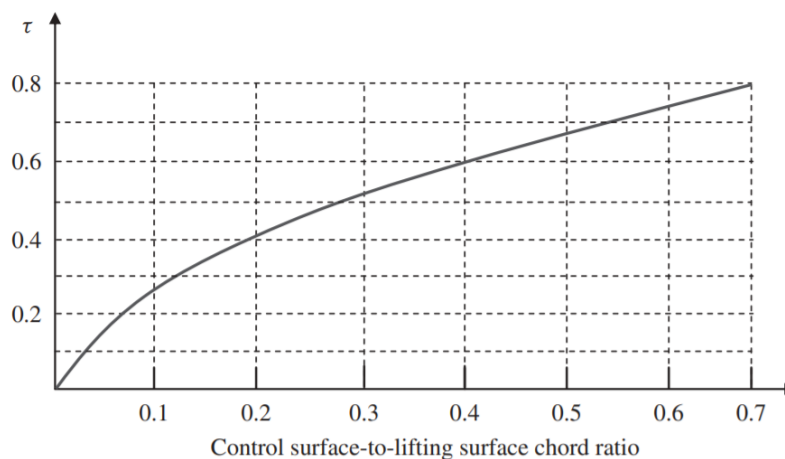


Figure 10.15: Control surface angle of attack effectiveness parameter [37].

The python tool was used to iterate over all sorts of aileron geometries to see when the geometries size would be minimised for a particular aileron deflection.

The final dimensions of the ailerons can be found in [Table 10.9](#). The ailerons start at 2.45 m and ends at 3.5 m on the wings.

Table 10.9: The final dimensions of the ailerons. Note, the dimensions of the total aileron surface.

Parameter	Value	Unit
S_a/S_h	0.21	-
b_a/b_h	0.35	-
c_a/c_h	0.60	-
S_a	1.89	m^2
b_a	2.10	m
c_a	0.9	m

10.8.2. Rudder control surface sizing

The rudder is designed such that the aircraft can achieve directional trim in the case of asymmetric thrust, for example one engine failure situation. During the iteration process the maximum deflection value is set to be 30 degrees, values above this one are considered high and another iteration is required. This value was used based on reference aircraft.

A tool is created in python for the rudder sizing, which takes the vertical tail size, S_v , as an input, and outputs the required chord ratio, C_r/C_p . Varying the chord ratio will change the rudder effectiveness τ_r , thus, the rudder control derivative will change as well according to Equation 10.9[37]:

$$C_{n\delta_R} = -C_{L\alpha_V} \bar{V}_V \eta_V \tau_r \frac{b_R}{b_V} \quad (10.9)$$

where:

$C_{L\alpha_V}$ is the vertical tail lift slope.

\bar{V}_V is vertical tail volume coefficient.

η_V is the vertical tail dynamic pressure ratio.

b_R/b_V is rudder span to vertical tail span ratio.

According to statistics, the chord ratio always lie in the straight part of the graph in Figure 10.15, as a result, it is approximated using the linear relation in the tool. Equation 10.10 then uses the control derivative to calculate the maximum rudder deflection[37]:

$$\delta_R = \frac{T_L y_T}{-\bar{q} S b C_{n\delta_R}} \quad (10.10)$$

Where:

T_L is the thrust of the operational engine.

y_T is the moment arm of the thrust generated by the operational engine.

\bar{q} is the dynamic pressure.

The parameters used in these calculations are either aircraft parameter obtained from other tools, or computed according to the method used in [37]. The velocity used in the calculations, however, is the minimum controllable speed V_{MC} , which is equal to $0.8 * V_s$. The program iterates till the angle is 30 degrees to give the minimum chord ratio. In some cases, if the ratio is big, it might be required to increase the vertical tail size. In this tool, the span ratio is set to be one, i.e. the rudder span equals the vertical tail span.

The final geometry dimensions of the rudder can be found in Table 10.10.

Table 10.10: The final dimensions of the rudder.

Parameter	Value	Unit
S_r/S_h	0.06	-
b_r/b_h	1	-
c_r/c_h	0.101	-
S_r	0.128	m^2
b_r	1.2	m
c_r	0.11	m

10.8.3. Elevator control surface sizing

The elevator sizing was actually the complex control surface to size at this stage of the design as it needs data from a lot of design departments in the design team. The reason for this is that the elevator sizing is usually critical during the take-off (TO) rotation. The horizontal tail needs to be able to produce enough force to rotate the nose up during take-off. To be able to calculate the force required, things like drag, lift and the size of the aircraft already need to be known. The method used to size the elevators originated from the book Aircraft Design: A Systems Engineering Approach [37]. The same book was used to size the rudder.

An important thing to consider here, is that the personal aircraft will not be taking off like an ordinary airplane. It will take off in VTOL mode, so a take-off rotation does not need to be considered. However, it was still found useful to try and size the elevators for a ordinary take-off situation as in the far future, this aircraft's operation extended to the point where it is able to take-off like an ordinary aircraft. However, if it would not be possible to get a feasible solution for the elevators for an ordinary take-off situation, the next most critical phase in flight needs to be considered, which is the landing. If there is a feasible solution for the elevators during landing, but not for ordinary take-off, this result will still considered to be acceptable.

The method works by first calculating the lift the canard (in this case) needs to generate to be able to rotate the aircraft during take off. This is done by setting up the moment equilibrium equation around the main landing gear in the take-off situation. However, the moment equilibrium equation that was presented in the method description did not apply to the design of the personal aircraft as it is a canard aircraft, which means that a few moment arms were not correct. In addition, in a canard design, the canard actually creates upward lift instead of downwards lift. The new moment equilibrium equation was set up, which can be seen in Equation 10.11. This equation is then rearranged, such that the lift created by the canard (L_h) can be determined.

$$-L_{TO}(x_{acw} - x_{mg}) + M_{ac_{wf}} - m_{TO}a(z_{cg} - z_{mg}) - m_{TO}g(x_{mg} - x_{cg}) + D_{TO}(z_d - z_{mg}) - T_{max}(z_T - Z_{mg}) + \quad (10.11)$$

$$L_h(x_{mg} - x_{ac_h}) = I_{yy_{mg}} \frac{d^2\theta}{dt^2}$$

The following assumptions were made to be able to perform this calculation at this stage of the design:

- ✈ For the calculation of the moment around the aerodynamic centre of the wing and fuselage, the moment coefficient of the wing and fuselage is assumed to be 0.05 [37].
- ✈ The surface area of the wing which include the flaps (S_{ref}) is equal to the wing surface area (S) [37].
- ✈ The total thrust of the aircraft is assumed to act in the aerodynamic centres of the MAC of both the main wing and canard. This means that the thrust arm of the total thrust can be determined using the moment equilibrium equation of both thrust components. This equation is then rearranged to obtain the thrust arm:

$$z_T = \frac{T_w z_{T_w} + T_h z_{T_h}}{T_w + T_h}$$
- ✈ At this stage of the design it is impossible to know the total drag of the aircraft. This is why the drag at take-off was estimated by calculating the drag that both wings create during take-off. The drag was also assumed to act in the aerodynamic centre of the wings in their MAC. The drag arm was calculated the same way as for the thrust. This means that the arms for the individual thrust components are the same as for the drag components:

$$z_d = \frac{D_{TO_w} z_{T_w} + D_{TO_h} z_{T_h}}{D_{TO_w} + D_{TO_h}}$$
- ✈ The profile drag coefficient (C_{D_0}) was assumed to be 0.03 [37].
- ✈ The rotation speed (V_R) is assumed to be the same as the stall speed (V_s).
- ✈ The Oswald efficiency (e) of the wing is assumed to be 0.88 [37].
- ✈ The rotational acceleration during rotation ($\frac{d^2\theta}{dt^2}$) at take-off is set to $5^\circ/s^2$ as specified by the CS-23 regulations [3].

The force equilibrium equation were used to calculate the acceleration during take-off, as can be seen in Equation 10.12, with $F_f = \mu_d(m_{TO} - L_w)$.

$$a = \frac{T - D - F_f}{m_{TO}} \quad (10.12)$$

The calculated lift of the canard during take-off is then converted to a lift coefficient that the canard needs to be designed for ($C_{L_{des}}$), by means of appropriately sized elevators.

Next, the elevator angle of attack (AoA) effectiveness coefficient (τ_e), which is done using Equation 10.13.

$$\tau_e = \frac{\alpha_h + (C_{L_h} / C_{L_{\alpha_h}})}{\delta_{e_{max}}} \quad (10.13)$$

The parameters in Equation 10.13 were determined as follows:

- ✈ The angle of attack of the canard during take-off is equal to:
 $\alpha_h = \alpha + i_h - \epsilon$.
 The value of the AoA (α) was assumed to be 2 degrees. The angle of incidence, in other words, the angle with which the canard is mounted to the fuselage (i_h) is 2 degrees. The downwash on the canard due to the main wing (ϵ) is zero.
- ✈ The lift coefficient slope of the canard is obtained from the aerodynamics department. The same value was used as the one for the X-plot.
- ✈ The maximum deflection of the elevators ($\delta_{e_{max}}$), which is set to be 30 degrees.

Once the AoA effectiveness of the elevator is determined, Figure 10.15 is used to determine the cord ratio of the elevator compared to the canard ($\frac{c_E}{c_h}$). Note that now, the value on the x-axis is read off by using the y-axis value instead of the other way around.

Now, the elevator deflection needed during take-off can be calculated using Equation 10.14.

$$\delta_e = \frac{(\frac{Tz_T}{qSc} + C_{m_0})C_{L_\alpha} + (C_{L_1} - C_{L_0})C_{m_\alpha}}{C_{m_\alpha} C_{m_{\delta_e}} - C_{m_\alpha} C_{L_{\delta_e}}} \quad (10.14)$$

The coefficients in Equation 10.14 are calculated as follows:

- ✈ The moment coefficient due to the elevator deflection:
 $C_{m_{\delta_e}} = -C_{L_{\alpha_h}} \eta_h V_h \frac{b_E}{b_h} \tau_e$
 - The ratio of incoming airflow speed of the canard and free stream:
 $\eta_h = \frac{V_h}{V}$, is assumed to be 0.96.
 - The ratio of the span of the elevator with respect to the canard (b_E / b_h) is set to be 1.
- ✈ The lift coefficient due to the elevator deflection:
 $C_{L_{\delta_e}} = C_{L_{\alpha_h}} \eta_h \frac{S_h}{S} \frac{b_E}{b_h} \tau_e$
 Where the tail size ratio is taken from the canard sizing with the X-plot.
- ✈ The moment coefficient slope:
 $C_{m_\alpha} = C_{L_{\alpha_{wf}}} (h - h_0) - C_{L_{\alpha_h}} \eta_h \frac{S_h}{S} (1 - \frac{dc}{d\alpha})$
 For the parameters in this equation the following things are assumed:
 - The lift coefficient of the fuselage and main wing ($C_{L_{\alpha_{wf}}}$) assumed to be the lift coefficient of the "aircraft minus tail" ($C_{L_{\alpha_{A-h}}}$).
 - The parameters h and h_0 are equal to:
 $h = (x_{mg} - x_{ac_{wf}}) / c$
 $h_0 = (x_{mg} - x_{cg}) / c$
 - Lastly, the down wash on the canard due to the main wing is not present, so the down wash term drops out.

Now that the elevator deflection can be calculated during rotation is the take-off, it needs to be checked if the elevator stalls during rotation. If so, it means that the elevator will not be as effective. This means that the geometry of the elevator needs to be changed to make sure that it does not stall during take-off.

The stall during take-off is checked by comparing the AoA of the canard during rotation and the stall angle of the canard with a fully deflected during rotation. These angles can be determined using Equation 10.15 and Equation 10.16 respectively.

$$\alpha_{h_{TO}} = \alpha_{TO} (1 - \frac{dc}{d\alpha}) + i_h - \epsilon_0 \quad (10.15)$$

It is assumed that the AoA during take off (α_{TO}) is 5 degrees below the airfoil stall angle. Just as before, all the down wash components drop out of the equation due to the canard configuration.

$$\alpha_{h_s} = \alpha_{h_{s_{\delta_e=0}}} - \Delta\alpha_{h_E} \quad (10.16)$$

The stall angle of the canard without any elevator deflection ($\alpha_{h_{\delta_e=0}}$) is obtained from the aerodynamics department. The parameter $\Delta\alpha_{h_E}$ is a factor in reduction of the canard stall angle due to the fully deflected elevator. This correction factor can be interpolated from Table 12.19 [37], which can be seen in Figure 10.16.

δ_E (deg)	Tail-to-elevator chord ratio C_E/C_h										
	0	0.1	0.2	0.3	0.4	0.5	0.6	0.7	0.8	0.9	1
0	0	0	0	0	0	0	0	0	0	0	0
±5	0	0.3	0.5	1.1	1.6	2.2	2.7	3.3	3.9	4.4	5
±10	0	0.6	1	2.1	3.2	4.4	5.5	6.6	7.7	8.9	10
±15	0	0.9	1.5	3.2	4.9	6.5	8.2	9.9	11.6	13.3	15
±20	0	1.2	2	4.2	6.5	8.7	11	13.2	15.5	17.7	20
±25	0	1.6	2.5	5.3	8.1	11	13.7	16.5	19.4	22.2	25
±30	0	1.9	3	6.4	9.7	13.1	16.5	19.9	23.2	26.6	30

Figure 10.16: The table that is used to determine how much lower the stall angle of the canard is during rotation, with a full elevator deflection [37].

If the AoA of the canard during rotation is lower than the stall angle of the canard with fully deflected elevators, the elevator size is valid.

This method for sizing the elevators was implemented in a python code. The figures and tables Figure 10.15 and Figure 10.16 were also implemented in the code to make it easy to iterate the size of the control surfaces. If the calculated elevator geometry passes the AoA test, the program will give the elevator geometry as an output.

For Figure 10.15 it was assumed to consists of two linear parts from 0.25 to 0.35 and from 0.35 to 0.7 on the x-axis. These parts were implemented in the code as two lines. The beginning part of the figure from 0 to 0.25 is approximated using a square root function: \sqrt{ax} , where a equals 0.8.

Figure 10.16 was implemented in the code as a matrix. by specifying the elevator deflection and cord ratio of the elevator with respect to the tail, it interpolates and determines the value of the factor in reduction of the canard stall angle due to the fully deflected elevator ($\Delta\alpha_{h_E}$). The final elevator size and geometry is given in Table 10.11.

Table 10.11: The final dimensions of the elevator.

Parameter	Value	Unit
S_e/S_h	0.200	-
b_e/b_h	1.00	-
c_e/c_h	0.200	-
S_e	0.456	m^2
b_e	3.81	m
c_e	0.120	m

For take-off, no feasible elevator size could be found with the described method. The elevator sizes would not meet the stall during rotation test. This is why the elevators were sized for landing, where a maximum thrust was assumed of 100 N of the proprotors on the main wings. This is because during landing, aircraft mostly do not use more than 30% of their cruise power [17]. In this case that would be about 100 N for 300 N of cruise power. The proprotors on the canard assumed to not produce any thrust during landing, as at this moment the landing gear size does not allow the canard proprotors to fully tilt to the horizontal position without the propellers striking the ground. Of course, the proprotors on the canard could be tilted at a particular angle at which they do not hit the ground, but produce lift as well as forward thrust. However, for the sizing, only the main wing engines were considered to make sure that the elevators are sized for the largest negatively contributing moment created by the thrust during landing. This situation results in bigger elevators and a higher safety margin.

10.8.4. Control surfaces code verification

In this section the verification processes for the control surface sizing code are discussed. The control surface sizing methods are quite preliminary, this is why the validation of these method is not performed. A margin of error will always exist between the control surface size estimated by code and the real control surface sizes of existing aircraft.

Ailerons and rudder

For the verification of the control surface codes, examples out of the book that contained descriptions for the control surface sizing was used [37]. For the aileron, it was first manually checked if the equation for the roll rate was implemented correctly. After this, the example was used to confirm this. The only thing that can be verified for the rudder

sizing is if the equations for the rudder deflection are implemented correctly. This was able to be confirmed by using an example from the book in which the method was described [37].

Elevators

To verify the code of the elevator sizing, an example was used that was mentioned in the book where the elevator sizing method was described [37]. This example allowed for unit, block and system testing as the example gave numerical values for all the separate calculations that were described in this section.

The implementation of [Figure 10.15](#) and [Figure 10.16](#) in the code could also be tested. This was checked manually. One would read of the values from a particular figure and the code would be used as well to see if the values matched. The result was that the code was able to give values from these figures that were relatively close to the ones read from the graph. The error between the figure and code was around 10% at most. The small deviation between the values is accepted as the method is now very easy to quickly iterate.

The code gave the same answer for particular subcalculations and similar values for the final elevator deflection as the example. The small deviations in the number of the elevator deflection are due to the errors induced in implementing [Figure 10.15](#) into code. In the next phase, more effort could be put into implementing [Figure 10.15](#) to reduce the errors.

10.8.5. Control surface sizing sensitivity analysis

Ailerons and rudder

The aileron and rudder were not the hardest control surfaces to size. It was always easily possible to obtain a new geometry for these control surfaces when an iteration changes design values of the personal aircraft. As far as sensitivity goes, the methods were the most sensitive to changes to the maximum deflection angle as well as their control derivatives. However, as explained before, it would always be possible to get a possible control surface geometry.

Elevators

The elevators were by far also the hardest control surfaces to size as it was hard to make a certain elevator geometry pass the stall during rotation test. This is because the way the method calculates the correction factor for the stall of the elevator during rotation. By intuition, one would expect the the elevator would stall earlier is the incident angle of the canard and the maximum elevator deflection are high, as this means that the canard is already at a higher AoA with respect to the incoming airflow. For a specific maximum elevator deflection in the described, a particular elevator AoA effectiveness ratio is calculated, which corresponds to a particular elevator to tail cord ratio. For which the stall correction angle can be read off in [Figure 10.16](#).

If a high maximum elevator deflection angle is selected, a lower chord ratio will correspond to this maximum deflection. However, a higher maximum deflection angle and lower chord ratio will still result in a large stall correction angle. A large stall correction angle means that the canard will stall at a much lower angle of attack during rotation. Also, if a smaller maximum elevator deflection is selected, the chord ratio of the elevator to tail that corresponds to this maximum elevator deflection will increase. A low maximum elevator deflection and high chord ratio will result in a large stall correction angle.

In short, all this means that small changes from other departments have drastic implications for the elevator sizing. For a particular set of inputs, the elevator sizing could still be adapted by selecting a different maximum elevator deflection and span ratio to see if it passes the stall during rotation test. For some input sets a few possible options of elevator geometries would exist, but it seemed like most input sets had little or no possible solution. Most elevator geometries were tried by using trial and error.

10.8.6. Ailerons and elevators deflection during the VTOL mode

During VTOL mode, the main wing and the canard block the propwash produced by the propellers. This does not effect the amount of thrust created by the propellers, however the dynamic pressure caused by the prop wash onto the wings will create a downwards force on the wings of the aircraft, reducing the effective thrust that lifts the aircraft.

To be able to let the wings block less of the airflow during the VTOL mode, it is decided to make the control surfaces that extend to the ends of the wing able to fold downward by 90 degrees during the VTOL mode. This means that the aileron and elevator are effectively a "flaperon" and "flapevator".

With regards to the main wing, just folding the ailerons down still leaves a large part of the wing to block the prop wash. This is why it is decided to also make the leading edge at the wing tip fold down by 90 degrees. This way, the wing box is still able to carry all the loads created by the propeller. However, note that the ailerons and elevator will never be used as flaps during an ordinary landing. The aileron and elevator will only be able to fold down by 90 degrees during the VTOL mode.

This chapter will explain the material choices and the important material characteristics. First a functional analysis will be given in [section 11.1](#). After this, the requirement analysis is done in [section 11.2](#). Then the material choices for primary structures is elaborated in [section 11.3](#), the one for the secondary structures is done in [section 11.4](#).

11.1. Functional analysis

Material selection is mostly affected by the functions related to production and the end-of-life of the aircraft, these functions are as follows:

- ✈ F1.1: "Obtain new materials":
During the production phase, the materials need to be delivered by the supplier.
- ✈ F1.2: "Obtain recycled materials":
Material selection should be as sustainable as possible.
- ✈ F1.3: "Shape material into different parts":
Selected materials are then shaped into the required design.
- ✈ F1.4: "Obtain pre-manufactured and refurbished parts":
Since the circular economy concept is embraced in this project, parts and materials that can be used from retired aircraft are used again, sometimes refurbished first.
- ✈ F1.8: "Certify the aircraft":
The material selection should meet the certification requirements, some materials are not allowed in the aerospace industry for example.
- ✈ F3.4: "recycle":
Materials will be recycled at the end of life of the aircraft.

11.2. Requirement analysis

According to the requirements that were set for this project, material selection has to meet the following requirements:

- ✈ **DSE-22-STAK-04:** The aircraft shall be designed according to the circular economy concept [6].
- ✈ **DSE-22-STAK-05:** The aircraft shall be environmentally friendly [6].
- ✈ **DSE-22-STAK-06:** The price of the aircraft shall be such that it is competitive on the market [6].
- ✈ **DSE-22-SYS-SR-03:** The aircraft shall have a minimum life time of 10 years [6].
- ✈ **DSE-22-SYS-RM-08:** A list of alternative suppliers for materials shall be provided [6].
- ✈ **DSE-22-SYS-S-03:** The aircraft shall have re-usable materials [6].

These requirements determine how well the design will for the circular economy concept as well as sustainability. Some risk mitigation requirements are also included.

11.3. Material choice for primary structures

The choice of material for the different components of the aircraft is important since it determines not only the resistance to different loading of the aircraft, but also the action taken at the end-of-life with respect to recycling or reusing the components or the aircraft as a whole. The primary structures will be the fuselage structure and the wingbox inside the wing.

The two main categories of materials taken into account for the primary structural components of the aircraft were metals (aluminium alloys) and composites (carbon fibre and glass fibre composites). For each of these, the criteria which were considered were their mechanical properties as well as their sustainability and recyclability potential. In terms of mechanical properties, the following elements were looked into: yield strength, ultimate strength, stiffness, fatigue strength, shear strength and density. For the sustainability, the cost, energy used in production and the CO_2 footprint were the primary focus, and lastly for the recyclability, the potential of the material being taken from old aircraft and recycled into new ones was looked into.

11.3.1. Mechanical Properties

From the aluminium alloy list, the three main competitors in the trade-off were the 2024 T6, 7075 T6 and 6061 T6 alloys. The T6 in each of these indicates the heat treatment process which was used for the alloy. In particular, T6 indicates a high temperature treatment, typically in the range from 100°C to 200°C. This ensures a faster ageing of the material, and thus shorter time to reach a stable condition. Moreover, the alloy's strength as a result of this process is higher than the one obtained for other treatments (natural ageing which occurs at any temperatures, and is indicated by T1, T2, T3, or T4)¹, therefore making these alloys interesting for this application. The 2024 (2xxx series, using copper as alloying element) and the 7075 (7xxx series, using Zinc as alloying element)² are the two of the most commonly used alloys in the aerospace industry³, due to their high performance properties. This is also the reason why they were selected for this trade-off. Similarly, the 6061 (6xxx series, using Magnesium and Silicon as alloying elements) was found to be an alloy with great potential, having as well the advantage of being weldable and having great corrosion resistance, meaning it does not have a significant effect on the skin thickness. This alloy was also found as a result of the search for recyclable alloys, and its recyclability advantage will be discussed in the next subsection.

For the composites, the choices were set between quasi-isotropic carbon fibre lay-up with either PEEK, Epoxy, Polyimide as matrix, and a quasi-isotropic glass fibre lay-up with an Epoxy matrix. The quasi-isotropic lay-up for the fibres is required for composites (as opposed to metals which are already isotropic), in order to ensure that the properties are maintained constant regardless of the direction in which the components are loaded in. Table 11.1 summarises the findings for the mechanical properties of the mentioned alloys and composites, as retrieved from the CES Edu-Pack 2019 [18]. For the glass fibre, the S indicates the type of fibre used, the S-type having a higher stiffness than the regular E-glass⁴. Composites are very good with corrosion resistance, but do need additives to have a high enough conductivity in the case of lightning strike.

Table 11.1 shows that the composites have better specific properties. This holds for both the strength and the elasticity. The strength of the carbon is twice or three times as high in comparison to aluminium. This could make the carbon a lighter solution for the aircraft. This analysis does not take into account the minimum thickness of a carbon sheet. The carbon needs (0/90/+45/-45/0/90/+45/-45) in order to have a quasi isotropic sheet. This would mean that the thickness that is required might be lower than the minimum thickness of the sheet thus meaning a heavier than an ideal structure obtained using carbon.

Table 11.1: Mechanical Properties Aluminium Alloys

Alloy	Ultimate Strength (MPa)	Specific Strength ($\frac{MPa}{g/cm^3}$)	Fatigue Strength (MPa)	Elastic Modulus (GPa)	Specific Stiffness ($\frac{GPa}{g/cm^3}$)	Shear Modulus (GPa)
Al 2024 T6	427-472	124	125-147	72-75	26	28-29
Al 7075 T6	434-580	129	152-168	69-76	25	26-28
Al 6061 T6	290-338	88.89	112-131	66-70	24	25-27
Composite	Ultimate Strength (MPa)	Specific Strength ($\frac{MPa}{g/cm^3}$)	Fatigue Strength (MPa)	Elastic Modulus (GPa)	Specific Stiffness ($\frac{GPa}{g/cm^3}$)	Shear Modulus (GPa)
PEEK + Carbon QI lay-up	460	296	253	56.1	36	21.5
Polyimide + Carbon QI lay-up	465	292	256	42.2	27	16.1
Epoxy + Carbon QI lay-up	603	389	137	49.7	32.06	19
Epoxy + S-Glass QI lay-up	457	248	23.3	19	10	9.16

11.3.2. Sustainability and Recyclability

As previously mentioned, certain aspects related to the sustainability and the recyclability of the different material types were also taken into account, as these are important for the overall aim of the project. Starting with the sustainability, Table 11.2 presents the summary of the characteristics of each considered material once again retrieved from [18].

¹http://www.aalco.co.uk/datasheets/Aluminium-Alloy-Temper-Designations_93.ashx, Accessed [15.06.2020]

²<http://www.alcotec.com/us/en/education/knowledge/techknowledge/understanding-the-alloys-of-aluminum.cfm>, Accessed [15.06.2020]

³<https://matmatch.com/blog/aluminium-alloys-in-aerospace-industry/>, Accessed [15.06.2020]

⁴<https://www.azom.com/article.aspx?ArticleID=769>, [Accessed 15.06.2020]

Table 11.2: Sustainability of Materials

Alloy	Cost (€/kg)	Energy usage Primary Production (MJ/kg)	Energy usage Recycled Production (MJ/kg)	CO₂ footprint (kg/kg)
Al 2024 T6	2.40	204	31.7 - 35	12.4
Al 7075 T6	4.50	203	31.6-34.9	13.8
Al 6061 T6	2.20	210	32.4-35.8	13.9
Composite	Cost (€/kg)	Energy usage Primary Production (MJ/kg)	Energy usage Recycled Production (MJ/kg)	CO₂ footprint (kg/kg)
PEEK + Carbon QI lay-up	102	781	-	53.9
Polymide + Carbon QI lay-up	135	791	-	54.5
Epoxy + Carbon QI lay-up	35.2	723	-	50.5
Epoxy + S-Glass QI lay-up	26.3	106	-	5.96

Lastly, in terms of recyclability, a number of comments can be made for each material. A difference should be made between reusability, which describes refurbishing the part to use it in another aircraft, and recyclability, which means taking the material back to the cycle of source materials. Parts that have not degraded, can be reused, and parts that have, need to be recycled.

The aluminium alloys present the advantage that they can be relatively easily recycled. The recycling of aluminium alloys is economically viable due to the low energy that is needed for this process. Through melting, these can be re-shaped into different components, however noting that once remelted, the properties of the high-performance alloys suffer changes which prevent them from being used for the exact same parts as before. In other words, a primary structure can not be molten and then used as a primary structure again. This is caused by the increased level of impurities, mostly of iron and silicon, that is introduced in the recycling process, and which is difficult to control⁵. A suitable solution to this problem would be to add virgin aluminium to the recycled material to dilute the impurities to an acceptable level. This however raises the required energy to produce the material.

Another aspect that has to be considered is the price. The price of the recycled material will be elevated by adding pure aluminium in order to combat the lower mechanical properties. From the current list, aluminium 6061 presents an advantage compared to the 2024 and 7075 alloys, because after recycling, the wrought material obtained from various aluminium alloys (including 6061) will present characteristics similar to fresh 6061 alloys, making that alloy usable straight away without any or sometimes only with a small amount of changes⁶.

A general issue when it comes to the recyclability of aluminium in the aerospace industry comes from the low industry volume compared to the use of aluminium alloys in other industries. This can result in a cost that is too high for the value that can be obtained out of the process. Additionally, as previously mentioned, remelting aluminium induces impurities, which are troublesome for aerospace applications, thus making recycling difficult for this application.

Moving on to the composite recyclability, the predominant issue is the difficulty of recycling any of these materials. Dividing the composites into two categories, the thermoplastic and thermoset, one can see that the process is to some extent possible with thermoplastic materials, due to their ability to be melted and reformed into another component, ability which is fully lacking for the thermoset ones. One option for these composites is to grind up the part and use it as filler for a new composite, however this method generates little value compared to the preceding part. For the thermoplastic materials, the recycling process could in theory be conducted multiple times in a row, by melting the matrix and retrieving the fibres. In reality this poses a challenge in terms of keeping the mechanical properties of the components unchanged and the fibres undamaged. The knowledge about recycling of thermoplastic composites with this process is lacking, mostly because of the financial unfeasibility. Composites could however be reused by 'patching up', in case small cracks are present in the matrix but not in the fibres, these could be fixed by heating the matrix and letting it reshape to close the cavities.

⁵<https://www.totalmateria.com/page.aspx?ID=CheckArticlesite=ktnNM=222> [Accessed 20.06.2020]

⁶ibid

11.3.3. Final Material Choice

Based on the previous two subsections, some conclusions about the material options can be drawn. Firstly, by looking at [Table 11.1](#) it is visible that with the exception of glass fibre which has a very low fatigue strength, the other materials have similar performances. However, a large problem can be found with regards to composites in the sustainability and recyclability areas. As can be seen in [Table 11.2](#), composite materials are not only way more expensive than aluminium alloys, but they also require on average a considerably higher amount of energy for production, and generate a significantly higher amount of CO_2 per kilogram, rendering them unsustainable in comparison with the metal alternatives. Moreover, as mentioned in the previous subsection, composites as a whole seem to lack in the recyclability area, since the process is at the moment still unfeasible from a technical standpoint. Adding to this the fact that thermoplastics while being the only ones that present a good potential for recyclability, are currently not certified for primary structures in aircraft, the final decision is to remove composites from the primary structural design choices as a whole.

Aluminium alloys present both good mechanical properties and sustainability/recyclability characteristics. The final choice for the design was set on the Al 6061 T6 alloy, due to the range of advantages it would bring to the design. While the mechanical properties are not the highest in the list, they are high enough to resist the loads to which the aircraft will be subjected. Moreover as mentioned before, this material has good corrosion resistance as well as good weldability which is not the case for the other alloys. Lastly, as mentioned previously, the recyclability and sustainability are both very positive for this alloy, which can be obtained from melting of various other types of alloys (including 6061).

11.4. Secondary structures and other components

The material choice for secondary structures, such as the skin fairing of the fuselage, the leading edge and the trailing edge of the wing is discussed here. Additionally, the materials used for other components, such as bolts and the canopy windshield, are introduced.

11.4.1. Secondary structures

The wingbox inside the wing will be the primary load-carrying structure, and therefore the LE (leading edge) and TE (trailing edge) of the wing are considered secondary structures. They do not have to be made as strong as the primary structure, and they can therefore be made out of a lighter material. Similarly, the fuselage will have a skin fairing, that will not be a load-carrying structure. Same materials are considered for these secondary structures.

As was discussed in the previous section, thermoplastics are reusable, because they are patchable, and they are recyclable to some extent, as they can be melted and reshaped. This process however is not widely used for high-performance plastics. The recyclability is significantly improved when the polymer is not reinforced with fibres, because the fibres are the most difficult part to keep in tact without reducing the mechanical properties of the composite.

Unfilled thermoplastics are considered for the LE and TE of the wing, and the fuselage fairing, for the two above mentioned reasons: lightweight and reusable. Thermoplastic parts can also be made by additive manufacturing methods, which reduces the amount of material waste in manufacturing. There are some thermoplastics that are widely used for industrial-scale 3D-printing purposes, such as PEEK and Ultem (PEI) ⁷, because both are high performance materials. One more material will be looked into in more detail: PLA. It is not a high performance material, but it is widely used in 3D printing and it is biodegradable, which is beneficial for sustainability of the aircraft.

In choosing a material for the secondary structures there are some important properties that need to be considered. The material has to perform well in outdoor use, and therefore the UV resistance and water resistance are of high importance. Additionally, the material should not be flammable. As PLA itself is flammable, flame-retarded additives should be used. The secondary structure will not carry the loads, but it will experience deflection and possibly impacts (bird strikes or foreign object damage), and it should be able to withstand those. The cost of the material does affect the choice as well. Lastly, but not least, four characteristics of sustainability are evaluated: recyclability, biodegradability, energy required in recycling process and CO_2 emissions of the recycling process. All of the values are found from [18], and they are summarised in [Table 11.3](#).

⁷<https://all3dp.com/1/3d-printing-materials-guide-3d-printer-material/> [Accessed 20.06.2020]

Table 11.3: Properties of Materials for LE and TE

	PEEK	PEI	PLA (flame-retarded)
UV resistance	Excellent	Excellent	Good
Water resistance	Excellent	Excellent	Acceptable
Flammability	Self-extinguishing	Self-extinguishing	Self-extinguishing
Elongation at break [% strain]	30-150	56-65	20-26
Impact strength, unnotched 23 deg [kJ/m ²]	no break	- ⁸	77-88
Cost [Euro/kg]	83	15	4
Recyclable	yes	yes	yes
Biodegradable	no	no	yes
Energy in recycling [MJ/kg]	97-107	67-74	20-22
CO ₂ in recycling [kg/kg]	5.4-6.0	3.6-4.0	1.1-1.2

From Table 11.3 it can be seen that PEEK clearly has the best performance outdoors and in the mechanical properties. However, the cost is significantly higher than that of PEI or PLA, and from sustainability perspective it is not as good as the other two. PLA is the best in sustainability and cost, but it might not last long in outdoor use, as it degrades in UV light and in humidity. As the mechanical properties are not the driving aspect in the choice of secondary structural material, PEI is for now chosen as the material for the LE and TE of the wing. In the future more research should be made into the durability of PLA in long-term outdoor use, so that it could replace the PEI.

11.4.2. Other components

One aspect that is still left, is the use of other materials which will go into the design, such as bolts, rivets, materials for the seats, cables, covers, etc. The reason these were left for the end is that the range of choices for these materials is not that large. Taking for example the material for the seats, this can be chosen based on current materials used in the industry, such as vinyl for seats (taking for example RECARO as a known provider of aircraft interior pieces⁹, acrylic (Plexiglas) for the windshields, steel for bolts and nuts, XLPE (cross linked polyethylene) for cable insulations, etc.

For the larger elements, such as the seats and the windshield a short description will be given in order to explain the choice in more detail. First of all, the vinyl for seats is a material that is easily recyclable, it is light and fire resistant¹⁰ which are key characteristics for the interior of an aircraft. In addition to this, the energy usage for production is at only 54 MJ/kg, and the CO₂ footprint at 2.2kg/kg produced, as retrieved from [18]. Lastly, for the windshield, acrylic is a light and strong alternative to glass, being up to 30 times stronger and half as light¹¹ making it a commonly used material for aerospace applications¹².

⁸Not given

⁹<https://www.recaro-as.com/en/aircraft-seats.html>, Accessed [15.06.2020]

¹⁰<https://www.azom.com/article.aspx?ArticleID=987>, Accessed [15.06.2020]

¹¹<https://plasticsheetsshop.co.uk/acrylic-advantages-and-disadvantages/>, Accessed [15.06.2020]

¹²<https://aviation.stackexchange.com/questions/673/what-materials-are-plane-windows-made-of/681>, Accessed [15.06.2020]

12

Structural Design

Similar to the previous chapters, this one starts with a functional and requirement analysis in [section 12.1](#) and [section 12.2](#). In [section 12.3](#), the design of the fuselage will be discussed. The landing gear in [section 12.4](#), the wingbox and the rest of the wing structure will also be discussed in [section 12.5](#). Lastly some joining method ideas are proposed in [section 12.6](#).

12.1. Functional analysis

By taking a look at [section 5.2](#), the structural design of the aircraft has to take care of the following functional blocks:

- ✈ F1.7.1 Perform a structural check of airframe.
- ✈ F2.4.1 Perform structural maintenance .

The structural design of the aircraft will be designed such that it will be easy to perform checks and maintenance on the aircraft.

12.2. Requirement analysis

The structural design of the aircraft has to fulfil the following requirements:

- ✈ **DSE-22-STAK-03:** The aircraft shall have a capacity of one person [6].
The size of fuselage will be mainly based on this requirement.
- ✈ **DSE-22-SYS-AC-02:** The aircraft shall have a maximum payload mass of 150 kg.
The payload mass is important for the loads on the aircraft, which will affect the whole structure of the aircraft.
- ✈ **DSE-22-SYS-AC-03:** The aircraft shall have a maximum wing span of 9m [6].
The dimensions of the wing will affect the wingbox dimensions and component material thicknesses.
- ✈ **DSE-22-SYS-AC-04:** The aircraft shall be able to accommodate pilots between 153.5cm and 185.5cm height [6].
This is again important for the fuselage design of the aircraft.
- ✈ **DSE-22-SYS-RM-03:** The aircraft shall be maintainable for the user [6].
The structure is designed to be sectional to allow for easy access to different parts of the aircraft.
- ✈ **DSE-22-SYS-SR-05:** The aircraft structures shall be designed with a safety factor of at least 1.5 [6].
This safety factor will be taken into account in the whole structural design. All determined material thicknesses will take this safety factor into account.

12.3. Fuselage design

The fuselage of the aircraft will have a big glider-like canopy. This means that the whole canopy-section will not be able to carry loads. The irregular fuselage form is therefore more easily achieved using a truss structure frame. A FEM process was used to analyse the characteristics of this structure as the shape will become quite complicated.

12.3.1. Design Process

The truss structure configuration was designed using an iterative process in CATIA and ANSYS. The attachment points for the wing and all the loads were first modelled in CATIA and some connecting structures were drawn. After that the structure was analysed in a static structural analysis using ANSYS Workbench. The load applied at this stage was the lifting force of the wings at the wing attachment points. The model was fixed at the heaviest mass concentration which was the payload and fuel. After this result it was clear where the structure would need to be reinforced. The iterative process led to the tube frame shown in [Figure 12.1](#). As soon as the location of the masses inside the structure were known, the load case was switched to the wing attachment points being limited in some directions and the whole model was given an acceleration corresponding with the maximum load factor. The main wing was fixed in x, y and z and the canard only in z to make sure no overconstraints were present. In [Figure 12.1](#) the orbs are point masses corresponding to for example the 150 kg payload or the 59 kg batteries. The locations of all the masses in the structure were determined after an empty centre of gravity was determined by the aerodynamic analysis. The design process also resulted in a tube radius of 20 mm and a wall thickness of 3mm throughout the whole frame. This wall thickness and radius can be optimised per tube section in the future.

The maximum allowed internal stress was set at 303 MPa. This is the yield strength of aluminium 6061 divided by

the safety factor 1.5. The result of the FEM analysis can be seen in Figure 12.2. From this figure a few things can be concluded. First it is clear that some of the tubes do not appear to have high internal stresses. This means that there is still a lot of room for optimising the tube thickness. The highest stress concentrations can be seen at the joints. This is mainly because in the joints, where tubes come together, the forces in the separate tubes are all introduced into one. These can be reinforced to account for these stresses. It should be noted that the scale in this analysis shows a maximum stress of 977 MPa. This stress is however reached in a connection in one of the joints where the mesh size is too large to properly calculate the internal stresses. This results in a very high but unrealistic stress concentration, because the numerical model becomes inaccurate when the stress jumps too much from one node to the other. This can be analysed in the future to remove the model defects. If the stress after improving the model is still too high, the joints need to be reinforced.

The fuselage fairing is decided to be made out of a thermoplastic material. The thickness of this lining should be optimised, and the feasibility of manufacturing the non-uniform shape by 3D-printing researched more. A thicker lining, of about 5cm, with an optimised infill pattern and infill percentage should be used in locations that need higher impact resistance. For lower weight a thin lining without infill can be used. For now a 2mm thick sheet is considered for the whole fairing. A lower thickness would lead to problems in manufacturing, because the stiffness would not be enough to hold the fairing together. The fairing will be made in parts to ease the manufacturing process by reducing the part size. This will also be beneficial for inspecting, maintaining and ultimately disassembling the aircraft. The joining method of the fairing to the trusses will be discussed in subsection 12.6.1.

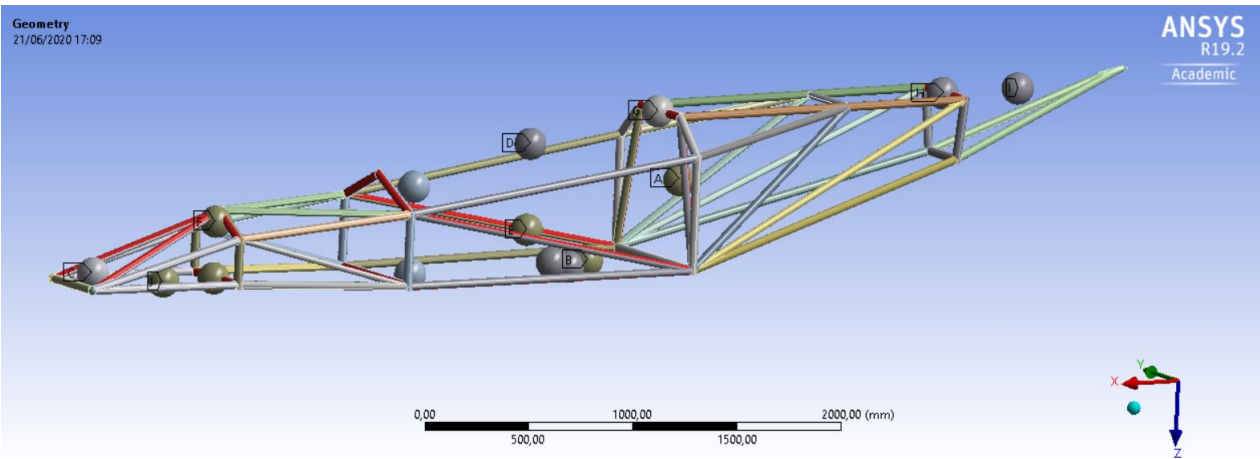


Figure 12.1: The tube frame with point masses

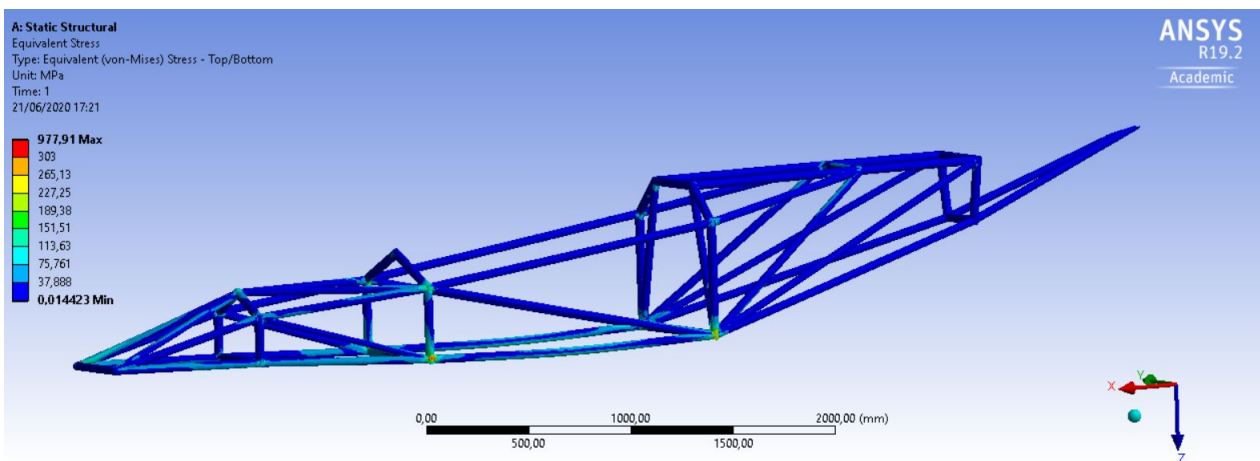


Figure 12.2: The tube frame with internal stress distribution

12.3.2. Verification and Validation

The FEM analysis was verified using a few methods. The FEM software settings were checked by analysing a very simple cantilever beam. It was a solid rod with a circular profile with a 10 mm radius and 100mm length. This can also be solved analytically. Comparing the two will verify that the software calculates the internal stresses correctly. The load case that was used in the model was also checked by comparing the reaction forces in the two wing constraints and comparing these to the values calculated for the wingbox analysis.

Cantilever Beam

To reduce the inaccuracies at the support surface, the internal stress was calculated 20 mm from the supported end. This is indicated as point A in Figure 12.3. A 100 N force is applied to the end of this beam. The moment of inertia for a circle is calculated using Equation 12.1.

$$I = \frac{1}{4}\pi r^4 \quad (12.1)$$

$$\sigma = \frac{M * c}{I} = \frac{100N * 0.08m * 0.01m}{\frac{1}{4}\pi 0.01^4} = 10.18MPa \quad (12.2)$$

In Figure 12.4 the result of the FEM analysis can be seen. A probe was used to look for the stress in exactly the same location as the hand calculation. In Figure 12.5 it can be seen that the internal stress calculated by ANSYS is the same as calculated by hand.

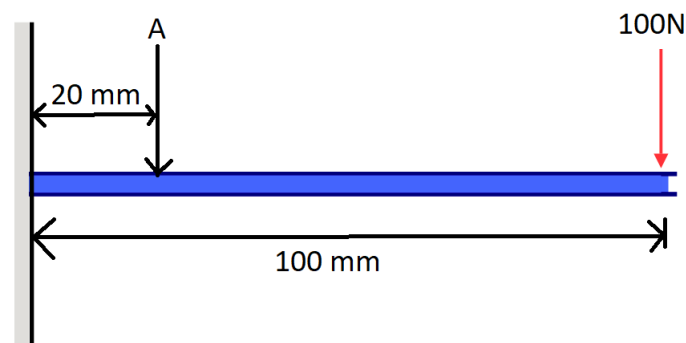


Figure 12.3: Supported beam loadcase

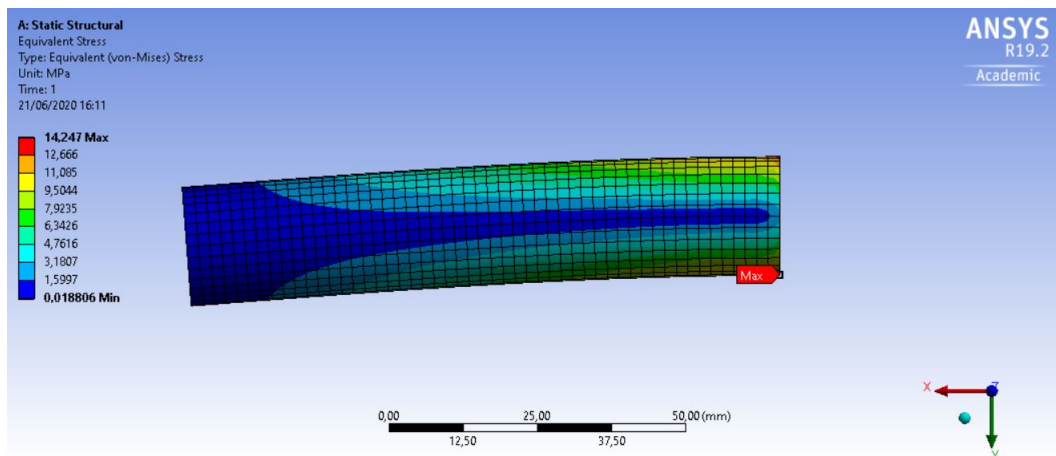


Figure 12.4: ANSYS internal stress result

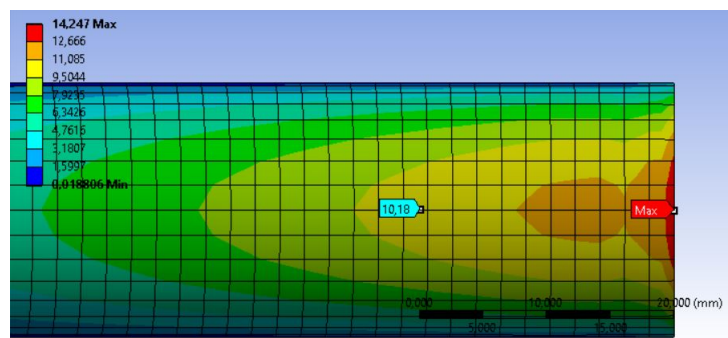


Figure 12.5: Probed value of σ in MPa

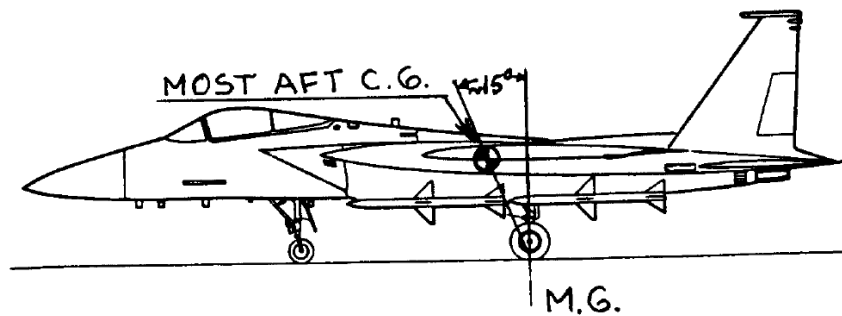


Figure 12.6: Tip-over criterion for tricycle gears [35]

Reaction force Another method used to verify if the model makes sense is by comparing the reaction force in one of the two constraints, the main wing in this case, to the reaction forces calculated in the wingbox design process. A acceleration of the maximum load factor, 2.92, was applied and the reaction forces in the displacement constraints were checked to match the calculations. The load at the root of the wingbox is 9318 N in the negative Z direction. The reaction force calculated by ANSYS at the main wing connection point is 12073 N. The 9318 N is for one wing and already includes the 1.5 safety factor. If we multiply this value by 2 and then divide by 1.5 it should match the ANSYS calculated value. This results in 12424 N. There is a 2.8 % difference. This can be considered within the model margins as the safety factor is 1.5.

12.4. Landing gear design

The landing gear was designed according to Roskam [35, part IV]. According to the book, retractable landing gear is strongly recommended if the cruise speed is above 150 knots (=77m/s) since the drag penalty will get unacceptably high. The design cruise speed of the tiltrotor is 61 m/s and hence fixed landing gear is a viable option. Also the design of this fixed landing gear will be less complex. Other advantages over the retractable gear are the low weight and the low maintenance cost.

It was chosen to design a tricycle landing configuration with 2 main landing gear and 1 nose gear. The advantages of this configuration are the good steering behaviour while taxiing and the stable ground-loop behaviour. The landing gear will be positioned in such a way that the longitudinal tip-over criterion of 15° (see Figure 12.6) and the lateral tip-over criterion of 55° (see p.84 Figure 12.9) according to Roskam [35] are fulfilled for the most aft c.g. possible. Both criteria also depend on the height of the c.g. which was assumed to be at half the height of the fuselage plus the height of the landing gear. Also a ground clearance of 5° must be ensured for the lower tip of the engine fairing if the propeller of the canard are in vertical mode (see p. 82 Figure 12.8). From the course Systems Engineering and Aerospace design slides [16], it is stated that, the nose landing gear should minimally take up 8% of the total aircraft weight to make sure the steering capability is guaranteed on ground and efficient braking is possible. The final positions of the aircraft landing gears are given in Table 12.1.

Table 12.1: Positioning of aircraft landing gears ¹

	Position [m] (wrt nose of a/c)
Most forward c.g.	2.50
Most aft c.g.	2.57
Nose gear	0.60
Main gear	2.90

To determine these landing gear positions multiple iterations were needed to fulfil all criteria. As a first step the static loads on the main and nose gears are calculated by a simple free body diagram analysis. The nomenclature of the forces and distances is shown in Figure 12.7.

¹The centre of gravity values are determined in the stability and control characteristics in chapter 10 and were iterated in the design for the landing gear.

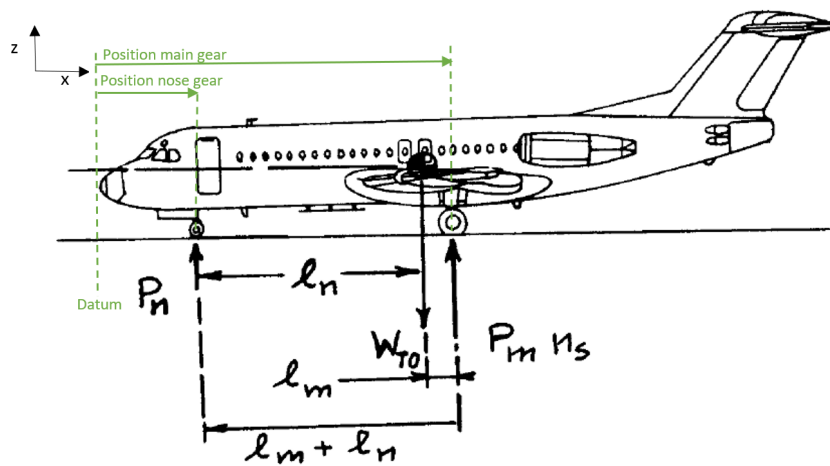


Figure 12.7: Geometry for static load calculation for tricycle landing gears [35] (and added datum)

The selected gear positions (Table 12.1) result in a static load of 1,008N on the nose wheel strut and 2,968N on each main gear strut. This means that at least 14.5% of the weight is on the nose gear which fulfils the 8% requirement. The position of the nose gear at 0.6m was selected since this is right at the trailing edge of the canard where a cut in the aircraft fairing will be made. The strut must coincide with a cut line in the fairing to allow the fairing to be disassembled (see subsection 12.6.1). The main gear was placed to just fulfil the tip-over criterion of 15° (Figure 12.6). For the tire selection of the nose wheel it is also important to know the maximum dynamic load on the nose gear. This was calculated using Roskam's formula [35, part IV] in Equation 12.3 which results in 317lbs, which equals 144 kg.

$$P_{n_{dyn}} = W_{TO} \frac{l_m + 0.35h_{cg}}{l_m + l_n} \quad (12.3)$$

12.4.1. Tire selection

In order to find the correct size of tires, use was made of a reference aircraft with similar total aircraft weight (Cessna 180). In the Cleveland product catalogue², it is stated that the aircraft has main landing gears of type 6.00-6. The first number represents the size of the tire itself in inches, the second digit gives the wheel diameter the tire is designed for³. With this information, it is possible to find a suitable main tire in an aircraft tire catalogue⁴. It was chosen to use a Michelin Air tire with the according 6.00-6 size for the main landing gear. This exceeds the requirements for the wheel during VTOL operations since that is less demanding for the tire. However to be ready for the possible STOL operations in a future mission profile a bigger tire was selected (see subsection 16.1.2). Then a suitable tube was selected from Michelin Airstop with similar size, a Cleveland wheel assembly was selected of type 40-97A and a braking assembly of type 60-63A, which are the recommended ones in the Cleveland product catalogue⁵.

For the nose landing gear, type 5.00-5 tires are used, as again based on the reference aircraft (Cessna 180⁶). Also here, the Michelin Air tire was selected and the Michelin Airstop tube with same dimensions in the aircraft tire catalogue⁷. The nose gear only needs to have a wheel assembly, and no braking assembly, as braking will only be done in the main landing gear. For the wheel assembly a Cleveland wheel assembly of type 40-77 was chosen.

12.4.2. Main gear strut design and suspension

Now that the main tires and assemblies are selected, the suspension and struts can be designed, connecting the tires to the fuselage. For the main landing gear, it is decided to use a spring steel strut design, which is a cantilevered beam under a sideways angle that will act as suspension. This type of suspension for the main gear was chosen as many general aviation aircraft use it⁸ and it is structurally less complex to design. The strut will have a simple solid rectangular cross section and will be made of steel 300M as it is used in the aircraft landing gear industry due to its high strength, toughness and fatigue strength⁹. This cross-sectional shape was chosen as it allows for for a lower bending

²<https://www.aircraftspruce.com/catalog/pdf/cleveland-wheel-brake.pdf> [Accessed 22.06.2020]

³<https://www.aopa.org/news-and-media/all-news/2013/april/15/whats-so-special-about-aircraft-tires#:text=The%20first%20numbers%20in%20the,tire%20is%20designed%20to%20fit>, [Accessed 18.06.2020]

⁴<https://www.skygeek.com/>, [Accessed 22.06.2020]

⁵<https://www.aircraftspruce.com/catalog/pdf/cleveland-wheel-brake.pdf> [Accessed 22.06.2020]

⁶<https://www.aircraftspruce.com/catalog/pdf/cleveland-wheel-brake.pdf> [Accessed 22.06.2020]

⁷ibid

⁸<https://www.boldmethod.com/learn-to-fly/systems/how-the-4-types-of-landing-gear-struts-work/> [Accessed 19.06.2020]

⁹<https://www.sciencedirect.com/topics/materials-science/landing-gear#:text=Landing%20gear%20materials%20must%20therefore,strength%20steel%20and%20titanium%20alloy>, [Accessed 11.06.2020]

stiffness (EI), such that the beam can bend sufficiently to allow for proper suspension. The sideways mounting is needed to increase the track width (lateral distance between main wheels) to comply with the lateral tip-over criterion and to load the strut in bending which is necessary to have suspension.

To determine the height and width of the cross-section, the expected force on the landing gear must be calculated. It is assumed that the vertical touch-down rate must be decelerated to 0 within the suspension of the landing gear. The vertical touch down rate of the aircraft was determined according to Roskam [35, Part IV] using the following formula:

$$w_t = 4.4 \cdot (W_{to}/S)^{\frac{1}{4}} \quad (12.4)$$

In this equation, take-off weight W_{to} is given in lbs (775 kg = 1708 lbs) and the wing surface area S is given in ft^2 ($9.0 m^2 = 96.8 ft^2$) and results in a vertical touch down rate of 8.82 ft/s (=2.69 m/s).

Assuming a constant deceleration the load factor can be calculated by Equation 12.5.

$$N_g = \frac{0.5 \cdot w_t^2}{\Delta y \cdot 9.81} \quad (12.5)$$

With w_t being equal to the vertical touch down rate in [m/s] and; Δy being the total vertical deflection in [m] from the rod (calculated using beam bending and compression) and the estimated tire deflection of 2cm.

Multiplying the load factor with the aircraft weight results in the force that acts on the main gears. The design iterations resulted in a strut length of 1.1m which is mounted at 43° with the horizontal. The strut length and angle with the horizontal were found by checking the minimum vertical distance of all landing gear (height of gears), that will guarantee the ground clearance angle between nose gear and canard rotor engine fairing as seen in Figure 12.8 and by checking the lateral distance between the main gear, to make sure the airplane does not tip-over laterally. This resulted in a ground clearance angle of 5.4° which meets the ground clearance criterion of 5° and a track width of 2.41m which fulfills the minimum of 2.32m. The normal force acting on the landing gear tire and then the strut can be split in a component in the direction of the strut, which causes compression, and in a component perpendicular to that, which causes bending. The cross-sectional dimensions are selected such that the maximum stresses due to the summation of the stresses due to bending and due to compression do not exceed the yield stress of the material. Optimising resulted in a cross-sectional width of 33mm and a cross-sectional height of 25mm of the main gear strut, as shown in Figure 12.8. Since the load factor depends on the deflection which depends on the force which again depends on the load factor an iteration was necessary. Trying out different dimensions for cross-sectional width and height had a big impact on the load factor. In general decreasing the bending stiffness resulted in lower load factors. Performing the iteration with the selected strut-dimensions a load factor of 1.94 was calculated. This load factor shows that the main gear is designed elastic enough to keep the load factors in an acceptable range even for the assumed touch-down rate which can be considered already a "hard landing"[35]. The weight of this strut was determined to be 7.14 kg.

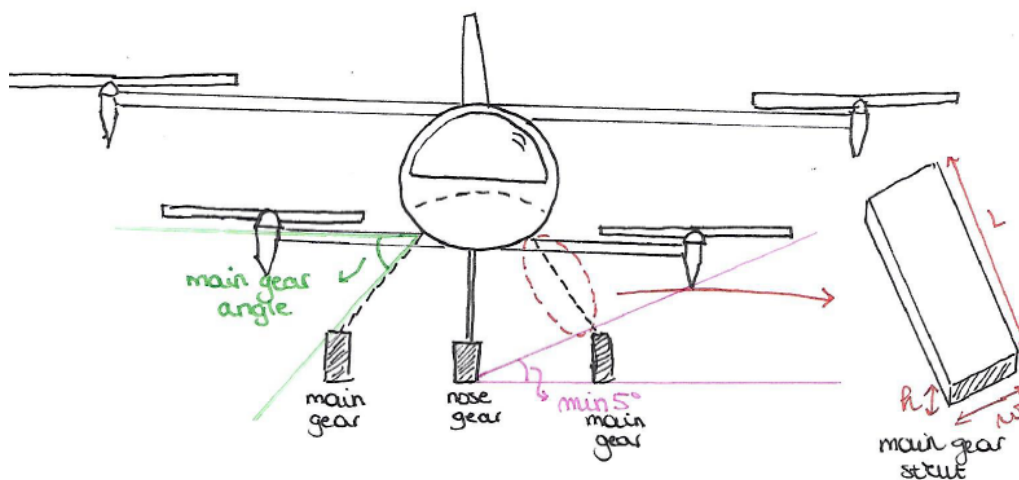


Figure 12.8: Sketch of landing gear ground clearance angle and main gear strut dimensions (not to scale)

Table 12.2: Main gear strut dimensions

Strut length [m]	Strut sideways angle [°]	Suspension height [m]	Cross section width [m]	Cross section height [m]
1.1	43	0.17	0.033	0.025

12.4.3. Nose gear strut design and suspension

For the nose gear a different approach is needed since a spring steel strut needs to be mounted at an angle to load it in bending. Whereas the angled mounting of the main gear was already necessary to comply with the minimum track width this is not needed for the nose gear. Still mounting it at an angle to have a spring steel strut is not beneficial for the nose gear since an angled strut increases the wetted area and makes the steering more difficult than a strut mounted vertically. Instead the suspension mechanism will consist of an off-the-shelf oleo pneumatic shock absorber which is 60cm long, weighs 4.5kg and costs € 783 (880\$¹⁰). Due to restrictions in access to more information about aircraft parts it is believed that this strut is not the most optimum yet but it was the best that could be found. Probably other shock absorbers are available that perform the function at a lower weight. The strut itself will again be made of steel 300M, with this time, a hollow circular cross section. The circular cross-section was chosen as it gives a more stiff structure, because for the nose gear the strut itself will not act as suspension, only the oleo pneumatic shock absorber will absorb the landing loads. The strut's height will be such that it is equal to the height of the main landing gear struts. This way, the aircraft will be in fully horizontal position on the ground, which eases the vertical take-off and landing as the aircraft is already correctly levelled. The cross-section diameter and thickness of the strut were determined to make sure no yielding or buckling of the strut occurs. the required shock absorber length for the oleo pneumatic absorber was found in Roskam [35, part IV]

$$S_s = [(0.5(P_n/g)(w_t)^2/(n_s L_{dynamic} N_g) - \eta_t s_t)/\eta_s] \quad (12.6)$$

where: P_n is the static load on the nose wheel strut in [lbs];

w_t is the vertical touch down rate in [ft/s];

n_s is the number of nose struts;

$L_{dynamic}$ is the maximum dynamic load on nose wheel strut in [lbs] ;

N_g is the load factor on the nose gear strut, which can be assumed to be equal to 3 according to [35, part IV];

η_t is the tire energy absorption efficiency, which is equal to 0.47 according to [35, part IV];

s_t is the maximum allowable tire deflection in [ft];

η_s is the oleo pneumatic energy absorption efficiency, which is equal to 0.8 according to [35, part IV]. For the final stroke of the shock absorber, it is suggested to add one inch to the calculated length in [Equation 12.6](#)

The nose gear strut dimensions found, are summarised in [Table 12.3](#). The cylindrical steel part weighs 0.15kg.

Table 12.3: Nose gear strut dimensions

Strut length [m]	Suspension height [mm]	Cross section outer diameter [mm]	Cross section thickness [mm]
0.76	133	26	2

12.4.4. Landing gear overview

In [Table 12.4](#) an overview is given of the different parts considered in the landing gear, together with their mass and cost. For the metal struts the material cost was multiplied by 10 to account for manufacturing. This must be seen as a preliminary guess which must be revised once the proposals are requested from the suppliers. The total mass results in 45.11kg. To account for bolts and mountings 10% is added to the weight resulting in 49.67kg. The total cost results in € 6062 for all the components. The wheel assembly includes the rim and all necessary parts to attach the wheel to the strut, except the brakes they are included in the brake assembly with all necessary small parts.

¹⁰<https://www.aircraftspruce.com/catalog/lgpages/oleoshockstrut.php?clickkey=54670>[Accessed: 22.06.2020]

Table 12.4: Overview of wheel parts

Part	Type	Amount	Cost p.p. [€] ^{11 12}	Total cost [€]	Mass p.p. [g] ¹³
Main tire	Michelin 6.00-6 Aircraft tire	2	184.23	368.46	4120
Main tube	Michelin Airstop 6.00-6 inner tube	2	146.88	293.75	750
Main wheel assembly	Cleveland 40-97A Wheel assembly	2	939.01	1,878.02	4000
Main brake assembly	Cleveland30-63A Brake assembly	2	681.18	1,362.36	2000
Nose tire	Michelin 5.00-5 Aircraft tire	1	195.99	195.99	2530
Nose tube	Michelin Airstop 5.00-5 inner tube	1	155.11	155.11	450
Nose wheel assembly	Cleveland 40-77 Wheel assembly	1	769.27	659.27	1500
Main strut	Designed spring steel strut	2	126.56	253.12	7140
Nose strut	Designed circular beam	1	2.70	2.70	152
Shock absorber	Oleo Shock Strut 05-08750	1	783.20	783.20	4500

12.4.5. Verification and Validation

The landing gear design considers three main parts: the calculated static and dynamic loads experienced on the wheels, the calculated position of the landing gear and lastly the landing gear strut design. All of these will be verified/validated by changing some of the input parameters.

The calculation of the static loads and the positioning of the landing gear to make the nose gear carry more than 8% of the load was done by taking the sum of forces and sum of moments in a simple free body diagram. The formulas were again derived by another person to ensure the correctness.

As a second check, the maximum take-off weight of the aircraft was doubled to check the sensitivity of the design solution. This action should have no effect on the position of the landing gear, as the centre of gravity locations are also unchanged. However, it will have an effect on the loads experienced by the wheel and therefore the strut design will need to be altered accordingly. Since the weight distribution remains unchanged the static loads per wheel should double as well. Also the dynamic load should double as Roskam's formula is proportional to the aircraft weight. Performing the change in the code indeed leads to the expected results.

The calculation of the required track width w (lateral distance between the main wheels) of the main gear based on the sketch in Figure 12.9 [35, Part II] involves a lot of trigonometry and is quite error-prone. Therefore a verification of this calculation seems useful.

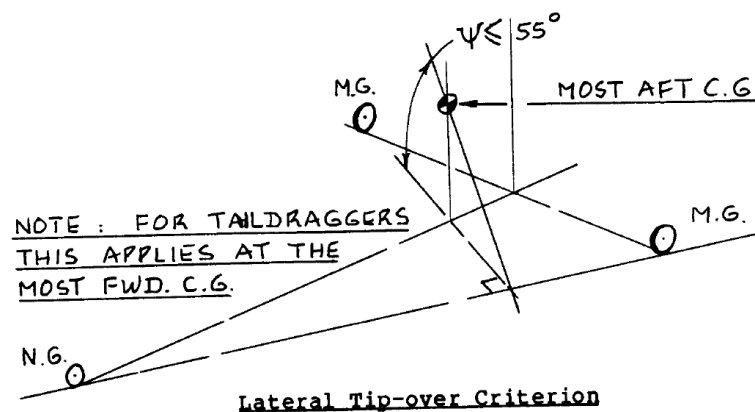


Figure 12.9: Lateral tip-over criterion

Firstly the formula used for that calculation was carefully re-derived on paper by hand. The resulting formula (see Equation 12.7) was the same as in the code and also gives the same results when using the same inputs.

$$w(h) = 2 \cdot (l_n + l_m) \tan \left(\sin^{-1} \left(\frac{h_{c.g.}}{\tan(\Psi) l_n} \right) \right) \quad (12.7)$$

¹¹p.p. = per part

¹²Cost estimate for all parts from <https://www.skygeek.com/>, [Accessed 11.06.2020]

¹³Mass estimate tires from https://www.tost.de/blog/category/aircraft_tires/?lang=en&post_type=katalog, [Accessed 11.06.2020], Mass estimate for tubes, wheel assemblies and brake assemblies from <https://www.skygeek.com/>, [Accessed 11.06.2020]

Where:

$w(h)$ is the minimum track width (lateral distance) between the main gear;

l_n is the longitudinal distance between main gear and nose gear and;

l_m is the distance between main gear and center of gravity (see [Figure 12.7](#)) and;

h_{cg} is the height of the center of gravity and lastly;

Ψ is the angle as given in [Figure 12.9](#).

Verification checks for limit values can be made. One would be to let the height of c.g. approach 0 (see [Equation 12.8](#)). The expected outcome is that the lateral distance between the main gears (track width w) will also converge to 0 since the lower the c.g. height the less track width is needed to not tip-over. This was checked in the code where the calculations were performed, and indeed showed the correct result, of the lateral distance converging to 0.

Secondly, the other part of the singularity can be investigated by letting the height of the center of gravity approach infinity (see [Equation 12.9](#)). This would result in a required track width going to infinity as well, as the wheels need to have a lateral distance that is infinitely large to make sure the aircraft does not tip over sideways. Also this test was confirmed by manually inputting the values in the code.

$$\lim_{h \rightarrow 0} w(h) = 0 \quad (12.8)$$

$$\lim_{h \rightarrow \infty} w(h) = \infty \quad (12.9)$$

After this, the design of the strut itself was checked. The first iteration of the main landing gear strut consisted of a circular cross-section beam made of aluminium 6061. The appropriate cross-sectional diameter and thickness were determined such that the strut would not yield under the applied loads. The g-forces experienced by the strut were determined using [Equation 12.5](#). It was found that the loads became very high, to an unacceptable level of about 14g. This means that the chosen cross-section shape and material did not provide the correct characteristics for proper suspension and high impact loads are encountered during landing. Therefore it was chosen to lower the bending stiffness (EI) of the landing gear rod, in order to make the beam bend more (without permanent deformation) and therefore lowering the loads on the landing gear.

This was achieved in a new design iteration where the material was changed to 300M Steel. The tensile yield strength of that steel is much higher than the one the Al 6061-T6 (1586 MPa¹⁴ vs. 276 MPa¹⁵). This allowed for a design with a height of 25mm and a width of 33mm resulting in a much lower moment of inertia (I). By that the bending stiffness (EI) was reduced which increased the deflection. This yields to lower and more achievable load factors around 2g.

In order to validate the design rod made of 300 M steel with a rectangular cross-section, it was decided to check with similar fixed landing-gear configurations and see whether it is in line with existing reference aircraft. As it can be seen in here¹⁶ spring steel struts are a common suspension method for the main gears of general aviation aircraft.

12.5. Wing Design

In this section, the design approach for the wingbox of the main wing, the canard and the vertical tail is considered.

12.5.1. Description and assumptions

The primary structure of the wing is the load-carrying wingbox. The secondary structures, LE (leading edge) and TE (trailing edge), will be looked into in [subsection 12.5.6](#). It is decided to design the wingbox with a trapezoidal cross-section, for the sake of simplicity. This means that the top web and the bottom web do not conform to the shape of the airfoil. The four webs of the wingbox are the top skin, the rear spar, the bottom skin and the front spar.

The y-axis is defined as direction along the span, positive towards the right wing of the aircraft when looking from behind, x-axis along the chord towards the nose and z-axis pointing to the ground. This becomes a right-handed coordinate system. If a different coordinate system is used for a part it will be explained in the section.

First the loads acting on the wing are determined, and the reaction forces at the root of the wing computed. The internal forces are then numerically integrated for each spanwise section, with a selected step size. The moment of inertia is calculated separately for each spanwise cross section, in this way accounting for possible taper of the wing, should any taper be required once the calculations are performed. Stress distributions are computed similarly for each section.

The assumptions are listed below, with a note about validity after:

¹⁴<https://www.azom.com/article.aspx?ArticleID=4370> [Accessed 19.06.2020]

¹⁵<http://asm.matweb.com/search/SpecificMaterial.asp?bassnum=MA6061T6> [Accessed 19.06.2020]

¹⁶<https://www.boldmethod.com/learn-to-fly/systems/how-the-4-types-of-landing-gear-struts-work/> [Accessed 19.06.2020]

1. All loads are carried by the wingbox, as it is the primary structure of the wing.
Design decision, additionally control surfaces are not yet considered for LE and TE.
2. The wingbox can be modelled as a trapezoid.
If the wingbox would conform to the curvature of the airfoil, it would have more cross-sectional area, and therefore more material, making it stronger.
3. No loads are acting in the y-axis, along the span.
Identified load cases do not have forces in the y-axis.
4. The cruise lift force, without any load factors, is equal to the MTOW.
This overestimates the loads, in cruise some fuel is already used and the mass is lower than the MTOW, this is therefore a safer design choice.
5. All loads are acting through the aerodynamic center.
Simplification of load cases.
6. The reaction forces in the structure are in an equilibrium state.
No accelerations present in the wing structure.
7. Wing has no sweep, no dihedral angle and no twist.
From aerodynamic design of the wing.
8. Assumption: The wingbox is a thin-walled structure: change in shear stress along the thickness is negligible and therefore shear can be studied as a shear flow within the structure.
Web thicknesses assumed to be in magnitude of 1mm.
9. The wingbox webs carry all shear stresses, not stringers.
Thin-walled closed-section with shear flow.
10. No buckling of the structure is allowed.
Buckling leads to failure faster, because the strength and therefore load-carrying capabilities of the structure are lowered.

12.5.2. Loads on wingbox

Firstly the loads on the wingbox are analysed. Two main load cases are identified based on the main positions of the propellers: loads during VTOL with MTOW, and loads in manoeuvres during cruise.

In cruise it is assumed, that the lift force acts vertically with respect to the wingbox, and that the lift force is equal to the MTOW, which overestimates the loads and is therefore a safer design choice. Usually, in manoeuvres, the lift force would not act exactly vertically.

The additional (external) maximum positive and negative load factors are identified in [section 7.3](#). In VTOL load factors of 2.0 and -0.5 are implemented for the thrust force, and in cruise manoeuvring load factors of 2.92 and -1.0 for the lift force. These are the limit loads that the structure will experience in flight. To reach the ultimate loads a safety factor of 1.5 is added to all loads.

The identified forces acting on the wingbox in VTOL are: VTOL thrust, weight of the wing, and weight of the motor. The forces in cruise are: lift, drag, thrust, weight of the wing, and weight of the motor. Additionally, control loads in z- and x- directions can be taken into account, and torque around z- or x-axis and torsion around y-axis caused by the motors added afterwards.

Using the known loads such as the thrust, weights and the aerodynamic loads, it was possible to determine the reaction forces at the fuselage of the aircraft. [Figure 12.11](#) shows the free body diagrams of the left wing, with the coordinate system being taken at the wing root.

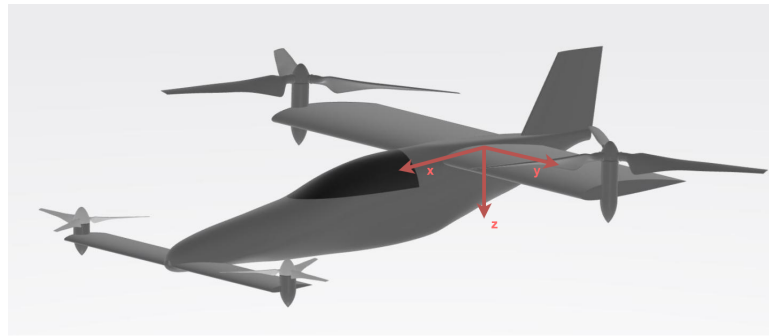


Figure 12.10: Coordinate System for Wing Structure Analysis

The diagrams present three different views of the wing (front, side and top) for the two identified loadcases, VTOL and cruise. In the diagrams the following loads and notations are used:

- ✈ R_x, R_y, R_z - reaction forces at the fuselage in the x, y, and z directions respectively.
- ✈ M_x, M_y, M_z - reaction forces at the fuselage around the x, y and z axis respectively.
- ✈ w_w, w_l, w_d - distributed loads of the wing weight, lift and drag respectively.
- ✈ W_{engine} - weight of the engine.
- ✈ L - resultant lift force (as seen from side view).
- ✈ T - thrust force. This varies based on the flight condition (T_{VTOL} and T_{cruise}).

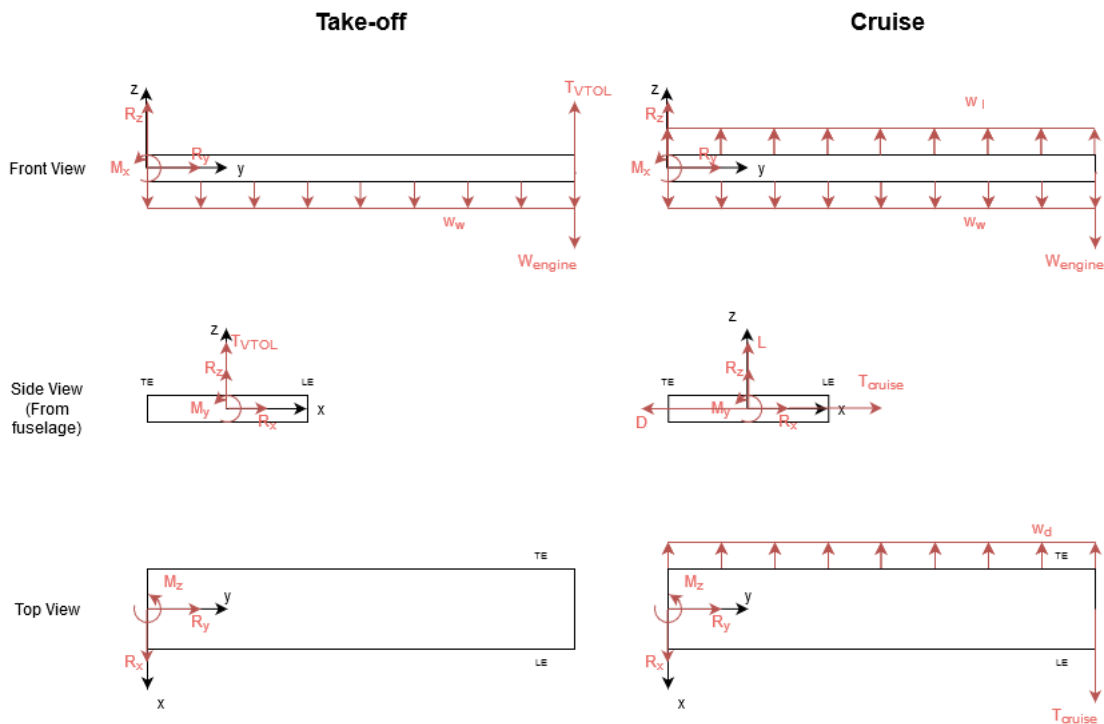


Figure 12.11: Free Body Diagrams of Left Wing during Take-Off (left) and Cruise (right)

With the assumption of equilibrium for both cases, the reaction forces can be determined for each case using the force and moment equilibria. Considering a length "l" for the halfspan, the equations for the VTOL configuration can be written as follows:

$$\begin{aligned}
\Sigma F_x : R_x &= 0 \\
\Sigma F_y : R_y &= 0 \\
\Sigma F_z : R_z - w_w \cdot l + T_{VTOL} \cdot l - W_{engine} \cdot l &= 0 \\
\Sigma M_y : M_y &= 0 \\
\Sigma M_z : M_z &= 0
\end{aligned}$$

Here the forces in x-direction can be determined looking at the side view and/or top view, the forces in y-direction from the front view and/or top view, the forces in z-direction from the front view and/or side view, the moments around the x axis are easiest seen from the front view, while the moments around the y and z axis can be observed from the side view and top view respectively.

A similar analysis can be performed for the cruise configuration, and considering once again the same halfspan length "l", the following equations are obtained:

$$\begin{aligned}
\Sigma F_x : R_x + T_{cruise} - w_d \cdot l &= 0 \\
\Sigma F_y : R_y &= 0 \\
\Sigma F_z : R_z - w_w \cdot l + w_l \cdot l - W_{engine} &= 0 \\
\Sigma M_x : M_x + w_l \cdot \frac{l^2}{2} - w_w \cdot \frac{l^2}{2} + -W_{engine} \cdot l &= 0 \\
\Sigma M_y : M_y &= 0 \\
\Sigma M_z : M_z + w_d \cdot \frac{l^2}{2} - T_{cruise} \cdot l &= 0
\end{aligned}$$

12.5.3. Moments of inertia of the cross-section

In order to determine the moments of inertia of the wingbox cross-section, the centroid has to be determined first. This however requires the determination of the centroid of each component of the wingbox, such as the top, bottom and side panels along with the stringers present on each of them. Figure 12.12 shows the cross section of the stringer used, which is divided into two sections, labelled with 1 and 2. The width of the stringer, labelled with w_s is equal to the height of the stringer h_s plus the thickness of the stringer t_s . Figure 12.13 shows in a similar fashion a cross-section of the wingbox, with only one additional stringer in the middle of the top panel, which is used for the sample calculations of the center of gravity and the moment of inertia of the box. In the actual design of the box, multiple stringers are used on both the top and the bottom panels. The code is built such that with each iteration, new stringers are added and the new centroid and moment of inertia of the wingbox are recalculated using the same method, based on the location of the new stringer(s). In this diagram, the panels' lengths and thicknesses are labelled with $l_1, l_2, l_3, l_4, t_1, t_2, t_3$ and t_4 respectively, starting with the top panel and moving in a clockwise direction. The angles α and β represent the angles with the horizontal of the top and bottom panels respectively. For both Figure 12.12 and Figure 12.13 the coordinate system used is indicated in red in the bottom left corner of each figure, while the dotted lines indicate an arbitrary position of the neutral axis, which is to be determined accurately in the following steps. In the calculations of the centroids and moments of inertia, the stringers are assumed to be in a perfect L shape, the inclination angle being taken into account only for the top and bottom panels of the wingbox. It must also be mentioned that the two figures presented are not to scale, they are simplified representations of the wingbox and its components.

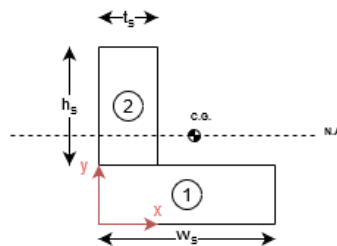


Figure 12.12: Stringer Cross-Section

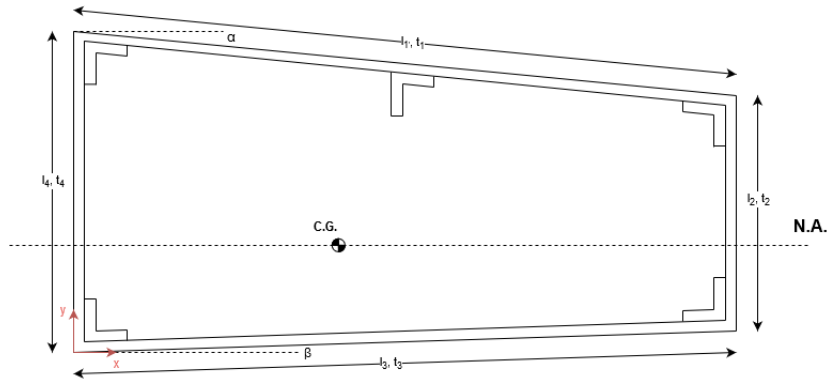


Figure 12.13: Wingbox Cross-Section

For determining the x and y coordinates of the centroid of a part, the following expressions are used:

$$\begin{aligned} \bar{x} &= \frac{\sum A_i x_i}{\sum A_i} \\ \bar{y} &= \frac{\sum A_i y_i}{\sum A_i} \end{aligned} \tag{12.10}$$

Here, A_i indicates the area of the individual components, and the x_i and y_i indicate the x and y coordinates of the same components.

For the stringer using the divisions shown in Figure 12.12, the centroid equations for the entire stringer can be applied as follows:

$$\begin{aligned} \bar{x}_s &= \frac{(t_s \cdot w_s) \cdot \frac{w_s}{2} + (t_s \cdot h_s) \cdot \frac{t_s}{2}}{(t_s \cdot w_s) + (t_s \cdot h_s)} \\ \bar{y}_s &= \frac{(t_s \cdot w_s) \cdot \frac{t_s}{2} + (t_s \cdot h_s) \cdot (t_s + \frac{h_s}{2})}{(t_s \cdot w_s) + (t_s \cdot h_s)} \end{aligned}$$

For the centroid of the wingbox without stringers, the centroids of the individual web panels must be determined with respect to the chosen coordinate system as shown in Figure 12.13.

$$\begin{aligned} \bar{x}_{bottom} &= \frac{l_3}{2} \cdot \cos(\beta) & \bar{x}_{LE} &= 0.5 \cdot t_4 \\ \bar{y}_{bottom} &= \frac{l_3}{2} \cdot \sin(\beta) & \bar{y}_{LE} &= 0.5 \cdot l_4 \\ \bar{x}_{top} &= \frac{l_1}{2} \cdot \cos(\alpha) & \bar{x}_{TE} &= l_3 \cdot \cos(\beta) - 0.5 \cdot t_2 \\ \bar{y}_{top} &= \frac{l_4}{2} \cdot \sin(\alpha) & \bar{y}_{TE} &= l_3 \cdot \sin(\beta) - 0.5 \cdot l_2 \end{aligned}$$

By plugging in all the values of the coordinates for the wingbox panels and stringers needed into Equation 12.10, the location of the center of gravity of the entire wingbox can be determined.

The mass moments of inertia can be determined using Steiner's Theorem, as follows:

$$\begin{aligned} I_{xx} &= I_{0x} + A \cdot dy^2 \\ I_{yy} &= I_{0y} + A \cdot dx^2 \\ I_{xy} &= I_{0xy} + A \cdot dx dy \end{aligned}$$

Here, the I_0 in each formula represents the moment of inertia of the component considered, A represents its area and dy represents the distance between the centroid of the component and the centroid of the box. The moment of inertia

of the components can be calculated using the standard equations due to the simple shapes. A rectangular shape such as the segments of the stringers and the panels labelled with 2 and 4 in [Figure 12.13](#) (trailing edge and leading edge respectively), the moment of inertia is given by [Equation 12.11](#).

$$I = \frac{b \cdot h^3}{12} \quad (12.11)$$

Where b is the side of the rectangle parallel to the axis considered for the moment of inertia and h is the side that is perpendicular to this axis.

The top and bottom panels of the wingbox as seen from [Figure 12.13](#) are at an angle, and therefore require a different expression for determining their moment of inertia. This can be seen in [Equation 12.12](#).

$$\begin{aligned} I_{xx} &= \frac{l^3 \cdot t \cdot \sin^2 \alpha}{12} \\ I_{yy} &= \frac{l^3 \cdot t \cdot \cos^2 \alpha}{12} \\ I_{xy} &= \frac{l^3 \cdot t \cdot \sin(2\alpha)}{24} \end{aligned} \quad (12.12)$$

Here, l is the length of the tilted panel, t is the thickness of the panel and α is the angle the panel makes with the horizontal.

12.5.4. Stresses on the cross-section

Shear flow and shear center

Firstly, all web lengths are divided into smaller segments. For now the number of segments is the same in all four webs, in order to ease the integration of the results. The segments are used to integrate numerically over the length of the web, by moving step by step through the segment points.

Here it must be noted that no boundary values are known for ending points of the webs, which are also the corner points of the wingbox cross section, and therefore the numerical integration has an inaccuracy when moving over the corner point to the next web. It is now assumed that the last found segment value will be the starting value of the next web, thus ignoring the missing corner values. This issue causes a difference between the first point of evaluation, and the last corner point of the fourth web, when the shear flow values have been integrated over the total cross section. This inaccuracy however does not have a major effect on the magnitude of the shear flow.

Steps of the method of computing shear flow and the shear center are introduced here, and they will be elaborated upon after.

1. Apply internal vertical shear force
2. Compute basic shear flow q_b
3. Assume shear force acting through shear center
4. Compute constant shear flow q_{s0}
5. Through moment equilibrium find x-coordinate of shear center

Afterwards same is repeated for forces in x-direction:

6. Apply internal horizontal shear force
7. Compute basic shear flow q_b
8. Assume shear force acting through shear center
9. Compute constant shear flow q_{s0}
10. Through moment equilibrium find y-coordinate of shear center

Now the location of the shear center is known for each cross section. As the internal shear forces in x and y are not actually acting through the shear center, the resulting q_{s0} will be differ from those computed in points 4 and 9. To compute the actual shear flow due to the forces a new constant shear flow must be calculated.

11. Add both basic shear flows q_b due to vertical and horizontal forces
12. Through moment equilibrium around intersection point of lines of action, compute q_{s0}
13. Add q_{s0} to q_b
14. Convert shear flow to shear stress
15. Find maximum shear stress for each web

Now looking into the steps in more detail. The wingbox experiences shear forces in both vertical and horizontal direction, applied at some distance away from the unknown location of the shear center, as presented in [Figure 12.14a](#). Starting with the first five steps, only the internal vertical shear force is shown in [Figure 12.14b](#), and as will be discussed later, it is now assumed to act through the shear center. This force causes a shear flow along the cross section, this is **step 1**. As the cross section is closed and unsymmetrical, the exact location of the shear center is not yet known. The internal shear force is depicted in [Figure 12.14](#). The used coordinate system is shown to start at the top left corner, and the angles α and β are the angles of the top and bottom skin with respect to the horizontal lines parallel to the x-axis.

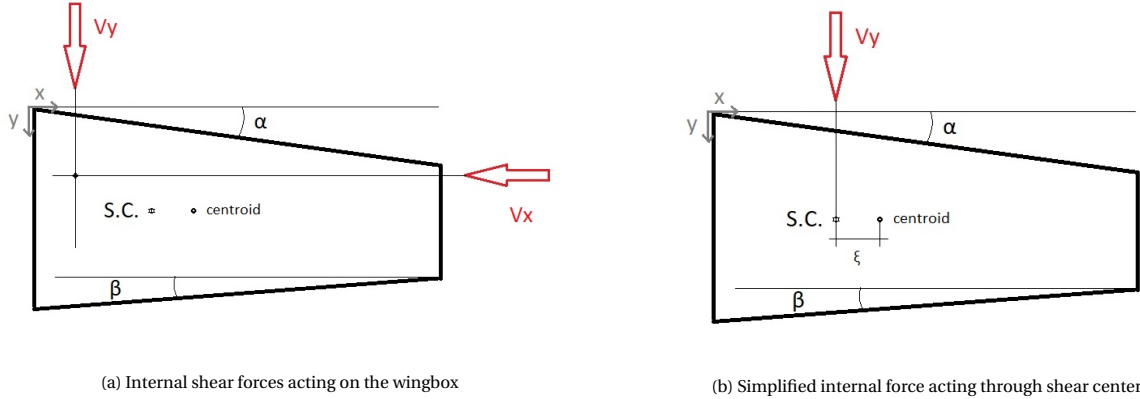


Figure 12.14: Shear forces in the cross-section

The shear flow due to internal forces in both x and y direction can be found with [Equation 12.13](#).

$$q_s = -\frac{V_y I_{yy} - V_x I_{xy}}{I_{xx} I_{yy} - I_{xy}^2} \int_0^s ty ds - \frac{V_x I_{xx} - V_y I_{xy}}{I_{xx} I_{yy} - I_{xy}^2} \int_0^s tx ds - q_{s0} \quad (12.13)$$

From this it can be seen that the shear flow has two components, that can be computed separately and then added together, using the principle of superposition [33], this is presented in [Figure 12.15](#). The basic shear flow, noted as q_b , is computed by applying an imaginary 'cut' in the cross section, making it an open section. Now it can be said that the starting point of the shear flow is the cut, where q_b is equal to zero. The basic shear flow for each web section is then computed from that point onwards, with [Equation 12.14](#), completing **step 2**.

$$q_b = -\frac{V_y I_{yy} - V_x I_{xy}}{I_{xx} I_{yy} - I_{xy}^2} \int_0^s ty ds - \frac{V_x I_{xx} - V_y I_{xy}}{I_{xx} I_{yy} - I_{xy}^2} \int_0^s tx ds \quad (12.14)$$

The assumed direction of the shear flow is indicated in [Figure 12.15a](#), together with the location of the cut. The cut is made at the top left corner, where the coordinate system starts. The integration in y is then performed separately for each web section. Once the basic shear flow is known, the shear center can be found.

In order to find the shear center, the constant shear flow q_{s0} needs to be computed. For this it is for now assumed, that the internal shear force is acting through the shear center, as mentioned in **step 3**, therefore not causing twist in the structure. Completing **step 4**, the constant shear flow is given by [Equation 12.15](#).

$$q_{s0} = -\frac{\oint (q_b / Gt) ds}{\oint ds / Gt} \quad (12.15)$$

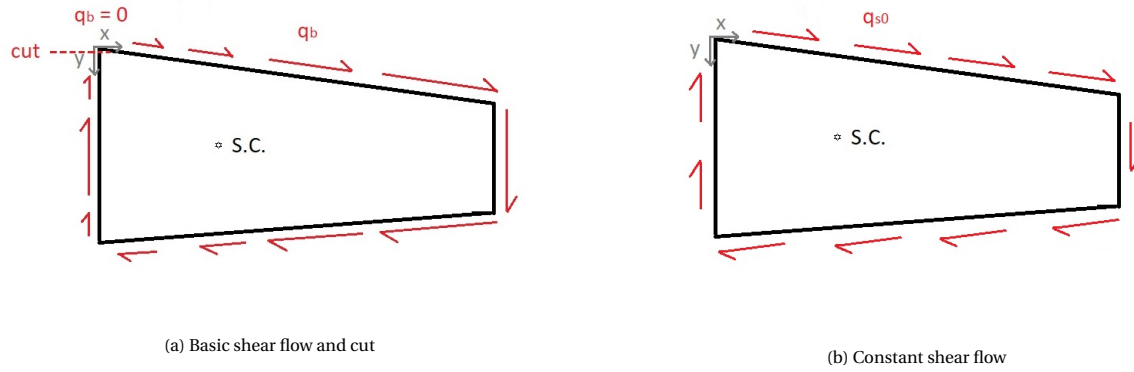


Figure 12.15: Superposition of shear flows

Having assumed, that the force is acting through the shear center, the x-coordinate of the shear center with respect to the centroid, here noted as ξ , is the only unknown.

As **step 5**, moment equilibrium of the shear force and the shear flows is taken around the top left corner, which is a convenient point, because the shear flow on the top skin and on the front spar do not create moments around this point. From [Equation 12.16](#) the x-coordinate of the shear center is first found regarding the top left corner point, and it can be converted to distance ξ from centroid.

$$V_y \xi = 2A_m q_{s0} + \oint \rho q_b ds \quad (12.16)$$

In [Equation 12.16](#) the variable ρ presents the moment arm of the shear flow to the chosen point of reference.

The same steps are taken for forces acting in horizontal direction, from **step 6** to **step 10**, and the y-coordinate of the shear center with respect to the centroid is found.

Finally, as the shear center location is known, the actual shear flows in the cross section are computed, going back to [Figure 12.14a](#). Previously, it was assumed, that the internal shear forces are acting through the shear center, but in reality, this is unlikely the case. Starting from **step 11**, the basic shear flows q_b due to the internal forces stay the same, and are added together. The constant shear flow is now computed with respect to the intersection point, which is found from the actual lines of action of the internal shear forces. This is **step 12**. The [Equation 12.17](#) is used, which is similar to [Equation 12.16](#), but now as the intersection point of lines of action is the reference, there is no moment contribution of V_y or V_x , and the moment arm ρ differs.

$$0 = 2A_m q_{s0} + \oint \rho q_b ds \quad (12.17)$$

When both parts of the total shear flow are computed, these can be added together according to the principle of superposition, as shown in [Figure 12.15](#), fulfilling **step 13**. An assumption was made, that for a thin-walled structure the shear stress variation through the thickness is negligible, and for this reason the shear flow representation could be used. In order to convert shear flows into shear stresses, [Equation 12.18](#) is used, considering **step 14**. As the final action, **step 15**, the maximum stress on the cross section is found.

$$\frac{q}{t} = \tau \quad (12.18)$$

Normal stress

In order to compute the normal stresses in the structure, first the four webs are divided into shorter segments, similarly to what is done for the shear stress. The same coordinate system is also used for the normal stress, as shown in [Figure 12.14](#).

The normal stress in each segment is computed with [Equation 12.19](#).

$$\frac{(M_x I_{yy} - M_y I_{xy})y + (M_y I_{xx} - M_x I_{xy})x}{I_{xx} I_{yy} - I_{xy}^2} \quad (12.19)$$

In this equations y and x are the distances from the neutral axes.

12.5.5. Buckling

The a material failing due to a tensile load is easily understood as it is one of the mechanical properties. For thin walled structures, loaded into anything other than pure tension, buckling could be the first failure mode. The three most likely buckling modes are described in this subsection.

Shear buckling When a high shear load is applied on an thin sheet, this skin could buckle. After the skin is buckled it will start to deform more. This is not beneficial for the structure itself and the subsystems it is attached to. The critical stress at which the skin would buckle was calculated with Equation 12.20. If the shear force in the skin would be higher than this value, the skin would buckle. The E-modulus (E) and Poisson's ratio (ν) are from the material that is used to fabricate the spar web. The value b was defined to be the height of the spar itself. The value k varied with the length over height ratio. For an ratio over 2: k = 6, a ratio of less than 2: k = 7, a ratio of less than 1.5: k = 8 and a ratio of less than 1: k = 9. The spars thickness was chosen in such a way that no buckling would occur in the spar.

$$\tau_{cr} = k \frac{\pi^2 E}{12(1 - \nu^2)} \left(\frac{t}{b} \right)^2 \quad (12.20)$$

When a high shear load is applied on an thin sheet, this skin could buckle. After the skin is buckled it will start to deform more. This is not beneficial for the structure itself and the subsystems it is attached to. The critical stress at which the skin would buckle was calculated with Equation 12.20. If the shear force in the skin would be higher than this value, the skin would buckle. The E-modulus (E) and Poisson's ratio (ν) are from the material that is used to fabricate the spar web. The value b was defined to be the height of the spar itself. The value k varied with the length over height ratio. For an ratio over 2: k = 6, a ratio of less than 2: k = 7, a ratio of less than 1.5: k = 8 and a ratio of less than 1: k = 9. The spars thickness was chosen in such a way that no buckling would occur in the spar.

Buckling of a stiffened panel

The top and the bottom skin are susceptible to buckling due to negative normal stresses, otherwise known as compression. To prevent these panels from buckling the thickness of the skin could be increased. The formula for the skin critical stress is given in Equation 12.21. This is however not the best method when optimising for the weight. The critical stress does not change significantly with a thicker skin but the weight certainly does. A better way is to stiffen the skin with the help of stiffeners. The new critical stress of the panel is calculated in different steps. First the crippling stress of the stiffener is calculated with Equation 12.22. The following variables are C: 0.425, b: the width of the stringer section, α : 0.8, n: 0.6. The last two values are equal for all aluminium alloys. If the output of this formula is above 1 the yield stress of the material of the stringers is used. With the crippling stress of the stiffener the stiffened area of the skin can be calculated in Equation 12.23. This width could be subtracted from the width of the skin (b). By adding the stiffener the panel is also divided into multiple sections further increasing the critical stress of the skin. To get the actual crippling stress of the panel, Equation 12.24 is used. For the Equation 12.23, a value of 6.98 was chosen for the C value. This value is correct with the assumption that the spacing between the stringers will not be less than 10 cm. The C value for the skin changes with the amount of stringers. For a panel with no stringers a value of 6.98 is appropriate because the spars will have a clamped connection on the side. With one stringers in the middle the C value changes to 5.41 because one side is now simply supported. With more stringers the panels in the middle will be simply supported on all sides and have a C value of 4.

$$\sigma_{cr} = C \frac{E\pi^2}{12(1 - \nu^2)} \left(\frac{t}{b} \right)^2 \quad (12.21)$$

$$\frac{\sigma_{cc}}{\sigma_y} = \alpha \left(\frac{C}{\sigma} \frac{E\pi}{12(1 - \nu^2)} \left(\frac{t}{b} \right)^2 \right)^{1-n} \quad (12.22)$$

$$2we = t \sqrt{\frac{C\pi E}{\sigma_{cc} 12(1 - \nu^2)} \left(\frac{t}{b} \right)^2} \quad (12.23)$$

$$\sigma_{cr_{panel}} = \frac{\sum \sigma A}{\sum A} \quad (12.24)$$

A loop was used to find the right number of stringers for the wingbox, each time calculating the critical stress of the panel and comparing it with the compressive stress in the panel. If the critical stress is lower a stringer was added to the skin.

Column buckling of the stiffeners

The stiffeners that support the skin from buckling can also buckle themselves. These stiffeners will experience Euler buckling due to their length. To prevent them from buckling, ribs were placed in the structure to divide up the length of the stiffeners. The formula for Euler buckling is given in Equation 12.25, where C is a coefficient determined based

on the type of constraints on each side of the stringer, E is the elastic modulus of the material of the stringer, I_{xx} is the moment of inertia of the stringer and L is the length of the stringer. Here, C is 0.25 due to the stringers being free at their end. Lastly, P_{cr} is the critical force to buckle the beam.

$$P_{cr} = C\pi^2 E \frac{I_{xx}}{L^2} \quad (12.25)$$

This can be converted to stress by dividing it by the area of the stringer. A rib is needed when the critical stress is lower than the highest compressive stress in that part of the skin.

12.5.6. Wing structure

In order to determine the number of reinforcements as well as their dimensions within the wingbox, a Python tool was created. This tool puts all of the previously described calculations from this chapter together, and is capable of iterating over a number of different situations, starting from a number of fixed inputs coming from the different departments (such as load distributions from aerodynamics, weights of the propellers from propulsion, material properties from structures, etc.). In the main combined wingbox design tool the following steps are taken:

1. Divide halfspan into sections
2. Define VTOL and cruise loads and reaction forces
3. Calculate internal loads for each spanwise cross-section
4. Compute cross-sectional properties, such as moment of inertia
5. Check shear and normal stresses in structure
6. Check for buckling: if critical buckling stress is exceeded, add stringer and repeat from step 4, with moments of inertia
7. If rib is needed to avoid buckling, add rib
8. Sum weights of webs and stringers of each spanwise section

A similar wingbox structure will be made for the canard, the wing and the vertical tail.

Both VTOL and cruise limit loads were taken into account, with maximum load factors of 2 and 2.92 respectively. The negative load factors of -0.5 and -1.0 were also tested. For the ultimate loads the safety factor 1.5 is added. The structure is allowed to break after three seconds when loaded in ultimate loads [3], with ultimate stress of aluminium 6061 being at least 290 MPa [18].

In order to reach a long lifetime for the wingbox structures of the canard and the main wing, the normal cruise and VTOL loads without any additional load factors from manoeuvres or gusts, are tested for fatigue strength. Here the safety factor is also left out. The fatigue limit of aluminium 6061 T6 is taken as 112 MPa [18], and the structures are designed such that this fatigue limit is not exceeded with the normal loads.

The final dimensions of the wingbox, canard and the tail are given in [Table 12.5](#), [Table 12.6](#), and [Table 12.7](#) respectively. The indicated number of stringers also includes the corner ones. Note that the mass value is the mass of the wingbox for a halfspan, not the total wing. Also this value does not include the LE and TE of the wing.

LE and TE

For the secondary structures in the wing, the LE and the TE, a thermoplastic material was chosen, and 3D printing thought as manufacturing process in [subsection 11.4.1](#).

These parts need more elasticity than strength, because they are not load-carrying structures, but they will experience deflections from the loads on the wing, as they are connected to the wingbox. The LE and TE are subjected to impacts from foreign object damage. For these reasons, the LE and TE do not have to be padded completely with the polymer, even if the print has a pattern with low infill percentage. A thick lining could be used instead of completely filling the cross-section, in order to reduce the weight of the wing structure. The thickness of the lining still has to be optimised for each section of the LE and TE, but for now thicknesses of around 5 centimetres are considered, because this would still allow for an infill. Additionally, it is important to note, that the thinner the structure, the more accuracy is also required from the printer.

A possible structural pattern for these linings could be a 2D or 3D honeycomb. 2D honeycomb is a strong, light-weight pattern, but 3D honeycomb would give it a more quasi-isotropic lay-out, offering same properties in all directions, which could be interesting for impact resistance. The 2D honeycomb is visualised in [Figure 12.16a](#)¹⁷. In the same figure different infill percentages are also presented. The infill percentage should be optimised for each location, but for the weight estimation an infill of 20% is assumed now, as this is commonly used in 3D prints for durability¹⁸. Lower infill percentage reduces the cost and makes the structure more flexible, but also weaker. The 3D honeycomb

¹⁷<https://pinshape.com/items/25524-3d-printed-display-tray-for-infill-pattern-and-infill-density> [Accessed 20.06.2020]

¹⁸<https://all3dp.com/2/infill-3d-printing-what-it-means-and-how-to-use-it/> [Accessed 20.06.2020]

Table 12.5: Main wing wingbox

Parameter	Value	Unit	Mode
Top web t	0.8	mm	-
Rear spar t	0.8	mm	-
Bottom web t	0.8	mm	-
Front spar t	0.8	mm	-
Stringer t	1	mm	-
Stringer h	10	mm	-
Max shear stress	13.91	MPa	Cruise
Max compressive stress	221.4	MPa	VTOL
Max tensile stress	272.9	MPa	VTOL
Top web stringers at root	21	-	-
Top web stringers at mid section	8	-	-
Top web stringers at tip	3		
Bottom web stringers at root	11		
Bottom web stringers at mid section	3		
Bottom web stringers at tip	3		
Number of ribs	11	-	-
Wingbox mass	14.4	kg	-

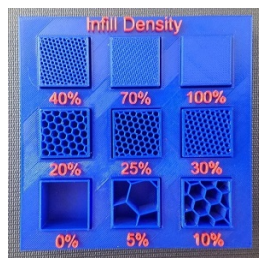
Table 12.6: Canard wingbox

Parameter	Value	Unit	Mode
Top web t	1.7	mm	-
Rear spar t	1.7	mm	-
Bottom web t	1.7	mm	-
Front spar t	1.7	mm	-
Stringer t	1	mm	-
Stringer h	10	mm	-
Max shear stress	16.83	MPa	Cruise
Max compressive stress	231.8	MPa	VTOL
Max tensile stress	285.1	MPa	VTOL
Top web stringers at root	7	-	-
Top web stringers at mid section	4	-	-
Top web stringers at tip	3		
Bottom web stringers at root	5		
Bottom web stringers at mid section	4		
Bottom web stringers at tip	3		
Number of ribs	7	-	-
Wingbox mass	12.5	kg	-

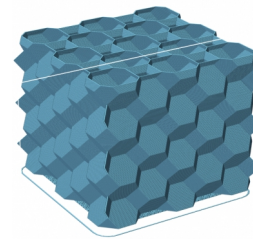
Table 12.7: Tail wingbox

Parameter	Value	Unit	Mode
Top web t	0.5	mm	-
Rear spar t	0.5	mm	-
Bottom web t	0.5	mm	-
Front spar t	0.5	mm	-
Stringer t	1	mm	-
Stringer h	10	mm	-
Max shear stress	31	MPa	Gust
Max compressive stress	124	MPa	Gust
Max tensile stress	148	MPa	Gust
Top web stringers at root	6	-	-
Top web stringers at mid section	3	-	-
Top web stringers at tip	3		
Bottom web stringers at root	6		
Bottom web stringers at mid section	3		
Bottom web stringers at tip	3		
Number of ribs	3	-	-
Wingbox mass	5	kg	-

is visualised in Figure 12.16b¹⁹. In a 2D honeycomb structure it would be possible to have small holes going through the honeycomb hexagon tubes, in order to allow for moisture to leave the structure. This should be studied in more detail in the future. In Figure 12.17 the structure is visually presented. Note that the dimensions in the figure are not to scale.



(a) 2D honeycomb with differing infill percentages



(b) 3D honeycomb

Figure 12.16: Possible infill patterns

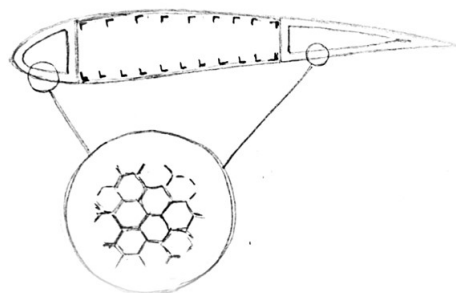


Figure 12.17: Wing cross-Section

Future improvements

First of all, to improve the structural design of the wingboxes, the effects of the assumptions need to be looked into further and possibly some simplifications removed. These include the assumption on the lines of actions of the forces, that all forces are acting through the aerodynamic center, and the forces acting purely in x, y or z. The first main

¹⁹<https://engineerdog.com/2015/03/08/3d-printing-a-3d-honeycomb-infill-concept/> [Accessed 20.06.2020]

improvement would come from making the wingbox top and bottom skin conform with the curvature of the airfoil, because for now a trapezoidal geometry was used.

Secondly, for now buckling is avoided completely, and due to that reason, in ultimate load the main wing structure does not reach the ultimate stress that the material can withstand. However, in reality, some buckling is allowed in the structure under the limit loads. This in turn will reduce the load-carrying capability of the structure itself, which means that the structure will in fact reach the ultimate stress under the ultimate load. More research should be made into how much buckling the structure is allowed to undergo and at what stress levels, how the buckling affects the strength, and from this the structure can be optimised to break exactly at the ultimate loading condition.

Thirdly, the deflections in the structures should be looked into, in order to verify that the wingboxes do not deflect unreasonably much. The deflections are also needed to optimise the LE and TE designs. Additionally, the number of segments for each web should be adjusted in the coding tool based on where the highest stresses are found. The higher the stresses the more accurate results can be found by increasing the number of segments.

12.5.7. Verification and Validation

In order to check the result of the calculations, verification and validation (where possible) have to be performed for the codes used in the structural analysis calculations.

Moments of inertia

In the moments of inertia code, the verification can be done through a number of unit tests, performed for the centroid calculations of individual parts, followed by unit tests for the moments of inertia of individual components.

All of these can be performed using an online calculator²⁰. This allows for the construction of simple shapes such as the plates of the wingbox, but also more complex shapes such as various types of stringers. By selecting the same dimensions for these components, the centroid and moments of inertia came out at the same values as the ones computed using the code, therefore indicating a successful verification.

Validation unfortunately is difficult to perform due to the lack of data present about the actual components used for aircraft, but also due to the nature of the project, this aircraft being on the newer side of development, meaning that not many similar sized aircraft exist for an accurate comparison to be made. The results of the unit tests are given in Table 12.8. Due to the high number of components, the table presents only two of the tests as an example, namely for the stringers and leading edge plate of the wingbox (denoted in the table as LE). The computations for the other plates were made using the same formulae, indicating they should be correct as well, however they have been tested individually as well just for good measure.

Table 12.8: Verification Centroids and Moments of Inertia

Tested Element	Calculated Value	Unit	Verification Value	Unit
Stringer Centroid (x-location)	6.238	mm	6.24	mm
Stringer Centroid (y-location)	6.238	mm	6.24	mm
Stringer I_{xx}	3883.238	mm^4	3.880	mm^4
Stringer I_{yy}	3883.238	mm^4	3.880	mm^4
Stringer I_{xy}	-2304.762	mm^4	-2.300	mm^4
LE Centroid (x-location)	0.625	mm	0.625	mm
LE Centroid (y-location)	80.775	mm	80.8	mm
LE I_{xx}	439.187	mm^4	439.000	mm^4
LE I_{yy}	26.294	mm^4	26.3	mm^4
LE I_{xy}	0	mm^4	0	mm^4

In some of the numbers, slight variations can be noticed. These could have been caused by the accuracy of the program used for verifying. The limitation comes from the number of decimals which can be imputed from the code into the external program. Due to roundings, the final values of the moments of inertia are also affected. For the calculations where exact values were easy to input (e.g. thicknesses and lengths of the stringers), the results were almost identical (e.g. centroid locations).

²⁰<https://clearcalcs.com/freetools/free-moment-of-inertia-calculator/au>, Accessed [21.06.2020]

Shear stress

For the verification of the shear stress a rectangular shape is used, because the centroid location, the shear center location and the shape of the shear flow distribution are all known. The centroid is at the intersection of the axes of symmetry, and the shear center coincides with the centroid. The coordinate system presented in Figure 12.14 is used.

The shear center location computed by the program is verified by comparing to the known centroid of the rectangle. A small inaccuracy is noted in the shear center computation. The expected location would be exactly at the centroid, with x- and y-coordinates of 0.75 and 0.10 respectively, when looking from the top left corner. The program however outputs the coordinates 0.76 and 0.12. This difference is expected to be caused by the missing boundary values for the corner points, as was explained in subsection 12.5.4. For the numerical integration it was assumed that the starting value of the shear flow in the next web has to be equal to the last value of the preceding segment. This however leads to a small inaccuracy when crossing each corner point, which then adds up to a larger inaccuracy in the shear flow values between the front spar and the top web, thus the last and first point of integration.

The error could also indicate an integration error in shear flow due to forces acting in x-direction, but the source of such an error could not be found. The inaccuracy in the shear center is of negligibly small magnitude in x-coordinate, but the error is too large in the y-coordinate for the shear center to be of use in computing twist.

When a shear force acting along y-axis is applied at the shear center, the shear flow distribution of Figure 12.18 should be obtained. The shear flow values that the shear flow calculator outputs are checked manually to see if they match the expected shape. This is done by looking at the values at the corners of the webs, to see that they match in both magnitude and sign, and at the known positions of the neutral axis, to ensure that the values are following the expected patterns. Additionally the change in shear flow within each segment is checked, to see that the pattern follows the correct shape, either increasing/decreasing linearly, or increasing parabolically until reaching the neutral axis, and then decreasing parabolically.

From this analysis it can be said that the shear flow outputs of the calculator follow the expected patterns in both cases, for the basic shear flow when a cut is made, and the total shear flow after superposition is applied.

The shape of the shear flow distribution could be verified by comparing to the expected result of a known simple shape. The magnitude of the shear flow was also only tested against manual computations. The inputs of the shear flow calculator are made to match example cases Structural Analysis course of the Aerospace Engineering Faculty [33], and the output values are compared to the solved results. The output of the program is found to be in the correct order of magnitude. Future improvements in calculations could be made by verifying the output values for unsymmetric shapes with FEM-analysis.

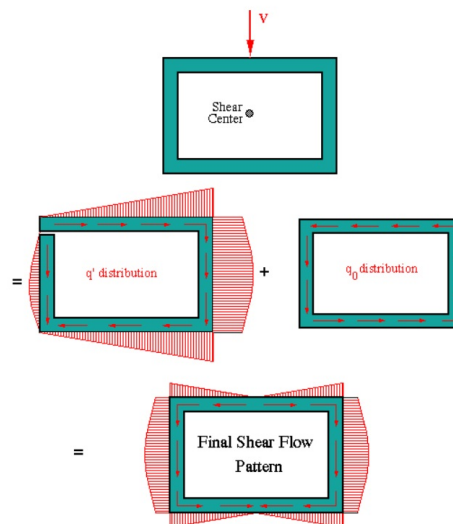


Figure 12.18: Expected shear stress distribution for thin-walled rectangular cross-section

Normal stress

The calculations of the normal stresses are very simple and can be verified by looking into the output values. A rectangular shape is used for the verification, as it is a simple shape, with two axes of symmetry. The centroid is known to lie at the intersection of the axes of symmetry, and the neutral axes are known to lie exactly on the axes of symmetry, when a pure moment is applied around one of the lines of symmetry of the cross-section. The shape of the normal stress distributions is also known for a rectangle in pure moment around x- or y-axis of the cross-section, it is visually presented in Figure 12.19.

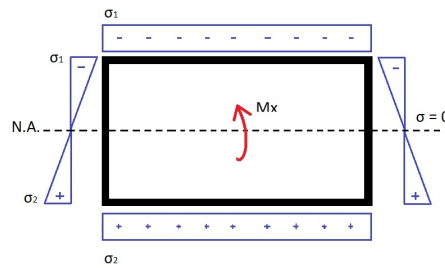


Figure 12.19: Normal stress distribution for thin-walled rectangular cross-section

When a known moment around the x-axis is applied, for example an assumed moment caused by the lift force acting on the wingbox, it is expected that the top skin will experience compression, and the bottom skin tension. This is depicted with the positive and negative signs in Figure 12.19. For a rectangle, the absolute distance of the top skin to the neutral axis the same as the absolute distance from the bottom skin. Therefore the normal stresses σ_1 and σ_2 should have the same magnitudes. On the neutral axis the normal stress should be equal to zero.

The shape of the normal stress distribution computed by the program is as expected, the obtained test results are shown in Table 12.9.

Table 12.9: Normal stress verification test

Parameter	Value	Unit
Web skin t	1	mm
Spar heights	0.2	m
Top and bottom web lengths	1.5	m
Ixx	0.00002	m ⁴
Iyy	0.00025	m ⁴
Mx	12,000	Nm
Max compressive stress	-60	MPa
Max tensile stress	60	MPa
Stress at mid-spar	0	MPa

Stringers and ribs

The stiffeners are calculated within a loop. At first it calculates the Critical stress of the panel without stiffeners. It compares this value with the maximum compressive stress in the panel. If the maximum stress in the panel exceeds the critical stress of the panel a stringer is added.

This stress calculation was tested by calculating the value both by hand and let the computer run the code. These two calculations matched for each of the three cases and thus verified that the equations where correctly implemented. The first case where there is no stringer, the second with one stringer and the third with more than one stringer. The last case is needed due to the different clamping case with more than one stringer. To verify that the code indeed found the correct number of stringers the intermediate outputs where printed and checked. If the critical stress was still below the normal stress it needed to iterate. If it had reached the part it needed to stop. By observing the code it was clear that it did not over- or undershoot the number of stringers that where needed. For the Euler buckling the code was checked by using hand calculations. The output of the program matched the value that was calculated by hand.

The validation of these formulas was achieved by looking at different sources. It was found that all sources had same approach to calculating the stiffened panel and the Euler buckling. These sources were [29],[33] and [23].

12.6. Circular economy principle: joining method

The joining method that will be used to join different systems and subsystems has a big impact on the ability to disassemble the aircraft. Easy disassembly will facilitate the circular economy principle where disassembled, recycled and refurbished parts will loop back into the manufacturing and joining phases of the aircraft. The ease of unfastening the joined parts is mainly determined by the following factors: the fastener type/process which comes from the material choice, the accessibility, the tool needed to unfasten and the end-of-life condition[40].

To follow the circular economy principle, the use of non-permanent fasteners and fastener types that can easily be unfastened, is beneficial. Therefore it was chosen to make use of bolts and screws. The parts/structures that will

be joined are made of aluminium types. With simple reinforcement to reduce the stress concentrations, aluminium provides the perfect material characteristics for joining with bolts or screws. For aerodynamic reasons, one should consider the bolts not interrupting the aerodynamic flow and join as much as possible from the inside of the structures. In order to achieve this, the structures should be easily accessible from all sides. As already described, the fuselage structure will be made out of trusses. The truss structure has the advantage of providing easy accessibility over the whole aircraft. The truss structure itself will be welded and form a rigid structure that carries all the loads. The fairing, wing, canard and tail will all be joined directly onto this truss structure to distribute the loads into the trusses, and will all be attached by non-destructively removable joints (bolts, screws) for easy disassembly. When a bar of the rigid truss structure is damaged, it first must be checked if other bars might be damaged as well. In case of a local damage the particular bar can be replaced by grinding or mechanically sawing the truss from the rest of the structure and welding a new part back together. After the repair the structure will have a slightly higher weight than before but resources and money are saved by not having to replace the whole truss structure. However, when the damage is too big for instance in case of a heavy collision during ground operations, it cannot be repaired and is considered a total loss. The same would apply to other general aviation aircraft hence it is not a disadvantage. An advantage of the CESTREL however is that all other components can be disassembled and the damaged truss structure can be melted in order to recycle it.

12.6.1. Fairing

The function of the fairing is to cover the fuselage to give it a more aerodynamic shape and to protect the payload and the components from external impacts like the weather or UV rays. The fairing itself is not used to attach any other component hence it must withstand only the aerodynamic loads. Since the fuselage is not pressurised the fairing does not need to be airtight but it shall be waterproof so that rain cannot enter into the fuselage.

The fairing will be split into different parts as it can be seen in the exploded view in [Figure 12.20](#). Splitting of the fairing allows for a quick disassembly which is beneficial for an easy maintenance. The cover of the cockpit (part 10) shall be transparent to allow for a good visibility and it shall be hinged to allow for entering the cockpit. The hinge will be at the front of the cockpit dome such that the door will hinge up and forward to open the cockpit.

From inside of the cockpit several bolts are within reach. Those bolts fixate the surrounding fairing parts (parts 3 L&R, 5 L&R and 9) from the inside. The fairing around the canard wing is split in an upper part (part 1) and a lower part (part 2). The leg-room is covered by two fairing parts (parts 3 L&R). They are fixed with bolts in the back (from inside) and the front will be hold by a pin that slides into a counterpart which is mounted to the truss structure. To disassemble the parts first the bolts need to be loosened then the part can slide back and out to detach the pin in the front. After removing parts 3 L&R bolts become visible that hold parts 1 and 2. Similar to part 3 they are fixed with a pin in the front and bolts in the back. The general direction to disassemble is to start from inside the cockpit and from there work towards the front and rear of the aircraft.

Also parts 9 and 8 L&R are mounted in the same way - bolts in the front and a fixation pin in the rear. Parts 4 and 6 can be unmounted once the side parts 5 L&R and 7 L&R are removed.

The mounting principle has the advantage that the fairing can be dismantled easily and non-destructively. For instance the wing root can be easily inspected by lifting up part 9. Also no fasteners are visible on the outside which could potentially have a negative impact on the aerodynamic behaviour.

The micro turbine and the generator are placed underneath the main wing (or between parts 7 L&R). Since the turbine needs frequent maintenance and inspections it would be convenient to have a simple access. Therefore fairing parts 7 L&R are a door with a hinge at the bottom to easily open without having to remove other fairing parts first.

The tolerance of the gaps between adjacent fairing parts shall be minimised to reduce aerodynamic drag but must be sufficiently large to account for imperfections during production. Within the gap a strip of rubber will be placed to seal the gap. The placement of the fairing cuts and the landing gear positioning are harmonized with each other such that the struts of the nose and main landing gear enter the fuselage right at a cut between two fairing parts (see [Figure 12.21](#)). A circular cut out is needed for the nose gear strut and rectangular ones for the main gear struts.

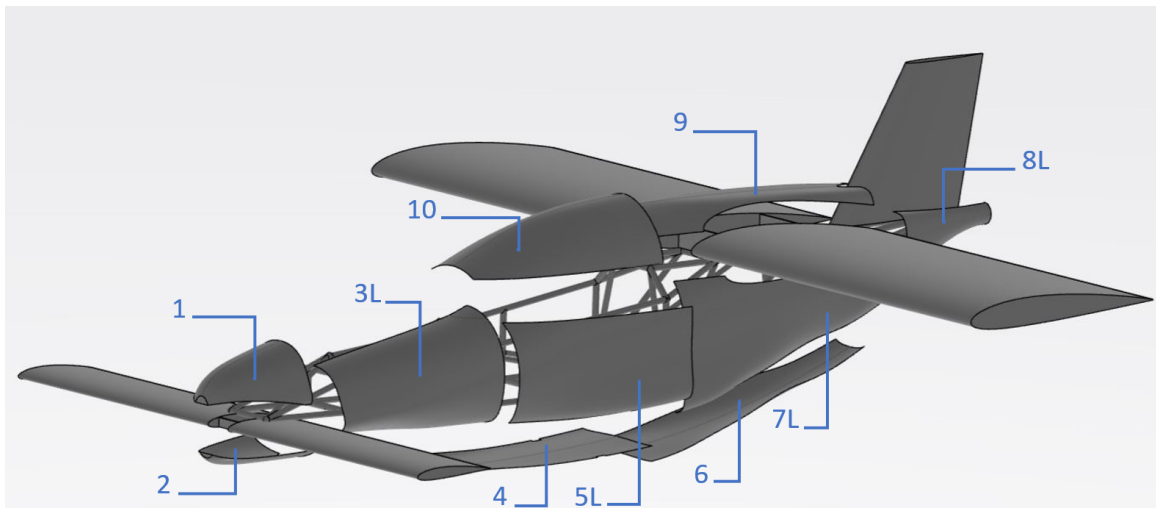


Figure 12.20: Exploded isometric view of fairing parts

12.6.2. Landing gear joining

Both main landing gear struts need to be mounted to the truss structure at an angle. As indicated in the sketch in Figure 12.22 the landing gear connection consists of 2 blocks, where the bottom block has a welded connection to the main gear strut. A similar technique was used by Zhao et al. in [44, Figure 3]. Each block will cover a side of the strut and both blocks are connected to each other by a bolt and nut connection. Further detailed calculations are necessary to assess whether the weld line itself is sufficient to carry the bending moment at the root or if additional strengthening elements are needed.

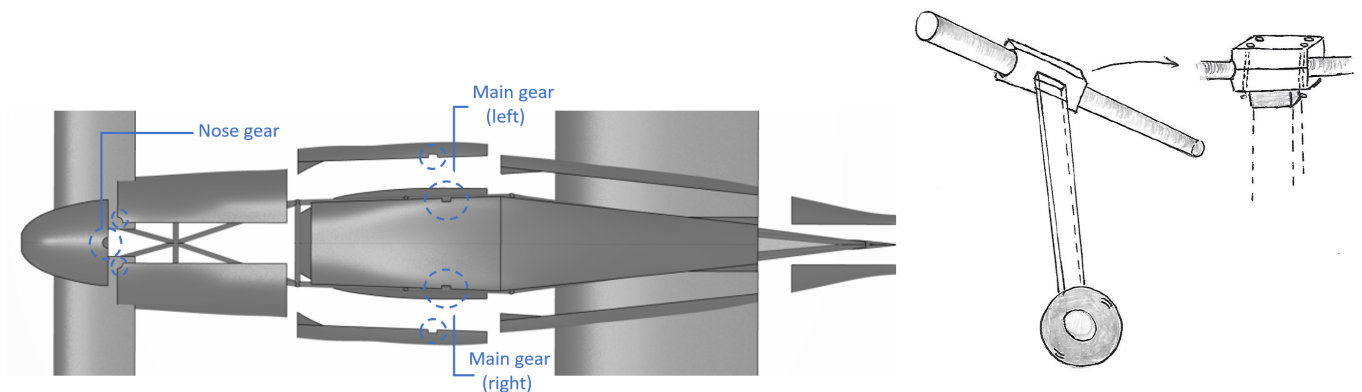


Figure 12.21: Bottom view of gear cut-outs in fairing

Figure 12.22: Sketch of landing gear connection to truss bar

12.6.3. Wing joining

Due to the forces acting on the wing, the wing joint should be able to carry the moments and forces at the spars of the wingbox root. Especially during horizontal flight the moments experienced around the x-axis can be rather high due to the high load factors that can be expected due to gusts. Those moments should not be introduced directly into the truss structure but should remain in the connection mechanism. Contrary to the moment the lift force should be introduced to the fuselage since that is the "useful" force. The connection mechanism consists of several lugs and a pin as seen in Figure 12.24, in order to connect both wings to each other. This will be done for the front spar of the wingbox as well as the rear spar, in order to take up the moment at the root around the z-axis due to the thrust forces of the rotors (in horizontal flight) and the drag forces. This mechanism can be very easily attached and detached, as it is a simple pin to be pushed or pulled from the top of the connection. The dimensions of the pin were determined as follows:

From the production course lecture slides on riveting and bolting [39], the ultimate force a pin can bear without fracturing due to the shear forces applied is given in the following equation:

$$F_{ult} = \frac{\pi}{4} D^2 \tau \quad (12.26)$$

By rearranging this formula, one can design for the minimum diameter of the pin, that is able to carry the shear forces at the root of the wingbox (F) without exceeding the shear strength of the material (τ). For the pin, a 12.9 class steel was considered due to its high shear strength of 732 MPa²¹

To determine the force acting on the pin the reaction forces of a free body diagram need to be studied. The load case that was considered for the design of the pin is cruise flight²². For cruise it is assumed that the thrust equals the drag and the maximum compression and tension forces experienced at the root spar were found by equating the equilibrium of forces and moments at the middle of the front and rear spar, due to the lifting forces on the wing itself.

Another assumption made is that the resulting lift force is applied exactly in the middle of the two spars. In reality the lift force is more forward, close to quarter-chord. This would result in higher forces in the front spar. Due to time constraints the structural analysis was simplified with this assumption but must be revisited before the design goes into manufacturing. For now the common safety factor of 1.5 accounts for all the assumptions.

The moment equations are given with respect to the distances as given in Figure 12.24 and are right hand-positive in sign convention:

$$\begin{aligned} \sum F_x : R_x &= 0 && \text{where } R_x \text{ is the reaction force at the spar in x-direction} \\ \sum F_y : R_y &= F_f && \text{where } R_y \text{ is the reaction force at the spar in y-direction} \\ \sum F_z : R_z &= L/2 && \text{where } R_z \text{ is the reaction force at the spar in z-direction} \\ \sum M_x : 4F_c h + Ld &= 0 && \text{where } M_x \text{ is the reaction moment at the spar around the x-axis} \\ \sum M_y : L - b/2 - R_z b &= 0 && \text{where } M_y \text{ is the reaction moment at the spar around the y-axis} \\ \sum M_z : F_c b - R_y b &= 0 && \text{where } M_z \text{ is the reaction moment at the spar around the z-axis} \end{aligned}$$

From these equations, it is possible to find the force F_f which is the shear force on the pin from:

$$F_f = \pm \frac{Ld}{4h} \quad \begin{array}{l} + \text{ for tension at bottom of spar} \\ - \text{ for compression at top of spar} \end{array}$$

The outcome of the sizing exercise is summarised in Table 12.10. The length of the pin was chosen to be 18cm to account for 1cm at top and bottom for the head and the nut of the bolt respectively.

The lug introduces the loads into the pin. It is sketched in Figure 12.23b. In the following the sizing of the lugs will be explained:

To be able to mount the lug to the end of the spars a flat Al 6061-T6 plate is welded onto the end of the spar. That plate will just have the same height as the front spar (16cm). The rear spar is less high but inside the fairing it is gradually increased in height to also have 16cm²³. Then the same metal plate is welded on it. The metal plate has a width of 13.2mm which is the same as the width of the spar including the flanges of the corner stringers. Onto this metal plate the lug can now be welded. Since the metal plate and the lugs are both made from Al 6061-T6 a welded joint is possible. The design of the lug is driven by the yield strength of Al 6061-T6 which is 276 MPa.²⁴ The cross-sectional area must be designed such that the force acting on the lug area will not yield the connection piece. The results of this calculation are given in Table 12.10. The lug is designed such that the cross-sectional area at the mounting line of the lug (A_1) is the same as the area at the hole for the pin (A_2) as can be seen in Figure 12.23b. The width of the lug is determined by the width of the metal plate which is 13.2mm. The thickness (t) can be calculated from the area which is necessary to stay below the yield stress. The hole diameter will be the same as the diameter which was calculated for the pin.

Table 12.10: Sizing of Pin and Lug

Part	Design for...	Material	F_f [N]	length [mm]	A [mm^2]		D_{pin} [mm]
Pin	Shear strength	12.9 class steel	68,145	180	93		10.9
Part	Design for ...	Material	F_f [N]	w [mm]	A [mm^2]	t [mm]	D_{hole} [mm]
Lug	Yield strength	Al 6061-T6	68,145	13.2	246.9	18.7	10.9

²¹<https://itstillruns.com/129-bolt-shear-capacity-11415080.html>, [Accessed 17.06.2020]

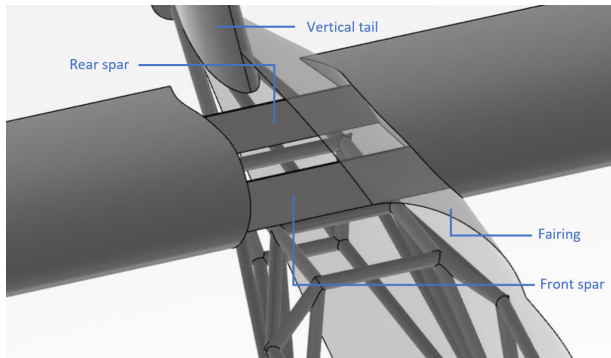
²²At a later stage it was figured out that the VTOL-phase creates higher moments even though the load factors are lower than during cruise flight. Therefore the sizing should be redone in the future. The procedure however stays exactly the same.

²³This is not optimal for the production process. In order to have the spar from one material only a lot of scrap material would remain. A possible solution would be to keep the height constant and to design the lug-pin joint for that. The loads would be higher though and calculating them is harder. Due to time-constraints the design was made with the same height of both spars.

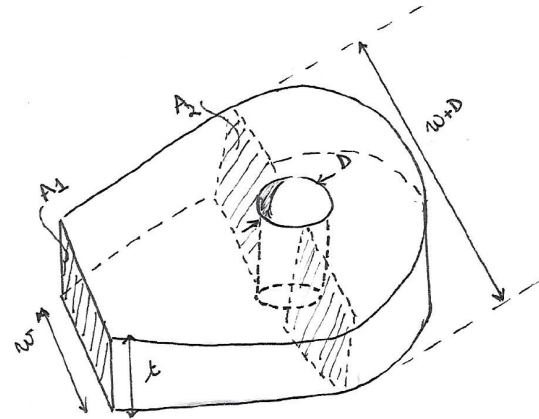
²⁴<http://asm.matweb.com/search/SpecificMaterial.asp?bassnum=MA6061T6>, [Accessed 17.06.2020]

A downside of this connection mechanism however is that the distance between the spars must be almost exactly the same for both wings. Inaccuracies in the dimensions will result in unacceptably high residual stresses. Hence a very high accuracy is needed to insert both pins at the same time. This will increase the production costs of these components.

The connection of the wing to the fuselage truss structure can be seen in [Figure 12.25](#). The spars of the wingbox structure will be connected by a connection piece which has a lug welded to a curved metal plate. The lug is connected to the spar with a bolt and a nut and the curved metal plate is bolted directly onto the truss bar. This connection makes sure that the lifting loads in the wingbox are directly distributed into the truss structure via an appropriate load path. As can be seen in [Figure 12.23a](#) the wing itself (skin, leading edge and trailing edge) will already stop right in front of the truss bar, whereas the spar only will continue into the fuselage truss structure. In the middle of the fuselage truss structure (at the symmetry line), the left wing front and rear spar will be connected to the relative spars of the right wing with the connection as previously explained in [Figure 12.24](#).



(a) Main wing connection with truss structure and fairing. The upper and lower skin as well as leading and trailing edge stop at the fairing. Only the spars are continued and go into the fuselage. Deviating from this figure the spars are not continuous but are connected with the lug-pin wing connection in the middle.



(b) Sketch of lug dimension parameters

The leading edge and trailing edge of the wing will be attached to the wingbox structure, which is then attached to the fuselage with above mentioned connection mechanism. The use of attachment screws and a joggle will be made, to attach the leading and trailing edge to the wingbox itself and to make sure the surfaces are flush to account for aerodynamic flows as seen in [Figure 12.26](#)²⁵.

In [Figure 12.27](#) the honeycomb connection is shown. On the left side the connection of the honeycomb to the aluminium spar is presented. The polymer would have a honeycomb structure, but on the locations where the screws are added, a thicker sheet of print could be made on top of the honeycomb. This would ease the connection of the two structural parts. On the right side a close-up is given, with a screw, the honeycomb pattern and the thicker lining to accommodate the screw. Figure is not to scale.

The leading and trailing edge are the parts that are very likely to get damaged either during ground operations by other objects or during flight for instance by bird strike. The modular design philosophy allows for an easy replacement of the wing leading or trailing edge. This is beneficial for the costs if a repair is necessary.

²⁵<https://www.heritageconcorde.com/the-wing>, [Accessed 16.06.2020]

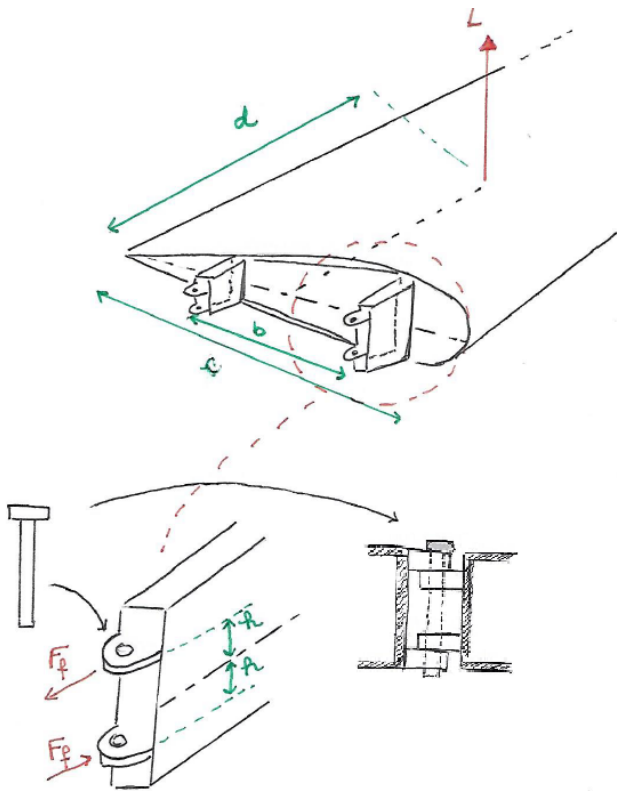


Figure 12.24: Sketch of wing connection

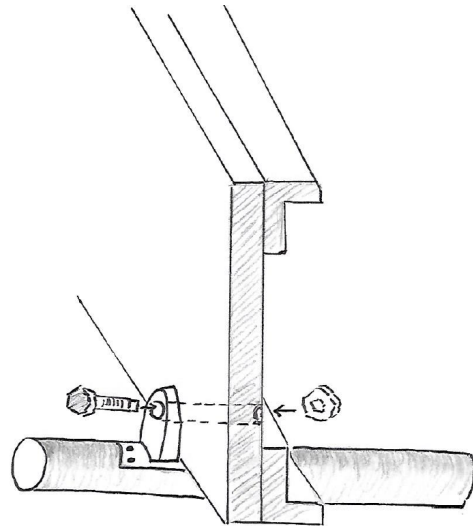


Figure 12.25: Sketch of wing connection to truss structure. For illustrative reasons the mounting mechanism between the lug and the bar is drawn too fragile. The real joint should be replaced by a joint similar to the one for the main gear in Figure 12.22.

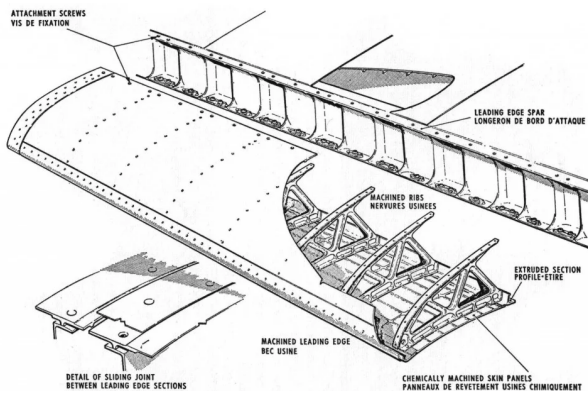


Figure 12.26: Leading edge connection with screws

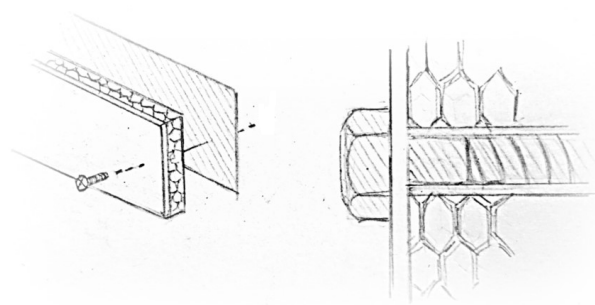


Figure 12.27: Leading edge connection of honeycomb. Attachment screws are used to mount the leading edge. Threaded holes are therefore needed in the front spar.

12.6.4. Canard joining

Joining of the canard will be done in the same way as the main wing, where the moments and forces are not directly introduced into the main structure, but only through the connection mechanism. For the connection between the canard wings, again the mechanism in Figure 12.24 is used. To connect the canard to the fuselage the connection mechanism in Figure 12.25 is used, only this time instead of bolting it to a lower bar, it will be bolted to an upper bar (which is the same connection mechanism but upside down).

12.6.5. Tail joining

The last structure that will be attached to the fuselage structure is the vertical tailplane. The vertical tail has two spars which are connected to the truss structure. Each spar will be mounted at two points in the truss structure in order to account for bending of sideways forces acting on the tail.

13

Final Design

This chapter describes the final design of the aircraft in detail, including a summary of the design in [section 13.1](#), followed by the budget breakdown in [section 13.2](#) the RAMS characteristics in [section 13.3](#). After this a cost breakdown and operation cost will be given in [section 13.4](#) and [section 13.5](#). Finally this chapter will provide the compliance matrix in [section 13.6](#).

13.1. Final Design Summary

To summarise the design, a tilting propotor has been designed. It has a main wing and canard to produce lift, with a tilting propeller at the edge of each wingtip. This is included to be able to take-off vertically, as well as fly horizontally during cruise. Now that the end of the final phase is nearing, a name for the aircraft has been selected as well: Cestrel. The Circular Eco-Friendly Short Take-off Range-Extended Lifter. The name is also partly inspired by a hovering bird called the Kestrel However, in this case, the K was exchanged for a C to indicate circular economy concept.



Figure 13.1: The lay-out of the aircraft Cestrel

13.2. Budget Breakdown

Throughout the iterations done, the resource allocation has also been updated, leading to the budget breakdown that can be seen in [Table 13.1](#). The last iteration was made with a MTOW of 775 kg. Due to the design still being conceptual, there are uncertainties in the mass, power and cost values. The structural design for example has not been optimised yet for low weight, and some component masses have not been accurately estimated. At the end of the last iteration the total MTOW comes to 585 kg, excluding the 'Other' components from [Table 13.1](#), which would include for example avionics, instrumentation and the cockpit interior. For now it is assumed, that the other components would fill the remaining 190 kg to reach 775 kg. However, in [Table 4.2](#) the other components were assumed to add up to 85 kg. If the total mass of the other components would be adjusted, a new lower MTOW could be found, and with the new MTOW another iteration of the structures should be made, as it would lead to lower structural weight. This means that the expected mass for convergence is lower than 775 kg. This indicates that there is at least a -25% uncertainty still present in the mass, taking the difference between the current extremes, 585 kg and 775 kg.

The uncertainties are assumed to cause a contingency of -25% in the mass, and a $\pm 25\%$ one for the power and cost estimations, as these depend on the mass as well. The power consumption could still increase as not all losses have been taken into account yet, as mentioned in [chapter 8](#). The cost also depends on multiple variables that are mentioned in [section 13.4](#), one of them being the break-even point, which could also increase the price. The contingencies are shown on the last row of the table.

Table 13.1: Updated budget breakdown

	Subsystem	Component	Mass [kg]	Power [kW]	Cost [Euro]
Preliminary estimation	Total		1180	421	450,000
Final design	Structure		194	-	?
		Wing	55	-	?
		Fuselage	60	-	?
		Canard	20	-	?
		Vertical tail	9	-	?
		Landing gear	50	-	?
	Propulsion		201	160	160,000
		Electric motors incl. controllers	71	provider	51,040
		Micro gas turbine	27 ¹	generator	?
		Batteries	59	storage	?
		Proprotor	24	160	7,150
		Fuel system	20	-	?
	Other		190	1	?
		Payload	150	-	?
		Fuel	40	-	?
	Total	775	161	317,000	
	With contingencies	585-775	121-201	238,000-397,000	

13.3. RAMS characteristics

As seen in the acronym, the RAMS characteristics describe the reliability, availability, maintainability and safety aspects of the design. This section will go over each of the characteristics and describe how it is reflected by the tilt proprotor design, Cestrel.

13.3.1. Reliability

The reliability is defined as the probability that the aircraft performs its mission without any failure that makes an unscheduled maintenance necessary [15]. In the following different aspects that drive the reliability are discussed.

- ✈ The flight control systems of the Cestrel are rather complex since the operation must be possible in VTOL-mode, in airplane-mode and in the conversion phase between those. Complex system generally tend to be less reliable.
- ✈ The structures including the landing gear are kept very simple with a minimised number of moving parts. This increases the reliability of those aspects. Electrical engines are also considered by far more reliable than combustion engines due to their reduced number of moving parts ².
- ✈ The reliability is also increased by the redundancy applied for instance in the truss-structure, according to the design philosophy "fail safe". If a component fails but still performs its function due to the redundancy it must be carefully assessed whether it is safe to continue the mission or to initiate an emergency procedure.
- ✈ In general the reliability can be increased by following the specified maintenance procedures.

13.3.2. Availability

The availability is defined as the probability that the aircraft is usable when it is needed [15]. A qualitative assessment of the Cestrel's availability is done for various aspects in the following.

- ✈ The Cestrel needs more power during VTOL than the turbine can deliver. The missing power will be provided by the batteries. To take-off the batteries hence must be charged. However if the operator forgets to charge the batteries prior to take-off the aircraft is not available. The charging can also be done with the turbine but still a certain time is required until the batteries are sufficiently charged to take-off.
- ✈ The availability of the aircraft also depends on the availability of fuel. The advantage over other aircraft is that the turbine can burn various different fuels. If one fuel type is not available another can be chosen as substitute. Fuels like (Bio-)Diesel or gasoline are widely available for road traffic. All this also increases the availability of the Cestrel.
- ✈ The aircraft can not be loaded in a way that would violate the most forward or most aft c.g. locations. This poses limits on the operation and makes the aircraft unavailable for load placements exceeding those limits. This is

¹ See Power and Propulsion Chapter.

² <https://www.forbes.com/sites/sap/2018/09/06/seven-reasons-why-the-internal-combustion-engine-is-a-dead-man-walking-updated/3c12a128603f> [Accessed 22.06.2020]

- ✈ opposite to a car where the placement of the load is nearly unrestricted. In an aircraft the limits are more strict.
- ✈ Due to the size of the propellers the aircraft is not available for a short take-off with the propellers in horizontal mode. The propellers would touch the ground. Putting them into a 59° position for main wing and 38° position on canard would be possible. Yet it was not analysed if a take-off in that configuration is possible and what the energy saving or increase in safety would be.
- ✈ The aircraft is designed to withstand the gusts that are specified in the CS23 regulations. Nonetheless it still might be that a less experienced pilot reacts irrational to heavy gusts. In later tests with a prototype it must be determined which limits should be posed on the operation in bad weather conditions. Since the use of this product is supposed to be possible for the wide public the operational limits should be more conservative than for professional aviation. This decreases the availability of the aircraft in favour of an increased safety.

13.3.3. Maintainability

The maintainability aspect of the Cestrel tilt proprotor design, will include the scheduled and non-scheduled maintenance design activities. Scheduled maintenance activities will be further explained in [section 16.4](#), but a short summary will already be provided here:

- ✈ The pilot should perform small checks prior to each flight. If critical systems show damage, an unscheduled maintenance is needed. In the current time frame, the aircraft is designed to only travel between different airports/hub stations, where the unscheduled maintenance checks will be performed in maintenance facilities.
- ✈ The aircraft will have an annual maintenance requirement.
- ✈ The aircraft will need to be checked after every 100 flight hours.

As mentioned, unforeseen maintenance can be required. These are considered to be non-scheduled maintenance activities which are often the worst kind of inspection and repairs and can be very costly and unpredictable. In order to enable these maintenance activities, maintenance facilities will be implemented in the small airports and hub stations as will be described in [section 16.4](#). In these facilities, small repairs can be performed. However, when specialised or larger repairs are needed the aircraft shall be transported to larger and more suitable facilities.

The design of the aircraft was such that it allows for easy maintenance. The truss fuselage structure was designed to have a good accessibility over the whole aircraft. Together with the removable fairing, fairing door and the non-permanent joints between different subsystems (see [section 12.6](#)), all critical parts can easily be checked and inspected. Also the material selection gives rise to easy maintenance. By using (mostly) aluminium alloys (see [chapter 11](#)), cracks and other impurities can easily be detected with non-destructive testing (NDT) which allows for better detection of material failure and repair of damaged parts. On top of that metals do not suffer delamination or fibre damage like composites do.

13.3.4. Safety

The safety of the aircraft is evaluated by listing the safety critical functions and the redundancy philosophy applied. The safety critical functions will describe the most critical components of the aircraft and its mission, where one should operate the aircraft with extra care. The safety critical functions identified are:

- ✈ The VTOL phase is a critical part of the aircraft's mission. When one of the engines is inoperative, it will not be able to take-off. When this happens during landing procedure, autorotation is not possible and it is impossible to safely land the aircraft on the ground. Therefore the engines should often be subjected to maintenance and handled with good care.
- ✈ If an engine failure occurs during the cruise phase the second engine on the side of failure needs to increase in power. A conversion to VTOL-mode is then not possible anymore since the aircraft would not be controllable with three motors in VTOL. Hence a horizontal emergency landing must be made.
- ✈ Also the conversion phase from VTOL to horizontal (and opposite) can be considered a critical part of the mission. One should always make sure that the speed is high enough to perform the conversion to horizontal mode, otherwise the aircraft will stall. For the conversion from horizontal to vertical landing, the function will be less critical, as the aircraft is designed to enable horizontal landing in case of emergency.

In order to increase the safety of the Cestrel, a some components/systems are designed to "fail safe". This philosophy refers to "inclusion of duplicate functional elements for protection against failure"³. Other components/systems are designed according to the "safe life" philosophy. Which means that these are very unlikely to fail. Some of these safety aspects are analysed more closely in the following:

- ✈ All structural elements were designed with a safety factor of 1.5 followed from requirement **DSE-22-SYS-SR-05**. This safety factor will account for uncertainties in the design. The downside of this safety factor is the increased weight of the structural elements.

³<https://www.webpages.uidaho.edu/morourke/443-phil/06-Spring/Handouts/Philosophical/443S06-Redundancy.htm>, [Accessed 22.06.2020]

Table 13.2: Cost break-down estimation for the Cestrel

	Man-hours	Rate, €/h	Total Cost	Cost per Unit	
Engineering	58,217	€82	€22,426,366	€8,971	
Development support			€343,888	€138	
Flight test operations			€68,285	€27	
Tooling	62,996	€54	€8,045,177	€3,218	
Certification Cost			€30,883,715		
Manufacturing labour	1,064,464	€47	€118,113,901	€47,246	
Quality control			€15,511,582	€6,205	
Materials/equipment			€23,901,804	€9,561	
Units produced in 5 years				2,500	
Quantity Discount Factor				0.5605	
				Without QDF	With QDF
Fixed landing gear discount				-€6,669	-€3,738
Power plant and engines				€280,799	€157,378
Propellers				€12,560	€7,040
Avionics				€29,953	€16,788
TOTAL COST TO PRODUCE				€392,007	€252,832
Manufacturer's liability insurance					€42,981
MINIMUM SELLING PRICE					€295,813
Total fixed cost					€30,883,715
Unit variable cost					€283,460
Number aircraft to break even					1,000
SELLING PRICE					€314,344

- ✈ For pure vertical take-off or landing, the landing gear wheels are essentially not needed. However it was decided to include wheels (and not some sort of skids) to allow for horizontal emergency landings and to enable taxiing. By that an alternative form to land is provided which is considered a redundancy. In horizontal landing the propellers however can not be pointed completely forward, but should remain tilted at a minimum angle of 59°(with the horizontal) for the rotors on the canard and 38°for the ones on the main wing, to ensure they do not touch the ground.
- ✈ The truss structure was designed to "fail safe", which means that a failure does not immediately leads to the truss structure not being able to provide its function anymore. For instance if one bar breaks the loads will use another path. The price of this design philosophy is that regular maintenance checks on the truss structure are required to spot cracks, flaws, failures due to load concentrations at the joints or due to the potentially limited fatigue life because of the welding. Due to the removable fairing these checks are quite easily done.
- ✈ The power supply has some redundancy, the batteries chosen are able to deliver more power than only in VTOL phase. This means that in case of the micro turbine generators not functioning properly, the batteries can take over and a safe flight of about 30 minutes can be performed to reach the next airport to diverge. The same is true for the opposite case where the batteries not functioning, the micro turbines are able to take over and ensure safe flight and a safe horizontal emergency landing.
- ✈ Others components and systems are designed according to the design philosophy "safe life". For instance this was done for the wing joint and the landing gear struts. These components are designed such that it is very unlikely that they fail.

13.4. Cost breakdown

In the market analysis performed in the Baseline report [6], a very preliminary cost estimate was conducted by looking into similar reference aircraft. This cost estimation is now revised for the exact aircraft characteristics of the final design. To determine a revised preliminary estimation of the sales price of the Cestrel a method was used whose approach is comparable to a Class II weight estimation since it groups together different components that make up the sales price. The used method is described in Prof. Snorri Gudmundsson's book *General Aviation Aircraft Design* [20]. The results of this method are shown in [Table 13.2](#).

The cost to develop the aircraft, to test it, to certify it and to develop the manufacturing process is summarized as certification cost. This is also considered as the fixed costs and described in [subsection 13.4.1](#).

The variable costs, described in [subsection 13.4.2](#), include the manufacturing labour, the quality control and the materials/equipment. The power plant, propellers, avionics and a fixed landing gear discount are treated separately but are also included in the variable costs.

The total cost including the quantity discount factor (QDF), a liability insurance and the profit margin is presented in [subsection 13.4.3](#). Also a break-even analysis is shown.

Gudmundsson's cost estimation are based on the year 2012 as the reference year. To correct for the inflationary trend the costs were corrected by using the consumer price index (CPI). According to the U.S. Bureau of Labor Statistics this index was 228 in 2012 and 256 in April, 2020⁴ which results in a correction factor of 1.1228. After this, the cost values were all converted from USD to Euro, as Europe is the target market of the aircraft. For this a conversion factor of 0.88923 €/€ was used (currency exchange on the 29.06.2020)⁵.

A couple of values which are used as input for the statistical relations are given below to allow the reader to reproduce the calculations.

- ✈ $W_{Airframe}$ is the Airframe weight was assumed to be 65% of the OEW (452kg) and needed to be converted to 648 lbf.
- ✈ V_H is the maximum level airspeed in knots TAS. The dive speed of the V_n -diagrams was used for this and results in 148 knots. Taking the dive speed is conservative since it is actually higher than the maximum level airspeed.
- ✈ N is the number of planned aircraft produced in the first 5 years. In the Baseline Report [6] it was planned to sell 7500 aircraft in 15 years which means on average 2500 aircraft per 5 years.
- ✈ F_{Cert} should be set to 1 if the aircraft is supposed to be certified with 14 CFR Part 23 which is the FAA equivalent to the CS23.
- ✈ F_{CF} should be set to 1 if a simple flap system is used. This is the case for the Cestrel since the flaperon basically is a plain flap.
- ✈ F_{Comp} is $1 + x \cdot f_{comp}$, where x is a factor that changes for each statistical relation and f_{comp} is the weight fraction of the weight of all composites in the airframe over the airframe weight. No composites are used for the aircraft but 12 kg of PEI are used. Due to the lack of experience with PEI it is more expensive to develop and manufacture something out of it but it is not as expensive as composites. Therefore f_{comp} was calculated using the 12 kg PEI and then halved, resulting in 0.02.

13.4.1. Fixed costs

The certification costs which are also the fixed costs contain the following four parts. All of them are based on statistical relationships.

1. **Engineering** The engineering part is the cost to develop the aircraft. Firstly the number of engineering man-hours is estimated to be around 58,200 hours. Assuming an hourly rate of €82 (including overheads) according to Gudmundsson the engineering cost can be calculated. The result needs to be corrected by the factor of 1.1228 for the inflation since 2012 and by a factor of 2.0969 to account for the CPI from 1986 which is when the models on which the estimation is based were developed. This would result in an engineering cost for the development of the aircraft of around €11,200,000. However it must be noted that the approach of Gudmundsson is for general aviation aircraft. The Cestrel is a much more complex system due to its VTOL capability and the ability to convert to an airplane mode. Additionally it can be assumed that the engineers have less experience with the design of tilt proprotors compared to conventional general aviation aircraft. To account for that the engineering costs were corrected by a factor 2 - leading to €22,400,000.
2. **Development support** Even though the overheads were already included in the engineering hourly rate another cost part is needed since the overheads do not scale linearly with the engineering men-hours. This part includes costs to support the development, for instance HR, facility management, logistics, overheads etc.. The cost estimation for this also depends on the number of prototypes that will be built. This number was assumed to be 3. One might eventually crash, another one is needed to demonstrate the operations and a third one will be built after updating and revising the design. The costs result in approximately €344,000.
3. **Flight test operations** The cost for the certification flight-test program is estimated to be approximately €68,300.
4. **Tooling** This includes the cost and time to develop the tools to manufacture the aircraft. The man-hours were estimated approximately 63,000 hours. Assuming an hourly rate of €53 the same correction factors as for the engineering are applied, except the factor of 2 for the design complexity since the development of the tooling is not necessarily more complex than for GA aircraft. It results in a cost of €8,045,000.

⁴https://data.bls.gov/timeseries/CUSR0000SA0?output_view=pct_1mth [Accessed 20.06.2020]

⁵<https://www.xe.com/currencyconverter/convert/?Amount=1From=USDTo=EUR> [Accessed 29.06.2020]

Summing all four parts results in a certification cost of about €30,900,000.

13.4.2. Variable costs

The variable costs include the following parts:

1. **Manufacturing labour** The manufacturing labour includes the man-hours to manufacture all the aircraft that are planned to be sold in the first 5 years. To manufacture those 2500 aircraft approximately 1,064,000 man-hours are needed. Assuming an hourly rate of €47 this results to €118,100,000 (including the CPI factors 2.0969 and 1.1228 only).
2. **Quality control** The cost for the quality control is estimated as €15,500,000 for 2500 aircraft.
3. **Materials/Equipment** The cost of the raw material and the equipment to produce 2500 aircraft is approximately €23,900,000. This approach is for conventional aircraft and thus considers only new materials and parts. Recycled and refurbished parts will lower the material and equipment cost. Hence it can be considered overestimated.
4. **Fixed landing gear discount** If the aircraft has a non-retractable landing gear, which is the case for the Cestrel, Gudmundsson advises to subtract €6,700 from the unit cost.
5. **Power plant and engines** The cost estimation of Gudmundsson is not designed for hybrid power plant. However reasonable numbers are obtained by using the formula for turbofan engines. The cruise thrust of $68N$ and $N_{pp} = 4$ (4 engines) are used. The result is multiplied by two to account for the generator and the fact that this power plant is yet less common on the market and therefore more expensive. This results in €280,800 per unit.
6. **Propellers** For fixed-pitch propellers a price estimation of €3,140 per propeller is given. With four propellers and the CPI factor 1.1228 this results in €12,560 per unit.
7. **Avionics** Gudmundsson suggests €13,400 for the avionics. The Cestrel basically requires two sets of avionics since it is able to fly in VTOL- and airplane-mode. Therefore it was decided to double Gudmundsson's suggestion to €26,800. Corrected by the CPI this results in €30,000 per unit.
8. **End-of-life recycling** The purpose of the Cestrel is to be recycled, refurbished and reused at the end of life. This process will create costs. In Gudmundsson's approach this was not incorporated however as said before the material/equipment costs are overestimated. This compensates for the recycling costs. The balance is even expected to be positive since the sustained value of the recycled parts and materials is higher than the recycling cost. This is already the case for conventional commercial airliners (e.g. the company AELS⁶) and since the Cestrel is designed for this, it will be even more profitable. The exact number can not yet be estimated but it has potential to decrease the final selling price in the order of a few thousand Euros since the Materials/Equipment cost are lowered and the manufacturing labour costs decrease if some parts do not need to be assembled anymore.

For the fixed landing gear discount, the power plant and engines, propellers and avionics a quantity discount factor (QDF) can be applied to correct for the fact that prices are lowered when buying parts in high quantity. The QDF depends on the experience effectiveness. Assuming a conservative value of 0.95 for that results in a QDF of 0.5605.

13.4.3. Total cost

The fixed costs are divided by $N = 2500$ aircraft to get a cost per unit. Now all the costs per unit can be summed together to get the total production cost (€252,800). According to Gudmundsson 17% of the production cost need to be added for the manufacturer's liability insurance (+ €43,000). This results in a minimum selling price of €295,800. With this price the break-even point would be reached after 2500 aircraft or 5 years.

If the break-even point shall be at 1000 sold aircraft the selling price must be increased to the price calculated in [Equation 13.1](#).

$$\text{Selling price} = \frac{\text{Fixed cost}}{\text{a/c to break even}} + \text{Variable cost} = \frac{30,883,715 \text{ €}}{1000} + 283,460 \text{ €} = 314,344 \text{ €} \quad (13.1)$$

To conclude, assuming a sales volume of 2500 aircraft in the first 5 years which are sold for €314,344 per unit results in a break-even after 1000 sold aircraft.

As discussed in the selling points (see [subsection 3.3.3](#)) the aircraft has a high scrap-value. A possible business strategy would be to have a subcompany which buys the aircraft from the customer at the end of life. The customer receives a payback which will depend on the condition of the aircraft. This motivates the customer to handle the product with care which is also in the spirit of sustainability. The payback can be connected with a discount campaign to the purchase of a new Cestrel. The recycling and refurbishing will be performed by the subcompany and the reusable parts can be sold to the holding company to install them in new aircraft.

⁶<https://aels.nl/> [Accessed: 30.06.2020]

Table 13.3: Operational cost estimation for the Cestrel

	Cost per year	Cost per flight hour
Maintenance	€4,439	€17.07
Storage	€2,995	€11.52
Fuel	€4,684	€18.02
Insurance	€5,160	€19.85
1-year inspection	€499	€1.92
Engine overhaul	€1,298	€4.99
Total cost	€19,076	€73.37
Flight hours per year [h]		260
Distance flown per flight hour [km]		200
cost per kilometer [€/km]		€0.367

13.5. Operational cost

Gudmundson also describes a method to estimate the operational cost of the aircraft [20]. All parts of the operational costs are calculated for one year. In the end the sum of all parts is divided by the annual flight hours to get a cost estimation per flight hour. According to Jos Sinke "in general every human being travels about 1 hour a day." [38] Therefore the number of flight hours per year was determined to be $1h \cdot 5 \cdot 52 = 260hrs$. With 1 hour a day one could travel a distance of around 200km per day with the Cestrel. This number shows the new dimension of flexibility of travelling. The parts that determine the total operational cost are the following. It must be noted that the cost for writing-off the purchase price is not included.

1. **Maintenance cost** For the maintenance cost a hourly rate of €53.35 was assumed for the mechanic. By multiplying this rate with the maintenance to flight hour ratio, the annual flight hours and the CPI correction the maintenance cost results in approx. €4,400 per year. The maintenance to flight hour ratio was determined to be 0.285 assuming that the pilot/owner is able to do some simple maintenance activities himself.
2. **Storage cost** For the storage cost Gudmundson recommends €222 per month. Corrected with the CPI this results in €3,000 per year.
3. **Annual fuel cost** The aircraft is supposed to run on Biodiesel. The average price over the last 2 years (excluding the price-drop due to the Covid-19 crisis) for conventional Diesel for road traffic in Europe was found to be roughly 1.25€/l (including taxes).⁷ Biodiesel was found to cost 5 to 10 cent/liter less. The current trend however is to reduce the consumption of all fuels. Therefore it is not unlikely that the taxes on fuels will be increased in the next decades. To give a conservative estimation the price of conventional Diesel was increased by 50% for the cost calculation. This converts to a fuel price of €7.05/gallon. The power plant has an average fuel flow of 2.554 gallons/hour which results in a fuel cost of €4,700 per year.
4. **Annual insurance cost** The insurance cost can be estimated using the selling price of €314,344 to be €5,160 per year.
5. **1-year-inspection cost** According to Gudmundson an inspection that is done once a year (irrespective of the actual flight hours) costs €445. Corrected by the CPI this is €499.
6. **Engine overhaul per year** For the Cestrel an engine service interval of 100 flight hours was found (see [Figure 16.5](#)). Assuming the engine overhaul also costs €499 this results in €1,298 per year.

Summing all these costs together leads to a final operational cost of €19,079 per year or €73.37 per flight hour. Assuming that an effective distance of 200km can be flown in one hour this results in a price of 37 €-Cent/km.

13.6. Compliance matrices

In this table the compliance of the design to the user requirements is given. When the design is proved to comply with a requirement, a '✓' is added to the compliance-column. The value computed for the aircraft is presented, and in case no numerical value is related to the requirement, it is indicated with '-'. If no value is available yet, the acronym 'tbd' is used. Reasoning in terms of a feasibility analysis is only given for those requirements that are not met. The requirement compliance matrices can be found in [Table 13.4](#) to [13.10](#).

⁷<https://www.dkv-euroservice.com/portal/en/web/customers/dieselpreis-index> [Accessed: 21.06.2020]

Table 13.4: The requirement compliance matrix of the stakeholder requirements.

Stakeholder requirements compliance matrix		
Requirement	Compliance	Reason
DSE-22-STAK-01: The aircraft shall have performance characteristics such that it is competitive on the market.	✓	An extensive market analysis was performed in chapter 3 . The aircraft characteristics are unique and the design is expected to perform well in the market.
DSE-22-STAK-02: The aircraft shall comply with the current safety and reliability requirements.	✓	The aircraft was designed with the CS-23 and CS-27 requirements in mind. In chapter 10 the aircraft was designed to be stable and controllable. In ?? , the aircraft was designed to comply with the minimum stall speed requirement.
DSE-22-STAK-03: The aircraft shall have a capacity of one person.	✓	The design of the Cestrel is based on a single pilot.
DSE-22-STAK-04: The aircraft shall be designed according to the circular economy concept.	✓	The circular economy was extensively taken into account in the structural design of the aircraft in chapter 12 . All parts in the aircraft are circular.
DSE-22-STAK-05: The aircraft shall be environmentally friendly.	✓	The propulsion system of the aircraft of the aircraft runs on biofuels, which is already a big step forward wrt fossil fuels (subsection 8.5.1). In addition, the entire aircraft is able to be recycled or reused.
DSE-22-STAK-06: The price of the aircraft shall be such that it is competitive on the market.	✓	The aircraft turned out to be cheaper than the maximum allowed unit price of the aircraft (412,500 euros [6]). The aircraft now costs around 314,000 euros. This was discussed in section 13.4 . This price is actually comparable to the prices of the futuristic reference aircraft described in Baseline report [6].
DSE-22-STAK-07: The project shall meet the Project Objective Statement.	✓	The aircraft was fully designed by 10 people according to the circular economy concept [8].

Table 13.5: The performance system requirements compliance matrix.

System requirements compliance matrix: Performance		
Requirement	Compliance	Reason
DSE-22-SYS-P-01: The aircraft shall have a range of at least 300 km.	✓	The aircraft has a range of 660 km as estimated in the propulsion chapter in chapter 8 . Because the aircraft has to meet the endurance requirement, it will be able to fly a longer range.
DSE-22-SYS-P-02: The aircraft shall have a minimum endurance of 3 hours.	✓	The aircraft has an endurance of 3 hours with an additional 45 minutes of loitering time, as determined in chapter 8 .
DSE-22-SYS-P-03: The aircraft shall have take-off and landing distance within 50m.	✓	Cestrel has a VTOL mode, which means that aircraft can land and take-off in 0 m.
DSE-22-SYS-P-04: The aircraft shall have a loiter time of minimum 45 minutes.	✓	The endurance of 3.75 hours includes a maximum of 0.75 hour of loitering time.
DSE-22-SYS-P-05: The aircraft shall have a maximum service ceiling of 3048 m.	✓	The aircraft's wing's were sized such that the aircraft is still able to manoeuvre well at 3048 m altitude as explained in ?? . However, the aircraft's operation is limited by humans not being able to get enough oxygen above this altitude without the aircraft having a pressurised cabin. This was a design decision to keep the aircraft design a bit simpler [6].
DSE-22-SYS-P-06: The aircraft shall have a minimum rate of climb of 304.8 meters per minute (during nominal flight).	✓	The aircraft is able to climb at a the specified ROC with a thrust of about 3.7 kN during the horizontal flight mode. Which is about half of the thrust that the aircraft has available.
DSE-22-SYS-P-07: The aircraft shall have a minimum cruise speed of 160 km/h.	✓	Cestrel has a cruise speed of 220 km/h. This cruise speed was determined in section 7.3 .

Table 13.6: The requirement compliance matrix for safety and reliability.

System requirements compliance matrix: Safety and Reliability		
Requirement	Compliance	Reason
DSE-22-SYS-SR-01: The aircraft shall be operational in the same weather conditions as other general aviation aircraft.	✓	The aircraft is able to handle crosswinds as specified by CS-23 as the aircraft's vertical was sized for something more critical: engine failure of a multi engine configuration in section 10.6 .
DSE-22-SYS-SR-02: The aircraft shall be stable in operation.	✓	The main wing and canard were positioned such that the aircraft is stable (and controllable) during all phases of flight.
DSE-22-SYS-SR-03: The aircraft shall have a minimum life time of 10 years.	tbd	It is impossible to prove that the aircraft will be able to operate for 10 years during this conceptual design phase. The aircraft would actually need to be in operation to put this to the test.
DSE-22-SYS-SR-04: The aircraft shall have no more than 50 accidents per 1,000,000 flights.	tbd	This cannot be proven during the conceptual design phase. The aircraft statistics would need to be monitored while the aircraft is in operation.
DSE-22-SYS-SR-05: The aircraft structures shall be designed with a safety factor of at least 1.5.	✓	During the structural design of the aircraft, this safety factor of 1.5 was taken into account.
DSE-22-SYS-SR-06: The aircraft shall only be landed on streets within the operational cross wind limit.	✓	The aircraft is able to handle crosswinds as specified by CS-23 as the aircraft's vertical was sized for something more critical: engine failure of a multi engine configuration in section 10.6 .

Table 13.7: The requirement compliance matrix for the aircraft characteristics.

System requirements compliance matrix: Aircraft characteristics		
Requirement	Compliance	Reason
DSE-22-SYS-AC-01: The aircraft shall have a maximum take-off weight of 1480 kg. (As determined by the Class I weight estimation [7]).	✓	The aircraft has a MTOW of 775 kg.
DSE-22-SYS-AC-02: The aircraft shall have a maximum payload mass of 150 kg.	✓	The aircraft is designed for a payload mass of 150 kg
DSE-22-SYS-AC-03: The aircraft shall have a maximum wing span of 9 m.	✓	The aircraft has a span of 6m as explained in ?? However, with the propellers at the ends of the main wing, the total wing span is 9 m.
DSE-22-SYS-AC-04: The aircraft shall be able to accommodate pilots between 153.5cm and 185.5cm height.	✓	The fuselage of the aircraft was designed to accommodate a pilot that is between 153.5 and 185.5 cm in height according to section 12.3 .

Table 13.8: The requirement compliance matrix for risk mitigation.

System requirements compliance matrix: Risk mitigation		
Requirement	Compliance	Reason
DSE-22-SYS-RM-01: Verification shall be done for all outputs of design calculations/simulations.	✓	Verification was performed for all the performed calculation and programmed tools.
DSE-22-SYS-RM-02: Validation shall be done for all outputs of design calculations/simulations.	-	This requirement was not met for the reasons that all methods were worth validating. An example can be found in subsection 10.8.4 .
DSE-22-SYS-RM-03: The aircraft shall be maintainable for the user.	✓	The fuselage of the aircraft was designed to be modular and this easily accessible for maintainance.
DSE-22-SYS-RM-04: Maintenance shall be performed according to supplier instructions for each of the pro-duction tools.	tbd	This can only be proven ones the aircraft is in operational use.
DSE-22-SYS-RM-05: Quality checks shall be performed to the produced structures.	tbd	This can only be proven ones the aircraft is in operational use. However, the fuselage was designed to be modular to allow for easy checking of the structure.
DSE-22-SYS-RM-06: In case of defects in materials/structures are detected, investigation shall be performed.	tbd	This can only be proven ones the aircraft is in operational use.
DSE-22-SYS-RM-07: Maintenance of the aircraft shall be performed after every 100 hours of flight.	tbd	This can only be proven ones the aircraft is in operational use. This number was used for the cost calculations.
DSE-22-SYS-RM-08: A list of alternative suppliers for materials shall be provided.	tbd	This will be finalised during the production phase of the design.
DSE-22-SYS-RM-09: All manufacturing workers shall have a certified training of at least 100 hours on the machine they operate.	tbd	This can only be proven ones the aircraft is in the production phase of the design.

Table 13.9: The requirement compliance matrix for sustainability.

System requirements compliance matrix: Sustainability		
Requirement	Compliance	Reason
DSE-22-SYS-S-01: The aircraft shall have emissions that do not exceed those of existing reference general aviation aircraft.	tbd	At this stage of the design, it is not possible to determine the exact emissions of the Cestrel. This is because a lot is still uncertain about the general efficiency of the entire propulsion and electrical system. Cestrel has a really low fuel flow of 2.6 gallons per hour. In addition Cestrel has a 40% combustion efficiency for its turbine, which is a generally higher efficiency compared to a internal combustion engine.
DSE-22-SYS-S-02: The aircraft shall use renewable sources.	✓	The design of the aircraft contains many efforts to introduce renewable sources.
DSE-22-SYS-S-03: The aircraft shall have re-usable materials.	✓	Effort was in to introducing re-usable material in to the design in chapter 11 .
DSE-22-SYS-S-04: The aircraft shall be entirely recycled or refurbished at the end of its life.	✓	The aircraft was designing to be fully recyclable/refurbishable after its end of life, as said in chapter 11 .
DSE-22-SYS-S-05: The noise level limitation shall be identical to motor vehicles (82 dB(A)).	tbd	At this conceptual design phase it is impossible to estimate or measure the noise of the aircraft. However, effort was put in minimising the noise in section 7.5 .

Table 13.10: The requirement compliance matrix for cost, design and development.

System requirements compliance matrix: Cost, design and development		
Requirement	Compliance	Reason
DSE-22-SYS-C-01: The aircraft shall have a maximum cost of 150% of similar existing personal aircraft: 412,500 euros [6].	✓	The aircraft has an estimated unit cost of around 314,000 euros. Which is lower then the 412,500 euros.
DSE-22-SYS-DD-01: Usage of resources shall be such that every member of the group has a task at all workingtimes.	✓	The Gantt chart and deliverable lists were extensively used to accomplish this.

13.7. Sensitivity analysis of the final design

This section features the sensitivity analysis of the whole aircraft design. This sensitivity analysis tried to combine the sensitivity of all the separate parts of the design, to see what the entire aircraft design is most sensitive to. The sensitivity analysis will be performed by changing the aspect ratio of the main wing of the aircraft (AR), which was one of the first design parameters that was set. It is only constrained by the requirement on maximum wing span of 9 meters, **DSE-22-SYS-AC-03**.

Within the aerodynamics department, nothing changes with regards to the airfoil selection as that is mostly based on the cruise speed the aircraft flies at. The cruise speed of the aircraft is not affected by this change. What must be ensured is that the maximum lift coefficient of the canard stays lower than that of the wing.

However, changing the aspect ratio of the design has a great impact on the geometry of the wings, which results in different lift distribution on the wings of the aircraft. This leads to different estimations for the wing lift coefficient and lift coefficient slope. A higher aspect ratio increases the slope, but causes the wing to stall at a lower angle of attack.

Changes in the lift coefficient and its slope affects the definition of the controllability and stability lines in the X-plot of the aircraft. In turn, this means that the position and size of the canard on the aircraft change drastically.

When the wing lift coefficient slope is higher than the slope of the canard, the stability is improved. The tail arm must be adjusted to allow for controllability, to increase controllability the tail arm needs to increase as well.

Adjusting the wing and canard position to stability and controllability has a drastic impact on the size of the electric motors and propellers at the ends of the wings, as the aircraft also needs to remain stable and controllable during the VTOL mode. Placing the wings at different positions changes the moments arms that the thrust on the wing tips act on with respect to the cg of the aircraft.

In addition, when talking about the cg, a new wing position will also alter the cg of the operational empty aircraft, which in turn could again influence the wing positions as the X-plot is most sensitive to changes in the width of the cg range.

The required power of the motors would also change, as different values of thrust are needed to keep the aircraft in balance during VTOL. If the tail arm increases, thus the distance between the cg and the canard becomes larger, bigger propellers should be used in the main wings. This is because they need to generate more thrust and would therefore require more power, and the power losses can be reduced by increasing the size of the propellers.

The structural lay-out would not change too much. The main structure that is affected by the change in the aspect ratio is the wingbox. Higher aspect ratio means that the moments at the root are higher, and the wingbox needs to be made stronger, thus more material is added.

After having adjusted the different design aspects of the aircraft, a new iteration should be made with the new masses of the structures, to balance the aircraft again.

Sustainability development logic

This chapter aims to show that the requirements with regard to circular economy and sustainability have been met for this design. This starts by first looking into a requirement analysis for circular economy and sustainability in [section 14.1](#). In addition, it aims to show how well the design performs in all the pillars of sustainability by using the sustainability checklist tools in [section 14.2](#). A look is also taken at the improvement in sustainability with respect to the midterm phase in [section 14.3](#), which is the section that concludes this chapter.

14.1. Requirement analysis

Circular economy and sustainability are one of the main driving factors in this design. This is why it is important to check if the requirements with regards to circular economy and sustainability have been met. The requirements that are important are listed here:

- ✈ **DSE-22-STAK-04:** The aircraft shall be designed according to the circular economy concept
- ✈ **DSE-22-SYS-SR-03:** The aircraft shall have a minimum life time of 10 years.
- ✈ **DSE-22-SYS-S-01:** The aircraft shall have emissions during operation that do not exceed those of existing personal aircraft.
- ✈ **DSE-22-SYS-S-02:** The aircraft shall use renewable sources.
- ✈ **DSE-22-SYS-S-03:** The aircraft shall have re-usable materials.

These requirements are considered to make sure that the sustainability and circular economy have been implemented well in the design.

14.2. Sustainability analysis: checklist

To determine if these requirements are met, an analysis is again performed using the sustainability checklists. The same was done during the midterm phase [7]. It was decided that a sustainability analysis using the checklists is sufficient for investigating the circular economy and sustainability of the design, instead of performing a LCA assessment as proposed for this final report in the baseline phase of the project [6]. This is because the sustainability checklist tools were developed using the LCA methods. This means that the sustainability checklist tools already incorporate the LCA methods, however, the analysis is performed in a more concise way. Each of the following subsection will go through the sustainability checklists. The questions are answered based on the results that were presented in the previous chapters on the design. The results of each sustainability checklist will again be presented in the form of a table.

14.2.1. Environmental sustainability

For the environmental checklist each of the questions will be discussed.

1. "The product/part does not involve any environmentally harming practises/procedures/materials/emissions."

Compared to the midterm, a lot more is now known about the design. As of now, it is clear that only recyclable materials will be used in the entirety of the aircraft. The only part that could be problematic are the batteries. Lithium batteries still contain chemicals that are toxic to the environment. However, nowadays more and more possibilities exist to recycle batteries and the chemicals they contain. Also as of now, no other technology exists to store electrical energy. This means that the design cannot go without batteries.

As far as the propulsion goes, a great improvement was made. Now, all the motors will be powered by electricity, which will be created using a turbine that can run on all sorts of fuels: biofuel, ethanol, hydrogen, plant oils and of course also fossil fuels. This means that the design is no longer restricted to using fossil fuels. However, the fuel type is restricted by the fuel tank that will be used. The fuel tank is only able to hold fuels that will be liquid at around room temperature. This means that at this stage, only biofuels or ethanol will be used as fuel. Being able to transition to biofuels and ethanol is a big step forward for the design. Unfortunately, using biofuels and ethanol means that CO_2 is still emitted by the aircraft. Yet, biofuels already have a much better circular economy as they are carbon neutral. All the carbon emissions they create were also taken out of the atmosphere when the fuel was created.

Compared to the midterm, quite some progress was made with this regard. So this question should get a higher score than during the midterm. However due to the chemicals in the batteries, the top score can not be awarded. The

questions will be answered with "Somewhat agree".

2. "The production methods used to produce the part/product use the minimum amount of energy for operation."

As will be said in the answer for question 9, it is difficult to be really specific about specification for production procedures at this stage of the design. This means that no exact numbers can be put on the efficiency and energy usage of particular production procedures. During this stage of the design it was possible to exclude production procedures that obviously use more energy than necessary to produce a particular part. Apart from this, not much effort was put into this during this stage of the design. This is why this question is answered with "neutral".

3. "The product/part contains the fewest possible (new) amount of material types."

The aircraft design does not use many types of materials at this point. Most of the aircraft will in fact be made out of Aluminium 6061. This is especially true for the structure of the aircraft, where all primary structures are made out of the alloy. Exceptions are made for the landing gear and the secondary structures like the leading and trailing edges of the wings.

For the landing gear type of steel was chosen to introduce more elasticity in landing gear struts to act as suspension during landing. The leading and trailing edges (LE and TE) of the wings, and the fairing of the fuselage will be reinforced using a type of plastic called PEI. The plastic was mainly selected to reduce the weight of the aircraft as it is not a load carrying part of the structure. Also, PEI is fully recyclable.

Although these materials were chosen for a good reason, they are still different types of materials. Making the gear struts and leading and trailing edges of wing out of aluminium 6061 would have been possible, but it would have required an entirely different engineering solution. This is why the top score cannot be awarded to this question in this case. If only the structure of the aircraft is considered, only three types of materials are used: Aluminium 6061, PEI (non primary structure or non load carrying parts) and Steel (landing gear). For a comparison, the Boeing 787 uses at least 5¹, This is why the score of this questions should still be in the good range, which is why the question will be answered with "Somewhat agree".

4. "The part/product can be produced by using currently integrated production methods."

For each part that was designed, the method of production for that particular part was taken into account. The parts were designed such that a currently existing production method would be available to produce the part.

An example of a production method that was looked into is 3D printing for the PEI of the LE and TE for lifting surfaces of the aircraft. This is because a honeycomb geometry was considered for the LE and TE reinforcements. This complex geometry is easy to produce using 3D printing. Industrial-scale 3D printing is already readily available and being used nowadays. The method is additive manufacturing, and it minimises the amount of materialistic waste created during part production. The only issue with 3D printing is that it can take quite some time to print a large part and will thus be hard to implement on an mass production scale. This would cause issues on the personal aircraft design if it would ever enter mass production.

Other production methods are more commonly used ones. As these methods already used for longer periods of time, their methods will be as efficient as possible. If a method was not already commonly in use, it would not have been considered for the production of the parts of the aircraft. This is why the question will be answered with "Completely agree".

5. "The product/part is designed to last for a long time."

The main structural components were designed to last until the end of the aircraft's operational life. Design for long lifetime is also true for other components on the aircraft like the body. However, the aircraft is designed to be modular to be able to easily replace parts if they were to get damaged.

To again take the example of the LE and TE reinforcements, the material PEI was selected over PLA. Both materials are easy to recycle and reuse. However, PLA is biodegradable, so the material will slowly degrade in operational life due to exposure to the environment, mainly UV light and humidity. This is not good from a structural standpoint, but the material is excellent from a sustainability standpoint as it will not leave anything harmful behind when it degrades. However, for the reason of degradation PEI was chosen above PLA for now, as the part would last for longer. Also, more research is needed for PLA to be chosen as the material for the LE and TE reinforcements.

In short, all parts of the aircraft were designed to make them last as long as possible. This question will therefor be answered with "Completely agree".

6. "The product/part is recyclable after its operational life." and

7. "The product/part is reusable after its operational life."

To hit two birds with one stone, question 6 and 7 are considered together as the answer to both questions will be more or less the same. As recyclability of the materials back into the cycle of source materials and reusability of parts that have not degraded, are of main importance to the design, they were always taken into account during the entire

¹<https://www.aircraftcompare.com/blog/what-are-planes-made-of/>, [Accessed 26.06.2020]

design process. If a particular option would have a bad effect on the recyclability or reusability of the aircraft, the option would only be considered if there is a very good reason for it. Generally though, recyclability was never traded for anything else.

Therefore "completely agree" are the answered to both questions.

8. "The product/part is designed/produced with a minimum amount of waste."

For as far as waste goes, it can only be commented on the what is know at this point, which is mostly material waste. Materialistic waste is of course also the most important for this design, and it was also considered from the beginning, by thinking a bit more about some production methods, such as modern production methods like 3D printing. The good thing about 3D printing is its very low amount of materialistic waste, as already mentioned. The only materialistic waste 3D printing creates is the material that is put in printing support pillars for the part that is being printed. This is however considerably less waste compared to other production methods.

More commonly used production procedures that create a lot of materialistic waste like milling parts out of big blocks of material were not considered. Unfortunately, the leftover production method for metals as an example still create a fair amount of materialistic waste. This is why the top score cannot be awarded to this question. This is why "somewhat agree" was given as the final answer to this question.

9. "The product/part is designed/produced with high efficiency methods."

At this stage of the design, not much was looked into the energy efficiency of most production methods. However, for most production methods, the energy efficiency is quite low. This sets a certain standard for the efficiency of most production methods. Unfortunately, not much effort was put into looking into the exact efficiency of the selected production procedures, which means that the production methods that were chosen do not have the best efficiency, but this does not mean that no effort was put into trying to select higher efficiency production methods. The production procedures that were looked into probably do not have the best efficiencies, but not enough time was spent on this to put exact numbers on them. Which is why this question's answer will be "neutral".

10. "The product/part is designed to meet its need and its need only (it does not have any additional functions)."

During the midterm phase, this question has quite a low score because of the VTOL capability. This VTOL capability was seen as a useful addition to the aircraft back in the midterm phase. However, at this point of the design process from a performance perspective, it is very probable that the personal aircraft design will not meet the 50 m take-off distance requirement if the aircraft did not have a VTOL mode. This is partly also the case because the personal aircraft does not have any high lift devices (HLDs) like most STOL aircraft. This means that the VTOL capability is becomes part of the need for the aircraft to be able to take off.

However, the one part of the aircraft that was designed for a need that exceeds the current need to the aircraft are the elevators. The elevators were attempted to be designed such that the aircraft is able to take off like an ordinary plane, by gaining forward speed on the ground. It is important to note that the propellers on the canard do not allow for this as they will strike the ground due to the low landing gear configuration. This means that the elevators will be a bit bigger than they are required to be. The personal aircraft will not need such big elevators during any of its phases of flight, not even during landing. However, the elevators were sized for an ordinary take-off, as in the far future it might be decided that it would also be essential for the aircraft to be able to take-off like any ordinary aircraft. However, in this case the aircraft will probably not be able to take-off in 50 meters. To cope with this the aircraft could do a VTOL assisted take-off where it still gains forward speed on the ground, but also uses the VTOL mode to create part of the lift. One could conclude that the elevator sizing does have a positive effect on the economical sustainability as the personal aircraft can more easily adapt to a different operational environment.

Due to the set back on the elevator sizing, this question will not get the top score. It will be answered with "somewhat agree".

In [Table 14.1](#), the filled in environmental sustainability checklist can be found. It contains all the answered specified by the questions described above. The summary of the scores of the environmental checklist is presented in [Table 14.2](#).

Table 14.1: The filled in environmental sustainability checklist for the final design of the personal aircraft.

Name of evaluated part/product:	VTOL personal aircraft						
Parameter	Questions	Completely agree	(Somewhat) agree	Neutral	(Somewhat) disagree	Completely disagree	Result
Hazardousness (toxicity)	1.	0	1	0	0	0	3
	2.	0	0	1	0	0	2
Energy usage	3.	0	1	0	0	0	3
	4.	1	0	0	0	0	4
Recyclability/reusability	5.	1	0	0	0	0	4
	6.	1	0	0	0	0	4
	7.	1	0	0	0	0	4
Waste & efficiency	8.	0	1	0	0	0	3
	9.	0	0	1	0	0	2
Need	10.	0	1	0	0	0	3

Table 14.2: The summary result table of the environmental checklist of the final design of the personal aircraft.

Final scores of:	VTOL personal aircraft
Parameter	Score
Hazardousness	3 /4
Energy usage	3 /4
Recyclability/reusability	4 /4
Waste & efficiency	2,5 /4
Need	3 /4
Total score	3,1 /4

All of the parameters mentioned in the summary table are important towards sustainability. However, it is important to note that the top score was not achieved for all the parameters. Of all the parameters, recyclability and reusability is the most important parameter during this design project. Therefore it is satisfying to see that the top score was achieved for this parameter of environmental sustainability.

14.2.2. Economical sustainability

The same plan of action will be taken as for the environmental checklist. Each question's answer will be accompanied with some argumentation. After the questions are answered, the result of the economical checklist will be presented. Note that some questions are not answered in as much detail as others. This is mainly because the answers to most questions is still the same as in the midterm.

1. "The product/part has no or little competition on the market."

After the final design phase, the opinion on how well this aircraft will perform in the market did not change. The aircraft is still expected to do well, as it is a unique and futuristic design that does not exist in the current market in the form of a personal aircraft. The answer to the question is still "completely agree".

2. "The product/part fulfils the needs of the future market."

The aircraft is also still expected to fulfil the needs of the future market due to the fact that personal aircraft is able to move people from A to B without having to make use of current transportation infrastructure. The answer to the question is also "completely agree".

3. "The product supports long-term economic growth of the company."

During the midterm, it was expected that this aircraft design would perform worse in the long term. Mainly because of the propulsion system using fossil fuels. During the final design phase, a different propulsion system was selected that is able to run on all sorts of fuels. This means that the propulsion system is no longer bound to using fossil fuels. The flexibility in terms of the fuel type now also increased, which is expected to be very beneficial for market competitiveness as in some locations, a particular fuel type might be more abundant.

Also, the aircraft was designed to be able to more easily adapt to changes in the market. Another example of this are the elevators, which were sized such that the aircraft is also able to take-off line an ordinary airplane by gaining

airspeed while still on the ground. This aircraft is thus able to operate in many different environments for years to come. This results in awarding the highest score to this question: "completely agree".

4. "The product/part uses the socio-economic resources to their full advantage."

During the midterm phase, it as indicated that the resources in terms of manpower were allocated well and that everyone worked to their strengths. However, it is safe to say that an improvement was made here compared to the previous project phase. This is because the Gantt chart as well as the deliverable lists created were used much more and more efficiently. On the other hand, there is still always room for improvement, which is why the top score will not be given here. The same score will be given as during the midterm phase even though some improvement was made. The question's answer is "somewhat agree".

5. "The product/part minimises the operation costs."

The this final phase of the design, more number were put on the operational cost of the aircraft. The operational cost of the aircraft was estimated to be around 83 US dollars per hour. This price includes things like fuel and monthly storage costs. Things like annual costs for maintenance are also included.

Compared to other modes of personal transport like a car, 73 euros per hour is still expensive. However, compared to a car, the personal aircraft is able to cut travel costs down significantly due to its cruise speed.

On the contrary, the personal aircraft is much cheaper per hour compared to general aviation aircraft of a similar size. These aircraft cost about 250 euros per hour [20]. This is significant difference in price. This means that the personal aircraft has quite a low operational cost per hour.

The low hourly operational cost of the aircraft mostly comes down to the maintenance being split over the owner and a mechanic. This is one effort taken to reduce the operational cost of the aircraft. In addition, the aircraft has a low cost due to its low fuel flow. Compared to general aviation aircraft, the personal aircraft uses less fuel. This helps to cut down the operational cost even more.

With these results, it can be said confidently that the operational costs are being minimised. There is not much more that can be done to minimise the operational cost of the aircraft even more. Thus, this question will be answered with "completely agree".

6. "The designed product/part does not negatively impact the social environmental sustainability pillars"

On the contrary, during the final design it became apparent that the VTOL capability is part of the need of the aircraft. Which has a positive effect on the environmental sustainability. This means that the VTOL capability is not just an addition to the aircraft to make it more competitive in the future market. In conclusion, the VTOL capability no longer negatively effects the other sustainability pillars.

During the midterm the top score was awarded to this question because the idea of not negatively affecting other sustainability pillars was taken into account in the design process. However, now the top score can be awarded as the economical sustainability no longer negatively effects the environmental sustainability pillar, as the VTOL mode was not just introduced to increase the economical sustainability. The results of the filled in economical sustainability checklist can be found in [Table 14.3](#). The summary score table of the economical sustainability can be found in [Table 14.4](#).

Table 14.3: The filled in economical sustainability checklist of the final phase of the design project.

Name of evaluated part/product:	VTOL personal aircraft						
Parameter	Questions	Completely agree	(Somewhat) agree	Neutral	(Somewhat) disagree	Completely disagree	Result
Market competition	1.	1	0	0	0	0	4
Business preservation	2.	1	0	0	0	0	4
	3.	1	0	0	0	0	4
Resource management	4.	0	1	0	0	0	3
Cost	5.	1	0	0	0	0	4
Sustainability awareness	6.	1	0	0	0	0	4

Table 14.4: The economical sustainability summary score table.

Final scores of:	VTOL personal aircraft		
Parameter	Score		
Market competition	4	/4	
Business preservation	4	/4	
Resource management	3	/4	
Cost	4	/4	
Sustainability awareness	4	/4	
Total score	3,8	/4	

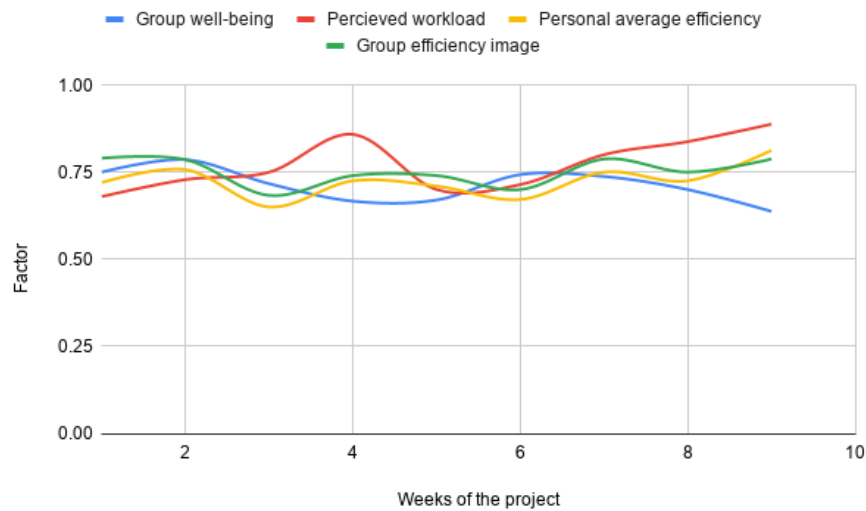


Figure 14.1: A table showing the percentage of the different metrics over the last 9 weeks

14.2.3. Social sustainability update

In Figure 14.1 the percentage of the four different metrics is presented. With the exception of the 4th and the 5th week where the group well-being had an average lower than 7. This was attributed to the deadline of the midterm report and the struggles of the group in isolating the best aircraft design. But after a long weekend, everyone got better while the perceived workload decreased. For the final design the perceived workload steadily rose again but the well-being stayed constant. Over the last week the well being went down again. This is partially due to the deadline that was set at the day the form was filled in. It does however show that although people suffer under the pressure the efficiency did go up. This is beneficial for the deadline but overall not sustainable. If the project was to continue for a couple more weeks there had to be a change. This would be either the workload per worker or the planning should be really updated. Unfortunately one of the group members also left the group in the middle of the project. This increased the workload for the other members. The fact that one group member quit means that it is very important to check up on the group members during the project to see how everyone is doing. It is especially important in a situation like this where anyone has even less social interactions and is trapped in their own homes.

From the beginning of the project there were two major improvements that could have been made. These were highly focused on the communication and structure during the meetings. This was affected by the low reliance on the planning tools from the start. During the project this greatly improved, even though the Gantt chart was not heavily used. The group preferred a google sheet where all the tasks were laid out and updated. The reason the group might have preferred this method was due to the ease of checking and updating by anyone. Due to the circumstances it was harder to communicate with someone else. It was therefore not preferred to ask the team manager for small updates every time.

The current situation was not a big hindrance throughout the project. The team quickly adapted to working in a virtual environment. The virtual environment did become an issue in the final design stage of the project. Designing and coding is very hard to do with multiple people, far away from each other. Discussing different theories or code structures was difficult and much slower in comparison with a situation where you are physically there. From the social side of the project these factors could be taken into account with the next project. Although the Gantt chart is very useful for the full project planning, a smaller more well known program or layout might be used for the day to day deadlines. The usefulness, of a program like the Gantt chart, is highly dependent on how it is used by the user. If the users find it too hard to work with it loses its usefulness. Furthermore, the use of an online workplace does not

have to be a handicap. It is only for the detailed design of the craft where better tools should be found. If possible the engineers should come together to collaborate on the design. An alternative would be to find/develop better tools to code or draw in real time with multiple engineers in the same document. This, in addition to a constant voice chat, could help with some of the problems that were faced. But there is no substitute for actually sitting together and working on the design.

The social sustainability of the final product is primarily affected after the design of the aircraft. There is one aspect of the design which could have an impact now. The aircraft is using bio fuels to power the range extender in the aircraft. Bio fuels are however made from plants, which need farmland to grow. It might affect the lives of other people if the demand for these fuels rises due to the aircraft being sold. With a higher demand farm land could be used for fuel production instead, thereby raising the food prices. This demand could decrease the equality because the route of the highest profit is chosen. This will decrease the availability of food for the less fortunate people. This could be a big problem to the project and should be one of the most important sustainability metrics to be checked throughout the life of the program. Beside the fuel the other parts of the project should also maintain equality and prevent negative effects to the people surrounding the project.

14.3. Sustainability development and conclusion

When seeing the results of the sustainability checklists, quite some progress has been made compared to the midterm phase. To see just how much progress was made, Table 14.5 and 14.6 are presented. In these tables the score summary tables of environmental and economical sustainability of the midterm and final phase of the design project can be seen.

Table 14.5: The environmental sustainability checklist scores of the midterm and final phase of the design project.

Final scores of:	VTOL personal aircraft		
	Midterm	Final	
Hazardousness	1	3	/4
Energy usage	3,33	3	/4
Recyclability/reusability	4	4	/4
Waste & efficiency	2	2,5	/4
Need	1	3	/4
Total score	2,27	3,1	/4

Table 14.6: The economical sustainability checklist scores of the midterm and final phase of the design project.

Final scores of:	VTOL personal aircraft		
	Midterm	Final	
Market competition	4	4	/4
Business preservation	3,5	4	/4
Resource management	3	3	/4
Cost	1	4	/4
Sustainability awareness	4	4	/4
Total score	3,1	3,8	/4

As can be seen, the sustainability scores went up during this final compared to the midterm phase. This is mainly because the recommendations that were set in the midterm report [7] were taken into account during the final phase.

Two things that were looked at during this final phase are the propulsion system and the operational cost. The propulsion system is now able to also run on more sustainable fuels. The operational cost was also calculated which came out to be quite low. Especially if compared to operational costs of general aviation aircraft. However, note that it is still more expensive compared to modes of personal transport such as the car.

As far as social sustainability goes, the Gantt chart and deliverable lists were now used more often to be able to more efficiently plan the tasks that needed to be performed. The well being of the group remained almost constant as well. The fuel that was chosen does directly compete with the natural resources humans need thus providing a place where inequality can occur. This needs to be monitored in order to maintain a high sustainability.

In the end, it was needed to exchange some economical sustainability and social sustainability to be able to obtain a higher score for the environmental sustainability. This way all pillars of sustainability were maximised.

Technical Risk Analysis

Throughout the different stages of this project, the organisational and then technical risks have been identified and actions for their mitigation were planned. With the final design being established, some of the identified risks were mitigated through the design choices by incorporating redundancies or replacing the elements which were considered more dangerous by elements that are safer, or easier to predict or check regularly, since safety by itself was deemed difficult to establish without some degree of subjectivity in many situations. The risks which have been mitigated are discussed in [section 15.1](#). Certain old risks however remain at the same stage as before, and this refers specifically to risks that are directly related to the production phase of the aircraft or post production risks related to the operation of the vehicle. As it will be seen in [section 15.2](#), the mitigation for these risks has already been planned, the only remaining action being to apply these mitigations once the aircraft enters the production phase and later on the operation phase.

15.1. Mitigated Risks

Technical risks have been identified before in both the Baseline Report [6] and Midterm Report [7], each risk being given an identifier, and a level based on the occurrence's likelihood and the resulting impact on the project development. The scores along with the descriptions given in these reports are once again presented below.

Likelihood scale:

1. Rare - less than 1 percent probability of occurrence within the project.
2. Unlikely - 1-5 percent probability of occurrence within the project.
3. Possible - 5-25 percent probability of occurrence within the project
4. Likely - 25-50 percent probability of occurrence within the project
5. Almost certain - more than 50 percent probability of occurrence within the project

Impact scale:

1. Insignificant - mission/production continues normally
2. Minor - aircraft still flyable, pilot decides whether to continue or land/ maintenance required asap, production manager decides whether production continues normally or is delayed.
3. Moderate - abort mission/production stops for few hours
4. Major - emergency landing/production stops for few days
5. Critical - mission failure/production stops for more than a week

The mentioned risk levels resulting from the combination of likelihood and impact were placed on a risk map which can be seen in [Figure 15.1](#)[6][7].

Risk Analysis		Impact Severity					
		1	2	3	4	5	
Likelihood of Event	1	L	L	L-M	M-H	XH	
	2	L	L	M	H	XH	
	3	L	L-M	M	H	XH	
	4	L-M	M	H	XH	XH	
	5	L-M	M-H	H	XH	XH	
		L	L-M	M	M-H	H	XH
		Low Risk	Low-Medium Risk	Medium Risk	Medium-High Risk	High Risk	Extremely High Risk

Figure 15.1: Risk Analysis Matrix

Table 15.1 presents the risks identified in the Midterm Report[7] and which have been mitigated as mentioned before through the design choices during the final design phase. The table shows each risk along with its identifier, initial likelihood and severity scores and the corresponding risk level for the combination, and lastly the design choice which lead to the mitigation of the risks. Table 15.2 following this analysis shows what the result of the design choice was on both the scores of the likelihood and severity, and as a consequence the new level of risk is presented.

Table 15.1: Risk Analysis and Mitigation Table

Risk ID	Risk Description	Initial Likelihood Score	Initial Severity Score	Initial Risk Level	Mitigating Design Choice
DSE-22-RK-06	Mistakes in the preliminary design. For example, wrong weight estimation or surface sizing. If happened, many units may be produced before realizing the problem which will result in huge losses.	1	5	XH	This was mitigated by performing the validation and verification in order to make sure the results are accurate.
DSE-22-RK-08	System/subsystem malfunctions during take-off and landing. These include but are not limited to the high lift devices, the landing gear, control surfaces, etc.	2	3	M	This risk includes numerous subsystems and therefore the solution involves multi-subsystem design choices. Firstly, the landing gear was designed such that it is non-retractable, reducing the risks of malfunctioning. Secondly, due to the VTOL capabilities, the HLDs are not required, and through the wing sizing and design, the aircraft can safely land in their absence even in standard configuration (in case of engine rotation malfunction). Lastly, the controls were designed to be mechanical instead of fly-by-wire, in order to reduce the chance of malfunctions for the control surfaces.
DSE-22-RK-14	Urban area integration. A risk for this aircraft could be that it is not easily integrated or accepted in urban areas which would mean the idea of a personal aircraft would be defeated.	3	5	XH	In order to avoid having an aircraft with no purpose and thus with no customers, the concept followed strictly all the requirements that diversify its functionality (e.g. range, endurance, short TOL, etc). By covering all of these this risk was mitigated through design.
DSE-22-RK-15	Propeller strikes. This risk appears for any aircraft having propellers since when spinning fast, the propellers are not visible and can cause harm to people/animals in the proximity.	3	3	M	As it was indicated in the midterm report [7], the visibility of propellers in motion can be improved by painting them at the ends with a different colour, or having patterns painted on the entire propeller. This was therefore added in the design of the propellers.

DSE-22-RK-16	Hybrid failure. The system uses a hybrid system for the propulsion, and therefore bears a risk of failure of one of the components due to its complexity.	3	5	XH	The aircraft was designed in such a way that the electric part can provide enough power for the take-off and cruise, and therefore the hybrid option serves as a range extender. Failure of this would still allow the aircraft to fly purely on its main propulsion system (electric).
--------------	--	---	---	-----------	---

Table 15.2: Post-mitigation Risk Levels

Risk Identifier	Risk Level Pre-mitigation	Likelihood Post-mitigation	Severity Post-mitigation	Risk Level Post-mitigation
DSE-22-RK-06	XH	1	1	L
DSE-22-RK-08	M	1	1	L
DSE-22-RK-14	XH	2	2	L
DSE-22-RK-15	M	1	3	L-M
DSE-22-RK-16	XH	3	1	L

As can be seen here, three of the risks which were identified as being dangerous for the project were reduced significantly through the design choices, while two other smaller risks were reduced further, to the point where their impact is deemed insignificant. It must be mentioned that for the risks related to any kind of failure of the aircraft it is possible to reduce the likelihood further during the operation of the aircraft by ensuring that proper maintenance is conducted after set amounts of time or after a set number of completed hours of flight. One aspect that has been pointed out in the past reports as well, is that it is important to note risks can be mitigated and therefore the level can be reduced, however full elimination of risks is simply not possible for any project. To some degree risks will always be part of a design activity, and later on production and operation of the concept. This is why for both [Table 15.2](#) and [Table 15.4](#), the minimum level that a risks can reach will be a Low (L) regardless of the mitigation strategy applied.

15.2. Current Risks

As mentioned previously, some of the risks could not be mitigated yet, and these are the production and operation risks, as well as newly identified risks specific to the subsystems that are used in the final aircraft configuration. In [Table 15.3](#), the risk identifiers up to DSE-22-RK-14 represent older identified risks along with the planned mitigation strategies, as taken from the midterm report[7]. The remaining risks are the ones originating from the final design, and these are either mitigated through the design, in progress of mitigating or have mitigation actions planned for the future. The distinction is made in the mitigation action section within the table. These are given as well with planned strategy for their mitigation. Lastly, [Table 15.4](#) shows the expected result of the mitigations, giving the new scores for likelihood, severity and the final risk level of each item.

Table 15.3: New Risks Analysis and Mitigation Table

Risk ID	Risk Description	Initial Likelihood Score	Initial Severity Score	Initial Risk Level	Mitigating Design Choice
DSE-22-RK-01	Injuries or health issues occurring during manufacturing. Incautious use of machines may cause injuries, other health issues may arise from using toxic materials for example.	2	3	M	This risk will be mitigated by introducing rules in the workspaces, using human friendly substances, and make sure all the workers are following the precautions. This can be ensured by having a responsible supervisor present at all times in order to enforce these rules.

DSE-22-RK-02	Economical Risk. Suppliers increase prices suddenly.	2	2	L	Long-term fixed-price contracts can be made with the suppliers. This way the risk of price fluctuations is borne by the supplier. Of course the supplier would want the extra risk that he is bearing to be compensated for at his turn, and this could have other consequences, i.e. setting a higher starting price.
DSE-22-RK-03	Shortage in supplies. Raw materials or parts required for manufacturing can not be provided by the supplier for a certain period of time.	1	4	M-H	A list of alternative suppliers or materials should be available and used in this situation.
DSE-22-RK-04	Production issues. Machines defects or network problems in the factory may result in stopping production.	2	4	H	Mitigation is achieved by proper maintenance planning for all the machines and the systems in the factory.
DSE-22-RK-05	Product defects. Bad surface finish for parts and structural flaws are not allowed, any of them will result in recycling this product.	1	4	M-H	Making sure that all workers are well-trained, machines are in good conditions, and quality checks are done properly in each production phase. If a flaw is detected, an investigation should be done immediately, recalling some items based on severity so that they don't end up on an aircraft, and documenting the event in order to prevent it from happening again.
DSE-22-RK-07	Engine failure. This can happen at any stage of flight, however the ratings are given for the most dangerous situations (landing and take-off, due to low speeds and altitude.	1	5	XH	Due to the way the electric motors work, this risk is now higher, since the failure of one motor automatically causes the diagonally opposite motor to fail as well. The mitigation includes using software for recovery once the engine has failed, in order to stabilise the aircraft. This software is still under development however but once ready, it can decrease the risk drastically.
DSE-22-RK-09	Structural failure. This can occur either due to external factors (physical damage/ weather) or internal (quality of materials, porosities, cracks, fatigue).	2	5	XH	This is to be avoided by performing regular maintenance checks.
DSE-22-RK-10	System/subsystem malfunctions during cruise.	3	2	L-M	Once again, redundancy should be considered together with the proper maintenance and training.
DSE-22-RK-11	Radio communication failure. This can lead to multiple complications especially in crowded airspace.	4	3	H	This risk can be mitigated or even avoided with proper maintenance, but also by having an alternative means of communication (portable radio station).

DSE-22-RK-12	Pilot error. This includes any types of error, ranging from lack of attention to mistakes in flight procedures.	4	3	H	Small errors (lack of attention) are sometimes unavoidable yet they also mostly (not always!) have a low risk factor. Large errors however can result in critical failures, thus the large range of severity given. These large errors shall be avoided at all costs, by proper training and rules being set in place for the pilots.
DSE-22-RK-13	Take-off/Landing single engine failure. For a VTOL aircraft this could be particularly dangerous since the speed during these phases is low and gliding is not possible. Thus this could lead to highly dangerous accidents.	1	5	XH	Similar to the previous failure, however the failure during take off is particularly dangerous and therefore added separately. The mitigation includes the use of the same software as well as extensive maintenance in order to ensure the correct functioning of the electric motor such that the failure likelihood stays low, or if it happens the aircraft can be made stable for safe landing.
DSE-22-RK-17	Overstressing the aircraft. During operation there is a chance that the aircraft could be pushed by the pilot over the limits mentioned in the loading diagrams. This could be either by accident or by intended improper use.	2	5	XH	This can be mitigated firstly by instructing pilots clearly about the limits of the aircraft in its book. Secondly, for future improvements of the software used (autopilot), a safety feature preventing the pilot from accidentally pushing the aircraft over the limit can be implemented, consisting of column shake, visual indicators etc.
DSE-22-RK-18	Noise levels. The noise level is unfortunately impossible to predict until the aircraft is build and functioning. Therefore, the risk of the aircraft exceeding the set noise requirement is present and must be looked into.	3	4	H	This is being mitigated already through the design by adding structures to the aircraft that are known to be reducing the noise. This will be checked at the end of the design as well, however, as previously mentioned, it is not possible to fully mitigate this risk due to current knowledge about noise and it's estimation.
DSE-22-RK-19	Battery/motors overheating. This is a risk that appears for any electric motor and battery powered vehicles.	3	3	M	In order to mitigate this, the design places the batteries and motors around aluminium components, since this material can be sued as a heat sink, dispersing the excessive heat. Moreover, the airflow from the propellers over the fairings of the motors will help cool it down as well. Additionally, the design could be modified such that more vents are present for airflow to reach the overheating parts. Lastly, a liquid cooling system can also be added for future iterations of the design if required.

DSE-22-RK-20	Motor not turning after cruise. In the landing phase, any failure to return to the VTOL configuration would lead to difficulty in landing, propeller strikes and many other issues.	2	4	H	This risk was mitigated by ensuring that the aircraft can land in the cruise configuration as well. Moreover, the landing design and propotor size were adjusted such that in the eventuality of landing in this configuration, the proprotors would not reach the ground, thus avoiding a strike and potential damage to the surroundings or hurting bystanders (possible when propellers spinning at high speeds break off).
DSE-22-RK-21	Damaged fairing/fuselage. This would be problematic especially from the point of view of aerodynamics and waterproofing of the aircraft since the fairing is not a main load carrying component, thus not generating a big problem with the structural integrity.	2	3	M	This is mitigated in the design by having the cables and other electrical components in the aircraft sealed using proper sealing materials such as XLPE or PVC. For the aerodynamics impact, the mitigation consists of regular maintenance that has to be conducted if flaws are being observed during operation (walk around checks by pilot or regular checks by mechanics).
DSE-22-RK-22	Landing gear integrity. After many flights, the components of the landing gear could get damaged. This includes the struts, as well as the tires.	2	3	M	This is only mitigatable through regular maintenance once the aircraft starts being used. Moreover, landing on surfaces that could damage the tires (broken glass, sharp rocks, etc) must be avoided by ensuring a clean area from where the aircraft usually takes off/lands.
DSE-22-RK-23	Galvanic corrosion. Since different metals are used in contact with each other in the landing gear especially (aluminium and steel), galvanic corrosion could occur.	3	4	H	This is mitigated in the design by using coatings over the different components in order to avoid the metals coming into contact. During operation the integrity of the coatings has to be checked regularly at each maintenance.
DSE-22-RK-24	Landing gear issues. These include any failures such as the breaks locking during taxiing, suspensions failing, steering wheel locking, etc.	3	2	L-M	These are regular issues that could occur during operation, and they must be mentioned in the aircraft book as part of the elements that are mandatory to check during maintenances, in order to prevent them from happening, or fix them in case they already did.
DSE-22-RK-25	CG shift. Due to the short CG range, any movement of the luggage to unexpected locations could cause the aircraft to become unstable.	2	3	L-M	This can be mitigated easily by having strict rules about the position of luggage in the aircraft that the pilot must follow at all times.

DSE-22-RK-26	Flapperon system stuck. If this happens during take off or landing, the flow of air from the proprotors will flow predominantly over the wing and therefore will not be efficient.	2	2	L	This risk can be mitigated through regular maintenance of the mechanism.
DSE-22-RK-27	Fuel leaks. Without a proper fuel lining, in the eventuality of a crash, the fuel can leak causing a fire and therefore more damage. The same can also happen if fuel leaks at any time due to a puncture or any other problems.	2	5	XH	This risk was mitigated by adding a Kevlar lining on the inside of the fuel tank. This risk mitigation was also issued in 2001 for different airlines, and especially for aircraft such as Concorde ¹ . Moreover, kevlar linings for the fuel tanks are used more commonly as well in formula cars ² .

Table 15.4: New Post-mitigation Risks

Risk Identifier	Risk Level Pre-mitigation	Likelihood Post-mitigation	Severity Post-mitigation	Risk Level Post-mitigation
DSE-22-RK-01	M	1	3	L-M
DSE-22-RK-02	L	1	2	L
DSE-22-RK-03	M-H	1	3	L-M
DSE-22-RK-04	H	1	3	L-M
DSE-22-RK-05	M-H	1	2	M
DSE-22-RK-07	XH	1	4	M-H
DSE-22-RK-09	XH	1	2	L
DSE-22-RK-10	L-M	2	2	L
DSE-22-RK-11	H	2	3	M
DSE-22-RK-12	H	2	3	M
DSE-22-RK-13	XH	1	4	M-H
DSE-22-RK-17	XH	1	3	L-M
DSE-22-RK-18	H	2	2	L
DSE-22-RK-19	M	2	2	L
DSE-22-RK-20	H	2	2	L
DSE-22-RK-21	M	2	2	L
DSE-22-RK-22	M	1	2	L
DSE-22-RK-23	H	1	2	L
DSE-22-RK-24	L-M	2	2	L
DSE-22-RK-25	L-M	1	3	L-M
DSE-22-RK-26	L	1	2	L
DSE-22-RK-17	XH	1	3	L-M

¹<http://www.concordesst.com/returntoflight/mods.html>, Accessed [26.06.2020]²http://www.formula1-dictionary.net/fuel_cell.html, Accessed [26.06.2020]

By the end of the DSE phase, the conceptual design of the aircraft is finished. However, the detailed design is not yet started and the aircraft it is not yet manufactured, tested, or certified. In this section, the post-DSE period will be discussed. This includes the Project Design Development logic (PDD logic) in [section 16.1](#) followed by the project Gantt chart in [section 16.2](#). The production plan is then discussed in [section 16.3](#). Finally, the operational and logistical aspects are then explained in [section 16.4](#), these include operations, ground support, maintenance, and environmental communication.

16.1. Project Design and Development Logic

This section discuss the Post-DSE project plans, the post DSE activities are shown in a diagram in [subsection 16.1.1](#). Then the mission lifetime cycle is discussed in [subsection 16.1.2](#).

16.1.1. PD&D Logic diagram

[Figure 16.1](#) includes all the post-DSE activities that can be executed in the future, which would serve the project goals by improving the urban air mobility. The diagram takes into account the uncertainties that might happen, for example the prototype not complying with the regulations, which might require another design iteration in that case. The project will always keep going, iteration will be made, however, it might be decided to stop the project completely; this will only happen in the case that the product did not succeed in the market, break-even point was not reached in the intended period, or the project can not get funds anymore to continue further. As shown in the diagram, the project is divided into four phases, the first one being the conception and initiation, the second one being the project definition and planning, then launch and execution and lastly, project close.

16.1.2. Product lifetime cycle

The project lifetime is explained in [Figure 16.1](#), however, the product lifetime cycle is not explained in details. The cycle is divided into several phases as follows:

Phase 0: Mission Analysis and Identification

This phase has already started in the early phase of the DSE, the findings of this phase were already discussed in the project plan [8].

Phase A: Feasibility

This phase was also done during the DSE period, its findings are discussed in earlier reports. It was done through a detailed market analysis, talking to the customer and checking the competitors.

Phase B&C: Preliminary & Detailed definition

These two phases were also started during the DSE, it starts with defining the requirements, and includes all the design phases of the product; namely, the conceptual design, the preliminary design, and detailed design. During the DSE, the conceptual design is finalized; where all the subsystems of the aircraft are designed and integrated, iterations are done till the design complies with all the requirements. It should be noted, however, that in the future the design process will continue further, preliminary and detailed designs will be done, and the conceptual design will be revised. Based on the investors inputs, some changes might be necessary as well. One change would be to explore the possibility of STOL if VTOL is not needed. This could potentially safe fuel and therefore it should be researched if that is possible. In the case of developing new products, these two phases together with the previous ones will be redone.

Phase D: Qualification and Production

Once the product design is finalised, the verification and validation process of the product will start. Different methods will be used depending on the subsystems. Earlier in the report the method used was explained in each section, however, different methods might be required for the detailed design. The production plan is then created, this will be explained more details in [section 16.3](#). Then the aircraft will be manufactured and tested, if passed all the tests and met all the regulations, it will be registered and delivered to the customers.

Phase E: Operations

After registration, the aircraft has the permission from the ATC to fly and to operate to and from the airports in the region as well. It is then ready to be delivered to the customers. It is designed to be flown by the customer himself, however, he will not be able to do all the maintenance work. Once the company starts to sell the product, maintenance

centres will open the regions where we will be operating for the bigger maintenance jobs that requires specialists. More details about operations and logistics are discussed in [section 16.4](#).

Phase F: End of life The entire project is implementing the circular economy concept, this means minimum waste during manufacturing, operations, and after the operational lifetime as well. Thus, the aircraft is designed to be recyclable. As mentioned in [Figure 16.1](#), a recycling facility will open in the company, once the aircraft is retired, it will be disassembled, some parts will be refurbished and reused in new aircraft and some will be recycled, more details about this are mentioned in [section 16.3](#). Some parts, however, might not be usable in new aircraft even after recycling, these parts can be sent to be recycled and used in other industries.

16.2. Project Gantt Chart

The project Gantt chart in [Figure 16.2](#) shows the post-DSE activities and their start and end date. These activities were listed earlier in [Figure 16.1](#), however, it was decided to include only the activities till the first flight of the prototype; that is because it is difficult to estimate time for the later ones, they also involve a lot of uncertainties, it is not yet certain how the project will succeed in the market, or whether the break-even point will be reached within the intended period or not, or when the company will be able to expand into new markets. The durations in the chart are initial estimates, they might change during the evaluation period based on the input of the fellow engineers or the feedback we receive from the customer after introducing the final design. For this version, the resources allocation is also not fixed, since the activities include hiring more staff members. During the evaluation, however, the activities prior to hiring staff will be allocated based on the interests of the team. During later phases of the project, the durations estimates will be refined.

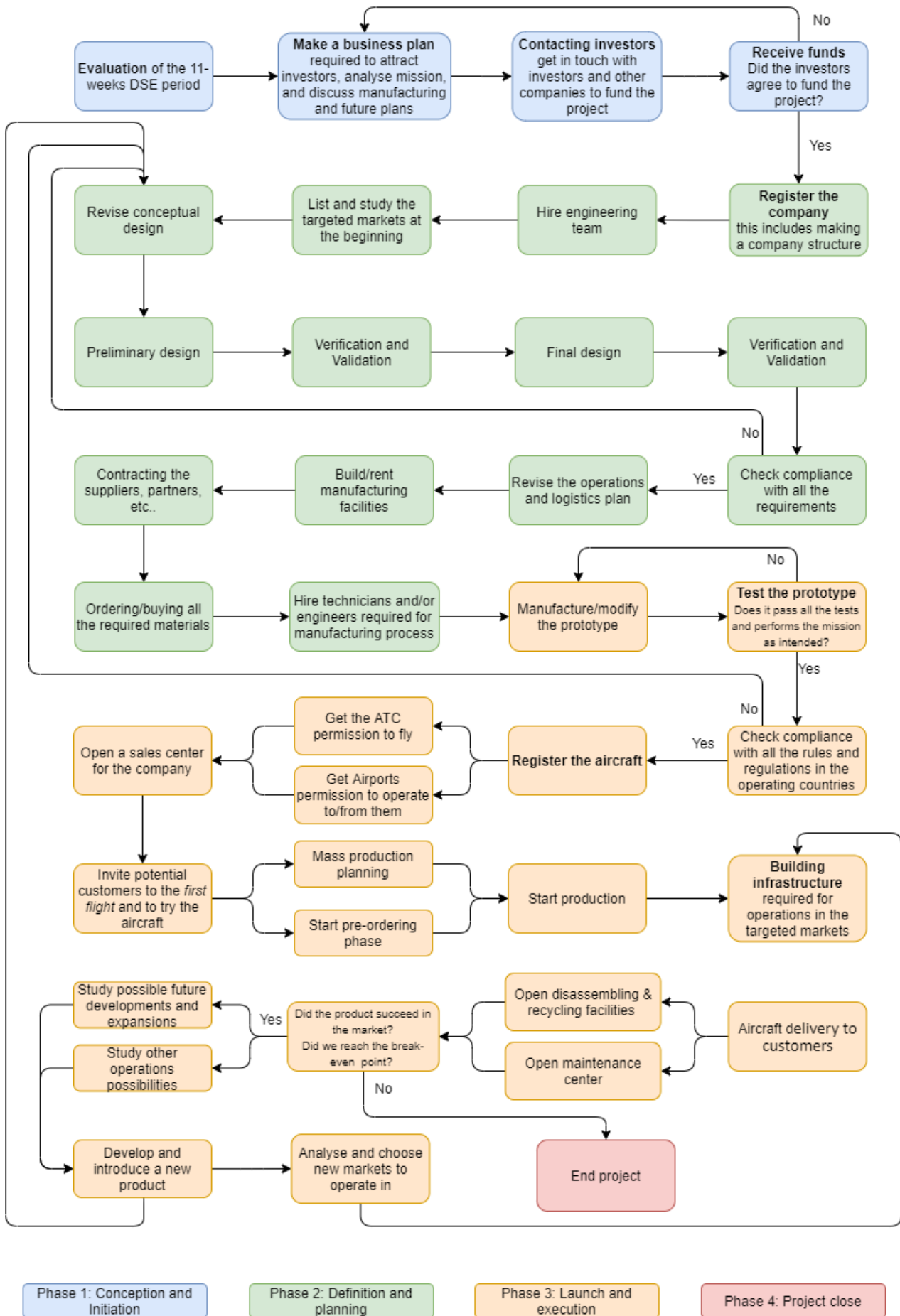
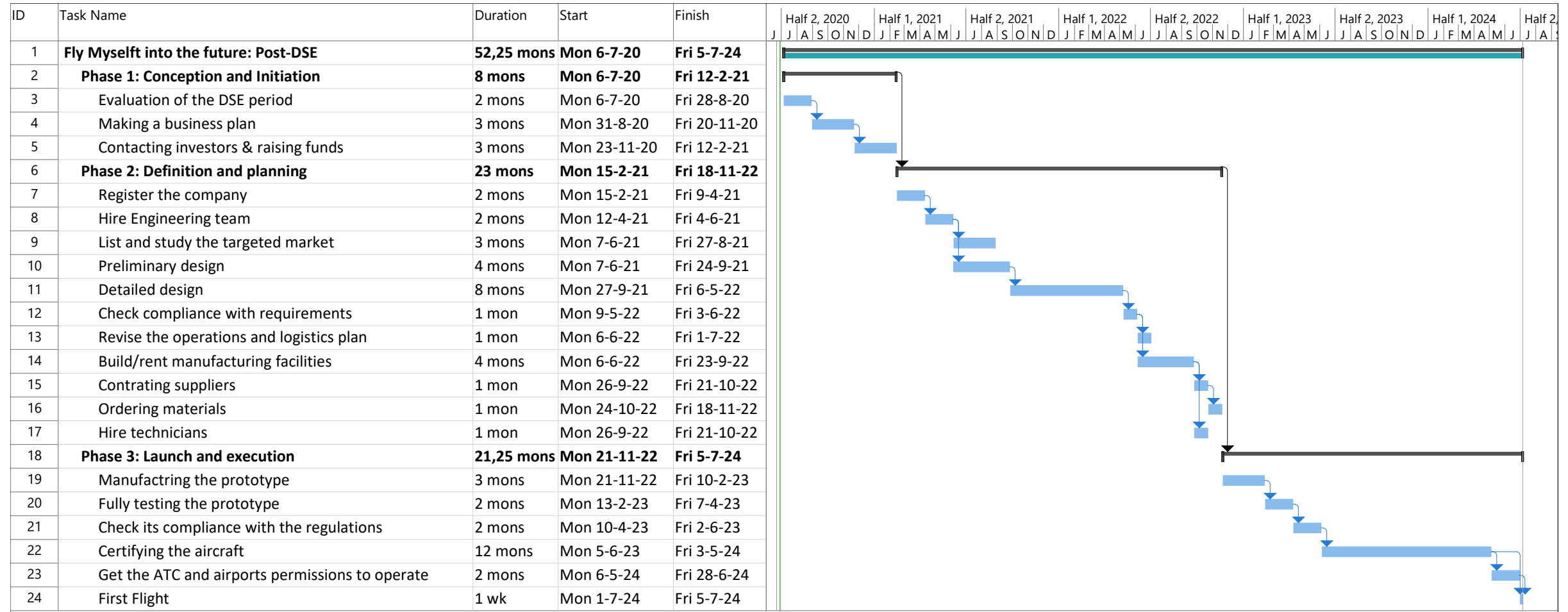


Figure 16.1: Project Design and Development Logic diagram



Project: Project Chart Date: Mon 29-6-20	Task		Project Summary		Manual Task		Start-only		Deadline	
	Split		Inactive Task		Duration-only		Finish-only		Progress	
	Milestone		Inactive Milestone		Manual Summary Rollup		External Tasks		Manual Progress	
	Summary		Inactive Summary		Manual Summary		External Milestone			

Figure 16.2: Project Gantt chart

16.3. Production Plan

In this section the production plan of the aircraft will be discussed, a time-ordered diagram will be presented in [subsection 16.3.1](#) and the different phases of the plan will be explained in [subsection 16.3.2](#). Lastly, the implementation of the circular economy concept in the production phase will be discussed in [subsection 16.3.3](#)

16.3.1. Production plan diagram

[Figure 16.3](#) shows the logical order of the production, divided into six different categories: manufacturing, components assembly, subsystems assembly, integration, quality control and testing, and circular economy. The different categories are colour-coded, and in addition, the ones related to the components and subsystems assembly are grouped together. The production process starts with part manufacturing, shown with an arrow pointing to the right on the top of the diagram. The main phases are also numbered in the diagram legend.

16.3.2. Production phases

The production process is divided into three main phases, manufacturing phase, assembly phase, and integration phase where all the subsystems come together.

Manufacturing

The production process of the aircraft starts with part manufacturing. This can be either done from scratch by ordering new materials from the supplier and shaping them, or by recycling the materials from the retired aircraft. When an aircraft is received in the disassembling and recycling centre, it is first disassembled, then materials are sorted into groups, and they will either be refurbished and reused, discarded, or recycled to new aircraft or to other industries; the recycling process also differs per material.

Some parts will be manufactured from scratch, with the recycled or new materials shaped into the required geometry. This shaping process will be different based on the geometry and the material used, for example manufacturing of the stringers and manufacturing of the fuselage skin require two completely different techniques; this indicates the need of having different machines for part manufacturing. Lastly, some parts will be ordered directly from the suppliers, this depends on whether it will be feasible to invest in a manufacturing facility for them or not. In addition, all the parts will have to pass the quality checks in order to proceed to the components assembly phase, failed parts will be discarded and re-manufactured/ordered.

Assembly

The assembly phase is divided into component assembly and subsystems assembly. That is because subsystems themselves usually have sub-assemblies as well and not only parts. Structural subsystems and other components of the aircraft can either be assembled from the manufactured parts, ordered from a supplier, or refurbished from a retired aircraft and reused again. All structural parts and components have to pass the quality checks before using them in the subsystems assembly. Once assembled, they have to pass new quality checks to proceed to the next step.

Integration

The last step in the production process is the integration. Once all the subsystems are approved, the integration process starts, where the aircraft starts to take its final shape. In this process, the order of the activities plays an important role in the entire production process. The components are integrated to the assembled structures when most convenient, for example, the propellers are attached to the wings only after the wings are attached to the fuselage. If the order is not planned, storage area is required, which might be expensive. In the next phase of the project, the exact time required for producing each part, component, or a subsystem will be estimated, dependencies will be determined, and a more refined plan will be made. This was already taken into account in [subsection 16.1.1](#).

16.3.3. Circular economy

In order to implement the circular economy concept in the production phase, the aircraft should be fully recyclable and the production methods should be sustainable as well and produce minimal waste. More details about the production methods will follow in the next phase of the project.

At the end of life of the aircraft, it will be disassembled and recycled as explained earlier in [subsection 16.1.1](#). A decision about recycling or refurbishing parts has to be made. As a general approach, the parts that have a longer lifetime than the aircraft as a whole, can be refurbished and used again, depending on how long they can further operate. It is most likely that structural parts that experience more fatigue or highly-loaded parts will be recycled instead. Financial aspects also play a role here, for example, the manufacturing process of the avionics is more expensive than that of the structural components, therefore, it would be favorable to reuse them instead of manufacturing/ordering new ones. Lastly, some materials change their characteristics when recycled, for example metals change their properties. If no new virgin material is added to improve the material so that it can be recycled into a new aircraft, it could be sold to other industries. Once the detailed design is finalized, more details about all the parts used, their characteristics, and their lifetime will be available. A more refined end-of-life plan can be made then.

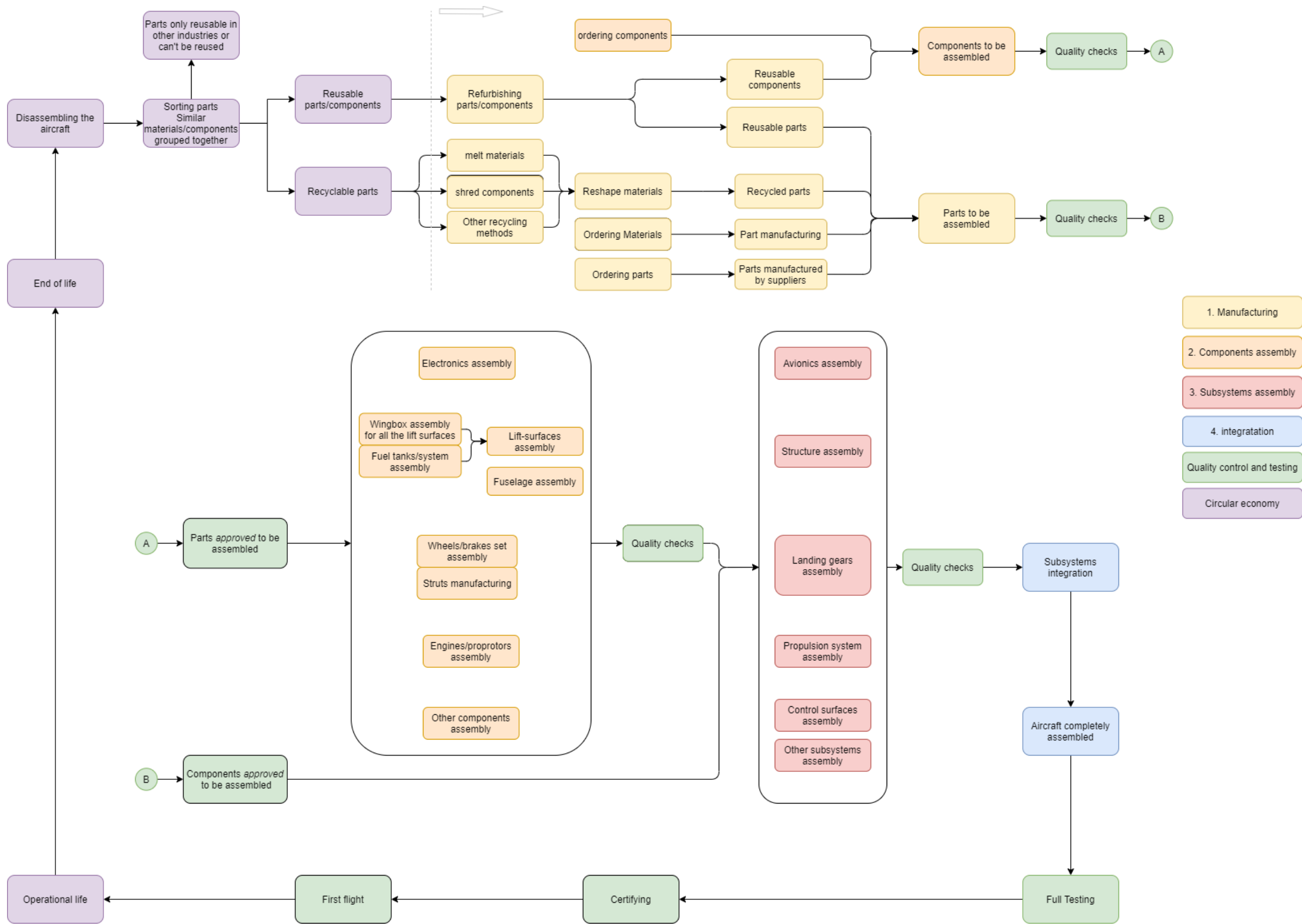


Figure 16.3: Production Plan Diagram

16.4. Operations and Logistics

This section will provide a description for the operations and logistics concept of the personal aircraft, which is a revised version of the one in the Midterm report [7]. A flow block diagram will explain the different phases encountered when travelling from home to a location of interest. First the operations aspect will be discussed in [subsection 16.4.1](#). The ground support aspect is covered in [subsection 16.4.2](#). The last part of the operations and logistics is the maintenance of the personal vehicle, explained in [subsection 16.4.3](#). In [subsection 16.4.4](#) the communication between the system and its environment is discussed.

16.4.1. Operations

The operations and logistics of the tilt proprotor design is depicted in a flow block diagram as seen in [Figure 16.5](#), which was also shown in the Midterm Report [7]. This diagram is given for an example use case for going from home to your preferred destination with the personal aircraft of the future. The 3 main phases are depicted in the upper blocks and consist of pre-flight, in-flight and post-flight activities. The in-flight operations contain the 3 main blocks: take-off, flying and landing/loitering. The functions in the operational phase are however not too detailed, as they were previously explained in the Functional Flow Diagram [section 5.1](#).

Before the aircraft control will be automated the pilot will need to have both PPL(H) and PPL(A) licenses, because the mechanical controls of the tilt proprotor resemble those of a helicopter in vertical flight mode and those of a general aviation plane in horizontal flight mode. As more automation is added, the pilot would only be required to have a PPL(A) license. The development of automation and urban operations would make it possible to travel in the aircraft just as a passenger, without any license.

16.4.2. Ground Support

Proper ground support is from importance during all phases, as clearly visible by the blue blocks in the diagram [Figure 16.5](#). Therefore this section will provide more information on the various ground support equipment present at the airport or in the aircraft.

Personal Garage

To store your personal aircraft safely, the airport will be equipped with personal garages/storage boxes. The storage facilities can be rented in a person's hometown airport on an annual bases. The renting of this garages will be very easy, similar to renting facilities to store a car.

Rent Garage

When travelling to other airport than the one in your hometown, the aircraft can be stored in similar garage boxes. These can be reserved by online or phone reservation for a couple of days or hours.

Leasing

When the aircraft becomes more automated, the company can also consider leasing the aircraft at airports, for an hourly rate for example. This however requires the company to be present at as many airports as possible, so that customers can leave the aircraft at the destination airport after travelling. In this case the company should cover the maintenance of the aircraft.

Recharging/Refueling Stations

The recharging or refueling procedure of the hybrid aircraft includes the following:

- ✈ **Biofuel** Current infrastructure at airports to refuel the aircraft with biofuel. However, additional refuelling stations will be needed, especially in urban areas. Additionally it must be noted that as biofuel is not used as widely as kerosene, some airports and areas are not yet equipped with the facilities or logistics chains.
- ✈ **Battery** The battery can be charged in flight through the range extender. To charge the battery on ground, a plug-in charging method is considered for now, meaning that there will be increased waiting time as the batteries are being charged. For future applications it could be considered, that the batteries could be taken out of the aircraft and changed. In this case the ground facilities would provide fully charged batteries to the operator of the aircraft, which would reduce the turn-around time. In order to increase the battery lifespan, they could be charged at ideal temperature and low charge rate at the ground facility. The batteries do need to be standardised and some assisting mechanisms might be required to lift the heavy batteries.

Last-Mile(s) Solution

The operations are now limited to landing at an airport close to the city, as operation in urban areas is not authorised yet. The so called last-mile concept means that the passenger would travel to the city center by public transport. In such operations, noise level in the cities is also not increased. In the future, UAM (Urban Air Mobility) will be authorized, and in this case there will be both manned and unmanned vehicles in the air. UAM requires a higher level of automation from all aircraft, since they require advanced detect-and-avoid capabilities to sense and avoid other flying objects in the air and obstacles on their way. New infrastructure is also required, since the aircraft will need to

be able to take-off and land on top of buildings and at multiple sites in cities. For this, vertiports and drone ports will be designed to accommodate both manned and unmanned vehicles.

16.4.3. Maintenance

Maintenance of the personal aircraft cannot be provided in-flight and are therefore only of importance in the pre-flight and post-flight phases as seen in the green boxes of the diagram [Figure 16.5](#). This section will explain the maintenance aspects encountered for this personal aircraft.

Pre-Flight Inspections

The pilot itself will need to perform the pre-flight inspection. The exact inspection procedure will be provided in the manual of the finished tested product. Example checks are:

- ✈ Check for external damage (e.g. flat tires, visibly broken structures, leaks)
- ✈ Check all cockpit instruments, including all switches, indicators and screens
- ✈ Check functionality of brakes
- ✈ Check functionality control surfaces
- ✈ Other equipment (according to the manual)

Regulations will pose some additional pre-flight checks to be performed before take-off. The pilot will be in charge of checking the fuel level before flight, as well as the expected weather conditions, to make sure it is safe to fly.

Futuristic developments may allow for the aircraft to fly fully autonomously. This will need automated pre-flight inspection methods to be set up.

Check after 100 Flight Hours

The aircraft will have an estimated total mass of 775 kg. According to the EASA relations, maintenance needs to be performed after every 100 hours of flight or on a yearly base. for aircraft with a MTOW up to 2703kg, [5]. For the design it is set to have a prescribed inspection in every 100-flight-hour interval by a professional.

In order to facilitate easy maintenance and inspections, the airport includes maintenance facilities. Maintenance and inspection services can be provided if one requests. When during this inspection it becomes clear larger maintenance should be provided, this could be done at larger/more suitable facilities.

16.4.4. Communication

The communication of the system with its environment is shown in the Communication Diagram [Figure 16.4](#). Here the system is shown to communicate through two possible ways: either through the pilot, or through automatic systems such as ADS-B. Additional network connections will be used in urban areas. Currently, as regulations do not yet allow for operations in urban areas, the aircraft will be used among general aviation traffic.

In the diagram the block 'environment' indicates the environment of currently allowed operations. This environment consists of ATC (Air Traffic Control) and other aircraft. During the in-flight phase, from take-off to landing, the system will communicate with the ATC through the pilot and the on-board ADS-B. The ATC commands rerouting if needed, and ensures that the aircraft has clearance to take-off, to fly through the zones along its path, and to land.

The future urban environment is shown in the diagram as 'extension', and this model is based on Swiss urban air traffic model plan [14]. The most important aspect of UAM regarding communication is the use of UTM (Unmanned Aircraft Systems Traffic Management), which regardless of its name would cover all unmanned and all automated operations in urban areas. UTM is needed to control the traffic in the low airspace, where for example drones are operated, and which in most countries is unregulated. U-space is the term used widely in Europe for the same concept.

All aircraft operators would need to be registered and connected to the UTM provider, that collects information about flight path planning and real-time traffic. The UTM provider would also be able to send commands to the operator, for example rerouting in case of colliding paths. In case of an automated aircraft, which the CESTREL design could become in the future, the on-board computer would process this command and act accordingly.

As there are multiple UTM providers, and each operator could choose their preferred provider, a UTM Interconnection provider is required, that combines the planning and real-time data of all providers. UTM should also be integrated to the existing ATM system, so that air traffic controllers and pilots of aircraft in high altitudes and near airports have information about operations in their vicinity. In case of unmanned or automated aircraft flying to the controlled airspace, air traffic controllers and pilots need to be able to communicate with the operators. The model architecture here would enable connecting UTM and ATM through a centralized FIMS (Flight Information Management System).

Additionally, to ensure security of all citizens, and critical infrastructure, the model includes a separate, secured authority network. This gives authorities the possibility to passively track all UAM traffic and disable operations through commands or to begin countermeasures in case of non-registered or disconnected aircraft in unauthorised areas.

NASA has concluded that tests have shown the ability of a secure and efficient cloud-based UTM network to coordinate and separate UAS in urban environments, and to remotely identify UAS within the network. The tests also presented complications: due to the high concentration of Wi-Fi routers and radio frequency equipment in the urban area, interference problems occurred in the command and communication link. The UAS compasses were affected by electromagnetic interference, and near tall buildings the UAS experienced GPS degradation ¹.

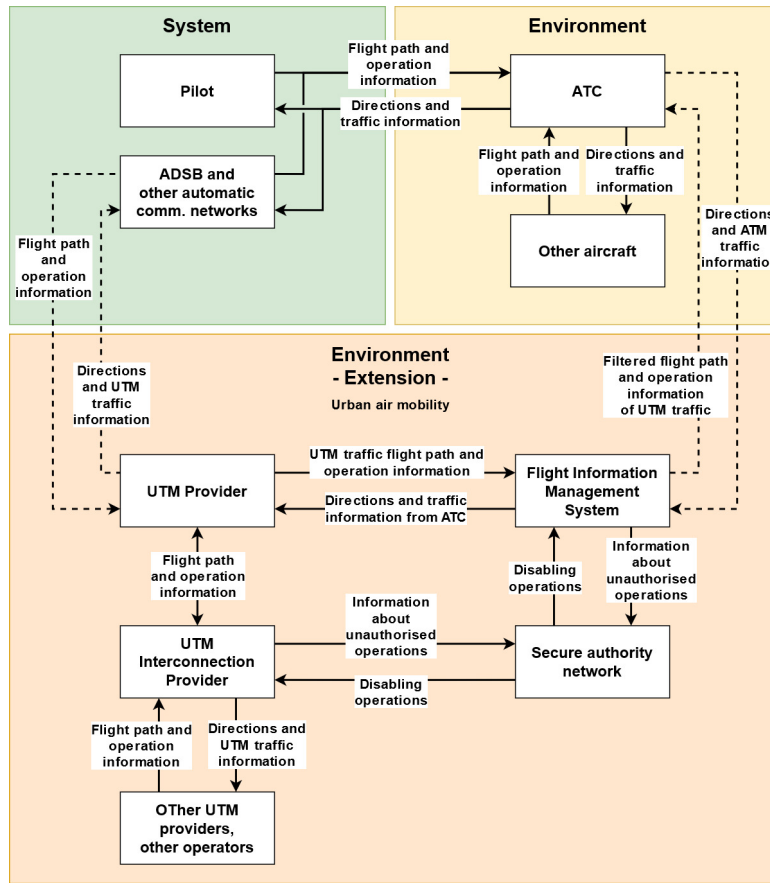


Figure 16.4: Communication Diagram

16.4.5. Emergency procedures

For now the pilot is assumed to have appropriate training to fly the aircraft, meaning a combination of both PPL(H) and PPL(A) licenses. The pilot is also required to have a multi engine rating. The pilot has been trained to respond to emergency situations. The procedures in case of emergencies will be specified in the aircraft manual, and these will be similar to current general aviation aircraft.

In the future, when operations in urban areas have started, there will most likely be new regulations regarding emergency situations and liability. The aircraft should have integrated safety systems on-board, for example for collision avoidance and back-up systems to avoid software failures. Through the UTM network emergencies can be notified to the authorities as soon as a system failure is detected.

Knowing how to handle emergencies is very important. This is why emergency procedures are mentioned in [Figure 5.3](#). The identified emergency procedures are first listed. The emergency procedures that were identified are mentioned here, note that all the emergency procedures get their own respective identifier. Note that the emergency procedures were based on the operational priority during flight: Aviate, Navigate, Communicate. In other words, make sure that you have the aircraft under control first, next identify where you are and navigate where you want to go. Only after this, add the extra work load of communicating with ATC.

✈ E1.0: Electric motor failure during VTOL:

Arguably, this is the most dangerous emergency situation as it is the hardest possible situation to stabilise the aircraft. This is because the thrust differential during a VTOL electric motor failure will be at its maximum. The aircraft should be vertically landed as soon as possible.

¹NASA. Unmanned Aircraft System Traffic Management (UTM)TCL 4. <https://ntrs.nasa.gov/archive/nasa/casi.ntrs.nasa.gov/20190030786.pdf> Accessed [19.06.2020]

✈ **E2.0: Electric motor failure during cruise:**

Although, less significant compared to E1.0, the differential thrust is still potentially dangerous. This is why a landing should be performed as soon as possible.

✈ **E3.0: Propeller tilt mechanism failure during VTOL:**

If during VTOL it turns out that the tilt mechanism of the aircraft is not functioning, the aircraft should be vertically landed again straight away.

✈ **E4.0: Propeller tilt mechanism failure during cruise:**

If it becomes apparent that the propellers cannot tilt to the vertical position during cruise, a nominal (non vertical) landing is unavoidable. Immediately, the most suitable aircraft with a long runway should be navigated to land the aircraft.

✈ **E5.0: Turbine range extender failure:**

In the event of a turbine failure, the aircraft will not be able to generate any more power and charge up the batteries. This means that a vertical landing should be performed as soon as possible. To save power for this vertical landing, the aircraft should descend to the transition altitude by gliding. If not enough power is available for the vertical landing, a nominal landing should be performed. Make sure to only use the battery power if absolutely necessary, as the power that is in the battery is the only power that is left.

✈ **E6.0: Out of or low fuel**

The same procedure should be followed as for E5.0.

✈ **E7.0: Bird strike**

A bird strike can have many possible consequences. A bird strike always leads to a different emergency situation. For example, if the bird damages the motor of the propeller, the emergency procedures of E1.0 or E2.0 should be followed. In the event of a bird strike, apply the correct emergency procedure accordingly.

✈ **E8.0: Unreliable airspeed indication:**

Unreliable speed indication mostly refer to a blocked pitot tube. This can be caused by ice or any other object. If the airspeed is unreliable, it is important to make sure that the aircraft keeps flying, so perform the memory items as specified for the aircraft (the memory items of the aircraft cannot be specified at this stage of the design and will not be discussed in this report). The next first thing to try it to see if the blockage is caused by ice. This can be determined by enabling the pitot heat or going to a lower altitude to melt the ice. If this does not solve the problem, something else is probably blocking the pitot tube. Keep flying the aircraft on memory item and try to transition the aircraft to VTOL mode as quickly as possible as the forward velocity is not important to keep the aircraft in the air during the VTOL mode. However, the transition could be risky at an unreliable airspeed. A decision could be made by the pilot to land nominally with the unreliable airspeed, which is also not without a risk. In both situations, the aircraft has risk of stalling.

✈ **E9.0: A control surface is stuck at a particular position:**

In the occurrence of a control surface getting jammed in a certain position, a similar procedure can be followed as for an engine failure. The aircraft first needs to be trimmed, next the emergency landing can be performed.

✈ **E10.0: The pilot is feeling unwell:**

If the pilot is feeling unwell, try to report this to ATC as soon as possible and immediately put the aircraft in the auto pilot mode and try to make the autopilot initiate an emergency landing.

✈ **E11.0: Turbine air intake blockage:**

The same procedures as for E5.0 and E6.0 should be followed.

16.4.6. Logistics

Ideally, the aircraft could be manufactured, assembled, and all components integrated in the same facility. However, it is likely that multiple facilities are needed, especially since some of the materials in the aircraft will be recycled after the end-of-life, which requires the appropriate disassembly and sorting facilities. Additionally, some parts and components are possibly ordered from other suppliers. A green supply line should be established between the facilities and suppliers. Additionally, the aircraft should be delivered to customers in the most sustainable transport method available.

The available logistics methods will be known at a later design stage, once all manufacturing processes are known.

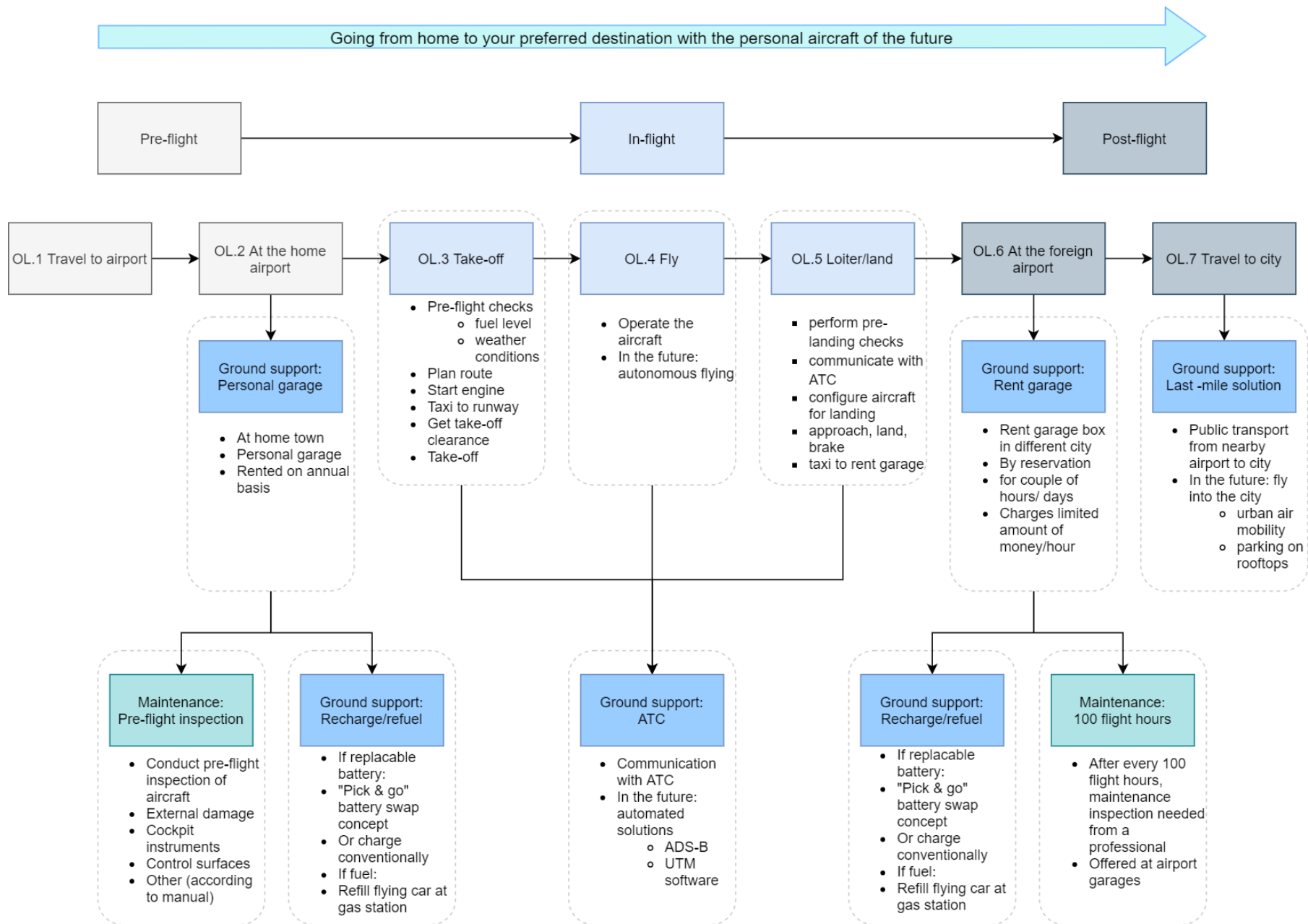


Figure 16.5: Operations and logistic concept description flow chart

Conclusion and Recommendations

The aim of this project is to design a sustainable personal aircraft to improve urban air mobility. The aircraft has to meet the requirements of a minimum range of 300km, take off and land in less than 50m, minimum endurance of 3 hours, and a minimum lifetime of 10 years. Most importantly, it has to fulfil the circular economy concept. At the beginning of the project, the project mission was identified, market analysis done, and an extensive trade of process was carried out in order to choose the design concept. It was then decided to design a tilt-proprotor canard aircraft with VTOL capability, named Cestrel. The aircraft therefore meets the 50m TOL requirements, and is still able to switch to a conventional aircraft during the cruise phase by tilting its rotors, which requires way less power.

This report discusses the findings of the final phase of the project, which is the conceptual design of the aircraft, and the future steps in the project. The design steps of each of the subsystems are discussed in detail throughout the report, as well as the design tools, and the verification and validation methods followed. It also discusses the technical risks associated with the design. The design process resulted in an aircraft with the following characteristics:

- ✈ Range: 660 km
- ✈ Endurance: 3 hours
- ✈ Dimensions: 6m length, 9m span
- ✈ Cruise Speed: 220 km/h
- ✈ Payload mass: 150 kg
- ✈ Cost 314k Euros

These characteristics comply with the requirements identified earlier in the project. In the future, the preliminary design and detailed design are to be continued, where more detailed sizing for all the subsystems will be done. Testing and production can be started afterwards. An initial production plan and development logic were also discussed in the report; however, they will be refined in the next phase of the project. The business aspects of the project are to be studied in more details in the next phase as well.

The aircraft mass does not yet converge, which means that more iterations should be made to reach the final mass. From current analysis it seems that the mass of the aircraft could be up to 25% lower than the estimated MTOW on which the calculations are based on, 775 kg. The structural masses for example are lower than those that were assumed for this MTOW. However, in order to reach a mass for which all calculations converge, the other components in the aircraft, such as avionics and instrumentation, also need to be studied more in depth, because for now their contribution to the mass is estimated based on a mass breakdown of an existing aircraft.

With the mass iteration the structures of the aircraft will be affected, because the mass directly affects the loads that the structures experience. With reduced loads the structures can be made lighter. Additionally, the wingbox structure can be designed in more detail by making the structure more complex. Firstly, the wingbox should follow the curvature of the airfoil, as for now a trapezoidal geometry was used. Secondly, more research should be made into how buckling would affect the structure and how much buckling the structure is allowed to experience. Thirdly, the deflections in the structures should be looked into, and these are also needed to optimise the LE and TE honeycomb structure. In a 2D honeycomb structure it would be possible to have small holes going through the honeycomb hexagon tubes, in order to allow for moisture to leave the structure. This should be studied in more detail in the future.

In order to improve the aerodynamic characteristics, more research will have to be performed on the airfoils. Right now, only 4-digit NACA airfoils were considered due to time constraint. However, 5-digit NACA airfoils are more detailed, which could lead to a more accurate airfoil selection, which in turn could lead to better aerodynamic characteristics. The stability and control characteristics could also be improved in a next phase of the design by widening the cg range of the aircraft. This would allow for a safer operation of the aircraft. Right now, if the pilot moves too much, the aircraft becomes uncontrollable according to the X-plot. In order to do this, the aerodynamic characteristics also need to be re-evaluated. Additionally, the fuselage of the aircraft should be incorporated into the AVL program that was used in order to be able to check the results more accurately.

Methods that need to be taken into account for noise reduction of the blades include serration of trailing edge, active flaps, and use of porous material. Additionally, to reduce noise of the micro gas turbine, acoustic linings and an optimised blade geometry could be used.

References

- [1] European Aviation Safety Agency. *CS-27: DECISION NO.2003/15/RM OF THE EXECUTIVE DIRECTOR OF THE AGENCY*. EASA, final edition, November 2003.
- [2] European Aviation Safety Agency. *Certification Specifications for Normal, Utility, Aerobatic, and Commuter Category Aeroplanes*. EASA, final edition, September 2010.
- [3] European Aviation Safety Agency. *Easy Access Rules for Normal, Utility, Aerobatic and Commuter Category Aeroplanes (CS-23) (Amendment 1)*. EASA, final edition, June 2018.
- [4] European Aviation Safety Agency. *CS-27: Certification Specification and Acceptable Means of Compliance for Small Rotorcraft*. EASA, amendment 5 edition, June 2018.
- [5] European Aviation Safety Agency. *Acceptable Means of Compliance (AMC) and Guidance Material (GM) to Annex Vb (Part-ML) to Commission Regulation (EU) No 1321/2014*. EASA, March 2020. Issue 1. Annex VI to ED Decision 2020/002/R.
- [6] Jonas Appels, Yasser Elnily, Quinten van Hilten, Roosa Joensuu, Thomas Keesom, Timo van Maarschalkerweerd, Elise Scheers, Kasper Sijmons, Andrei Stefanidi, and Aïcha van Veen. *Fly Myself Into the Future Baseline Design Report V2*. Technical report, 2020.
- [7] Jonas Appels, Yasser Elnily, Quinten van Hilten, Roosa Joensuu, Thomas Keesom, Timo van Maarschalkerweerd, Elise Scheers, Kasper Sijmons, Andrei Stefanidi, and Aïcha van Veen. *Fly Myself Into the Future Midterm Design Report V2*. Technical report, 2020.
- [8] Jonas Appels, Yasser Elnily, Quinten van Hilten, Roosa Joensuu, Thomas Keesom, Timo van Maarschalkerweerd, Elise Scheers, Kasper Sijmons, Andrei Stefanidi, and Aïcha van Veen. *Fly Myself Into the Future Project Plan V2*. Technical report, 2020.
- [9] Paul Breeze. *Micro-Turbiens*. Technical report, 2016.
- [10] Paolo Candeloro, Tiziano Pagliaroli, Daniele Ragni, and Silvia Di Francesco. *Small-Scale Rotor Aeroacoustics for Drone Propulsion: A Review of Noise Sources and Control Strategies*. *Preprints*, 2019.
- [11] Robinson Helicopter Co. *R22 Pilot's Operating Handbook - Section 1 General*, revised edition, 2012.
- [12] M. Schmid M. Buchwald D.B. Schwinn, P. Weiand. *Structural Sizing of a Rotorcraft Fuselage Using an Integrated Design Approach*. 31st Congress of the International Council of the Aeronautical Sciences, 2018.
- [13] Dr.F.Oliviero. *Aerospace Design and Systems Engineering Elements II – AE2111-II*, 2020.
- [14] Federal Department of the Environment, Transport, Energy and Communications DETEC and Federal Office of Civil Aviation FOCA. *Swiss U-Space*, 2019.
- [15] A.A. Ghobbar. *Implementing reliability, availability, maintainability and supportability rams for the mro industry: A case study at european airlines*. 2008.
- [16] E. Gill, A. Cervone, F. Oliviero, and B.V.S Jyoti. *AE3211-I - Systems Engineering Aerospace Design*. Delft University of Technology, Delft, Netherlands, 2020. Lecture slides.
- [17] DIAMOND AIRCRAFT INDUSTRIES GMBH. *AIRPLANE FLIGHT MANUAL DA40*. DIAMOND AIRCRAFT INDUSTRIES GMBH, June 2000.
- [18] Granta Design Limited. *CES EduPack 2019*, 2019. Version 19.2.0.
- [19] Snorri Gudmundsson. *General Aviation Aircraft Design: Applied Methods and Procedures*.
- [20] Snorri Gudmundsson. Chapter 2 - Aircraft Cost Analysis. In Snorri Gudmundsson, editor, *General Aviation Aircraft Design*, pages 33 – 53. Butterworth-Heinemann, Boston, 2014. ISBN 978-0-12-397308-5.
- [21] Martin Hepperle. *JAVAFOIL User's Guide*, final edition, December 2017.
- [22] ICCAIA, NASA, DLR, ONERA, and JAXA. *Helicopter Noise Reduction Technology, Status Report*. Technical report, 2015.
- [23] Dr. Ir. C. Kassapoglou Ir. W.A. Timmer, D. van Helvoort. *AE2111-I Systems Design: reader - Aircraft Work Packages 4 5*. Delft University of Technology, Delft, Netherlands, 2018. First year project work packages.
- [24] EASTMAN N. JACOBS and ALBERT SHERMAN. *AIRFOIL SECTION CHARACTERISTICS AS AFFECTED BY VARIATIONS OF THE REYNOLDS NUMBER*. Technical report, 1939.
- [25] W. Johnson. *Helicopter Theory*. Dover Publications, 1994.
- [26] Kenneth and Wernicke. *Tilt Prop-rotor Composite Research Aircraft*. Technical report, 1968.
- [27] Jim Hileman Dennis Huff Takeshi Ito Alain Joselzon Yuri Khaletski Ulf Michel Luc Mongeau Brian. J. Tester Magdy Adib, Fernando Catalano. Report by the Second CAEP Noise Technology Independent Expert Panel: Novel Aircraft-noise Technology Review and Medium- and Long-term Noise Reduction Goals. Technical report, 2014.
- [28] Martin Hepperle. *JavaProp Software*, 2018. Version 1.69.
- [29] T.H.G. Megson. *Aircraft Structures for Engineering Students*. Elsevier Ltd., sixth edition, 2017.
- [30] Jean-Baptiste Maurice Peter Konstanzer Oliver Dieterich, Antoine Rabourdin. *Blue Pulse TM: Active Rotor Control by Trailing Edge Flaps at Airbus Helicopters*. Technical report, 2015.
- [31] F. Oliviero. *Aircraft aerodynamic analysis – Mobile surfaces on the wing*, 2018. Course: *AE2111 – II Aerospace Design and Systems Engineering Elements II: Aircraft part*.
- [32] B.T.C. Zandbergen R. Vos, J.A. Melkert. *Aerospace Design and Systems Engineering Elements I – AE1222-II*, 2020.
- [33] Dr. Calvin Rans and Ir. Joris Melkert. *AE2135-I - Structural Analysis and Design*. Delft University of Technology, Delft, Netherlands, 2018. Lecture slides.
- [34] P.C. Roling. *Flight and orbital mechanics AE2230-I*, 2020.
- [35] Dr. Jan Roskam. *Aeroplane design*. Roskam Aviation and Engineering Corporation, 1985.

-
- [36] Rutan. *VaiEze Owners manual*, third edition edition, 1979.
- [37] M. H. Sadraey. *Aircraft Design: A Systems Engineering Approach*. Wiley, 2012.
- [38] Jos Sinke. *AE3211-II Production of Aerospace Systems Reader*. Delft University of Technology, 2020.
- [39] Jos Sinke. 7. rivetingbolting, 2020. AE3211- Production of Aerospace Systems.
- [40] MANUELA SONNENBERG. FORCE AND EFFORT ANALYSIS OF UNFASTENING ACTIONS IN DISASSEMBLY PROCESSES . Technical report, 2001.
- [41] Y. Liu Y. Wang B. Huang W. Li Y. Li, Y. Yang. Aerodynamic and Aeroacoustic Analyses of a UAV Propeller with Trailing Edge Serrations. *Hear to Listen - Acoustics Adelaide*, 2018.
- [42] Long P. Yip. Wind-Tunnel Investigation of a Full-Scale Canard-Configured General Aviation Airplane. Technical report, 1985.
- [43] L.A. Young, D. Lillie, M. McCluer, and G.K. Yamauchi. Insights into Airframe Aerodynamics and Rotor-on-Wing Interactions from a 0.25-scale Tiltrotor Wind Tunnel Model. Technical report, 2002.
- [44] Xianzhong Zhao, Shen Yan, Yiyi Chen, Zhenyu Xu, and Yong Lu. Experimental study on progressive collapse-resistant behavior of planar trusses. *Engineering Structures*, 135:104–116, 03 2017. doi: 10.1016/j.engstruct.2016.12.013.